

The Safety and Immunostimulatory Properties of
Amorphous Silica Nanoparticles <10 nm in Diameter

Bradley Vis

Hughes Hall College
University of Cambridge

This dissertation is submitted for the degree of Doctor of Philosophy at
the University of Cambridge

August 2017

Preface

This dissertation is the result of my own work and includes nothing which is the outcome of collaborative work except that declared here and specified in the text. It is not substantially the same as any work that I have submitted or is being concurrently submitted for a degree, diploma or other qualification at the University of Cambridge, any other university or similar institution. It does not exceed the word limit specified by the Degree Committee for the Faculty of Biology

The work presented in this dissertation was predominantly carried out at the Medical Research Council Elsie Widdowson Laboratory (MRC-EWL, formerly MRC-Human Nutrition Research, HNR) in Cambridge, UK. I collaborated with several members of the Biomineral Research group at MRC-EWL as well as the Department of Pathology at the University of Cambridge and the MRC Cancer Unit (MRC-CU), all in Cambridge, UK, and Lakehead University in Canada. In Chapter 3, the ^{29}Si NMR analyses were conducted at the University of Manitoba, Canada, by Dr Kirk Marat. Sample preparation for the NMR studies was conducted by myself or Mr Christian O'Brien in the Department of Chemistry at Lakehead University, Canada, under the supervision of Prof. Stephen Kinrade. Data analyses was the outcome of my own work. The titration of a nanosilica dispersion and the preparation of the iron hydroxide nanoparticles were conducted by Mr Carlos Bastos (MRC-EWL). In Chapter 4, IL-1 β analyses were conducted by Dr Laetitia Pele (MRC-EWL). The gene microarray analyses were performed by Dr Mark Boekschoten at Wageningen University (Netherlands). In Chapter 6, intracellular TCR and CD3 analyses were conducted by Miss Camilla Fairbairn in Dr Suzanne Turner's laboratory in the Department of Pathology (University of Cambridge). In Chapter 7, an alternative nanosilica synthesis was developed for translation into *in vivo* studies by Dr Nuno Faria and Mr Carlos Bastos (both MRC-EWL). Animal work was conducted either by Translational Drug Development (TD2) at Translation Genomic Research Institute (TGen) or at the MRC-CU in Cambridge (UK) by Drs Jacqueline Shields and Luisa Pedro. Sera samples from the study conducted at TGen were sent to Myriad RBM for a serum cytokine analyses. In Appendix 2, the clearance of nanosilica after intravenous injection in the mice was conducted by Dr Ravin Jugdaohsingh (ICP-OES analyses) and by Drs Jacqueline Shields and Luisa Pedro (animal work). In Appendix 3, flow imaging of fluorescent bead uptake was conducted by Dr Rachel Hewitt. All other data (analyses and interpretation) is the outcome of my own work.

Acknowledgements

I would first like to thank HS Pharma for sponsoring my PhD studies. I would also like to express appreciation to Dr Jonathan Powell, whose advice really helped shape this project. I would next like to thank Dr Rachel Hewitt, who guided me through the ways of flow cytometry and immunology. I would also like to thank my committee, Prof Serena Best and Dr Lee Roberts, for their guidance, Prof. Stephen Kinrade for his endless grounded advice, and Dr Nuno Faria for his scientific enthusiasm and guidance. Additionally, I would like to thank the past and present students in the BMR research group, particularly Mohamad Aslam, Carlos Bastos, and William Thom, from making my time in Cambridge so enjoyable. Finally, I would also like to express great thank to my supervisor, Dr Ravin Jugdaohsingh, whose guidance and calm temperament were always welcome and grounding.

Lastly, I would like to thank my parents and family for their constant support. Most of all, I would like to thank my wife, Tiffany, and my son, Renly, for being so amazingly supportive throughout my studies and for being my anchor to the real world.

Contents

Preface	i
Acknowledgments	iii
Contents	v
List of Figures	ix
List of Tables	xvi
Abbreviations	xvii
Symbols	xx
Abstract	xxi
Chapter 1. Introduction	1
1.1 Silicate chemistry.....	1
1.2 Exposure to silicon	4
1.2.1 Silicon in the diet	4
1.2.2 Biomedical applications	5
1.2.3 Inhalation.....	5
1.2.4 Silicate clearance and excretion	6
1.3 Biological role and safety of silicon	6
1.3.1 The safety of silicate nanoparticles.....	7
1.3.2 Insoluble silicates and the immune system.....	8
1.4 Cell Biology	9
1.4.1 Cell death	9
1.4.2 Cell lines, cell matrixes	10
1.5 General immunology	10
1.5.1 Innate immune responses	10
1.5.2 Adaptive immune responses	13
1.5.2.1 T cell immunology	13
1.5.2.2 T cell subsets.....	14
1.5.2.3 T cell signalling	17
1.5.2.4 T cell signalling models.....	20
1.5.2.5 General markers of T cell activation	20

1.5.2.6 Defective activation mechanisms	21
1.5.2.7 T cell activation by silica and nanoparticles	21
1.5.3 Cells that bridge innate and adaptive immune cells	22
1.6 Rationale and Aim of the Thesis	22
Chapter 2. Methods.....	25
2.1 Chemistry	25
2.1.1 Nanosilica preparation	25
2.1.2 Control particles	25
2.1.3 Characterization of nanoparticle dispersions	26
2.1.4 Tumour digestions	27
2.1.5 ICP-OES analyses.....	28
2.2 Cell assays.....	28
2.2.1 Transfected cells and cell lines	28
2.2.2 Primary cells.....	28
2.2.3 Gene array	29
2.2.4 Flow cytometry assays	30
2.2.4.1 Cell treatment.....	30
2.2.4.2 Cell staining	31
2.2.4.3 Flow cytometry analyses.....	33
2.2.5 Western blot analyses	35
2.2.6 Enzyme-linked immunosorbent assay	36
2.2.7 Statistical analysis	36
2.3 <i>In vivo</i> studies.....	37
Chapter 3. Synthesis and characterization of amorphous silica nanoparticles	39
3.1 Introduction.....	39
3.2 Results and discussion	39
3.2.1 Synthesis and characterization	39
3.2.1.1 Nanosilica stability and size	39
3.2.1.2 Nanosilica dissolution and size in dilute conditions (physiological concentrations)	41

3.2.1.3 Effect of aluminum, heat and pH on nanosilica size and dissolution.....	42
3.2.1.4 Low pH synthesis of particles.....	44
3.2.1.5 Silicon-29 NMR analysis of nanosilica dispersions.....	45
3.2.1.6 Charge of nanosilica particles.....	48
3.2.2 Stabilization of nanosilica dispersions.....	51
3.2.3 Preparation and characterization of control particles.....	55
3.3 Conclusions.....	57
Chapter 4. The effect of nanosilica on cell viability and function.....	59
4.1 Introduction.....	59
4.2 Results and discussion.....	59
4.2.1 EBV transformed B cells.....	59
4.2.2 Leukemic monocytic cell line – THP-1 cells.....	62
4.2.3 Primary peripheral immune cells.....	64
4.2.4 Gene array analysis.....	76
4.3 Conclusions.....	80
Chapter 5. Effect of nanosilica on T cell activation.....	83
5.1 Introduction.....	83
5.2 Results and discussion.....	83
5.2.1 The effect of nanosilica on CD4 T cells.....	83
5.2.1.1 General markers of activation.....	83
5.2.1.2 The effect of nanosilica on helper (CD4(+)) T cell lineage.....	89
5.2.2 The effect of nanosilica on cytotoxic lymphocytes.....	97
5.2.2.1 The effect of nanosilica on CD8 T cells.....	97
5.2.2.2 The effect of nanosilica on $\gamma\delta$ T cells and NK/NKT cells.....	101
5.3 Conclusions.....	104
Chapter 6. Investigations into the mechanism of T cell activation by nanosilica.....	107
6.1 Introduction.....	107
6.2 Results and discussion.....	107
6.2.1 Role of antigen-presenting cells (APCs).....	107

6.2.2 Induction of intracellular signalling pathways	112
6.2.3 Incomplete signalling in nanosilica induced T cell activation	114
6.2.4 Nanosilica-T cell interactions	117
6.2.4.1 Primary screening	117
6.2.4.2 Particle specificity for inducing T cell activation	124
6.3 Conclusions.....	130
Chapter 7. Effect of nanosilica on peripheral cells in whole blood and <i>in vivo</i>.....	133
7.1 Introduction.....	133
7.2 Results and discussion	133
7.2.1 Activation and toxicity in whole blood – preliminary investigations	133
7.2.2 Activation and toxicity in whole blood – dynamic whole blood environment	143
7.2.3 Assessing dispersions for use in future <i>in vivo</i> trials	148
7.2.4 <i>In vivo</i> trials	153
7.2.4.1 Preliminary study and post termination studies	153
7.2.4.2 Follow up investigations	159
7.3 Conclusions.....	160
Chapter 8. Conclusions	163
8.1 Summary of the project.....	163
8.2 Future perspectives	166
References	169
Appendix 1. Examples of gating strategies used in flow cytometry studies and integrations used in western blot studies.....	193
Appendix 2. Clearance of amorphous nanosilica from the periphery after intravenous injection.....	213
Appendix 3. The effect of nanosilica on bead and bacterial uptake by monocytes in enriched cultures from PBMC – flow imaging analysis	215

List of Figures

Figure 1.01. Solubility of amorphous silica at pH 0-14.....	2
Figure 1.02. A. General mechanisms of growth of amorphous nanosilica particles. B. Detailed mechanism of growth by Ostwald ripening.....	3
Figure 1.03. Gastrointestinal tract translocation of nanomaterials	5
Figure 1.04. The main helper T cells phenotypes and the factors that induce them	15
Figure 1.05. T cell signalling pathway after T cell recognition of cognate antigen presented on a MHC receptor by an APC or a target cell	19
Figure 3.01. A. Measured particle size distribution over time after neutralization (to pH 7) of a 23 mM Si silica dispersion. B. Particle size distribution of silica dispersions (ca. 23 mM Si, pH 7) containing different concentrations of saline, 24 h after neutralisation and incubation at room temperature	40
Figure 3.02.A. Effect of particle size on dissolution rate after dilution of silica dispersions (23 mM Si, pH 7.0) to ca. 1 mM Si in HEPES buffer (pH 7.0-7.3). B. Percentage of silicon that passed through a 3 and 1000 kDa ultrafilter following dilution of a nanosilica dispersion (23 mM Si, pH 7.0) to ca. 0.8 mM Si in RPMI media containing 10% FBS media and incubation at 37 °C for 0.5-1 h. C. Percentage of Si that passed through a 3 kDa ultrafilter following dissolution of a nanosilica dispersion (23 mM Si, pH 7.0) to ca. 0.8 mM Si in RPMI containing 10% FBS at 37 °C.....	42
Figure 3.03. The effect of A) Al doping and B) heating (70 °C) on the dissolution rate of nanosilica dispersions (23 mM Si, pH 7) after dilution to ca. 1 mM Si in HEPES buffer (pH 7.0-7.3)	43
Figure 3.04. The effect of incubation time at pH 10 on the dissolution rate of nanosilica dispersions (100 mM Si) after dilution to ca. 1 mM Si in HEPES buffer (pH 7.0-7.3)	44
Figure 3.05. Particle size distribution of a nanosilica dispersion (500 mM Si incubated at pH 0.8 and at room temperature for 24 h, A) and its dissolution rate (B) after dilution to ca. 1 mM Si in HEPES buffer (pH 7.0-7.3).....	45
Figure 3.06. Representative size (A.) and dissolution rate (B.) of the two nanosilica dispersions (40 mM Si, see below for formulations, denoted as A and B) employed in the ²⁹ Si-NMR analyses. C. ²⁹ Si NMR spectra (99.35 MHz) of the aqueous nanosilica dispersions containing 40 mM Si (²⁹ Si enriched) at 25 °C.	47
Figure 3.07. A. Representative dissolution rates of three 40 mM nanosilica dispersions, following dilution to 1 mM Si in HEPES buffer (pH 7.0-7.3). B. Zeta-potentials of the three nanosilica dispersions between pH 1.5 and 9 in water	49
Figure 3.08. Titration of 5 mL of a nanosilica dispersion (similar dissolution profile to material A in Figure 3.10) with 69 mM NaOH	49
Figure 3.09. Formation of the β-silicomolybdate complex over time, as measured by the absorbance at 400 nm, following dilution of silicate stocks (silicic acid or nanosilica dispersion (1-2 nm, 500 mM Si incubated at pH 0.8 for 24 h and at room temperature)) to 1 mM Si in a molybdic acid solution (pH ~ 0.8).	52
Figure 3.10. Formation of the β-silicomolybdate complex over time, as measured by the absorbance at 400 nm, following dilution of aged 500 mM (A.) and 40 mM (B.) nanosilica dispersions (prepared at pH 1) to 1 mM Si in a molybdic acid solution (pH ~ 0.8). The area under the absorbance curves (in A. and B.) was determined and plotted against age of the dispersion (C.), showing an increase in condensation with ageing.....	53

Figure 3.11. A. The area under the absorbance curve (measured at 400 nm between 0 and 5 h), corresponding to the formation of the β -silicomolybdate complex, after dilution of aged 40 mM nanosilica dispersions (prepared at pH 1, 7.4 and 9) to 1 mM Si in a molybdic acid solution. B. The effect of incubation time at pH 7 on dissolution rate of nanosilica dispersions after dilution to ca. 1 mM in HEPES buffer (pH 7.0-7.3)	54
Figure 3.12. A. Percentage of silicon in a nanosilica dispersion (40 mM, pH 1.5) that passed through 3 and 50 kDa ultrafilters before and after adjustment to pH 7. B. Particle size distribution (by DLS) of the nanosilica dispersion after pH adjustment to 7. C. Percentage of silicon in the nanosilica dispersion (40 mM, pH 1.5, as shown in A.) that passed through 3 and 50 kDa ultrafilters after dilution to 0.4 mM Si and incubation for 10 min..	55
Figure 3.13. Particle size distribution of (11-mercaptopundecyl)tetra(ethylene glycol) functionalized gold nanoparticles (Sigma-Aldrich, 687863)	56
Figure 3.14. A. Particle size distribution of an aluminium hydroxide dispersion (100 mM Al at pH 4.2. Percentage of aluminium that passed through 3 and 1,000 kDa after addition to BSS (B.) and complete growth media (RPMI+10% FBS, C.) at 1 mM Al	57
Figure 4.01. The effect of silicic acid and 3.6 nm nanosilica on transformed B cell proliferation after 24 h (A.) and 48 h (B.) incubation at 37 °C. C. The effect of 3.6 nm nanosilica on cell viability and proliferation of viable cells. D. The effect of 3.6 nm nanosilica on transformed B cells from separate donors.....	60
Figure 4.02. The effect of nanosilica size on transformed B cell proliferation	61
Figure 4.03. A. The effect of 1.9 nm and 3.6 nm nanosilica on the proliferation of transformed B cells. B. Dissolution of the nanosilica particles after dilution to ca. 1 mM Si in HEPES buffer (pH 7.0-7.3).	62
Figure 4.04. A. The dissolution of nanosilica particles ca. 4.6 nm in size prepared at different pHs after dilution to ca. 1 mM Si in HEPES buffer (pH 7.0-7.3). B. The effect of these particles on transformed B cell proliferation	62
Figure 4.05. The effect of 3.6 nm nanosilica and silicic acid on THP-1 viability	63
Figure 4.06. Representative FACS plots showing the effect of nanosilica on monocyte, B cell and T cell viability in PBMC culture at 24 h	65
Figure 4.07. The effect of nanosilica on percent viability and the viable cell counts of CD11c, CD19, and CD3 cells in PBMC culture at 24 h	66
Figure 4.08. The effect of nanosilica on monocyte apoptosis and necrosis	68
Figure 4.09. The effect of silicic acid and nanosilica on IL-1 β levels in PBMC culture supernatants.....	68
Figure 4.10. A. Representative histograms showing the effect of nanosilica on TCR $\alpha\beta$ cell staining within a T cell FS-SC selection gate at 0.5 h. B. Gating strategy for selection of CD4 and CD8 cells. C. Representative histogram plots showing the effect of nanosilica treatment on CD4 and CD8 cell Annexin V and 7-AAD positivity at 8 h.....	71
Figure 4.11. The effect of nanosilica on CD4 (A, B) and CD8 (C, D) cells apoptosis and necrosis/pyroptosis	72
Figure 4.12. The effect of nanosilica and silicic acid on the phagocytosis of polystyrene fluorescent beads by monocytes.....	73
Figure 4.13. The effect of nanosilica on the phagocytosis of fluorescent <i>S. aureus</i> by monocytes	75

Figure 4.14. The effect of nanosilica on PD-L1 expression by monocytes.....	75
Figure 5.01. The effect of SEB, silicic acid and nanosilica on the expression of CD25 and CD69 on CD4 T cells in PBMC culture after 24 h.....	85
Figure 5.02. The effect of nanosilica concentration on the percentage of CD4 T cells positive for CD25 and CD69 in PBMC culture after 24 h.....	86
Figure 5.03. The effect of nanosilica on CD4 T cell proliferation in PBMC culture after 3 and 5 d.....	87
Figure 5.04. The effect of nanosilica on the expression of CD95 on CD4 T cells in PBMC culture after 24 h.....	88
Figure 5.05. The effect of nanosilica on intracellular FoxP3 levels in activated CD4 T cells in PBMC culture after 24 h.....	90
Figure 5.06. The effect of nanosilica on LAP and GARP expression on activated CD4 T cells in PBMC culture after 24 h.....	91
Figure 5.07. The effect of nanosilica on IL-10 levels in PBMC culture supernatants after 24 h.....	92
Figure 5.08. The effect of silicic acid and nanosilica on IFN- γ levels in PBMC culture supernatants after 24 h.....	93
Figure 5.09. The effect of nanosilica on CD40L (CD154) expression on CD4 T cells in PBMC culture after 24 h.....	95
Figure 5.10. The effect of nanosilica on iCOS (CD278) expression on CD4 T cells in PBMC culture after 24 h.....	96
Figure 5.11. The effect of nanosilica on IL-4 levels in PBMC culture supernatants after 24 h.....	97
Figure 5.12. The effect of SEB, silicic acid and nanosilica on the expression of CD25 and CD69 on CD8 T cells in PBMC culture after 24 h.....	98
Figure 5.13. The effect of nanosilica on CD8 T cell proliferation in PBMC culture after 3 and 5 d.....	100
Figure 5.14. The effect of nanosilica on the expression of CD95 on CD8 T cells in PBMC culture after 24 h.....	101
Figure 5.15. The effect of nanosilica on CD25 and CD69 expression on $\gamma\delta$ T cells in PBMC culture after 24 h.....	102
Figure 5.16. The effect of nanosilica on CD25 and CD69 expression on NK/NKT (CD57(+)) cells in PBMC culture after 24 h.....	104
Figure 6.01. The effect of nanosilica on CD25 and CD69 expression on CD4 and CD8 T cells in enriched T cell cultures.....	109
Figure 6.02. The effect of nanosilica on Jurkat T cell CD25 and CD69 expression.....	110
Figure 6.03. The effect of nanosilica on Karpas 299 cell CD25 and CD69 expression.....	111
Figure 6.04. Effect of nanosilica on the phosphorylation of Zap70 in enriched T cell cultures.....	113
Figure 6.05. Effect of nanosilica on the phosphorylation of LAT in enriched T cell cultures.....	113

Figure 6.06. The effect of 400 μ M nanosilica, 0.5 μ g/mL ionomycin and 0.2 μ g/mL PdBu on IL-2 levels in PBMC culture supernatants at 24 h.....	115
Figure 6.07. The effect of nanosilica and anti-CD28 on CD4 and CD8 T cell proliferation at 3 d	116
Figure 6.08. Representative dot plots showing the expression of TCR $\alpha\beta$, CD3 ϵ , CD4 and CD8 in cultures exposed to SEB and nanosilica for 5 min.....	118
Figure 6.09. Percentage of the cells positive for TCR $\alpha\beta$, CD3 ϵ , CD4 and CD8 in cultures exposed to SEB and nanosilica for 5 min.....	119
Figure 6.10. Percentage of the T cells positive for internal TCR and CD3 after treatment with nanosilica for 30 min	120
Figure 6.11. Percentage of the cells positive for TCR $\alpha\beta$, CD3 ϵ , CD4 and CD8 in fixed cell cultures exposed to nanosilica (800 μ M) for 10 min	120
Figure 6.12. (Left y-axis) Percentage of the cells positive for TCR $\alpha\beta$, CD3 ϵ , CD4 and CD8 in cultures exposed to nanosilica (800 μ M) for 0.1-4 h. (Right y-axis) Dissolution of nanosilica in cell-free growth media.....	122
Figure 6.13. Effect of nanosilica on $\gamma\delta$ TCR and CD8 antibody staining.....	123
Figure 6.14. Effect of nanosilica particle size on expression of CD25 and CD69 on CD4 and CD8 T cells	125
Figure 6.15. Effect of nanosilica particle lifetime in dilute conditions on expression of CD25 and CD69 on CD4 and CD8 T cells	128
Figure 6.16. Percentage of the cells positive for TCR $\alpha\beta$, CD3 ϵ , CD4 and CD8 within a T cell selection gate (based on FSC versus SSC profiles) after treatment with 400 μ M nanosilica for 10 min.....	129
Figure 6.17. The effect of nanosilica and iron nanoparticles on expression of CD25 and CD69 on CD4 and CD8 T cells after 24 h	130
Figure 7.01. The effect of nanosilica on the percentage of CD3 T cells positive for CD25 and CD69 in whole blood culture after 24 h	135
Figure 7.02. Representative size (A.) and dissolution rate (B.) of nanosilica dispersions (40 mM Si, various formulations denoted as materials A and B) employed in the whole blood assays (Figure 7.03)	137
Figure 7.03 The effect of nanosilica on the percentage of CD4 and CD8 T cells positive for CD25 and CD69 in whole blood culture after 24 h	138
Figure 7.04. The effect of nanosilica on the percentage of $\gamma\delta$ T cells and NK/NKT cells (CD57(+)) positive for CD25 and CD69 in whole blood culture after 24 h.....	140
Figure 7.05. The effect of 4 mM nanosilica on neutrophil, monocyte (CD14), T cell (CD3) and B cell (CD19) in whole blood culture after 24 h	142
Figure 7.06. The effect of nanosilica on the percentage of CD4 and CD8 T cells positive for CD25 and CD69 in whole blood culture	145
Figure 7.07. The effect of nanosilica on the percentage of monocytes within the cell distribution in whole blood culture	146
Figure 7.08. The effect of nanosilica and dilution schedule on the percentage of CD4 and CD8 T cells positive for CD25 and CD69 in whole blood culture	147

Figure 7.09. The effect of the nanosilica dilution schedule on the percentage of monocytes within the cell distribution in whole blood culture	148
Figure 7.10. The effect of nanosilica particle age on the percentage of CD4 and CD8 T cells positive for CD25 and CD69 in whole blood culture	150
Figure 7.11. The effect of the particle age on the percentage of monocytes within the cell distribution in whole blood culture	151
Figure 7.12. The effect of nanosilica (material C and D) on the percentage of CD4 and CD8 T cells positive for CD25 and CD69 in whole blood culture	152
Figure 7.13. The effect of nanosilica (material C and D) on the percentage of monocytes in the cell distribution in whole blood culture	153
Figure 7.14. Tumour sizes after 14 d from mice injected subcutaneously with B16-F10 melanoma and treated daily with saline, temozolomide and nanosilica (23 mM Si, 400 µL) for 10 d	154
Figure 7.15. A. Concentration of Si in tumours from the murine melanoma model B. Correlation between tumour size and concentration of Si	155
Figure 7.16. Serum cytokine levels from mice injected subcutaneously with B16-F10 melanoma and treated daily with saline and nanosilica (DV0.5 = 3.6 nm) for 10 d.....	156
Figure 7.17. A. Serum lymphotactin levels from mice injected subcutaneously with B16-F10 melanoma and treated daily with saline and nanosilica (DV0.5 = 3.6 nm) for 10 d.). B. Correlation between tumour size and lymphotactin levels after nanosilica treatment C. Correlation between tumour size and lymphotactin levels after saline treatment. D. The effect of silicic acid and nanosilica on lymphotactin levels in PBMC culture supernatants after 24 h.	157
Figure 7.18. Serum IgA (A), IgG (B) and IgM (C) levels from mice injected subcutaneously with B16-F10 melanoma and treated daily with saline and nanosilica for 10 d. Correlation between tumour size and IgM/IgG (D).....	158
Figure 7.19. Treatment schedule (A.) and tumour sizes (B.) after 8-15 d of mice injected subcutaneously with B16-F10 melanoma and treated with saline and nanosilica. Treatment schedule (C.) and number of surface lung nodules (D.) 21 d after intravenous injection with B16-F10 melanoma and treated with saline and nanosilica.....	160
Figure 8.01. Proposed mechanism of nanosilica induction of T cell activation.....	165
Figure 9.01. Gating strategy for the assessing transformed EBV B cell proliferation without a viability stain	193
Figure 9.02. Gating strategy for the assessing transformed EBV B cell proliferation with a viability stain	194
Figure 9.03. Gating strategy for assessing THP-1 viability	195
Figure 9.04. Gating strategy for assessing viability of monocytes (CD11c), T cells (CD3) and B cells (CD19) in PBMC cultures	196
Figure 9.05. Gating strategy for assessing apoptosis and necrosis of monocytes (CD11c) in PBMC cultures.....	197
Figure 9.06. Gating strategy for assessing apoptosis and necrosis of CD4 and CD8 cells in PBMC cultures.....	197

Figure 9.07. Gating strategy for assessing fluorescent bead and bacteria by monocytes in enriched monocyte cultures	198
Figure 9.08. Gating strategy for assessing PD-L1 expression by monocytes in PBMC cultures	199
Figure 9.09. Gating strategy for assessing CD25 and CD69 expression on CD4 and CD8 T cells in PBMC cultures	200
Figure 9.10. Gating strategy for assessing proliferation of CD4 and CD8 T cells in PBMC cultures	201
Figure 9.11. Gating strategy for assessing CD95 (Fas) expression on CD4 T cells in PBMC cultures	202
Figure 9.12. Gating strategy for assessing FoxP3 levels in activated CD4 T cells in PBMC cultures	202
Figure 9.13. Gating strategy for assessing LAP/GARP expression on activated CD4 T cells in PBMC cultures	203
Figure 9.14. Gating strategy for assessing CD40L (CD154) expression on CD4 T cells in PBMC cultures	203
Figure 9.15. Gating strategy for assessing iCOS (CD278) expression on CD4 T cells in PBMC cultures	203
Figure 9.16. Gating strategy for assessing CD95 (Fas) expression on CD8 T cells in PBMC cultures	204
Figure 9.17. Gating strategy for assessing CD25 and CD69 expression on $\gamma\delta$ T cells in PBMC cultures	204
Figure 9.18. Gating strategy for assessing CD25 and CD69 expression on NK/NKT (CD57(+)) cells in PBMC cultures	204
Figure 9.19. Gating strategy for assessing CD25 and CD69 expression on Jurkat and Karpas 299 cells	205
Figure 9.20. Gating strategy for assessing cell distribution in enriched T cell cultures.....	206
Figure 9.21. Integration strategy for the determination of pZap70 and vinculin levels in cell lysates	207
Figure 9.22. Gating strategy for assessing $\alpha\beta$ TCR, CD3, CD4 and CD8 antibody binding inhibition in PBMC cultures	208
Figure 9.23. Gating strategy for assessing $\gamma\delta$ TCR and CD8 antibody binding inhibition in PBMC cultures	208
Figure 9.24. Gating strategy for assessing CD25 and CD69 expression on CD3 T cells in whole blood cultures	209
Figure 9.25. Gating strategy for assessing CD25 and CD69 expression on CD4 and CD8 T cells in whole blood cultures	209
Figure 9.26. Gating strategy for assessing CD25 and CD69 expression on $\gamma\delta$ T cells in whole blood cultures	210
Figure 9.27. Gating strategy for assessing CD25 and CD69 expression on NK/NKT cells in whole blood cultures	210

Figure 9.28. Gating strategy for assessing viability of T cells and B cells in whole blood cultures	211
Figure 9.29. Gating strategy for assessing viability of neutrophils and monocytes in whole blood cultures	212
Figure 10.01. Concentration of silicon in blood after mice were intravenously injected with 200 μ L nanosilica (40 mM Si)	214
Figure 11.01. The effect of nanosilica on the phagocytosis of polystyrene fluorescent beads by monocytes.....	217
Figure 11.02. The effect of nanosilica on the phagocytosis of fluorescent <i>S. aureus</i> by monocytes	218

List of Tables

Table 1.1. Silicon terminology	1
Table 2.01. Human antibodies and markers used throughout the investigations	34
Table 2.02. Mouse antibodies and markers used throughout the investigations.....	35
Table 3.01. Distribution of silicon in the two nanosilica dispersions (40 mM) determined through the spectral integration of the ²⁹ Si NMR spectra.....	47
Table 3.02. Zeta-potential and derived count rate of nanosilica dispersions (as defined in Figure 3.10) in PBS and RPMI.....	50
Table 4.01. Individual genes in EBV transformed B cells whose expression was significantly altered by nanosilica compared to that of the control	77
Table 4.02. Gene pathways in EBV transformed B cells whose expression was significantly altered by nanosilica compared to that of the control	77
Table 4.03. Gene pathways associated with apoptosis in EBV transformed B cells whose expression was significantly altered by nanosilica compared to that of the control.....	78
Table 4.04. Individual genes in THP-1 cells whose expression was significantly altered by nanosilica compared to that of the control.....	78
Table 4.05. Individual genes in PBMC culture whose expression was significantly altered by nanosilica compared to that of the control.....	79
Table 4.06. Gene pathways in PBMC culture whose expression was significantly altered by nanosilica compared to that of the control.....	80
Table 6.01. Statistical analysis of the induction of CD25 and CD69 on CD4 and CD8 T cell between nanosilica dispersions of different sizes (shown in Figure 6.14). Green denotes significant, red denotes non-significant	126
Table 7.01. The percentage of T cells activated (expressing CD25 and CD69) in the 16 mM Si, 25 s nanosilica pulse.	145

Abbreviations

7-AAD – 7-aminoactinomycin D
Abs - absorbance
AICD – activation induced cell death
APC – antigen presenting cells
APC - allophycocyanin
APC-Cy7 – allophycocyanin cyanine 7
ATP – adenosine triphosphate
DC – dendritic cell
BSA – bovine serum albumin
BSS – balanced salt solution
CD – cluster of differentiation
CCL – chemokine (C-C motif) ligand
CFDA-SE – carboxyfluorescein diacetate succinimidyl ester
CGM - complete growth media
CLIP - class II-associated li peptide
CRTAM – class-I MHC-restricted T-cell associated molecule
CTL – cytotoxic T lymphocyte
CTLA-4 – cytotoxic T lymphocyte associated protein 4
CTLs – cytotoxic T cells
DAMPs - damage-associated molecular patterns
DC – dendritic cell
DDW – distilled deionised water
DED – death effector domain
DLS – dynamic light scattering
DMSO – dimethyl sulfoxide
DNA – deoxyribonucleic acid
DV – volume median diameter
EBV - Epstein-Barr virus
ECL – enhanced chemiluminescence
ELISA – enzyme-linked immunosorbent assay
FACS – fluorescence activated cell sorting
FADD – Fas-associated death domain protein
FBS – foetal bovine serum

FDR – false discovery rate
FITC – Fluorescein isothiocyanate
FLICE- FADD-like IL-1 β -converting enzyme
FoxP3 - foxhead box P3
FSC – forward scatter
Fyn - proto-oncogene tyrosine-protein kinase Fyn
GARP - glycoprotein A repetitions predominant
GCP - granulocyte chemoattractant protein
GPNMB – glycoprotein nonmetastatic melanoma protein B
HEPES – 2-[4-(2-hydroxyethyl)piperazin-1-yl]ethanesulfonic acid
HRP - horseradish-peroxidase
iCOS – inducible T cell coostimulator
ICP-OES - inductively coupled plasma-optical emission spectroscopy
IFN- γ – interferon gamma
Ig - immunoglobulin
IL – interleukin
IL-2R – interleukin-2 receptor
ITAM- immunoreceptor tyrosine-based activation motif
iTreg - inducible regulatory T cell
kcps – kilo counts per second
KS – kinetic segregation
LAT – linker for activation of T cells
LAP - latency-associated peptide
LCK - lymphocyte-specific protein tyrosine kinase
LEAF – low endotoxin, azide free
LPS – lipopolysaccharide
MARCO - macrophage receptor with collagenous structure
MAPK – mitogenic-activated protein kinases
MIP – macrophage inflammatory protein
MHC – major histocompatibility complex
MMP-9 - matrix metalloproteinase 9
MOPS – 3-(N-morpholino)propanesulfonic acid
MPO - myeloperoxidase
MWCO – molecular weight cut-off

NETs - Neutrophil extracellular traps
NES – normalized enrichment scores
NF- κ B – nuclear factor kappa-light-chain enhancer of activated B cells
NK cells – natural killer cells
NFAT – nuclear factor of activated T cells
NKT – natural killer T cells
NMR – nuclear magnetic resonance
nTreg - natural regulatory T cell
PAMPS - pathogen-associated molecular patterns
PBS – phosphate buffered saline
PBMC – peripheral blood mononuclear cells
PD-1 – Programmed cell death protein 1'
PD-L1 – programmed death-ligand 1
PdBu - phorbol 12, 13-dibutyrate
PE - phycoerythrin
PE-Cy5 – phycoerythrin cyanine 5
PE-Cy7 – phycoerythrin cyanine 7
PG - peptidoglycan
PHA – phytohaemagglutinin
PIPES - piperazine-N,N'-bis(2-ethanesulfonic acid)
pMHC - peptide loaded MHC receptor
OVA - ovalbumin
PRR- pattern-recognition receptors
PS – phosphatidylserine
Q – quadrifunctional (silicate centre)
RPMI medium – Roswell Park Memorial Institute medium
RND3 – Rho family GTPase 3
pMHC – peptide-loaded MHC receptor
pTreg - peripheral regulatory T cell
pLCK - phosphorylated lymphocyte-specific protein tyrosine kinase
pZap-70 - phosphorylated zeta-chain associated protein kinase 70
RNA – ribonucleic acid
RPMI – Roswell Park Memorial Institute medium
SAg – superantigen

SD – standard deviation
SDS – sodium dodecyl sulphate
SEB – *Staphylococcal enterotoxin B*
SLAM – signalling lymphocytic activation molecule
SLP-76 – lymphocyte cytosolic protein 2
SSC – side scatter
STAT - signal transducer and activator of transcription
TBS - tris buffered saline
TBST - tris buffered saline with TWEEN20
TCR – T cell receptor
TEM – transmission electron microscopy
TGF- β – transforming growth factor
TLR – Toll-like receptor
TNF- α – tumour necrosis factor alpha
TNFR2 - tumour necrosis factor receptor 2
Treg – Regulatory T cell
tTreg - thymic regulatory T cell
Th1 – Type 1 T helper cell
Th2 – Type 2 T helper cell
TWEAK – tumour necrosis factor-like weak inducer of apoptosis
Tyr - tyrosine
Zap-70 – zeta-chain associated protein kinase 70

Symbols

δ – NMR chemical shift

Abstract

Humans are exposed to high levels of amorphous silica on a daily basis, via the diet and the use of cosmetic and pharmaceutical products. Amorphous silica particles (10-200 nm) have also been developed for use in biomedical applications, including as binding agents in tissue repair, drug and gene therapy delivery agents, coatings for medical contrast agents and as vaccine adjuvants. Numerous studies have already been conducted to evaluate the cellular toxicity of these silica particles but still little is known about their effects both *in vitro* and *in vivo*, especially of nanosilica particles under 10 nm in diameter. The aim of this thesis was to investigate the cellular and *in vivo* activity of < 10 nm diameter nanosilica particles with different properties (e.g., size and dissolution rate in dilute conditions) as it may infer upon safety after exposure via the diet and intravenous administration (biomedical applications).

First, the cytotoxicity of sub-10 nm nanosilica particles, fully characterized by size, dissolution rate, zeta-potential and by NMR spectroscopy, on immune cell function was assessed using transformed and cancerous cell lines and primary cells. The particles were toxic to the immune cells in a dose dependent manner and impaired certain cellular functions. Primary cells were most susceptible to nanosilica induced death and, of the primary cells, phagocytes were most susceptible to its cytotoxicity. Further investigations were conducted to assess the effect of nanosilica on T cells, as there was evidence suggesting that nanosilica particles were directly interacting with these cells.

Nanosilica particles 3.6 nm in diameter were found to have a significant effect on T cell function. The particles induced numerous markers of T cell activation, including CD25 and CD69 on CD4 T cells, CD8 T cells, gamma-delta T cells and NK/NKT cells, CD95 on CD4 and CD8 T cells, CD40L, FoxP3, LAP, GARP on CD4 T cells, and IFN-gamma production, but it did not induce T cell proliferation. The particles were found to activate T cells regardless of their antigenic specificity. Further investigations showed that nanosilica interacts with the T cell receptor complex, the first documented case of a non MHC-coated nanoparticle directly interacting with this receptor complex. The nanoparticulate induced signalling through Zap70, LAT, and, eventually, through NFAT but not through MAPK. Similar signalling in the literature has been shown to induce a hyporesponsive T cell state (anergy) or activation induced cell death. The induction of the CD25 and CD69 T cell activation markers was limited to nanosilica particles below 10 nm in size, while similarly sized iron hydroxide nanoparticles (3-5 nm) only induced low levels of CD69 expression on T helper cells.

Finally, it was shown that nanosilica is capable of inducing T cell activation in whole blood, though the T cell responses were greatly attenuated. Although identification of activation pathway *in vivo* remains elusive, the nanosilica particles were shown to have therapeutic value, decreasing murine subcutaneous tumour growth rate and significantly reducing the

formation of lung metastases. Whether these *in vivo* responses are related to T cell activation identified *in vitro* remains unclear.

Chapter 1 - Introduction

1.1 Silicate chemistry

Silicon is the second most abundant element in the Earth's crust and is present throughout the geosphere, found in forms including soluble orthosilicic acid ($\text{Si}(\text{OH})_4$) and insoluble silica particles (both amorphous and crystalline in structure) (Belton et al., 2012; Clarke and Washington, 1924; Sommer et al., 2006; Winter, 2012). A brief list summarizing the silicon terminology used throughout this report is shown in Table 1.01. Amorphous silica nanoparticles were the primary focus of the investigations conducted in this thesis.

Table 1.01. Silicon terminology in this thesis

Term	Properties
Silicon	<ul style="list-style-type: none">- Elemental silicon- Form not defined
Silicic acid	<ul style="list-style-type: none">- $\text{Si}(\text{OH})_{4(\text{aq})}$- Dissolved inorganic silicon- Also referred to as orthosilicic acid, monosilicic acid, monomeric silica, and soluble silica
Silicate	<ul style="list-style-type: none">- Refers to an anionic silicon compound- Most commonly denotes the oxide form of silicon, specifically silica and its soluble form
Amorphous silica	<ul style="list-style-type: none">- Insoluble silicon with a long-range formula of SiO_2- No defined structure, contains silicon centres connected to 2, 3 or 4 other silicon centres through oxygen linkages (Si-O-Si)- Also referred to as polymeric or colloidal silica
Nanosilica	<ul style="list-style-type: none">- Silica particles below 100 nm in size- In this report, "nanosilica" refers to amorphous particles (unless stated otherwise)
Crystalline silica	<ul style="list-style-type: none">- Insoluble silicon with a long-range formula of SiO_2- Structured, contains silicon centres connected to 4 other silicon centres through oxygen linkages (Si-O-Si). Form depends on crystal symmetry- Most common forms (polymorphs) include α-quartz and tridymite
Organic silicon	<ul style="list-style-type: none">- Refers to silicon species containing a Si-C bond- Not naturally occurring

The solubility of amorphous silica is low at physiological pH and it increases with pH, as shown in Figure 1.01. Insoluble colloidal silica is formed when the concentration of Si exceeds its solubility limit, and the properties of these colloidal particles depend on factors such as temperature, pH and ionic strength (Iler, 1979; Stumm and Morgan, 1981). Formed by condensation of orthosilicic acid, colloidal silica consists of tetraoxosilicon centres (denoted previously as \underline{Q} for quadrafunctional) bound through siloxane linkages. The degree of condensation refers to the number of siloxane linkages a silicate centre contains, commonly denoted by superscripts. For example, orthosilicic acid ($\text{Si}(\text{OH})_4$) is denoted as \underline{Q}^0 while a silicate centre linked to 3 other centres (through siloxane linkages) is denoted as \underline{Q}^3 . Amorphous particles consist of silicate centres linked to 2-4 adjacent silicate centres (\underline{Q}^2 - \underline{Q}^4) (Jantschke et al., 2014; Kalia et al., 2016) while crystalline particles are comprised of fully condensed centres (\underline{Q}^4) (Downs and Palmer, 1994; Kihara et al., 1986; Wright and Lehmann, 1981). The structure of amorphous and crystalline particles also differ, where the former has no inherent structure (amorphous) and the latter has a specific crystal structure (Downs and Palmer, 1994; Glinnemann, 1992; Kihara et al., 1986; Wright and Lehmann, 1981). In dilute conditions, crystalline silica particles are more persistent than amorphous silicates (Kalia et al., 2016; Rimstidt, 1997).

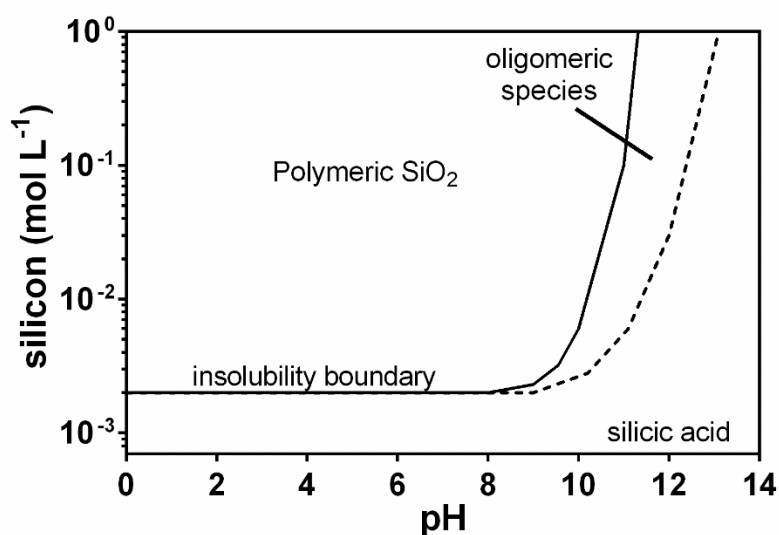


Figure 1.01. Solubility of amorphous silica at pH 0-14. Reproduced from Jugdaohsingh *et al.* (Jugdaohsingh et al., 2008).

Colloidal silicate dispersions are metastable and follow similar growth processes as other nanoparticles, mainly Ostwald ripening and agglomeration (Figure 1.02). Ostwald ripening occurs when silicon from the smaller particles dissolves and re-precipitates on the surface of larger particles (Belton et al., 2012; Kobayashi et al., 2005). This process is highly dependent on the solubility of the monomeric unit, *i.e.*, silicic acid, as it does not occur with materials that are completely insoluble or soluble (Fairhurst and Lee, 2008; Lifshitz and Slyozov, 1961; Nancollas, 1979). Agglomeration is the clustering of the smaller base particles resulting in the formation of larger particles (Belton et al., 2012). The clusters can be loosely bound or strongly assembled, which will be referred to as agglomerates and aggregates, respectively (classification set out by Powell *et al.* will be used) (Nichols et al., 2002; Powell et al., 2010). The rate of silicate agglomeration is greatest at pH 5-7 (Bergna and Roberts, 2005).

An important property of colloidal silica particles, and all nanoparticles, is their charge. Charge also plays a role in how the particles interact with other materials such as proteins, cells, metals, and even self-particles (*i.e.*, aggregation). Silica particles are known to be negative at physiological pH (Bergna and Roberts, 2005). The pKa of amorphous silica has been determined to be between 6.8 and 7.1 (Belton et al., 2012; Hair and Hertl, 1970), which would suggest that 50% of the surface hydroxyl groups are deprotonated at this pH. Nanosilica particles are known to be neutral at low pH, conditions in which they are most stable (Bergna and Roberts, 2005).

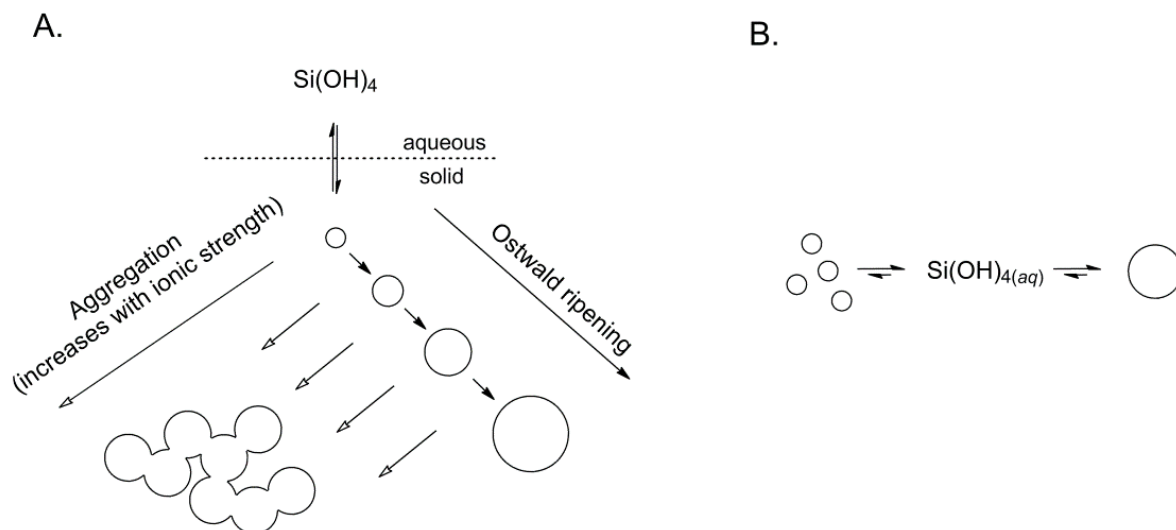


Figure 1.02. **A.** General mechanisms of growth of amorphous nanosilica particles. **B.** Detailed mechanism of growth by Ostwald ripening. Reproduced from Belton, Bolt, Iler and Kobayashi (Belton et al., 2012; Bolt et al., 1997; Iler, 1979; Kobayashi et al., 2005)

Silicon-29 NMR spectroscopy has also been used to characterize silicate condensation (Bergna and Roberts, 2005; Kalia et al., 2016). Chemical shifts of the silicate centres with ranging condensation levels (Q^0 to Q^4) have been assigned. The spectra of amorphous silicates have broad signals corresponding to the insoluble Si. The lack of repeating structure within the particle results in slightly different chemical environments for silicate centres of similar condensation levels, resulting in slightly different chemical shifts and broad signals.

1.2 Exposure to silicon

1.2.1 Silicon in the diet

Humans are exposed to high levels of silicates from their diet. High dietary sources of silicon include drinking water, cereal grains and products such as beer, nuts and some fruits and vegetables (Jugdaohsingh, 2007). In addition to natural sources, amorphous silica is commonly added to foods, pills/drugs, and beverages. It is used as an anti-clumping agent, thickening and stabilizing agents, and as fillers and abrasives (Jugdaohsingh, 2007). However, silicon is only markedly absorbed in its soluble form, meaning most dietary silicon is excreted in the urine (Jugdaohsingh et al., 2002; Sripanyakorn et al., 2009).

Notwithstanding, some ingested solid phase (particulate) silica probably is absorbed from the mammalian gut. Although many of the silicate particles that humans ingest are resistant to degradation in the gastrointestinal tract, some can potentially be taken up via the numerous gastrointestinal particle uptake mechanisms, as depicted in Figure 1.03 (reviewed by Powell *et al.*) (Powell et al., 2010). Firstly, epithelial cells can take up small particles (< 20 nm) via endocytosis. Secondly, large particles, > 20 nm, can undergo transcytosis by microfold cells (M cells). Thirdly, small and large particles can passively cross the gastrointestinal tract via holes created by the loss of endothelial cells. Lastly, disturbances in the tract, caused by drug or diet allow small nanoparticles to translocate. Most of these transport mechanisms are not efficient, but given the exposure to large numbers of particles, significant numbers may still be absorbed and interact with mucosal immune cells.

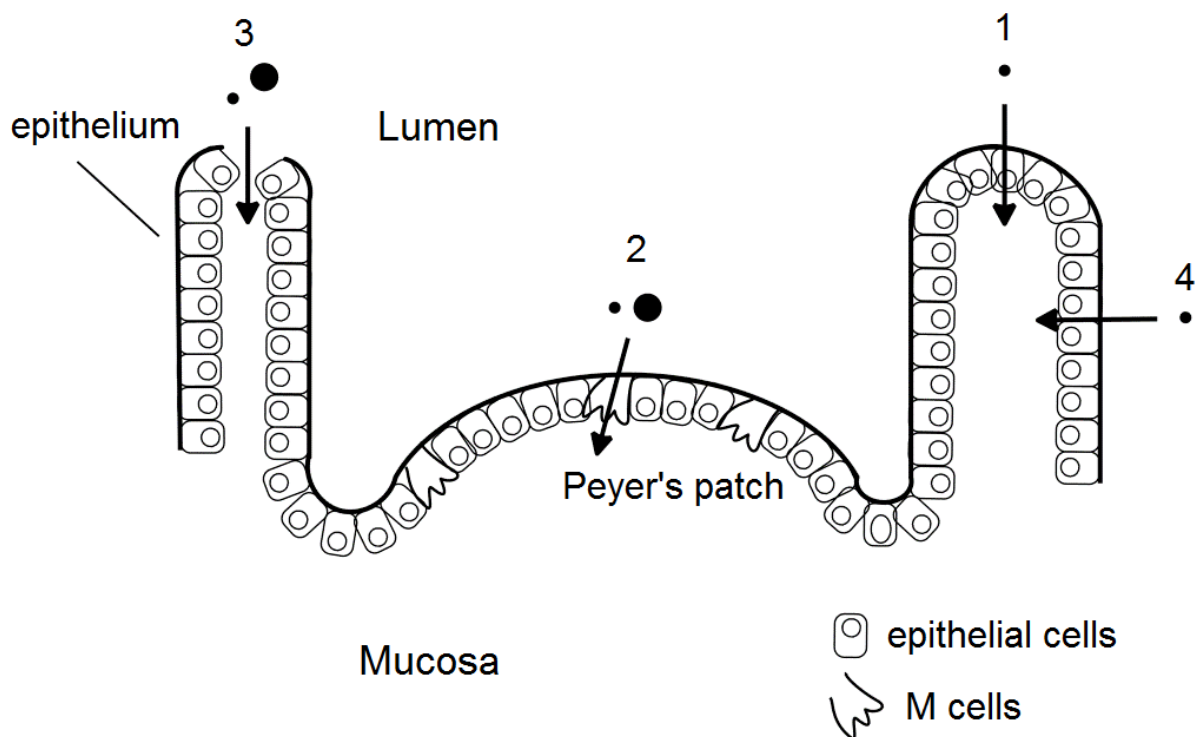


Figure 1.03. Gastrointestinal tract translocation of nanomaterials by: 1) Endothelial cells endocytosis of small particles (< 20 nm). 2) Microfold cells (M cells) translocation of large particles, > 20 nm. 3) Passive transfer of small and large particles via holes created by the loss on endothelial cells. 4) Translocation of small particles through disturbances in the endothelium. Reproduced from Powell et al. (Powell et al., 2010)

1.2.2 Biomedical applications

More recently, amorphous silica nanoparticles have been developed for use in biomedical applications. Silica nanoparticles have been shown to be an effective vaccine adjuvant, with comparable responses to the Al-based vaccine adjuvants for which many adverse reactions are associated (Scaramuzzi et al., 2016; Skrastina et al., 2014). These particles have also been shown to be effective binding agents in sutures, cross-linking soft tissues leading to increased closure and healing of wounds (Meddahi-Pellé et al., 2014). Lastly, silica particles have been used as agents to delivery drugs, in gene therapies and as contrast agents (for use in medical imaging) (Bitar et al., 2012). Silica is commonly used for these applications due to its highly tailorable properties.

1.2.3 Inhalation

Inhalation is another common route of exposure to silicates. Chronic exposure to crystalline silica, most commonly in the workplace, leads to inflammation of the lung and pulmonary fibrosis (Leung et al., 2012; Mazurek and Attfield, 2008). The inhalation of amorphous silica is also quite common, though its effects are less well understood as trace crystalline silica contaminants have skewed the results from many studies (Merget et al., 2002). More recently,

amorphous silica nanoparticles 14 nm in diameter were shown to transiently induce pulmonary inflammation (Choi et al., 2008).

1.2.4 Silicate clearance and excretion

The natural levels of silicon in the periphery are low, ranging from 100-600 µg Si/L (Dobbie and Smith, 1982; Sripanyakorn et al., 2009). Blood silicon levels peak 1 to 4 h after consumption of silicon containing materials (where time depends on silicon source) and return to baseline within ca. 6 h, being rapidly cleared in urine (Jugdaohsingh et al., 2002; Sripanyakorn et al., 2009).

The clearance of intravenous administered nanosilica particles is less well understood. Silica nanoparticles 50-200 nm in size have been shown to be predominately excreted in both urine and faeces within 72 h (Cho et al., 2009). No particles were detected in the excretions 1 week after dose. Organically modified silica nanoparticles were shown to be completely excreted (or broken down) over a 15 day period (Kumar et al., 2010). Silica nanoparticles (20 nm and 80 nm) have also been shown to remain in the liver, spleen and, to a lesser extent, lungs for upwards of 30 days (Xie et al., 2010). Nanosilica accumulation in these organs has been shown to induce, for example, the formation of granulomas, hydrotropic degeneration of hepatocytes, and pulmonary interstitial thickening (Ivanov et al., 2012; Yu et al., 2013)

1.3 Biological role and safety of silicon

In animals, silicon as orthosilicic acid is required for normal growth and a lack of Si (*i.e.*, Si deficiency) results in abnormal (stunted) growth (Carlisle, 1976; Carlisle, 1982; Carlisle, 1986). Silicon-deficiency also results in bone and connective tissue defects (Carlisle, 1976; Carlisle, 1982; Carlisle, 1986; Jugdaohsingh, 2007; Jugdaohsingh et al., 2008; Nielsen, 1998; Reffitt et al., 2003). In contrast, higher dietary silicon intake has been linked to higher bone mineral density (Calomme et al., 2006; Eisinger and Clairet, 1993; Jugdaohsingh et al., 2004; Macdonald et al., 2005; Spector et al., 2008). Silicon has also been shown to increase type I collagen formation in human osteoblast cells and dermal skin fibroblasts *in vitro*, and thus it has been suggested to play a role in wound healing (Arumugam et al., 2006; Reffitt et al., 2003). Indeed, silicon-substituted materials (*e.g.*, Bioglass™ and Si-substituted hydroxyapatite) are now widely used for bone healing (Hench et al., 2004; Porter et al., 2004). A mammalian Si transport protein has recently been identified, thus confirming its requirement in animals (Garneau et al., 2015; Ratcliffe et al., 2017).

Silicon has been shown to have a high affinity for aluminum (Jugdaohsingh et al., 2013; Taylor et al., 1997), a property that is utilized in nature to lock-up Al in the form of aluminosilicates (Al-Si). The freshwater snail *Lymnaea stagnalis* has been shown to actively increase its intracellular silicon levels to sequester toxic aluminum in the form of hydroxyl Al-Si (Desouky et al., 2002; Dobranskyte et al., 2004; White et al., 2008). Oligomeric silicon prevents Al

absorption and increases its excretion in humans (Jugdaohsingh et al., 2000), thereby protecting from Al associated Alzheimer's disease (Edwardson et al., 1993; Exley et al., 2002; González-Muñoz et al., 2008; Jacqmin-Gadda et al., 1996; Rondeau et al., 2000; Rondeau et al., 2001). The oligomeric silica has recently been shown to be an amorphous silica nanoparticle of ca. 2.4 nm in diameter (Jugdaohsingh et al., 2013). Nano-sized silica species are also formed in the snail lysosomes that sequester toxic Al (White et al., 2008).

1.3.1 The safety of silicate nanoparticles

The safety/toxicity of amorphous nanosilica particles > 14 nm in diameter has been extensively studied, as they are used in numerous commercial and pharmaceutical products (Fruijtier-Pölloth, 2012). Most commonly, the nanosilica particles used in these studies were generated at high temperatures and dissolve in dilute conditions relatively slowly (suppliers include W.R. Grace & Co (Ludox), Nanoamor and PolySciences, and are commonly prepared via the Stöber mechanism using alkoxy-substituted silicon (Stöber et al., 1968)).

In vitro testing has shown that these amorphous nanosilica particles (ranging from 14-500 nm in size) are toxic towards a range of cell types, e.g., lung carcinoma A529, liver carcinoma HepG2 and embryonic kidney HEK293 cells, in a dose dependent manner (Ahmad et al., 2012; Akhtar et al., 2010; Fede et al., 2012; Li et al., 2011; Lin et al., 2006; Lison et al., 2008; Lu et al., 2011; Mu et al., 2012; Wang et al., 2009a; Wottrich et al., 2004). More specifically, amorphous nanosilica has been shown to damage cell membranes (Akhtar et al., 2010; Chang et al., 2007; Li et al., 2011; Lin et al., 2006; McCarthy et al., 2012; Napierska et al., 2009; Wang et al., 2009a), damage DNA (Choi et al., 2011; Duan et al., 2013; Mu et al., 2012; Nabeshi et al., 2011), increase levels of intercellular reactive oxygen species and other oxidative stress markers (Ahmad et al., 2012; Akhtar et al., 2010; Duan et al., 2013; Fede et al., 2012; Klein et al., 2013; Li et al., 2011; Lin et al., 2006; Liu and Sun, 2010; Lu et al., 2011; McCarthy et al., 2012; Nabeshi et al., 2011; Park et al., 2013; Radonski and Medina-Martin, 2011; Ye et al., 2010), and, in some cases, increase cytokines and analytes such interleukin (IL)-6, IL-8 and matrix metalloproteinase 9 (MMP-9) (Liu and Sun, 2010; McCarthy et al., 2012; Wottrich et al., 2004).

The effects of silica nanoparticles on primary peripheral cells have also been investigated. In peripheral blood mononuclear cell (PBMC) cultures, nanosilica decreased cell viability and induced an inflammatory reaction (Fedeli et al., 2013; Mendoza et al., 2014). Monocytes and macrophages were shown to be more susceptible to nanosilica induced cell death than lymphocytes and epithelial cells, a trend that was assigned to the phagocytic nature of the cells (Fedeli et al., 2013). In the presence of protein, the nanosilica particles were shown to induce monocyte pyroptosis while necrosis was induced in the absence of protein (Fedeli et al., 2014).

In vivo testing has shown that mice injected with amorphous nanosilica have increased levels of oxidative and inflammatory markers. Specifically, Park *et al.* showed that after intraperitoneal injection of 50 mg/kg nanosilica particles 12 nm in diameter, nitric oxide levels progressively increased over 72 h and blood levels of IL-1 β , TNF- α , and IL-6 increased to a maximum at 12-24 h and decreased thereafter (Park and Park, 2009). Cho *et al.* showed that intravenous injection of 50 nm nanosilica particles did not induce an inflammatory response, while 100 and 200 nm nanosilica particles increased the incidence of inflammation in the liver (Cho *et al.*, 2009). These studies would indicate that amorphous silica nanoparticles induce an inflammatory response, which is similar, only a magnitude lower, to that caused by crystalline silica particles.

1.3.2 Insoluble silicates and the immune system

Silica nanoparticles have also been shown to have adjuvant and immunomodulatory properties. Antigen presentation by dendritic cells (DCs) increased after exposure to nanosilica (51 nm), leading to increased T cell responses to cognate antigen when compared to unstimulated DC-T cells (Chen *et al.*, 2014; Hirai *et al.*, 2012). Similarly, greater antibody production was induced *in vivo* when antigen was co-administered with 5-90 nm silica nanoparticles (Brandenberger *et al.*, 2013; Marzaioli *et al.*, 2014). Other silicate containing materials have also been shown to be immunomodulatory. Cargo-free mesoporous silica nanoparticles (104 nm) have been shown to increase the population of effector memory T cells and induce cytokine production (Wang *et al.*, 2016). Alkaline mineral solutions with a high silicate content (Barodon®) have been shown to increase peripheral T cell numbers and increase the response of the T cells to antigen (Koo *et al.*, 2006; Park *et al.*, 2000; Yoo *et al.*, 2001).

The interactions between crystalline silica and immune cells have also been well studied due to its involvement in silicosis and other pulmonary diseases. Crystalline silica is known for its chronic pro-inflammatory properties, which occurs through a cyclic macrophage recruitment-destruction pathway (Chu *et al.*, 2012; Greenberg *et al.*, 2007). These particles have been shown to be much more toxic towards macrophages than other non-Si particles of similar sizes (Allison *et al.*, 1966).

In addition to the toxic effects on monocytes and other phagocytes, crystalline silica has been shown to affect other immune cells. Circulating regulatory T cells, a suppressive helper T cell subset, in silicosis patients showed decreased function compared to those found in healthy individuals. Specifically, the regulatory T cell populations had decreased levels of FoxP3, a regulator of this T cell subset, decreased CTLA-4 function, which is an immune checkpoint inhibitor, and increased levels of the CD95 death receptor, whose engagement can suppress an immune response or induce apoptosis (Hayashi, 2010; Hayashi *et al.*, 2009; Wu *et al.*, 2005b). The ratio of effector T cells to regulatory T cells was also greater in silicosis patients

(Hayashi, 2010; Hayashi et al., 2009). Additionally, exposure to crystalline silica has been shown to chronically activate T cells *in vivo* (silicosis patients) (Hayashi et al., 2009; Wu et al., 2005b) and in cell culture (Ueki et al., 1994; Wu et al., 2005a).

There have also been studies conducted assessing the effect of crystalline silica on B cell function. Patients with silicosis have been shown to have higher immunoglobulin levels (Balamuralikrishnan et al., 2014; Doll et al., 1981; Kalliny and Bassyouni, 2011). Interestingly, short term exposure to crystalline particles does not result in increased immunoglobulin levels, but instead a marked decrease (Brown et al., 2003). Silicosis patients have also been shown to have increased autoantibody levels (Beshir et al., 2015; Brown et al., 2003; Doll et al., 1981; Kalliny and Bassyouni, 2011; Otsuki et al., 2006; Pfau et al., 2004), though few studies suggest otherwise (Aminian et al., 2009)

1.4 Cell biology

1.4.1 Cell death

As outlined in Section 1.3.1, the effect of amorphous nanosilica on cells has been extensively studied (Frujtier-Pölloth, 2012). These particles are toxic to cells in a dose dependant manner and have been shown to induce necrosis and pyroptosis of monocytes (Ahmad et al., 2012; Akhtar et al., 2010; Fede et al., 2012; Fedeli et al., 2014; Fedeli et al., 2013; Li et al., 2011; Lin et al., 2006; Lison et al., 2008; Lu et al., 2011; Mu et al., 2012; Wang et al., 2009a; Wottrich et al., 2004)..

Cells can undergo death through various mechanisms, including apoptosis, necrosis and pyroptosis. Apoptosis is a regulated mode of cell death and it can occur naturally (due to cell development and aging) or in response to external stimulus (noxious agents, corticosteroids, radiation, cell damage) (Elmore, 2007). The process is initiated by caspases -2, -8, -9 or -10 which activate caspases -3, -6 and -7. These caspases execute apoptosis by inducing a pathway which involves endonuclease activation, degradation of chromosomal DNA, and the degradation of nuclear and cytoskeletal proteins. The changes in cytoskeletal makeup, specifically the expression of surface phosphatidylserine (PS), are recognised by phagocytic cells and the apoptotic body is then phagocytosed without releasing its cellular components, thus preventing inflammation (Elmore, 2007; Jorgensen and Miao, 2015).

Necrosis was initially considered to be an unregulated mechanism of cell death, though recent studies have shown that it can occur in a controlled manner (Berghe et al., 2014). Non-regulated necrosis can occur through the rupturing of the cellular membrane, which leads to the release of its cellular components (Lohmann et al., 2009). In controlled necrosis, pores on the mitochondrial membrane are opened and protons, which are required for ATP synthesis, are lost into the cytosol. The lack of ATP leads to cellular dysfunction and necrosis (Dorn, 2013).

Another mechanism of cell death is pyroptosis. Pyroptosis is regulated by the activation of caspase-1, which can be induced by the presence of intracellular pathogens. Caspase-1 induces the production of IL-1 β and IL-18, both of which are inflammatory cytokines, and the formation of pores in the cellular membrane. The formation of pores causes cellular swelling (due to influx of water), cells lysis and release of its cellular components (Bergsbaken et al., 2009; Jorgensen and Miao, 2015).

1.4.2 Cell lines, cell matrixes

When using in vitro assays for assessing the effects of materials on cells, cell type and culture type will significantly impact the findings. Commonly, cell lines are used to study the effects of nanoparticles on cells. The effect of nanosilica particles on various cell lines have been extensively studied and reviewed by Fruijtier-Pöllöth (Fruijtier-Pöllöth, 2012). Although cell lines are inexpensive to work with and can generate highly reproducible results, they are known to not completely mimic primary cell cultures (Kaur and Dufour, 2012). Primary cells, which are more expensive and more challenging to work with, have been found to respond to different stimuli and have differing sensitivities compared to cell lines, and have also been shown to yield more varied results due to inter-donor variance (Gazdar et al., 2010; Krebs et al., 2002; Norian et al., 2000; Van Belle et al., 2016).

In addition to differences in cell type/origin, the matrix in which experiments are conducted influence the results. For example, primary monocytes treated with silica nanoparticles either undergo necrosis or pyroptosis depending on the protein concentration in culture (Fedeli et al., 2014). Therefore, even results from studies conducted on primary peripheral cells in culture would likely differ from those conducted in whole blood.

Whole blood is a complex matrix containing a high protein concentration, plasma, platelets, red blood cells and neutrophils in addition to the PBMCs. Interestingly, each of these additional components has been shown to interact with amorphous silica (Clemments et al., 2015; Gryshchuk and Galagan, 2016; Lehman et al., 2016; Zhang et al., 2012; Zimmerman et al., 1986). These interactions would likely impact the cellular response to the particles.

1.5 General immunology

1.5.1 Innate immune responses

The innate immune system is the body's first line of defence and consists of the cells which provide an immediate response to infection. These cells detect infection using cell surface receptors, specifically Toll-Like receptors (TLR) and cytosolic pattern-recognition receptors (PRR) (Iwasaki and Medzhitov, 2015). These receptors have evolved to detect sequences from essential components of foreign pathogens (pathogen-associated molecular patterns (PAMPs)) and stress signals from infected cells (damage-associated molecular patterns (DAMPs)) (Rock et al., 2011). There are also innate cells capable of detecting unhealthy cells

that do not express the receptors present on healthy cells (*i.e.*, MHC class I receptors) (Vivier et al., 2008). Upon recognition of these ligands (or lack of self-ligands), the innate cells release pro-inflammatory signals, including cytokines and chemokines.

Many innate cells have endocytic capabilities, *i.e.*, the ability of taking up foreign materials. There are many types of endocytic pathways, which have been extensively reviewed (Doherty and McMahon, 2009). The endocytic mechanisms of nanoparticles have also been investigated. It has been found that silica nanoparticles are recognised by scavenger receptors (macrophage receptor with collagenous structure (MARCO), CD204 or CD36) and phagocytosed by cells (Hamilton et al., 2006). Cellular death was found to be associated with scavenger receptor mediated silica nanoparticle uptake, where no toxicity was evident with cells lacking scavenger receptors (Hamilton et al., 2006). Other cell lines have been shown to non-specifically endocytose nanosilica particles (Chu et al., 2011; Mohamed et al., 2011).

After phagocytosis, the material is contained in an early endosome where the fate of the cargo is determined (sorted). The material can be immediately recycled back to the surface, transferred to the *trans*-Golgi network (for transfer back to the plasma membrane or for transfer to early- or late-endosomes) or it can stay within the endosome which then undergoes maturation (into late-endosomes, for material transfer to the *trans*-Golgi network or lysosomes) (Grant and Donaldson, 2009; Huotari and Helenius, 2011). These processes have plasticity (*i.e.*, allow for continuous exchange and communication) until the material is transferred to the lysosome, a process that is irreversible (Huotari and Helenius, 2011). During the transfer of the cargo from early endosome to lysosome, the pH drops for the degradation of the materials, where early endosomes have a pH of 6.1-6.8, late endosomes have a pH of 4.8-6.0, and lysosomes have a pH of *ca.* 4.5 (Huotari and Helenius, 2011).

Silica nanoparticles have been identified in the endo-lysosomes of primary phagocytic cells (Fedeli et al., 2013). The high silica nanoparticle load, especially that present in cell culture studies, and the low pH environment of the late endosome and lysosomes leads to the accumulation of the silicate particles in phagocytes. As outlined in Section 1.1, the solubility of amorphous silica is low at and below physiological pH (Jugdaohsingh et al., 2008). In a low pH environment like that found in endosomes (early and late) and lysosomes, the dissolution rate of the nanosilica particles would be slow. Additionally, the solubility of silicic acid would likely be exceeded in these localized compartments, thus preventing particle dissolution. Amorphous nanosilica particles have been found to accumulate in the acidic compartments of cells and can lead to their rupture (Fedeli et al., 2013). Other studies have also shown silica nanoparticle accumulation in endosomal and lysosomal vesicles (Al-Rawi et al., 2011; Chu et al., 2011; Corbalan et al., 2011; Drescher et al., 2011; Mohamed et al., 2011).

Phagocytic cell subsets of particular interest in this study are neutrophils and monocytes. Both are responsible for clearing foreign material in the periphery, though their functions differ.

Neutrophils are the most abundant cell subset in the periphery, making up >50% of peripheral cells (Kruger et al., 2015; Young, 1972). In addition to phagocytosis and breakdown of foreign materials in phagosomes as outlined above, neutrophils can employ extracellular traps to kill foreign pathogens. Neutrophil extracellular traps (NETs) are comprised of decondensed chromatin, histone and granular proteins which are capable of breaking down pathogens (Kruger et al., 2015). Neutrophils also release reactive oxygen species, proteases, antimicrobial peptides, cytokines and chemokines (Kruger et al., 2015). Little is known of silica-neutrophil interactions, though limited studies have shown that silica decreases neutrophil phagocytosis of bacteria (Zimmerman et al., 1986)

Blood monocytes are a less frequent peripheral cell comprising ca. 5-10% of the circulating cells and are precursors for macrophages, dendritic cells and osteoclasts (Sprangers et al., 2016). These cells have well established phagocytic capabilities and are involved in adaptive immunity as they present antigen to T lymphocytes via their MHC class II receptors. After phagocytosis of foreign pathogen or antigen, the proteins are processed with various proteases in endosomal and phagosomal compartments (Roche and Furuta, 2015). The MHC class II receptor is present in the endosome either from its expression on the cell membrane and internalization during the phagocytosis of the foreign material or from transportation to the endosome by the Golgi. The receptor then exchanges its class II-associated li peptide (CLIP) for antigenic peptide and is transported to the cell membrane for presentation of the antigenic epitope (Neefjes et al., 2011). Monocytes and its derived cells also provide secondary and tertiary signals to the T lymphocytes. Secondary signals, which are costimulatory or inhibitory receptors, and cytokines (referred to as signal 3) further mediate the T cell response (Chen and Flies, 2013; Iwasaki and Medzhitov, 2015; Sckisel et al., 2015).

Silica nanoparticles have been shown to effect monocyte function. Some studies have shown increased antigen presentation by dendritic cells after silica nanoparticle treatment, leading to increased T cell responses (Brandenberger et al., 2013; Chen et al., 2014; Hirai et al., 2012; Marzaioli et al., 2014). Other studies have shown that silica decreases monocyte function and induces cell death (Fedeli et al., 2014; Fedeli et al., 2013; Zimmerman et al., 1986).

Natural killer cells are a lymphocyte subset part of the innate immune system (Turvey and Broide, 2010). Natural killer (NK) cells do not have a T cell receptor (TCR) to recognize antigen. Instead, NK cells are activated through a number of different receptors, including NKp30, NKp44, and CD160, which recognize stress signals presented on other cells (Long et al., 2013; Vivier et al., 2008), and cytokines, including IL-2, IL-12, and IFN- γ (Zwirner and Domaica, 2010). These cells have cytotoxic capabilities and can release factors, mainly perforin and granzymes, to induce cell death of stressed and diseased cells (Aktas et al., 2009; Alter et al., 2004).

1.5.2 Adaptive immune response

The adaptive immune system is the secondary response to an infection. Adaptive immune cells, mainly B and T lymphocytes, are recruited to the site of infection by the cytokines and chemokines released by the innate immune cells (Alberts, 2002). The response of the adaptive immune cells is specific to the infection, thus preventing damage to the host organism. The adaptive immune response can be either cell or antibody (humoral) mediated. T lymphocytes facilitate the cell mediated adaptive immune response while B lymphocytes facilitate the humoral response, which can be either T cell dependent or independent (Alberts, 2002; Nutt et al., 2015). Since the majority of the work in this thesis investigated the effects of amorphous silica on T cells, a thorough discussion on these cells was included.

1.5.2.1 T cell immunology

T lymphocyte precursor cells are produced in the bone marrow and are developed in the thymus (Miller, 2011). In the thymus, the cells develop a T cell receptor (TCR), CD4 and CD8 receptors before they undergo the selection process. The thymic selection process is comprised of both positive and negative selection. Positive selection is the process where T cells which have a productive interaction with a self-antigen MHC complex expressed on thymic epithelial cells are selected for survival (Carpenter and Bosselut, 2010). T cells which lack this interaction die of neglect. These weak interactions with self-peptide are required for circulating T cells as they maintain a low level TCR signal and naïve T cell homeostasis, both of which impact the eventual response of the T cell to cognate antigen (Hogquist and Jameson, 2014). The positive selection process also dictates whether the cells become a helper T cell (CD4+), through an interaction with a MHC class II receptor) or a cytotoxic T cell (CD8+), through an interaction with a MHC class I receptor). If a T cell interacts too strongly with self-antigen, *i.e.*, it is autoreactive, the cells are eliminated through TCR mediated apoptosis (Palmer, 2003). This process is referred to as negative selection. Autoreactive T cells found in circulation have either escaped the negative selection process or are specific to an antigen not presented in the thymus (Bluestone et al., 2015; Ohashi, 2002). These T cells are known to contribute to various autoimmune diseases (Bellone, 2001; Janeway et al., 1997).

An adaptive immune response is specific to the infection. T lymphocytes orchestrate an infection specific response through antigen recognition by the T cell receptor (TCR), which are developed in the thymus to recognize a specific antigenic epitopes. In the periphery, *ca.* 10^6 clonotypes (different epitopes in which the TCR can recognise) have been identified and modelling suggests that 10^{15} to 10^{20} different TCR clonotypes can be developed in the thymus (Laydon et al., 2015; Warren et al., 2011). B cells are also equipped with receptors, referred to as B cell receptors (BCRs), to recognize a wealth of antigens. However, unlike traditional TCRs, BCRs can recognise both soluble antigen and presented antigen, though induced

activation is more efficient when antigen is presented (Avalos and Ploegh, 2014; Yuseff et al., 2013).

1.5.2.2 T cell subsets

The thymic selection process dictates whether a T cell is CD4(+) or CD8(+) (Carpenter and Bosselut, 2010). Upon activation, these T cell subsets, helper and cytotoxic respectively, respond differently to infection.

CD4, or helper, T cells mediate the immune response after activation (Geginat et al., 2015). Helper T cells recognise cognate antigenic epitope presented in MHC class II receptors on antigen presenting cells (APC) with their TCR. The CD4 co-receptor on T cells binds the TCR:peptide-loaded MHC class II interaction and downstream signalling commences, leading to activation (Chakraborty and Weiss, 2014). Upon activation, CD4 T cells respond by producing cytokines and expressing a range of cell surface markers. The cytokines produced and surface markers expressed depend on the helper cell phenotype that is induced. The main types of helper T cell phenotypes, specifically T helper 1 (Th1), T helper 2 (Th2) and regulatory (Treg) (Geginat et al., 2015), are shown in Figure 1.04.

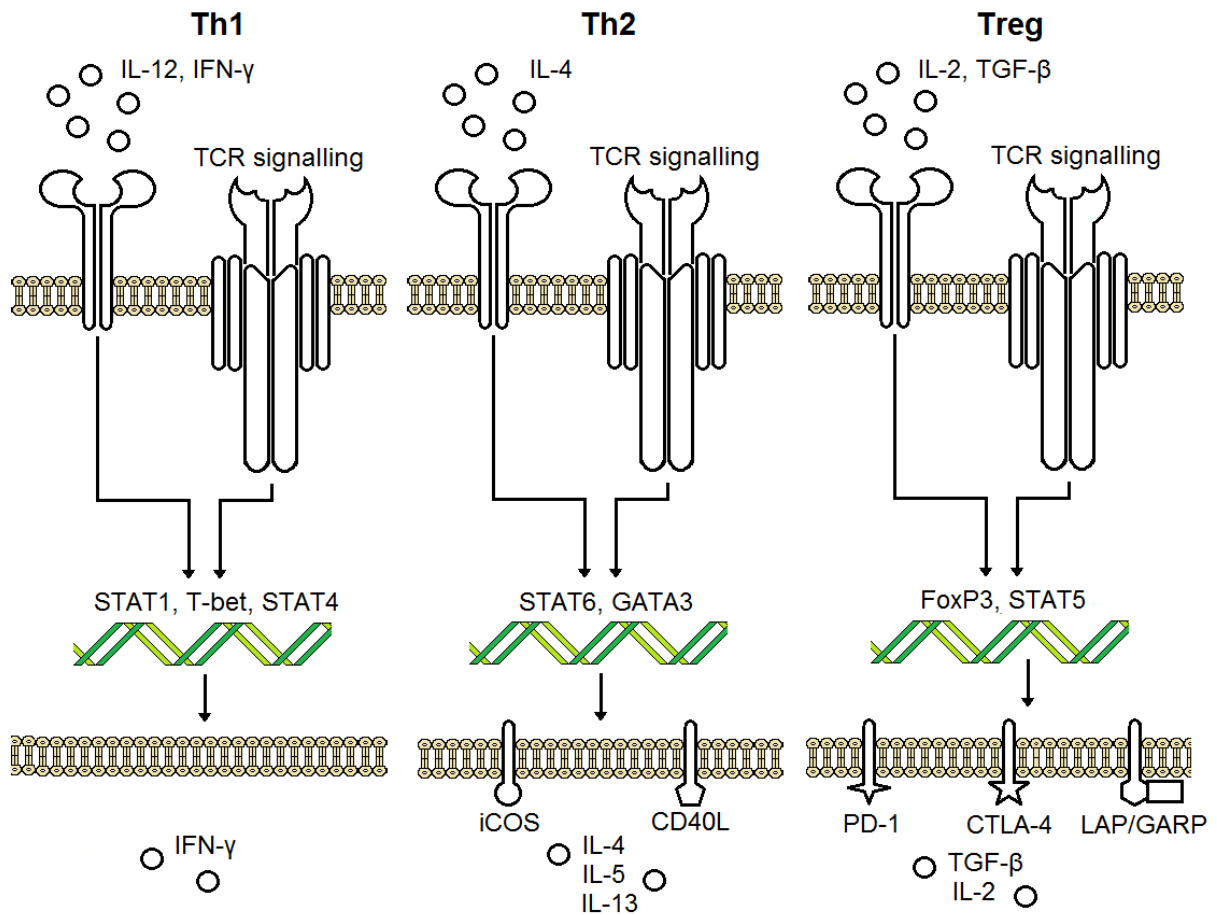


Figure 1.04. The main helper T cells phenotypes and the factors that induce them. Th1 cells are induced by TCR signalling in the presence of IL-12 and IFN- γ , inducing signalling through the STAT1, T-bet and STAT4 transcriptional factors, leading to IFN- γ production. Th2 cells are induced by TCR signalling in the presence of IL-4, inducing signalling through the STAT6 and GATA3 transcriptional factors, leading to IL-4, IL-5 and IL-13 production and expression of iCOS (CD278) and CD40L (CD154). Treg cells are induced by TCR signalling in the presence of IL-2 and TGF- β , inducing signalling through the FoxP3 and STAT5 transcriptional factors, leading to IL-2 and TGF- β production and expression of PD-1 (CD279), CTLA-4 (CD154) and LAP/GARP. Figure adapted from DuPage, Elgueta, Gauthy, Geginat, Janeway Jr, Sahoo and Stockis (DuPage and Bluestone, 2016; Elgueta et al., 2009; Gauthy et al., 2013; Geginat et al., 2015; Janeway Jr et al., 2001; Sahoo et al., 2016; Stockis et al., 2009)

Th1 cells are responsible for activating monocytes and cytotoxic T cells. A Th1 response is induced by strong signalling through the TCR and the cytokines IL-12 and IFN- γ (DuPage and Bluestone, 2016). These signals induce the transcriptional factors STAT1 (signal transducer and activator of transcription (STAT)), STAT4 and Tbet, leading to the production of IFN- γ (DuPage and Bluestone, 2016; Lazarevic et al., 2013). This cytokine further supports the induction of Th1 cells, activates macrophages (increases their anti-microbial activity), and enhances cytotoxic lymphocyte activity (Schroder et al., 2004; Zhu and Paul, 2008)

Th2 cells are responsible for mediating a response against parasites and are also involved in an allergic response (Sahoo et al., 2016). This cell lineage shares many functions with T follicular helpers cells, which mediate B cell responses including their survival, proliferation and

antibody production (Crotty, 2015). Th2 cells are induced by a weak TCR signal in the presence of the cytokine IL-4, inducing the transcriptional factors STAT6 and GATA3 (DuPage and Bluestone, 2016). Activated Th2 cells produce the cytokines IL-4, IL-5 and IL-13, which effect antibody production by B cells and further support the induction of Th2 cells (Sahoo et al., 2016). Th2 cells also express CD154 (CD40 ligand, CD40L) (Jenkins et al., 2008), a ligand that engages the CD40 receptor on B cells and it induces its proliferation and survival (Crotty, 2015; Elgueta et al., 2009). CD278 (inducible costimulatory, iCOS) is also expressed on Th2 cells and its engagement further induces a Th2 response (Sahoo et al., 2016; Wikenheiser and Stumhofer, 2016; Yong et al., 2009).

Regulatory T cells (Tregs) inhibit immune responses to prevent damage to the surrounding tissues and autoimmunity (Arpaia et al., 2015). A regulatory response is induced by TCR signalling in presence of the cytokine TGF- β (Chen et al., 2003; Zou, 2005). Transcriptional factors foxhead box P3 (FoxP3) and STAT5 are induced leading to the production of IL-10 and TGF- β (DuPage and Bluestone, 2016). Tregs express PD-1 (CD279) and CTLA-4 (CD152), both of which further support a suppressive environment (DuPage and Bluestone, 2016; Francisco et al., 2010; Walker and Sansom, 2015). Regulatory T cells also express latency-associated peptide (LAP) and glycoprotein A repetitions predominant (GARP) on their surface. Both of these proteins are components of the latent-TGF- β complex, which is responsible for the release of immunosuppressive cytokine TGF- β (Gauthy et al., 2013; Stockis et al., 2009). Two types of regulatory T cells have been identified, natural (nTreg), and inducible (iTreg) (Mellanby et al., 2009). nTreg, also referred to a thymic Tregs (tTreg), are positive for the transcriptional protein FoxP3 in the thymus. Although these cells express the regulatory transcriptional factor, they are not polarized Tregs, as they are still capable of taking on all other T helper cell phenotypes (DuPage and Bluestone, 2016). iTregs, also referred to as peripheral Tregs (pTreg), are cells that leave the thymus negative of the transcriptional factor FoxP3 but take up a regulatory phenotype upon activation. These cells can be both positive and negative for the FoxP3 protein (Mellanby et al., 2009)

CD8 T cells, also known as cytotoxic T lymphocytes (CTLs) when activated, are responsible for executing an immune response (Tscharke et al., 2015). CTLs engage stressed, abnormal, infected, and cancerous cells and induce their cell death by releasing factors or engaging receptors that will induce apoptosis of the target cell (Aktas et al., 2009; Alter et al., 2004; Arakaki et al., 2014). These cells can also release IFN- γ to further mediate a cytotoxic response (Schroder et al., 2004). CTLs are activated when they recognize their cognate antigen presented on an MHC class I receptor (Chakraborty and Weiss, 2014). Peptides presented on MHC class I receptors are a sampling of the intercellular proteins, unlike peptides presented on MHC class II receptors which are phagocytosed and processed foreign antigen (Neefjes et al., 2011). The peptides presented on MHC class I receptors, which are expressed

on all cell types (Tourdot and Gould, 2002), are an indication of the function of the cell (Comber and Philip, 2014). The peptide that is presented on a virally infected, cancerous or stressed cells is different than that of a healthy cell. After engagement of the peptide loaded MHC class I receptor by the TCR on CTLs, the CD8 co-receptor binds the TCR:MHC complex and activation is initiated (Chakraborty and Weiss, 2014). CTLs can execute an immune response in a number of different ways. After engagement of an unhealthy cell, a CTL can release the contents of its granules (perforin, granzymes) which induce apoptosis of the target cell. Classically, the perforin is thought to form pores in the target cell membrane that the granzymes move through to induce target cell apoptosis through the activation of caspases (Voskoboinik et al., 2015). Another mode in which CTLs induce target cell death is through the Fas death receptor. Target cells, including activated T cells (below), can express the Fas death receptor (CD95) that, when engaged, will induce apoptosis. CTLs can express FasL (CD195) on its surface or produce and release soluble FasL (sFASL) (Hassin et al., 2011; Stinchcombe and Griffiths, 2007). There are other cytotoxic lymphocytes present in circulation, specifically $\gamma\delta$ T cells and natural killer T cells (NKT), which are thought to bridge the adaptive and innate immune responses (below).

1.5.2.3 T cell signalling

The signalling induced upon T cell activation is complex and a simplified signalling network is shown in Figure 1.05. In a healthy interaction, T cell activation is initiated when the TCR engages the peptide loaded MHC receptor (pMHC). Upon engagement, the immunoreceptor tyrosine-based activation motif (ITAM), which is located on the intracellular tail of the CD3 chains and the CD247 protein (also referred to as CD3 ζ and TCR ζ), becomes accessible for phosphorylation (Chakraborty and Weiss, 2014). The exact mechanism in which the ITAM becomes accessible for phosphorylation is not known, though there are numerous proposed models (the most common models outlined below). Lymphocyte-specific protein tyrosine kinase (LCK), which is located on the intercellular end of the CD4 and CD8 co-receptors, phosphorylates the ITAM when the co-receptors binds the TCR:pMHC complex (Brownlie and Zamoyska, 2013). Proto-oncogene tyrosine-protein kinase Fyn ("Fyn") has also been found to phosphorylate the ITAM, specifically (Love and Hayes, 2010). The phosphorylated ITAM then is bound by zeta-chain associated protein kinase 70 (Zap-70), and this kinase is also phosphorylated by LCK or Fyn (Goodfellow et al., 2015). The phosphorylated Zap-70 protein (pZap-70) propagates the signal by phosphorylating the linker for activation of T cells (LAT) (Malissen et al., 2014). Most responses are associated with the engagement of the TCR signal through the phosphorylated LAT (pLAT) protein, as it serves as a nucleation point for downstream signalling (Malissen et al., 2014). For complete T cell activation, there must be sufficient signalling through mitogenic-activated protein kinases (MAPK) and nuclear factor of activated T cells (NFAT) (Macian, 2005; Smith-Garvin et al., 2009). When signalling does not

occur through both pathways, only certain T cell activation markers are induced and other markers, such as clonal expansion and IL-2 production, are not (Chen and Flies, 2013; Pennock et al., 2013; Reddy et al., 2004; Sprent et al., 1997). The lack of complete signalling can lead to defective activation states such as activation induced cell death (AICD) and anergy (below). With efficient TCR antigenic stimulation, both of these signalling pathways are sufficiently induced, by downstream signalling through the DAG protein (Macian, 2005; Smith-Garvin et al., 2009). When there is inefficient TCR antigenic stimulation, co-stimulatory signals provided by the cells presenting antigen are required for a complete T cell response (Csencsits and Bishop, 2003; Wang et al., 2000). For example, inefficient TCR ligation requires co-stimulation through CD28 for induction of signalling through MAPK (Boomer and Green, 2010; Fathman and Lineberry, 2007)

In addition to CD28, there are numerous T cell costimulatory receptors, reviewed by Chen *et al.* (Chen and Flies, 2013). Engagement of these receptors, including CD30, iCOS, OX40 and signalling lymphocytic activation molecule (SLAM), by their respective ligands can induce T cell proliferation, differentiation, survival, cytokine production, cytotoxic function and formation of memory cells. Coinhibitory signals, including Fas (CD95), programmed cell death protein 1 (PD-1), CTLA4 and CD160, limit T cell responses upon their engagement by inhibiting the cell cycle and effector function and also by inducing exhaustion and apoptosis.

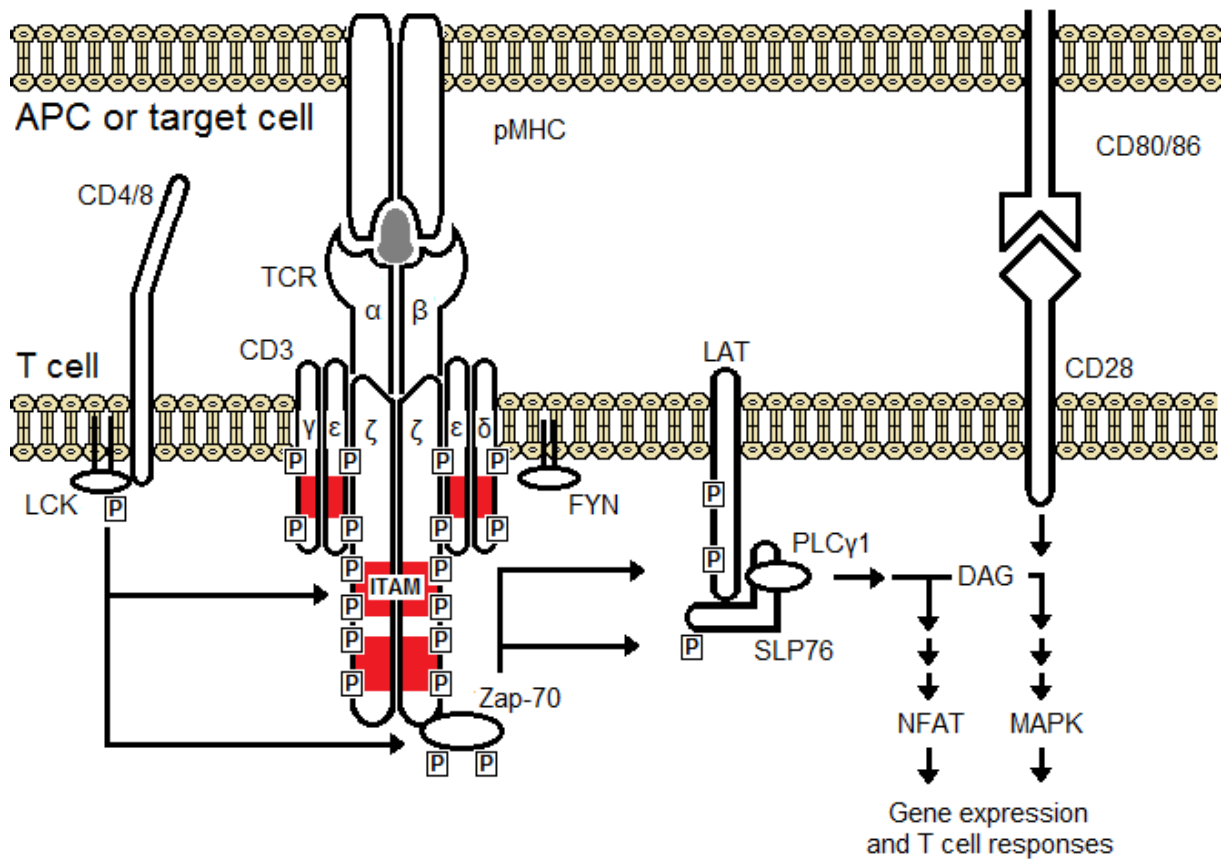


Figure 1.05. T cell signalling pathway after T cell recognition of cognate antigen presented on a MHC receptor by an APC or a target cell. After recognition of cognate antigen, the ITAM is phosphorylated by LCK (located on the intracellular end of CD4/CD8) or Fyn. Zap-70 then binds the ITAM and is phosphorylated. pZap-70 propagates the signal by phosphorylating LAT and SLP76. The signalling cascade continues through NFAT and, if TCR ligation is efficient, through DAG and MAPK leading to complete T cell responses. Co-stimulation also induces signalling through MAPK. Adapted from Acuto, Browlie and Zamoyska, Dupage and Bluestone, and Fesnak (Acuto et al., 2008; Brownlie and Zamoyska, 2013; DuPage and Bluestone, 2016; Fesnak et al., 2016).

A third signal, specifically cytokines, further mediate and enhance the T cell activation response. For example, dendritic cells can produce IL-12 to induce a Th1 cell phenotype (Geginat et al., 2015; Sckisel et al., 2015). Interestingly, if a CD4 T cell receives the signals out-of-sequence, its response could be suppressed or the T cell could become paralysed (Sckisel et al., 2015). For example, a CD4 T cell that encounters high concentrations of cytokine prior to TCR engagement may have impeded responses.

There are materials that can induce T cell activation in the absence of antigenic presentation and co-stimulatory signalling. Calcium ionophores, such as ionomycin, and phorbate esters, such as phorbol 12, 13-dibutyrate (PdBu), are known to induce signalling through NFAT and MAPK respectively (Bell, 2002; Chatila et al., 1989). These compounds, can therefore be used to induce complete T cell activation when added to culture together. There are other compounds that can directly engage the TCR/CD3 complex without needing to be presented by an APC or a target cell, specifically superantigens and mitogenic antigens. Superantigens,

which are produced by bacteria or pathogenic viruses, induce chronic T cell activation by binding the TCR and cross-linking it to an MHC receptor (Li et al., 1998). Superantigens are also capable of cross-linking to the CD28 costimulatory receptor (Arad et al., 2011; Fraser, 2011). *In vivo*, superantigens can induce toxic shock syndrome, with adverse effects such as vomiting, rash, fever, and hypotension, and even lethal shock (Fraser, 2011). Synthetic mitogenic antibodies, specific for protein sequences on the TCR, CD3 and CD28 receptors, can also be used to induce chronic T cell activation *in vitro* and *in vivo* (Suntharalingam et al., 2006; Trickett and Kwan, 2003).

1.5.2.4 TCR signalling models

The most common models on the initiation of T cell signalling, specifically regarding the phosphorylation of ITAM, include kinetic segregation and conformational change (though there are others which are also reviewed by Chakraborty and Weiss (Chakraborty and Weiss, 2014)). Briefly, the kinetic segregation (KS) model suggests that the segregation of negative regulators of tyrosine initiates T cell activation. Phosphatases, such as CD45, are known to oppose the phosphorylation of tyrosines, such as LCK (*i.e.*, CD45 de-phosphorylates LCK). The KS model suggests that the forces caused between the cells during the TCR:pMHC interaction sterically segregates CD45 from LCK, thus leaving LCK phosphorylated until it passes on the phosphate group to the ITAM. The conformational change model suggests that, after the TCR binds the pMHC complex, the torsion caused by the moment of the cells initiates T cell activation. The torsion forces the TCR (which does not have any intracellular signalling motifs) to contact a CD3 receptor, thus initiating intracellular downstream signalling.

1.5.2.5 General markers of T cell activation

T cells express numerous receptors and produce cytokines upon activation. Some markers of activation are expressed on all T cell subsets, including helper T cell subsets and cytotoxic lymphocyte subsets. Generally, these markers are essential for the survival of the activated cells. For example, all activated T cells express the CD25 surface receptor. CD25, with CD122 and CD132, make up the receptor for the cytokine IL-2, a complex commonly referred to as IL-2R (Létourneau et al., 2009; Malek and Castro, 2010). Activated T cells require IL-2 for late stage proliferation and T cell differentiation, and therefore express IL-2R (D'Souza and Lefrançois, 2003; Malek and Castro, 2010). Certain T helper cell subsets, specifically Tregs, constitutively express IL-2R as IL-2 is required for their homeostasis, development and function (Malek and Castro, 2010). Another common marker of T cell activation is the CD69 receptor. CD69 is expressed on the surface of activated T cells quickly after recognition of cognate antigen and it is involved in immune suppression and T cell migration (Mackay et al., 2015; Radulovic et al., 2013). CD69 is a more sensitive measure of T cell activation than CD25 and other activation markers (Fazekas De St. Groth et al., 2004). Another general marker of T cell activation is proliferation, though, unlike the previous two markers of activation, it requires

complete signalling to be induced (Chen and Flies, 2013; Pennock et al., 2013; Reddy et al., 2004; Sprent et al., 1997).

1.5.2.6 Defective activation mechanisms

When a T cell is not activated properly, it can take up a hyporesponsive state known as T cell anergy (Schwartz, 2003). T cell anergy is induced when there is TCR ligation in the absence of costimulation, by chronic TCR stimulation, or by TCR stimulation in conditions of high coinhibitory signals (Schwartz, 2003; Wells, 2009; Zheng et al., 2008). Treating cultures with calcium ionophores, which induce signalling through NFAT and mimic TCR ligation, in the absence of phorbate esters is commonly used to induce T cell anergy *in vitro* (Bell, 2002; Macián et al., 2002). Different anergic T cell states have been identified, and reviewed by Schwartz (Schwartz, 2003). The properties of T cells in the different anergic states differ slightly, where some will respond to restimulation while others do not. However, general properties of anergic T cells include a lack of clonal expansion (or an abortive proliferation response) and lack (or diminished rate) of cytokine production (Wells, 2009).

Incomplete or chronic stimulation of T cells can also induce activation induced cell death (AICD). AICD is a process in which activated T cells undergo apoptosis via death receptors (Arakaki et al., 2014). AICD is initiated when the death/coinhibitory receptor CD95 (Fas) is engaged by its ligand (CD178 or FasL). The CD95 receptor then trimerizes and is bound by the Fas-associated death domain protein (FADD) in the intracellular region. After the binding of FADD to the Fas trimer, FADD-like IL-1 β -converting enzyme (FLICE), which is a pro-caspase-8 protein, binds the complex through the death effector domain (DED) site and caspase-8 is released in the cell. Caspase-8 induces cell apoptosis, as reviewed in Section 1.4.1 (Krammer et al., 2007). Activated CTLs and NK cells are known to express FasL and therefore can induce AICD (Arakaki et al., 2014)

1.5.2.7 T cell activation by silica and nanoparticles

There is some evidence of uncoated nanoparticles effecting T cell function in the literature. Insoluble silicates, both amorphous and crystalline, have been found to alter T cell function through a phagocyte mediated mechanism (Chen et al., 2014; Pernis, 2004). Specifically, amorphous nanosilica increases T helper cell response through the enhancement of antigen presentation by dendritic cells (Brandenberger et al., 2013; Chen et al., 2014; Hirai et al., 2012; Marzaioli et al., 2014). Chronic exposure to crystalline silica has been shown to impair suppressive and enhance inflammatory function of T cells (Hayashi, 2010; Hayashi et al., 2009; Matsuzaki et al., 2016). *In vitro* exposure of peripheral cells to the crystalline silica particles was shown to increase T cell CD69 expression (at day 5) and IL-2 production (Ueki et al., 1994; Wu et al., 2005a).

Other silicate containing materials have also been shown to enhance T cell function, though the mechanism behind these responses remains unknown. The addition of an alkaline mineral solution containing *ca.* 4 M Si has been found to increase peripheral T cell numbers and enhance T cell responses to antigen in horses and pigs (Koo et al., 2006; Yoo et al., 2001). Cargo-free mesoporous silica nanoparticles were shown to increase the population of effector memory T cells and induce cytokine production (Wang et al., 2016).

Non-silicate nanoparticles have been well established to induce T cell activation. These materials, which are engineered with a peptide loaded MHC receptor coating, mimic antigen presentation by an APC or a target cell (Serra and Santamaria, 2015). They can also induce T cell activation through the delivery of antigen or drugs to APCs for enhanced responses (Serra and Santamaria, 2015). The effect of non-coated nanoparticles is less well understood. The addition of cobalt nanoparticles and fullerenes to T cell containing cultures increases the levels of IFN- γ in the supernatant (Liu et al., 2009; Petrarca et al., 2005). The mechanism of activation induced by these materials remains unclear.

1.5.3 Cells that bridge innate and adaptive immune cells

There are immune cells, mainly natural killer T (NKT) cells and $\gamma\delta$ T cells, which are considered to bridge the adaptive and innate immune systems, as they share characteristics from both branches of immunity.

NKT cells are a lymphocyte subset that shares properties of NK cells and T cells. These cells have an invariant TCR that recognises the MHC-like CD1b receptor but also can recognize stress signals on cells (Vivier et al., 2012; Wesley et al., 2008). $\gamma\delta$ T cells are a less frequent T cell subset with a TCR consisting of γ and δ chains rather than the classical α and β chains (Girardi, 2006). The angle between the constant and variable domain of the $\gamma\delta$ TCR is smaller than that of the $\alpha\beta$ TCR (Allison et al., 2001). $\gamma\delta$ T cells do not recognize antigen presented in MHC receptors but instead recognize soluble antigens, CD1 receptors (MHC-like) and other proteins expressed on cell surfaces (Dar et al., 2015; Vantourout and Hayday, 2013; Wiest, 2016; Wu et al., 2014). The recognition of antigen by $\gamma\delta$ TCRs is similar to that of IgG (Wiest, 2016).

1.6 Rationale and Aim of the Thesis

As indicated previously, humans are exposed to high levels of amorphous nanosilica daily. Although many studies have already been conducted, amorphous silica comprises of particles with such a vast range of sizes and properties (e.g., the degree of condensation) that their cellular activity and toxicity is not well understood. With its increasing use in biomedical applications, interactions between peripheral cells and nanosilica deserve further scrutiny, especially the small and very poorly studied particle sizes (< 10 nm). The aim of this PhD study

is to determine the effect of amorphous nanosilica 1-10 nm in diameter on peripheral cell activity and how select properties (e.g., size, resorbability) change this activity.

First, in Chapter 3, investigations were carried out to characterize small amorphous silica particles, both in concentrated stock solutions and after dilution to physiological concentrations. In Chapter 4, the toxicity of the particles was assessed on cancerous, transformed and primary peripheral cells and genomic analyses were conducted to determine if the particles induce specific, or unique, cellular responses. Chapters 5-7 investigated the effects of the nanoparticles on T cell activation, the mechanism of activation, and likelihood of such activation occurring *in vivo*. Finally, investigations were conducted to determine whether these responses could be exploited for use as a therapeutic.

Chapter 2 - Methods

2.1 Chemistry

2.1.1 Nanosilica preparation

Nanoparticle dispersions (< 4 nm) were prepared by diluting sodium silicate (#338443; Sigma-Aldrich Chemical Co., Gillingham, UK) in distilled deionized water (DDW; 18 M Ω /cm) to 20-40 mM Si and adjusting pH with hydrochloric acid (HCl, 4-5 M or 37%). The dispersions were left to equilibrate for 2-24 h at room temperature. Nanosilica particle size was increased (>4 nm) by adding a concentrated saline solution (ca. 1.5 M) immediately after pH adjustment or by increasing Si concentration. Micron-sized silica particles (ca. 57 nm) were prepared by freezing the nanoparticle solutions at -20 °C for 16-24 h immediately after pH adjustment. Heat-treated nanosilica particles were prepared by incubating the nanosilica dispersion at 70 °C immediately after pH adjustment. The particles were doped with aluminum (Al) by adding concentrated aqueous AlCl₃ (ca. 0.5 M) to the nanosilica dispersions (> 16 h after preparation) and incubating for 1 h. Low pH stabilization of dispersions was conducted by rapidly dropping the pH of a nanosilica dispersion to 1 with concentrated HCl (37%).

Ultra-small amorphous nanosilica dispersions (<2 nm) were prepared according to Bastos *et al.* (Bastos *et al.*, 2015). Briefly, 40-500 mM silicic acid was rapidly adjusted to pH 0.9 with concentrated HCl (37%). The dispersions were left to equilibrate for 0-24 h at room temperature. Size was increased by raising the pH of the dispersion to 4, incubating until the desired particle size was obtained, and dropping the pH back below 3.

pH measurements were conducted using pH test stripes (Sigma-Aldrich Co., #P3536) or a combined pH/reference electrode (VWR, #662-1761), following a 2 point calibration using appropriate buffers.

2.1.2 Control particles

Ludox SM30 (W.R. Grace & Co., US) was selected as a highly condensed nanosilica control based on its size (7 nm) and counterion (Na⁺). Its hydrodynamic diameter after dilution to ca. 25 mM was ca. 10 nm as determined by dynamic light scattering.

Min-u-sil® 5 was acquired from US Silica Company for use as a crystalline silica positive control. A dispersion was prepared by baking the powder at 200 °C overnight (to break down any endotoxins) (Satpathy *et al.*, 2015) and suspending in H₂O (Sigma-Aldrich, #W3500).

Aluminium clusters were prepared using methods based on those set out by Fu *et al.* (Fu *et al.*, 1991). Briefly, an aluminium chloride solution (100 mM Al) was adjusted to pH 4.2 with NaOH. The resulting dispersion, which contained visible precipitation, was incubated for 24 h and resulted in a dispersion with a median particle size < 2 nm. Attempts were made to increase particle size using pH and heat, but none were successful.

Gold nanoparticles, (11-mercaptoundecyl)tetra(ethylene glycol) functionalized, were acquired from Sigma-Aldrich (#687863). The hydrodynamic diameter of the dispersion after dilution to ca. 40 mM Au was ca. 10 nm as determined by dynamic light scattering. Attempts were made to re-disperse the particles with sonication, pH and dispersing agents (citrate) but none were successful.

Iron hydroxide nanoparticles coated with adipate and tartrate were prepared by C. Bastos according to methods set out by Powell *et al.* (Powell *et al.*, 2008). Particles were dispersed in water at a concentration of 40 mM Fe prior to being employed in cell assays.

2.1.3 Characterization of nanoparticle dispersions

Hydrodynamic particle sizes of the dispersions were determined by dynamic light scattering (DLS) on a Zetasizer NanoZS or NanoZSP (Malvern Instruments). Acquisition parameters for silicon dioxide were used for nanosilica (refractive index = 1.45, absorption = 0.01), bernalite for nanoiron (refractive index = 1.92, absorption = 0.10), gold for gold nanoparticles (refractive index = 0.20, absorption = 0.10), and aluminium hydroxide for the aluminium clusters ((refractive index = 1.53, absorption = 0.01) all in a water solvent at room temperature (0.8872 cP, refractive index = 1.33)), using a 173° backscatter angle. Three replicate measurements were recorded and their average volume particle distribution, at which 10%, 50% and 90% of the particles were smaller (DV0.1, DV0.5 and DV0.9 respectively), was calculated.

The particle size of the micron-sized silica was determined on a Malvern Mastersizer 2000 (Malvern Instruments), using parameters for silicon oxide (refractive index = 1.45, absorption = 0.01) and a range of mixing speeds (500-5000 rpm) and sonication levels. Three replicate measurements were recorded and their average DV0.5 was calculated.

Zeta-potential was determined using a Zetasizer NanoZSP (Malvern Instruments) using the same properties for silicon dioxide and water as the size measurements. A capillary cell cuvette (DTS1070) and the Smoluchowski model with $F(\kappa a) = 1.50$ were used. The nanosilica dispersion was adjusted to pH 1.5 to 9 immediately prior to analysis. Zeta-potential in PBS was determined by adding 10% v/v 10x PBS to the nanosilica dispersion and adjusting to pH 7.0 to 7.1. Zeta-potential in RPMI was determined by adding 50% v/v RPMI1640 to the nanosilica dispersion and adjusting to pH 7.4 to 7.5. Three independent dispersions and 3 replicate measurements were averaged.

The dissolution of nanosilica was assessed using a molybdic acid dissolution assay derived from Alexander (Alexander, 1953). Briefly, 200 μ L of a molybdic acid solution (0.0375 M H_2SO_4 + 34.5 mM Mo (as $NH_4Mo_7 4H_2O$) or 0.15 M H_2SO_4 + 34.5 mM Mo) was added to 100 μ L of the test solution (nanosilica at 1 mM Si in HEPES buffer (10 and 50 mM, pH 7.4)) in a 96 well plate. After mixing for 10 min, the absorbance at 400, 405 or 450 nm was measured on a Labsystems Multiskan RC V1.5-0 plate reader (ThermoScientific, UK) or a FLUOstar Omega

microplate reader (BMG Labtech). The concentration of silicic acid in solution was determined using standard curves generated with SiF₄ (1,000 mg/kg Si, Sigma-Aldrich Co). Due to the presence of phosphate, it was not possible to determine silicic acid concentrations in media by the molybdic acid assay. For this reason, dissolution and size in complex media was determined using ultrafiltration and ICP-OES elemental analysis. The dispersions (in concentrated stock and after dilution in various media) were ultrafiltered through 3, 50, 100, and 1,000 kDa filters (13,000 rpm, 10 min) or centrifuged (1,500 rpm, 5 min). The Si levels in the flow through or supernatants were determined by ICP-OES. MWCO and pore size has been correlated and will be used to determine the phase distribution (size) of the materials (Guo and Santschi, 2007). For both the molybdic acid assay and ultrafiltration, the proportion of Si(OH)₄ was presented as a percentage of the total Si concentration (%Si as Si(OH)₄ = [Si(OH)₄]/[Si_{total}] x 100%)

A molybdic acid release assay, derived from Iler (Iler, 1979), was used to assess the formation of the nanosilicates and the condensation rates of labile nanosilica particles. Briefly, aliquots of concentrated nanosilica stocks were transferred to a 96 well plate (3.0 x 10⁻⁷ moles Si per well, triplicate wells prepared). Immediately after diluting the samples to 100 uL with DDW, 200 uL molybdic acid solution (34.5 mM Mo (as NH₄Mo₇O₂₄4H₂O) in 0.15 M H₂SO₄) was added and the absorbance at 400 nm was measured every 60 s for 5 h, agitating (400 rpm) briefly before each measurement. Silicic acid was used as an assay control. Area under the absorbance curves (Abs x h, ΔX * (Y1+Y2)/2) was calculated and used to represent relative condensation

Silicon-29 nuclear magnetic resonance (NMR) spectra were acquired on a Bruker AMX500 (at 99.35 MHz) using a silicon-free probe, a 53 s inter-pulse delay and >3000 π/2 pulses. Nanosilica dispersions were prepared and stabilized at pH 1 prior to being loaded into a Kel-F NMR tube.

2.1.4 Tumour digestions

In vivo tumour inhibition by nanosilica was tested by HS Pharmaceuticals, LLC, at Translational Drug Development (TD2, Scottsdale, Az, US) in 2012. Upon study termination, the tumours were excised, frozen down and couriered on dry ice (along with sera for ELISA studies (below)). Elemental analysis was conducted by digesting the tumours in nitric acid and analyzing by ICP-OES. Briefly, a section of the tumours (ca. 100 mg, freeze dried) and 500 uL 17% HNO₃ (high purity, Fluka Ltd) were added to clean PTFE vessels and the digestion was carried out in an Milestone UltraWave acid digestion system (Milestone S.r.l., Italy) at 140 °C (10 min ramp to 140 °C and 15 min at 140 °C). Sample blanks were similarly prepared without samples to determine Si levels in the nitric acid and contamination from the tubes. The digests were transferred to clean polypropylene tubes, diluted appropriately, spiked with strontium as an internal standard and ICP analysis was conducted.

2.1.5 ICP-OES analyses

Elemental analysis was conducted by ICP-OES on a JY Ultima-2 (Horiba Scientific) fitted with a V-groove nebulizer and a flow rate of 0.83 mL/min was used. Media samples containing silica were diluted with a NaOH solution (*ca.* pH 10) to promote silicate dissolution and then analyzed for total Si at 251.611 nm. Silicon standards (0.2 to 70 ppm) were prepared in a similar matrix with SiF₄ (1,000 or 10,000 mg/kg Si, Sigma-Aldrich Chemical Co). Media samples containing aluminium clusters were diluted with an HCl solution (50% w/w, 1 M) to promote particle dissolution and then analyzed for total Al at 396.152 nm. Aluminum standards (0.2 to 30 ppm) were prepared in a similar matrix with an Al standard (1,000 mg/kg Al, Sigma-Aldrich Chemical Co).

Tumour digests were analysed for Si and Sr at 251.611 nm and 346.446 nm respectively. Standards were prepared in 17% HNO₃ (high purity, Fluka Ltd) and matrix matched standards were prepared using pooled digest to identify wavelength interference by the matrix.

2.2 Cell assays

This study was approved by the University of Cambridge Human Biology Research Ethics Committee (ref. HBREC.2015.10).

2.2.1 Transfected cells and cell lines

Epstein-Barr virus transformed B cells were generously supplied by Dr Mark Wills (University of Cambridge, Dept. of Medicine, Addenbrookes site), transformed from two healthy donors. Epstein-Barr virus, a gamma-herpesvirus, infects resting B cells and causes them to proliferate (Chen, 2011). THP-1 cells were acquired from ATCC. Jurkat and Karpas 299 cells were supplied by Dr S. Turner (University of Cambridge). The cells were maintained in RPMI media containing 10% FBS, 0.3 g/L L-glutamine, 1% penicillin-streptomycin.

2.2.2 Primary cells

Peripheral blood mononuclear cells (PBMC) were isolated from single leukocyte cones purchased from the National Blood Service (Cambridge, UK) using density gradient centrifugation. Cells were used after resting 2 h or froze down in freezing media (10% DMSO, 50% FBS, 40% RPMI 1640). Frozen cells were thawed, washed in RPMI, and rested 2 h in RPMI containing 10% FBS, 0.3 g/L L-glutamine, 1% penicillin-streptomycin and 0.01 µg/mL DNase prior to use. The enrichment of monocytes and T cells was conducted through monocyte adherence. For monocyte enrichment, PBMC cultures were added to a 6 well plate. After incubating for >1 h, non-adherent cells were discarded and adherent cells were scraped and transferred to a fresh 6 well plate. After repeating 3 times, cells were counted and used after resting for 2 h. For T cell enrichment, PBMC cultures were added to a 6 well plate. After incubating for >1 h, non-adherent cells were transferred to a fresh 6 well plate and adherent

cells were discarded. After repeating 3 times, cells were counted and enrichment was assessed using flow cytometry. T cell enrichment was also conducted using a Pan T cell isolation kit (MACS Miltenyl Biotec, #130-096-535). Briefly, PBMC cultures were resuspended in PBS+0.5% BSA, Pan T Cell Biotin Antibody Cocktail was added (to stain all non-T cells), and the cells were incubated for 5 min at 4 °C. After addition of more buffer and Pan T Cell Microbead Cocktail, cells were incubated at 4 °C for 10 min and passed through a LS Column in the magnetic field of a MACS Separator. After enrichment, cells were rested for a minimum of 2 h prior to use and cells enrichment was assessed using flow cytometry.

Whole blood from healthy, consenting individuals was collected in heparin tubes and briefly mixed. The blood was transferred to fresh tubes in a sterile environment and more heparin was added (to a concentration of 0.5 mg/mL) to prevent coagulation.

T cells from transgenic mice were isolated by cutting up, crushing and grinding freshly isolated spleens with frosted microscope slides. Spleens were provided by C. Fairbairn in Dr S. Turner's laboratory in the Department of Pathology at the University of Cambridge. The cells were passed through 100 and 40 µm cell strainers before centrifuging at 350 g for 10 min. After discarding the supernatants, cells were resuspended in RPMI and centrifuged at 1500 rpm for 5 min. The cells were suspended in warm tissue culture media and rested 1 h prior to treatment.

Staphylococcal enterotoxin B (SEB, Sigma Aldrich #S4881), peptidoglycan (PG), anti-CD3, anti-CD28, OVA 323-339 (Scientific Laboratory Supplies, #01641) and PHA (Sigma) were as positive controls.

2.2.3 Gene array

For investigations using the cell lines (EBV B cells, THP-1), 0.5 mL of a cell suspension (at 1.2×10^6 cells/mL in RPMI + 20% FCS) was mixed with 0.5 mL RPMI +/- 300 µM nanosilica (giving 0.6×10^6 cells/mL, 150 uM nanosilica). Cells were incubated for 4 h and RNA was collected using an RNeasy Mini kit (Qiagen, #74104, below), according to manufacturer's suggested protocol (below). RNA was also collected from cells at time 0.

Freshly isolated PBMCs (Section 2.2.2) were rested in RPMI + 10% FCS for 2 h prior to testing. Cells were resuspended in RPMI + 20% FCS at 2×10^6 cells/mL and 6 mL was added to 50 mL falcon tubes followed by 6 mL RPMI +/- 300 µM nanosilica (giving 1.0×10^6 cells/mL, 150 uM nanosilica). Cells were incubated for 4 h and RNA was collected using an RNeasy Mini kit (Qiagen, 74104, below). RNA was also collected on cells prior to treatment (time 0).

RNA was collected according to the manufacturer's suggested protocol. Briefly, after incubating, centrifuging and decanting the supernatant, the RLT buffer and an equivalent volume of ethanol (70%) was added to pellet. After mixing thoroughly (through tituration), the lysate was transferred to the RNeasy Mini spin column and centrifuged at 8,000 g for 15 s. The

RNA (retained on the column) was washed with RW1 and RPE buffer (spinning at 8,000 g for 15 s) followed by another wash with RPE buffer (8,000 g for 2 min). RNase-free water was used to elute the RNA (spinning at 8,000 g for 1 min).

RNA quantity and quality (by gel electrophoresis) was determined and RNA was stored at -80 °C. Samples were shipped on dry ice to Wageningen University for analysis.

Differences in expression were calculated using an R package limma based on the log₂ intensities using the following calculations:

For cell lines

$$\text{Fold change} = 2^{(\log_2(\text{avg}(\text{nanosilica})) - \log_2(\text{avg}(\text{control})))}$$

For PBMCs

$$\text{Fold change} = \text{avg}_{\text{donore A-D}}(2^{(\log_2(\text{nanosilica, donor A-D}) - \log_2(\text{control, donor A-D}))})$$

2.2.4 Flow cytometry assays

2.2.4.1 Cell treatment

Test media was prepared immediately prior to addition to cells (with the exception of silicic acid). Silicate stocks were filter sterilized (0.2 µm) prior to or after addition to RPMI medium, with the exception of the > 100 nm particles which were filter sterilized (0.2 µm) immediately after pH adjustment (*i.e.*, before freezing or sterile saline addition). Treatments from low pH nanosilica stocks were prepared by either adding the silicate to RPMI, neutralizing with NaOH, and filter sterilizing or by added sterile NaOH to RPMI media and adding the sterilized silicate. RPMI supplemented with silicic acid was prepared by diluting sodium silicate (ultrapure, supplied by Prof. S.D. Kinrade) or Sigma-Aldrich sodium silicate into RPMI, mixing for 5-30 minutes (spiral mixer) and neutralizing with HCl. After pH neutralization, the media was sterilize filtered. The control solution (vehicle) was prepared with NaOH in place of sodium silicate.

Cells were also treated in Basic Salt Solution (BSS) media. BSS was prepared as according to Pereira *et al.* (Pereira et al., 2015). Briefly, 1.52 g piperazine-N,N'-bis(2-ethanesulfonic acid) (PIPES) was dissolved in 500 mL DDW at ca. 60 °C. After cooling, pH was adjusted to 6.5 and NaCl (3.80 g), KCl (0.37 g), MgSO₄ (0.06 g), glucose (0.45 g) and CaCl₂ (0.11 g) was dissolved in the solution. The pH was adjusted back to 6.5 and the media was filter sterilized prior to use.

2.2.4.2 Cell staining

CFDA-SE based proliferation assays

Proliferation was measured by staining the cells with carboxyfluorescein diacetate, succinimidyl ester (CFDA-SE, 90%, Sigma-Aldrich Chemical Co., UK). A 10 mM CFDA-SE (in

DMSO, stored at -20 °C) aliquot was thawed and diluted to 10 µM in sterile PBS. The CFDA-SE was diluted further with PBS to a working concentration of 0.1 µM, in which the cells (at ca. 10⁶ cells/mL) were suspended. After incubating at 37 °C for 7 min, 1 mL FBS and ca. 6 mL RPMI + 10% FBS were added to the suspension followed immediately by centrifugation at 1500 rpm for 5 min. The supernatant was decanted and the pellet was washed twice with 1 mL FBS and >10 mL RPMI + 10% FBS. The intensity of CFDA-SE (excitation filter 488 nm and emission filter 588 nm) in the cells after the incubation period was used to determine the number of cell divisions. For EBV transformed B cells, the proliferation index was calculated using:

$$\text{Proliferation index (PI)} = \frac{\sum_{i=1}^{N_1} x_i}{\sum_{i=1}^{N_1} 1}$$

where “N” is the number of events within the generation “i.” The gating of the generations was determined by taking the intensity mean of the CFSE stained cells fixed at experimental time 0 (generation 0) and gating in between the calculated mean intensities of each generation (the daughter generation has half the intensity of the parent generation). Representative plots of gating are shown in Appendix 1. Data is represented as a percent of the vehicle control. As the sodium levels of the nanosilica treatments varied significantly (and consequently their vehicle controls), the effect of sodium on cell proliferation was determined. There was only a ca. 5% reduction of cell proliferation at the highest sodium concentration that is used in a nanosilica stock (data not shown).

For T cell assays (conducted in PBMC), proliferation was represented as % divided, which corresponds to the % of CD4 or CD8 T cells that had undergone one or more rounds of division. Representative plots of gating are shown in Appendix 1.

Lysing

Prior to staining with fluorescence antibodies (below), whole blood cultures and spleen isolates required additional lysing steps to remove red blood cells. Briefly, 2 mL 1x BD Pharm lyse (#555899) solution was added to the sample tubes and the samples were gently vortexed. After 15 min at room temperature (not exposed to light), the tubes were centrifuged at 200 g for 5 min and the supernatants were carefully aspirated. Cells were washed twice with PBS + 1% BSA (for 7-AAD viability staining, below) or PBS (for Invitrogen live-dead staining, below) and the supernatants were aspirated. The cells were washed once more with the respective buffers followed by centrifuging at 1500 rpm for 5 min.

Samples using the 7-AAD viability stain

Cells were stained for flow cytometry analysis according the manufacturer’s suggested protocol with minor changes. Briefly, the cell suspensions were topped up with cold PBS + 1% BSA (BSA source: Labtech, #PM-T1725) and centrifuged at 1500 rpm for 5 min. After

decanting the supernatants, the cell surface antibodies (in a mixed cocktail) were added to the cells in the remaining supernatant (<100 μ L). The samples were incubated on ice for 20 min. The 7-AAD viability stain was then added and the cultures were incubated for 10 min at room temperature. The cells were washed with cold PBS + BSA and fixed in PBS + 2% paraformaldehyde. Flow cytometry analyses were conducted within hours.

Samples using the Invitrogen live-dead stain

Cells were stained for flow cytometry analysis according to the manufacturer's suggested protocol with minor changes. Briefly, the cell suspensions were topped up with cold PBS and centrifuged at 1500 rpm for 5 min. After decanting and blotting the supernatants, the Invitrogen live dead stain was added to the cells in the remaining supernatant (<100 μ L). The samples were incubated on ice for 20 min and washed with cold PBS + BSA. The cell surface antibodies (in a mixed cocktail) were added to the cultures and the samples were incubated on ice for a minimum of 20 min. The cells were washed with cold PBS + BSA and fixed in PBS + 2% paraformaldehyde. Flow cytometry analyses were conducted within hours

Bacterial and bead uptake studies

Enriched monocytes cultures were treated with nanosilica followed immediately by addition of fluorescent beads (final concentration 25 μ g/mL) or bacteria (final concentration 3 μ g/mL) (details of beads and bacterial can be found in Table 2.01). Cultures were incubated for 1 or 3 h, stained (using the Invitrogen live-dead stain) and flow cytometry was conducted within hours

Apoptosis-necrosis staining

Apoptosis and necrosis was measured using the manufacturer's suggested protocol. Briefly, the cell suspensions were topped up with cold PBS + 1% BSA and centrifuged at 1500 rpm for 5 min. After decanting the supernatants, the cell surface antibodies (in a mixed cocktail) were added to the cells in the remaining supernatant (<100 μ L). The samples were incubated on ice for 20 min. Cultures were then washed twice, once with PBS + 1% BSA and once with PBS. After decanting the supernatant, 100 μ L annexin buffer (10 mM HEPES, 140 mM NaCl, 2.5 mM CaCl_2 , pH 7.4), annexin V and 7-AAD were added to the cells. Cultures were incubated for 15 min at room temperature. Annexin buffer (400 μ L) was then added and the cells were stored on ice followed immediately by flow cytometry analyses.

Intracellular FoxP3 staining

Cells were stained for the intracellular FoxP3 protein through permeabilization of the cell membrane. Briefly, after staining for surface receptors (*Samples using the 7-AAD viability stain*, without the addition of PBS+2% paraformaldehyde), cells were washed with cold PBS + 1% BSA. After discarding the supernatant, 250 μ L permeabilization solution (100 mL FACS lysing solution (BD Biosciences, #349202), 400 mL H₂O and 250 μ L TWEEN 20 (Sigma), at

room temperature) was added to each tube and mixed. After incubating for 10 min (not exposed to light), the cells were washed twice with cold PBS + 1% BSA (centrifuged at 1800 rpm for 8 min, at 4 °C). The intracellular fluorescent antibody was added to the remaining supernatant after decanting and cultures were incubated for 20 min on ice. The cells were then washed with cold PBS + 1% BSA (centrifuged at 1800 rpm for 8 min, at 4 °C), resuspended in cold PBS + 1% BSA, and flow cytometry was conducted immediately.

2.2.4.3 Flow cytometry analyses

Flow cytometry was conducted using a Beckman Coulter CYAN ADP flow cytometer (“Cindy”), equipped with 405, 488 and 642 nm solid-state lasers and 11 detectors in standard configuration. Beckman Coulter Summit software was used for analyses and acquisition. The flow cytometer was calibrated with alignment beads (Spherotech, USA), and the coefficients of variation for each channel was within the range set by manufacturer. For EBV transformed B cells, a minimum of 30,000 gated events were acquired for each suspension. For THP-1, Karpas 299, Jurkat, PBMC, enriched T cell cultures, 400,000 events or the complete suspensions were acquired. For whole blood and cells extracted from mouse spleens, total suspensions were acquired. All cultures were filtered through 35 µM nylon mesh prior immediately prior to analysis.

Table 2.01. Human antibodies and markers used throughout the investigations

Marker	Stain	Supplier
annexin	Pacific Blue	ThermoFisher Scientific (#A35122)
TCR	FITC	BD Pharmingen (#555547)
TCR $\gamma\delta$	PE	BD Pharmingen (#333141)
	FITC	BD Pharmingen (#347903)
CD3 ϵ	PE-Cy5	BD Pharmingen (#555334)
	PE	BD Pharmingen (#555340)
	VioGreen	Miltenyi Biotec (#130-096-910)
	PE-Cy7	BD Pharmingen (#557851)
	FITC	BD Pharmingen (#555332)
CD3-LEAF	APC-Cy7	BD Pharmingen (#557832)
	unconjugated	Biolegend (#300414)
CD4	PE	BD Pharmingen (#555347)
	PE-Cy5	BD Pharmingen (#555348)
	FITC	BD Pharmingen (#555346)
	PE-Cy7	BD Pharmingen (#557852)
CD8	APC	Miltenyi Biotec (#130-091-076)
	APC-Cy7	BD Pharmingen (#557834)
CD11b	PE	BD Pharmingen (#555635)
	PE-Cy7	Biolegend (#101216)
CD11c	APC	BD Pharmingen (#559877)
	PE-Cy5	BD Pharmingen (#551077)
	PE-Cy5.5	Invitrogen (#MHCD11C18)
CD14	Alexa Fluor 488	BD Pharmingen (#557700)
CD16b	PE	BD Pharmingen (#550868)
CD19	APC-Cy7	BD Pharmingen (#557791)
	PE-Cy5	BD Pharmingen (#555414)
CD25	FITC	BD Pharmingen (#555431)
	APC-H7	BD Pharmingen (#560225)
CD28-LEAF	unconjugated	Biolegend (#302914)
CD56	APC	BD Pharmingen (#555518)
	PE-Cy7	BD Pharmingen (#557747)
CD57	VioBlue	Miltenyi Biotec (#130-096-530)
CD69	APC	BD Pharmingen (#555533)
	FITC	BD Pharmingen (#555530)
CD95 (Fas)	APC	BD Pharmingen (#558814)
CD107a	FITC	BD Pharmingen (#555800)
CD142	PE	BD Pharmingen (#550312)
CD154 (CD40L)	APC	BD Pharmingen (#555702)
CD172a,b (SIRP- α)	PE	BD Pharmingen (#563441)
CD178 (FasL)	PE	BD Pharmingen (#564261)
	PE	BD Pharmingen (#557924)
	APC	BD Pharmingen (#563741)
CD274	FITC	BD Pharmingen (#558065)
	PE	BD Pharmingen (#557802)
CD278 (iCOS)	PE	BD Pharmingen (#557802)
CD279 (PD-1)	FITC	BD Pharmingen (#557860)
Forkhead box P3 (FoxP3)	Alexa Flour 647	BioLegend (#320214)
Glycoprotein A repetitions predominant (garpin, GARP)	APC	BioLegend (#352506)
IgG	FITC	BD Pharmingen (#555786)
Latency associated peptide (LAP)	PE	eBioscience (#12-9829)
Polystyrene fluorescent beads	FITC	Bangs Laboratories (#FS03F/5069)
Proliferation	CFDA-SE (FITC)	Sigma-Aldrich (90%, #150347-59-4)
<i>S. aureus</i> (wood strain without protein A)	FITC	Life Technologies (#S2851)
Target cell	Violet	ThermoFisher Scientific (#C34557)
	Violet fluorescent reactive dye	Invitrogen (#L34955)
Viability	7-AAD	Life technologies (#A1310), Biolegend (#420404)

Table 2.02. Mouse antibodies and markers used throughout the investigations

Marker	Stain	Supplier
TCR V α 2	PE	BioLegend (#127808)
CD3	V500	BD Pharmingen (#560773)
CD4	PE-Cy5	BD Pharmingen (#561836)
	PE-Cy7	BD Pharmingen (#552775)
CD8b	PE	BD Pharmingen (#550798)
CD25	FITC	BD Pharmingen (#558689)
CD69	APC	BD Pharmingen (#560689)

2.2.5 Western blot analyses

Western blot analyses was conducted on lysates of T cells enriched from PBMC cultures (using the Pan T cell isolation kit, above). After treatment with nanosilica, the cultures were incubated for 0.2-6 h, centrifuged (1,500 rpm, 5 min) and the supernatants were discarded. The cells were lysed with 100 μ L lysis solution (1 x NuPAGE LDS Sample buffer (Invitrogen, #NP0007), 1 x Halt Protease and Phosphatase Inhibitor Cocktail (Thermo Scientific, #78440) in H₂O), titrated, and diluted with 300 μ L H₂O. Lysates were stored at -80 °C until protein analyses were conducted.

For the western blot analyses, cells lysates were diluted in a reducing agent cocktail (6.5 μ L lysate, 5 μ L NuPAGE LDS Sample buffer, 2.5 μ L NuPAGE Reducing agent (Invitrogen, cat# NP0004), 11 μ L H₂O) and were heated at 70 °C for 10 min. The gels (4-12% Bis-Tris, Invitrogen, #NP0321/0322) were loaded with 15 μ L diluted lysates (with the appropriate ladders/blanks) and run at 100-150 V in a SDS MOPS running buffer (Invitrogen, #NP0001), where the SDS MOPS running buffer in the inner chamber contained NuPAGE Antioxidant (Invitrogen, #NP0005). After electrophoresis, the protein was transferred to the membrane (PVDF, Invitrogen, cat# LC2005, pre-soaked in methanol) in transfer buffer (10% methanol, 1 x NuPage Transfer buffer (Invitrogen, #NP00061), 0.1% NuPAGE antioxidant) between filter paper and blotting pads, run at 30 V for 60 min. The membrane was then removed from the blot module and immersed in block buffer (Thermo Scientific, #37571) for 1 h. The membrane was then transferred to a 50 mL centrifuge tube (protein facing in) with 3 mL block buffer containing primary antibody (1:1000 dilution, antibody specification below) and was incubated overnight at 4 °C (while mixing). The membrane was then rinsed with tris buffered saline with TWEEN20 (TBST, Cell signalling, #9997) followed by 5 wash steps (5 min on a shaker in TBST). The secondary antibody (HRP-conjugated) was then added and incubated for 30 min (while mixing) at room temperature. The membrane was washed with TBST (rinse + 5 x washes, as before) and Pierce ECL Plus Western Blotting Substrate (Thermo Scientific, #32132) was added. After incubated (while mixing) for 5 min at room temperature, the excess substrate was blotted off with filter paper and the membrane was analysed on a GeneGnome XRQ digital imager using the ECL Plus reagent settings. Acquisition time was incrementally

increased until a signal band (of interest) was saturated. Band volume was determined through integration using GeneTools (Syngene) software. An example of the integrations is shown in Appendix 1. Antibodies used in the western blot analyses were vinculin (Thermo Scientific, #7000626, 1:1000 dilution), pZap70 (Cell Signalling Technology, #2701, 1:1000 dilution) pLAT (Cell Signalling Technology, #3584, 1:1000 dilution), Goat anti-rabbit IgG Secondary Antibody, HRP-Conjugated (#A16096, 1:1000 dilution) and Precision Protein StrepTactin-HRP Conjugate (Bio-Rad, #1610380, 1:10,000 dilution). Precision Plus Protein Western C Standards (Bio-Rad, #1610376) was used as the ladder.

2.2.6 Enzyme-linked immunosorbent assay

Cytokine analysis was conducted using duoset ELISA kits according manufacturer's specifications. Briefly, 100 μ L capture antibody (in PBS) was added to each well of a 96 well plate (R&D Systems, #DY990). After incubating overnight, the wells were washed 3 times with PBS + 0.05% TWEEN 20, inverting the plate and blotting on paper towel (for the last wash). Block buffer (PBS + 1% BSA, 300 μ L) was added to each well and incubated for >1 h. After washing (3 times, as before), 100 μ L sample (or standard made up in CGM or tris buffer saline (TBS) + 0.1% BSA + 0.05 TWEEN 20) was added to each well and incubated for 2 h. Plate was washed (as before) and 100 μ L detection antibody (in TBS + 0.1% BSA + 0.05 TWEEN 20) was added to each well followed by incubation for 2 h. After washing (as before), 100 μ L Streptavidin horseradish-peroxidase (HRP) was added to each well and incubated for 20 min followed immediately by addition of 1 M H₂SO₄ (Stop solution). Absorbance at 450 nm and 540 nm (wavelength correction) were made using a FLUOstar Omega microplate reader (BMG Labtech). A 4-parameter logistic regression was used to interpolate for the unknown values. For analyses of IFN- γ levels, normal goat serum was used in place of BSA in the diluent containing the detection antibody (according manufacturer's specifications). IL-2 (#DY202), IL-4 (#DY 204), IL-10 (#DY217B), IFN- γ (#DY285) and lymphotactin (#DXCL10) ELISA kits were acquired from R&D Systems. Mouse IgG (#ab151276) and IgM (#ab133047) ELISA kits were acquired from Abcam plc, for the analysis of the sera from mice in the *in vivo* tumour growth inhibition studies conducted at Translational Drug Development (TD2, Scottsdale, Az, US) in 2012 (methods available upon request). Upon study termination, sera was collected and stored at -80 °C and shipped on dry ice prior to analyses. Sera was also sent to Myriad RBM for a thorough assessment of serum analyte levels.

2.2.7 Statistical analysis

Statistical analyses employed are indicated in Figure caption. Most commonly, data is expressed as means \pm standard deviation (unless otherwise stated). Statistical analyses commonly employed include two-tailed Student T-test and a Two-way Anova, where a *P* value of > 0.05 was not considered significant.

2.3 In vivo studies

In vivo studies were conducted under project licence 80/2574 by Drs J. Shields and L. Pedro (MRC-CU). For the subcutaneous melanoma tumour model, female C57BL/6 mice were injected with 2.5×10^5 B16-F10 cells (ATCC) on both shoulders. Tumour growth was monitored for 14 days or until tumour sizes reached the maximum legal limit (12 mm diameter). Mice were treated with nanosilica or saline (200 μ L) intravenously on days 4, 6, 8, and 11. Tumour volumes were calculated by: $\text{Volume} = \pi/6 \times \text{small}^2 \times \text{longest}$. In the metastatic melanoma model, mice were intravenously injected with 1.5×10^5 B16-F10 cells. Mice were intravenously treated with 200 μ L nanosilica or saline on days 1, 4, 7, 11, 14, and 18. Animals were sacrificed on day 21 and nodule counts were performed.

Chapter 3. Synthesis and characterization of amorphous silica nanoparticles

3.1 Introduction

Silica particles can be prepared using various synthetic routes, including the Stöber reaction, Sol-gel synthesis, fuming, and precipitation, the lattermost being the focus of the investigations conducting here.

Amorphous silica nanoparticles are inherently metastable and can undergo processes such as Ostwald ripening and agglomeration. Ostwald ripening, as described in the Introduction, occurs when the monomeric unit of the system, monosilicic acid for nanosilica, dissolves from the smaller particles and resorbs onto the surfaces of larger particles (Belton et al., 2012; Iler, 1979; Kobayashi et al., 2005). Agglomeration is the formation of larger particles through the clustering of the smaller base particles (Belton et al., 2012). The clusters can be loosely bound or strongly assembled and are referred to as agglomerates and aggregates, respectively (Nichols et al., 2002; Powell et al., 2010). The rate of colloidal silica agglomeration has been shown to be greatest at pH 5-7 (Bergna and Roberts, 2005).

Silica nanoparticle dispersions prepared using the precipitation synthetic route, which can produce nanoparticles under 10 nm in size, were the primary focus of these investigations. The properties of colloidal silica produced via this method are highly dependent on the conditions during preparation. Total Si concentration, pH, temperature, time, and the presence of salts (alkali metal salts and ammonium salts) can alter the particle properties significantly (Gorrepati *et al.*, 2010; Musić *et al.*, 2011). Using such influences, colloidal silicate suspensions of different sizes and properties (mainly dissolution rate in dilute condition) were generated, as outlined in the Methods, and were characterized in this chapter for use in subsequent cellular investigations (Chapters 4-7).

3.2 Results and discussion

3.2.1 Synthesis and Characterization

3.2.1.1 Nanosilica stability and size

Silica nanoparticles were prepared here by adjusting the pH of an alkaline sodium silicate solution at a concentration that exceeded the solubility of silicic acid at the desired final pH (see Chapter 1). Figure 3.01A and B show the resulting dispersion from adjusting a 23 mM $\text{Si}(\text{OH})_4$ solution (pH~11) to pH 7 and incubating for >12 h. The first size measurement was conducted >12 h after preparation to allow time for the pH and particle distribution to equilibrate. At 24 h, the median particle size was ca. 3.6 nm (Figure 3.01B), with a narrow size distribution (2-8 nm). The stability of the nanosilica dispersion was investigated beyond 24 h, as these dispersions are known to be inherently unstable at physiological pH (Belton et al., 2012; Bolt et al., 1997; Iler, 1979; Kobayashi et al., 2005). Figure 3.01A shows the particle size

distribution of a nanosilica dispersion at pH 7 over 28 days. Over time, the size distribution broadened, yielding particles ca. 80% larger on day 28 (Figure 3.01A).

Ionic strength was used to generate larger particles at a more rapid rate. Concentrated saline was added to the silica dispersion immediately after pH neutralization and prior to incubating for 16-24 h. Figure 3.01B shows the particle size distribution of nanosilica dispersions containing different concentrations of Na^+ . Particle size increased with the concentration of Na^+ . As increased ionic strength is known to promote agglomeration rather than Ostwald ripening (Belton et al., 2012; Iler, 1979), it is likely that these large particles are agglomerates, comprised of small particles subunits. Unfortunately, this method of increasing particle size also increases the particle size range within the dispersion (*i.e.*, it increases polydispersity). The particle size distributions are reported as volume median diameter (DV0.5).

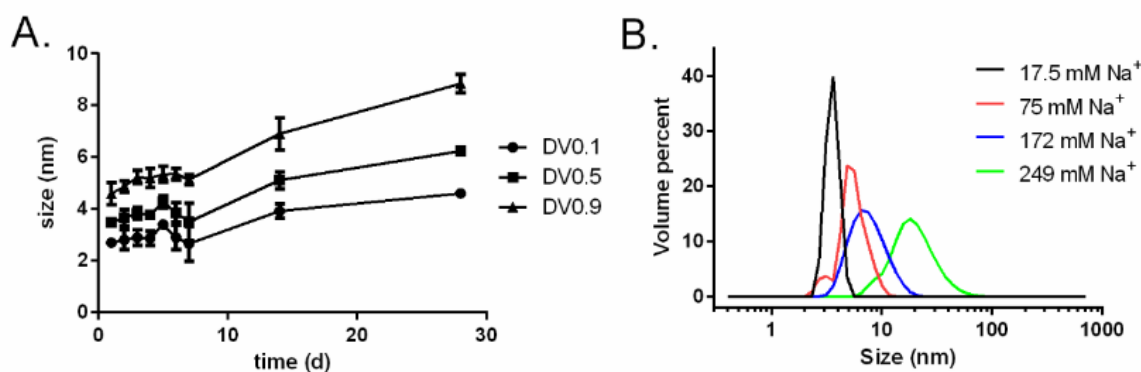


Figure 3.01. A. Measured particle size distribution over time after neutralization (to pH 7) of a 23 mM Si silica dispersion. Size is represented as DV0.1, DV0.5 and DV0.9, *i.e.*, the size where 10%, 50% and 90% of the particles have a smaller diameter. Data are means and SD of 3 replicate measurements per dispersion **B.** Particle size distribution of silica dispersions (ca. 23 mM Si, pH 7) containing different concentrations of saline, 24 h after neutralisation and incubation at room temperature. Data are means of 3 independent dispersions with 3 replicate measurements per dispersion

3.2.1.2 Nanosilica dissolution and size in dilute conditions (physiological concentrations)

An important property of nanosilica particles is their dissolution rate in dilute conditions, *i.e.*, at a concentration below the solubility limit of amorphous silica (*ca.* 1.7 mM Si at pH 7), as it more closely mimics *in vivo* concentrations. The importance of this property is exemplified by crystalline silica, which has chronic inflammatory properties due in part to its longevity/persistence, a product of its very slow dissolution rate (Greenberg et al., 2007; Rimstidt, 1997). Amorphous silica particles have been shown to dissolve readily after dilution while crystalline silica particles do not (Kalia et al., 2016; Rimstidt, 1997). Figure 3.02A shows the effect of particle size on dissolution rate. Particle size, which was increased using the previous techniques, had very little effect on nanosilica dissolution, all particles <19 nm in diameter being > 85% dissolved after 24 h. These data would indicate further that the increase in particle size is through weak agglomeration (not aggregation or Ostwald ripening) and, when diluted to *ca.* 1 mM Si, the agglomerates slowly break apart and release their small particles subunits which dissolve at the same rate. The larger, micron sized silica particles had a slower dissolution rate, suggesting that the particles are more strongly assembled (*i.e.*, are aggregates) and remain intact when diluted to *ca.* 1 mM Si.

Further investigations were carried out in cell culture media, which contains a higher ionic strength, amino acids and other components that may affect the particle size and dissolution rate. However, due to the dilute concentrations and low light scattering properties of nanosilica, along with the presence of proteins from the serum added, dynamic light scattering size measurements were not possible. Additionally, the presence of phosphates, which react with molybdic acid in a similar fashion to silicates, in the media prevented the use of molybdic acid assays for determining dissolution rates. Therefore, 1,000 kDa ultrafilters (11 nm average pore size (Guo and Santschi, 2007)) were used to determine whether particle size was maintained while the dissolution rate was determined with 3 kDa ultrafilters (1-2 nm average pore size (Guo and Santschi, 2007)). Figure 3.02B shows the percentage of silicon that passed through 3 and 1,000 kDa ultrafilters after a 3.6 nm nanosilica dispersion was diluted in RPMI + 10% FBS media and incubated at 37 °C for 0.5 and 1 h. The majority of the silicon passed through the 1,000 kDa ultrafilter, suggesting that significant agglomeration does not occur after dilution in cell culture media. At 1 h, 30-50% of the silicon passed through the 3 kDa ultrafilter, suggesting that the nanosilica readily dissolves or breaks up into particles under 1 nm in size after dilution. Indeed, >90% of the silicon passed through a 3 kDa ultrafilter 8 h after dilution (Figure 3.02C). Given that the nanosilica particles completely dissolved within 24 h at room temperature (Figure 3.01A) and that dissolution rates increase with temperature (Amram and Ganor, 2005; Cama et al., 2002), it is likely that the silicon that passed through the 3 kDa ultrafilter is predominantly silicic acid, and not particles <1 nm in size.

3.2.1.3 Effect of aluminium, heat and pH on nanosilica size and dissolution

As persistence in dilute conditions is viewed as a very important property of nanoparticles, methods were developed to generate particles with longer lifetimes after dilution. Figure 3.03A shows the dissolution rate of a nanosilica dispersion doped with Al prior to dilution in HEPES buffer. Nanosilica dispersions (ca. 25 mM Si) prepared using Sigma-Aldrich sodium silicate naturally contain ca. 0.04 mM Al, giving a Si to Al ratio of 599:1. The ratio was increased to 74 Si:1 Al by adding further Al to the dispersion and incubating for 1 h. Increasing the Al levels beyond this ratio resulted in complete agglomeration of the dispersion. The additional Al prevented a fraction of silicon from solubilizing. This corroborates with studies that showed that Al added to dilute silicate solutions (ca. 0.15 mM Si) leads to the formation of aluminosilicate nanoparticles, which have a lifetime of greater than 50 d (Jugdaohsingh et al., 2013; Taylor et al., 1997).

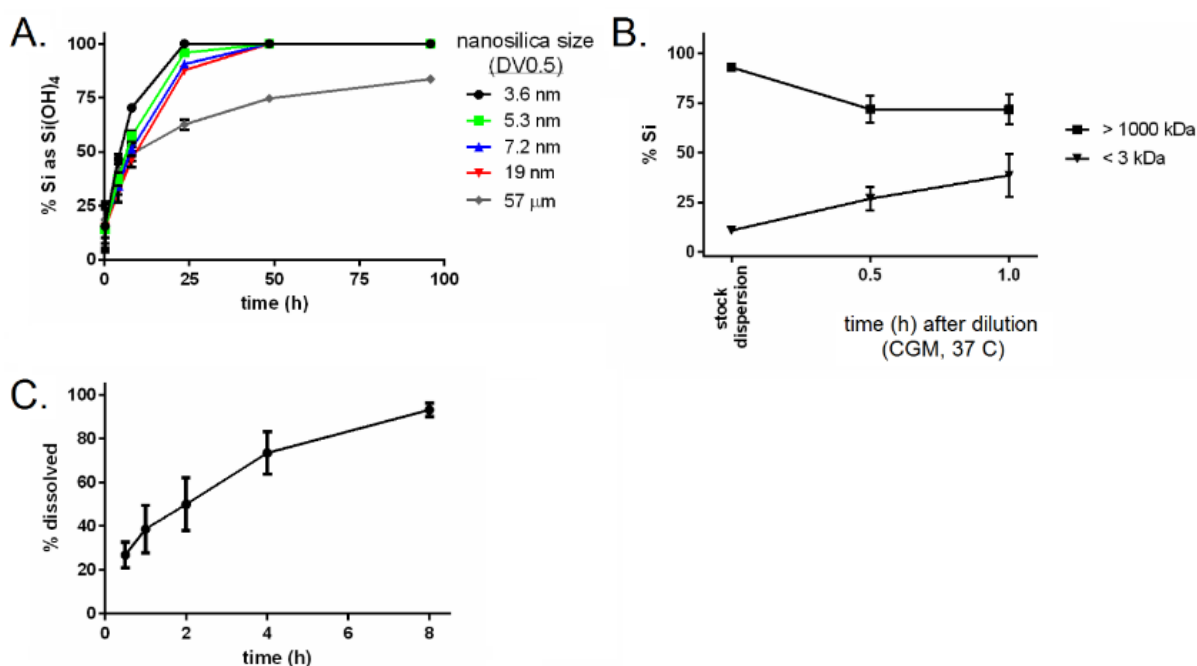


Figure 3.02.A. Effect of particle size on dissolution rate after dilution of silica dispersions (23 mM Si, pH 7.0) to ca. 1 mM Si in HEPES buffer (pH 7.0-7.3). Data are means and SD of 3 replicate measurements per dispersion. **B.** Percentage of silicon that passed through a 3 and 1000 kDa ultrafilter following dilution of a nanosilica dispersion (23 mM Si, pH 7.0) to ca. 0.8 mM Si in RPMI media containing 10% FBS media and incubation at 37 °C for 0.5-1 h. Data are means and SD of >6 independent dispersions (for 3 kDa) and 3 independent dispersions. **C.** Percentage of Si that passed through a 3 kDa ultrafilter following dissolution of a nanosilica dispersion (23 mM Si, pH 7.0) to ca. 0.8 mM Si in RPMI containing 10% FBS at 37 °C. Data are means and SD of >6 independent dispersions.

Another way to increase particle lifetime is heat. Figure 3.03B shows the dissolution rate of a nanosilica dispersion heated to 70 °C. The particle size increased with heating time, yielding particles 6.9 nm in size after 24 h at 70 °C (data not shown). There was an observed decrease in dissolution rate with heating time (Fig. 3.03B), where, for example, the non-heat treated particles were completely dissolved within 24 h and only ca. 50 % of the 24 h heat-treated particles were dissolved at 96 h. It is likely that heat induces particle ripening, either through Ostwald ripening or the formation of aggregates, and consequently increases silicate condensation (as determined using ²⁹Si NMR spectroscopy (below)). A highly condensed commercial silica nanoparticle (Ludox SM30, DV0.5 = 11 nm) was shown for comparison. These particles, which are produced at high temperatures (Bechtold and Snyder, 1951), dissolve very slowly in dilute conditions.

Lastly, pH can be used to increase particle condensation. Figure 3.04 shows the dissolution rate of nanosilica particles prepared at 100 mM Si and pH 10. The proportion of soluble silicon is greater at pH 10 than at pH 7, as evident from the initial measurements (time 0) which indicated that ca. 30% of the silicon is readily soluble at pH 10 compared to less than 20% at pH 7 (Figure 3.02 & 3.03). A higher concentration of silicic acid is known to promote exchange between soluble and particulate silica, *i.e.*, particle ripening (Lifshitz and Slyozov, 1961). Indeed, particle lifetime in dilute conditions increased with an increasing period of incubation (of the stock dispersion) at pH 10. The stability of nanosilica dispersions is also greater at high pH (Bergna and Roberts, 2005), and therefore longer incubation times can be used without there being significant particle agglomeration. All dispersions tested here ranged from 3.6 nm to 5.3 nm in diameter and there was no correlation between size and incubation time.

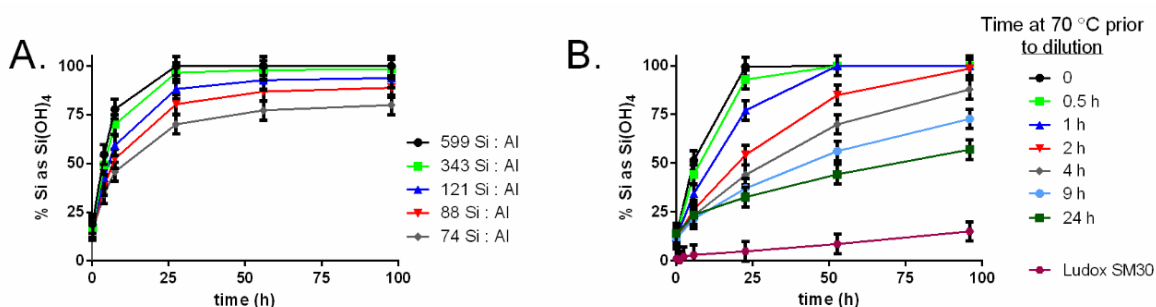


Figure 3.03. The effect of **A)** Al doping and **B)** heating (70 °C) on the dissolution rate of nanosilica dispersions (23 mM Si, pH 7) after dilution to ca. 1 mM Si in HEPES buffer (pH 7.0-7.3). Both Al-doping and heating at 70 °C increased the size of the particles (in their stocks) but all remained between 3.6 and 6.9 nm. (Note - data similar to B (at 60 °C) was previously patented (Bastos et al., 2015)). Data are means and SD of 3 replicate measurements per dispersion.

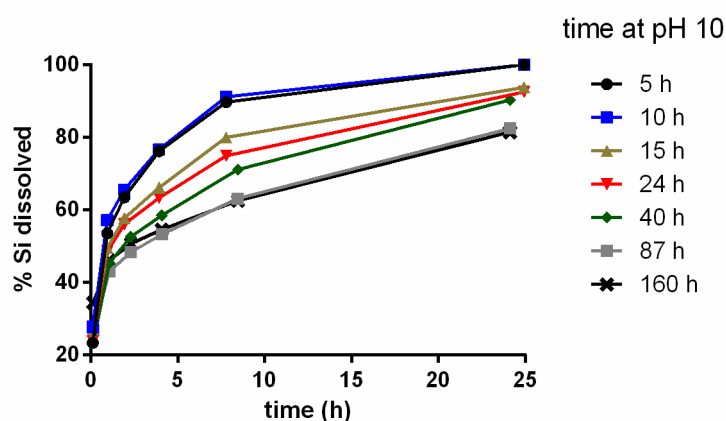


Figure 3.04. The effect of incubation time at pH 10 on the dissolution rate of nanosilica dispersions (100 mM Si) after dilution to ca. 1 mM Si in HEPES buffer (pH 7.0-7.3). After incubating at pH 10, the dispersions were stabilized by rapidly adjusting pH to 1 (see Section 3.2.7). All particles were between 3.6 and 5.3 nm in size (DV0.5) and there was no correlation between size and incubation time. The error associated with the values is 5% but error bars were left out for clarity (Note - this data was previously patented (Bastos et al., 2015)). Data are means of 3 replicate measurements per dispersion.

3.2.1.4 Low pH synthesis of particles

The previous synthetic strategy, *i.e.*, precipitation at near-physiological pH, successfully generates the particles > 3 nm in size. As it does not consistently generate particles < 2 nm in diameter, an alternative synthetic strategy was employed. By rapidly adding a concentrated acid to an alkaline silicic acid solution, nanosilica particles ca. 1 nm in diameter can be generated at high concentrations (Bastos et al., 2015; Bronder, 1999; Kerek, 2010). Figures 3.05A and B show the size and dissolution rate of a nanosilica dispersion prepared at 500 mM and pH 0.8 (after 24 h incubation). The particles were smaller than those produced at pH 7, despite being prepared at a much higher Si concentration (>10 times more concentrated). These results might suggest that rapid adjustment to low pH increases the number of nucleation points, thereby generating a greater number of smaller particles. The particles prepared at low pH dissolve very rapidly upon dilution to 1 mM Si (Figure 3.05B). Approximately 50% of the particles were dissolved 0.2 h after dilution and 100% dissolution was reached before 2 h. The increased dissolution rate is likely in part due to the increased surface area of the particles. Whether an increased degree of amorphousness, *i.e.*, a decrease in the amount of silicate connectivity/condensation within the particle, also contributes to the increased dissolution rate is unknown. The rapid formation of the particles could be inducing precipitation of silicic acid in a less organized fashion.

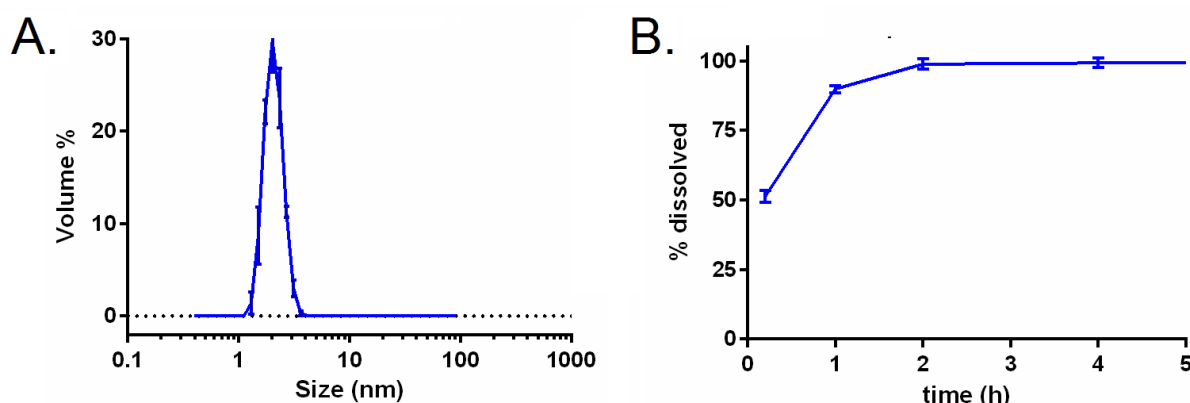


Figure 3.05. Particle size distribution of a nanosilica dispersion (500 mM Si incubated at pH 0.8 and at room temperature for 24 h, **A**) and its dissolution rate (**B**) after dilution to ca. 1 mM Si in HEPES buffer (pH 7.0-7.3). Data are means and SD of 3 replicate measurements per dispersion.

3.2.1.5. Silicon-29 NMR analysis of nanosilica particles

Silicon-29 NMR spectroscopy has been used to characterize the degree of condensation of insoluble silicate dispersions (Fedeyko et al., 2004; Kalia et al., 2016). The chemical shifts of silicate centres with varying degrees of condensation (*i.e.*, Q^0 - Q^4) have been assigned and provide a method to quantify the proportion of the silicate centres within a dispersion.

Here, ^{29}Si NMR spectroscopy was used to characterise two dispersions of approximately the same size with varying dissolution rates (the representative size and dissolution plots are shown in Figure 3.06A & 3.06B). To maximize signal intensity, dispersions were prepared using isotopically enriched silicic acid (99.35% ^{29}Si) which contain a higher sodium concentration than the non-enriched stock. Therefore, the particle size distribution of the dispersions could potentially be larger than what is shown in the representative plots (which show dispersions prepared from normal sodium silicate). Figure 3.06C shows the ^{29}Si NMR spectra of the nanosilica dispersions stabilized at pH 1.5. The signals at 0 and -9 ppm correspond to orthosilicic acid (Q^0) and the silicic acid dimer (Q^{1_2}) respectively, while the broad signals below -15 ppm correspond to the insoluble portion of the dispersion. The lack of definition (sharpness) in the signals corresponding to the insoluble portion of the silicate dispersion is due to the environmental heterogeneity of the silicate centres. For example, the particles contain many Q^4 silicate centres and, as there is a complete lack of structure (*i.e.*, it is amorphous rather than crystalline), each of these silicate centres is subjected to a slightly different chemical environment. Each silicate centre consequently has a slightly different chemical shift and, as a result, broad signals (lumps) are present rather than sharp signals. The signals from -15 ppm to -32 ppm were assigned to partially condensed silicate centres (Q^2 and Q^3) and those further down in frequency (-32 ppm to -52 ppm) were assigned to fully condensed silicate centres (Q^4), as previously assigned by Kalia *et al.* (Kalia et al., 2016).

Table 3.01 shows, for the two dispersions, the percentage of soluble and insoluble silicon and the distribution of silicate centres (or the condensation of silica) within the insoluble portion, as determined by spectral integration. Despite storage at the same final pH, the soluble silicon content of the materials differed and both were higher than the solubility limit of amorphous silica (*ca.* 1.7 mM Si (Jugdaohsingh *et al.*, 2008)). The distribution of silicate centres within the insoluble portion of the dispersion differed significantly between the two materials. The fully condensed portion (*i.e.*, a Q⁴ centre) was greater in the more persistent material (material B). Consequently, the partially condensed portion (*i.e.*, Q²+Q³ centres) was lower in material B than in material A. Whether this change in is truly due to particle condensation or is due to the slight differences in size is unclear. A small increase in size would significantly increase the proportion of core (internalized) silicate centres (likely Q⁴), as there is a cubic relationship between radius and the internal volume of a sphere (as the volume of a sphere (V) = $4\pi r^3/3$).

The percentages of partially condensed silicate centres in the two dispersions tested here were lower than those previously tested. Kalia *et al.* showed that a 1.5 nm nanosilica dispersion (by TEM) was comprised of $83 \pm 2\%$ fully condensed (Q⁴) silicate centres (Kalia *et al.*, 2016). Although particle size was smaller than those tested in the present study, as determined by ultrafiltration (96% Si <10 kDa (Kalia *et al.*, 2016) vs *ca.* 70% Si <50 kDa for material B in the present study, data not shown), the percentage of fully condensed silicate centres (Q⁴) was higher. As fully condensed silicate centres can only exist in the core of the particle (not on the surface), this may suggest that there is a percentage of partially condensed centres in the core of the materials tested here.

Silicon-29 NMR spectroscopy has been shown to effectively measure nanosilica condensation. However, the extensive experimental requirements (long acquisition times (>40 h), isotopic enrichment and glass free NMR equipment) and the meta-stability of the silicate dispersions make these experiments costly and difficult to build up a large sample dataset. For this reason, further studies using ²⁹Si NMR spectroscopy were not conducted.

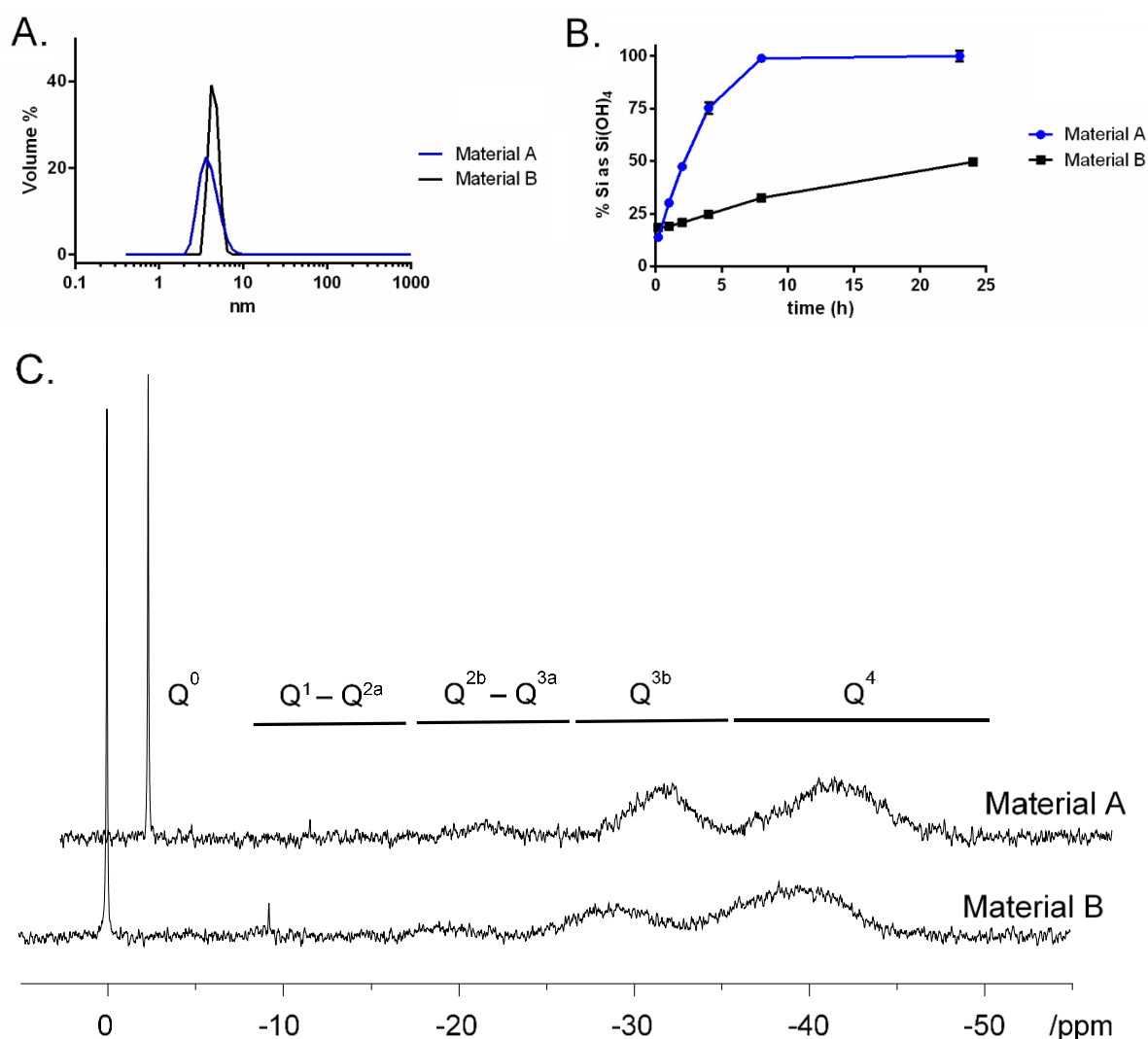


Figure 3.06. Representative size (**A.**) and dissolution rate (**B.**) of the two nanosilica dispersions (40 mM Si, see below for formulations, denoted as A and B) employed in the ²⁹Si-NMR analyses. **C.** ²⁹Si NMR spectra (99.35 MHz) of the aqueous nanosilica dispersions containing 40 mM Si (²⁹Si enriched) at 25 °C. The signal corresponding to silicic acid was referenced to 0 ppm. For material A the silicic acid signal was clipped in the display to maximize the signals corresponding to the insoluble silicate. Material A was prepared by adjusting a 40 mM silicic acid stock to pH 7, incubating for 2 h and adjusting to pH 1.5. Material B was prepared by adjusting a 40 mM silicic acid stock to pH 9, incubating for 18 h at 40 °C, and adjusting to pH 1.5 after cooling to room temperature.

Table 3.01. Distribution of silicon in the two nanosilica dispersions (40 mM) determined through the spectral integration of the ²⁹Si NMR spectra

Material	% Si (+/- 3)		% NP (+/- 2)	
	Soluble	Insoluble	<u>Q² + Q³</u>	<u>Q⁴</u>
A	6	94	44	56
B	12	88	32	68

3.2.1.6 Charge of nanosilica particles

Next, the charge of various nanosilica dispersions was determined. The interactions between the nanosilica particles and cells, proteins and other components in the culture media is largely dependent on the charge of the particles. In solution, the charge of a particle is measured at the edge of the diffuse layer (*i.e.*, the slipping plane, the point in at which the surrounding solution is no longer associated with the particle) (Clogston and Patri, 2011). The charge at this point is referred to as the zeta-potential.

Figure 3.07 shows the zeta-potential of three nanosilica dispersions between pH 1.5 and 9. Although the dissolution characteristics of the three nanosilica dispersions (particle size ranging between 1 and 5 nm) varied significantly (Figure 3.07A), there was no significant difference in zeta-potential (Figure 3.07B). This may suggest that the degree of condensation, at least within the narrow range tested here, has little effect on zeta-potential. The zeta-potentials of the nanosilicates increased with pH. The nanosilica particles carried no charge at low pH (< pH 4), which is consistent with nanosilica particles of larger diameters (Bergna and Roberts, 2005). As the pH increased above 5.5, there was a significant increase in zeta-potential. The zeta-potential of the dispersions was not assessed above pH 9 as solubility of silicic acid increases significantly above this pH (Jugdaohsingh et al., 2008). The relationship between pH and zeta-potential shows a point of inflection at pH 7-7.5, which would suggest that at this pH *ca.* 50% of the surface hydroxyl groups are deprotonated (*i.e.*, $pK_a = 7-7.5$). To investigate this further, a nanosilica dispersion was titrated with dilute NaOH (Figure 3.08). The dispersion was buffered between pH 6-8 by the nanosilica particles, which would corroborate the results indicating that the pK_a of the particles is *ca.* 7. Additionally, the ionization constants reported in the literature corroborate these results, where larger silica particles were determined to have a pK_a of 7.1 (Hair and Hertl, 1970) and 1 nm nanosilica “oligomers” were found to have a pK_a of 6.8 (Belton et al., 2012).

Studies have previously shown that nanosilica particles are quite stable under conditions where they carry no charge (reviewed by Bergna and Roberts (Bergna and Roberts, 2005)), contrary to other nanoparticles which are most stable in conditions where they carry significant charge (Gören et al., 2012). Both kinetic and thermodynamic models have been proposed to explain this phenomenon, but the problem remains unresolved (Bergna and Roberts, 2005). One possible solution is that deprotonation is required for condensation and agglomeration of the particles. It has been hypothesised that the polymerization of silicates occurs through the electrophilic attack of neutral silicic acid by a negatively charged silicate species (Kinrade and Swaddle, 1988). It is plausible that a similar mechanism is occurring with the nanosilica particles, *i.e.*, a negative region of a nanosilica particle attacking a neutral area of another nanosilica particle. Indeed, it has previously been suggested that negative silicate regions are

required for oligomer growth (Iler, 1979). This would address the observations of increased stability and decreased condensation rates (below) at low pH.

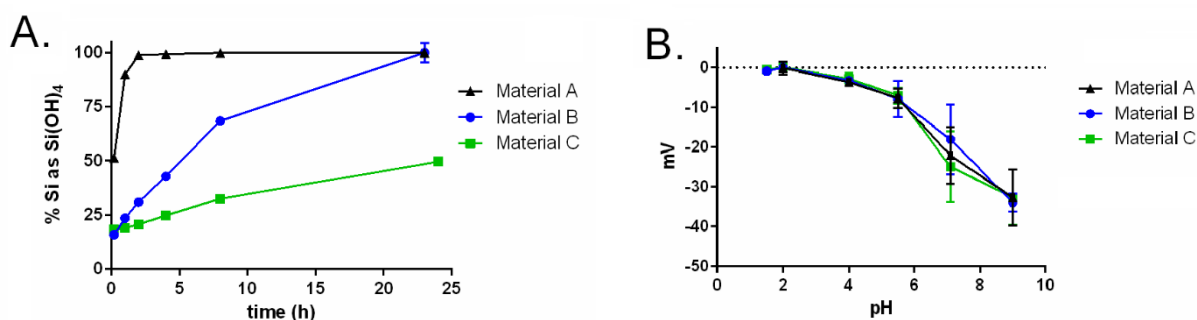


Figure 3.07. A. Representative dissolution rates of three 40 mM nanosilica dispersions, following dilution to 1 mM Si in HEPES buffer (pH 7.0-7.3). **B.** Zeta-potentials of the three nanosilica dispersions between pH 1.5 and 9 in water. Material A was prepared by rapidly adjusting a 500 mM silicic acid stock to pH 0.8, incubating overnight and diluting to 40 mM. Material B was prepared by adjusting a 40 mM silicic acid stock to pH 9, incubating for 18 h at room temperature. Material C was prepared by adjusting a 40 mM silicic acid stock to pH 9, incubating for 18 h at 40 °C, and cooling to room temperature.

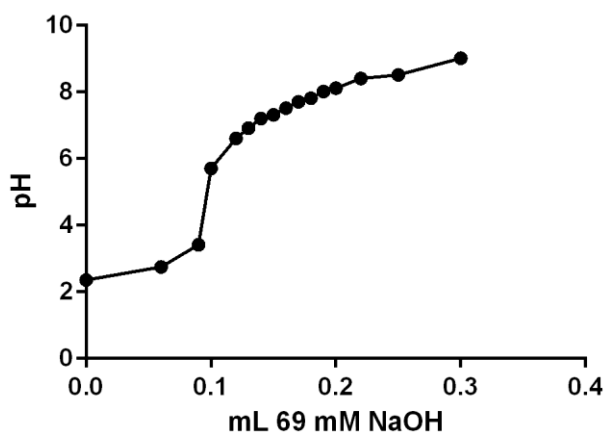


Figure 3.08. Titration of 5 mL of a nanosilica dispersion (similar dissolution profile to material A in Figure 3.10) with 69 mM NaOH (conducted by C. Bastos).

The zeta-potential measurements were previously conducted in the dispersion stock, with the required HCl/NaOH to adjust pH. As cells would only encounter the nanoparticulate in more complex media, the charge of nanosilica was assessed in two biologically relevant fluids, phosphate buffered saline (PBS) and RPMI. Protein was not included in the media as proteins would interfere with the DLS measurement and produce artefactual signals. Table 3.02 shows the zeta-potentials of the three nanosilica particles (as previously defined in Figure 3.10) in PBS and RPMI. Both media stocks alone (*i.e.*, without nanosilica particles) had negative zeta-potentials, *ca.* -22.4 mV and -11.2 mV for PBS and RPMI, respectively. The zeta-potential of the nanosilica particles in these media was very similar to that of the media alone. This might suggest that the particles cannot be detected in the complex matrix. One method of determining whether particles are detected by DLS techniques is the derived count rate. Derived count rate is the calculated concentration/density of the dispersion, determined by the average scattering intensity and the attenuation (a filter is used at the detector) required to obtain that intensity. By comparing the derived count rates, it may be possible to determine whether nanosilica particles are detected in the media. The nanosilica containing media had a higher derived count rate than the media alone, indicating that the nanosilica particles were detected in these complex matrixes. These results would suggest that the zeta-potential measurements correspond to the nanosilica particles, not the negatively charged species from the media formulations. The zeta-potential of the nanosilica particles was similar, but slightly less negative, in the complex media compared to stock dispersions. These results corroborate with trends reported in the literature, which show that zeta-potential decreases in higher ionic strength media (Kobayashi et al., 2005). Further investigations are required to confirm the charge of the nanosilicates in more complex media (*i.e.*, media containing proteins from FBS).

Table 3.02. Zeta-potential and derived count rate of nanosilica dispersions (as defined in Figure 3.10) in PBS and RPMI. Data are means and SD of 3 independent dispersions with 3 replicate measurements per dispersion. ND – not determined

Material	In PBS		In RPMI	
	mV	kcps	mV	kcps
A	-14.0+/-1.5	1717+/-2348	-14.6+/-1.8	419+/-488
B	-20.8+/-0.9	1755+/-1841	ND	ND
C	-22.1+/-0.4	837+/-416	-17.3+/-3.0	293+/-236
PBS	-22.4+/-0.9	222 +/- 22	-	-
RPMI	-	-	-11.2+/-1.6	29.0+/-7.8

3.2.2 Stabilization of nanosilica dispersions

The metastability of silica nanoparticle dispersions, especially at physiological pH, prevents preparation of the suspensions in advance. This instability inserts a degree of complexity into more experimentally demanding studies, such as *in vivo* toxicological studies, as staff need to be fluent in the preparation of the materials and would also require the analytical tools for characterization. For these reasons, investigations were conducted to identify the conditions of greatest nanosilica stability, in an attempt to prolong shelf life of the dispersions.

An alternative molybdic acid assay was employed to assess the formation and ripening processes of labile insoluble silicates. Instead of diluting in a buffer at pH 7 and adding aliquots to the molybdic acid solution (pH ~ 0.8, as conducted previously), the silicate dispersion was directly diluted with the molybdic acid solution and the optical density at 400 nm (which corresponds to the formation of the β -silicomolybdate complex and the amount of silicic acid released from the particles) was measured over time (Iler, 1979). Figure 3.09 shows the absorbance at 400 nm after silicic acid (40 mM Si, pH ~ 11) and a nanosilica dispersion (500 mM Si incubated at pH 0.8 for 24 h, as shown in Figure 3.05) were diluted to 1 mM in an acidic molybdic acid solution. The optical density reached a maximum ca. 0.5 h after molybdic acid was added to the silicic acid solution, which would suggest that silicic acid is completely complexed by molybdic acid during this time. There was a slight decrease in absorbance after 1 h, which is likely due to the instability of the β -silicomolybdate complex (Kley et al., 2014). The formation rate of the β -silicomolybdate complex was slower for nanosilica particles compared to soluble silica, as silicic acid had to be released from the particles before it could be complexed by molybdic acid. The release of silicic acid from the particles was slower under the conditions of this assay compared to the previous dissolution assay (Figure 3.05), most likely due to difference in pH of the diluent (pH ~ 0.8 here compared to pH 7). Using this assay, which has a decreased rate of reaction and therefore greater sensitivity, the ripening and formation processes of nanosilicates could be assessed.

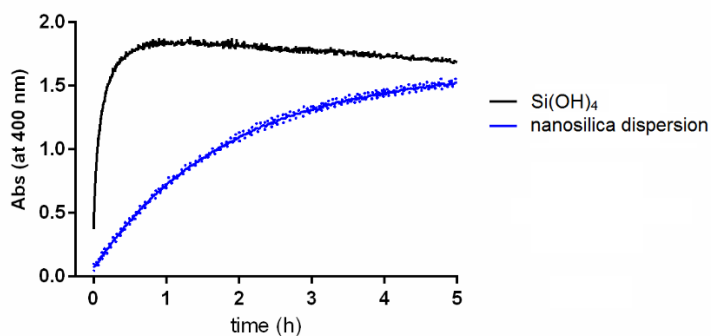


Figure 3.09. Formation of the β -silicomolybdate complex over time, as measured by the absorbance at 400 nm, following dilution of silicate stocks (silicic acid or nanosilica dispersion (1-2 nm, 500 mM Si incubated at pH 0.8 for 24 h and at room temperature)) to 1 mM Si in a molybdic acid solution (pH \sim 0.8). Data are means and SD (dotted lines) of 3 replicate measurements per dispersion.

The effect of concentration on particle formation, ripening and, therefore, stability was first investigated. Nanosilica dispersions were prepared at 40 and 500 mM (both at pH 0.8-1) and incubated for 0-24 h at room temperature. Figure 3.10A shows the silicic acid release, as determined by the formation of the β -silicomolybdate complex, from the 500 mM nanosilica dispersions. The formation rate of the β -silicomolybdate complex decreased with longer incubation at room temperature (*i.e.*, with increased ageing of the dispersion). There was also a similar decrease in β -silicomolybdate formation rate with increased ageing of the dispersions prepared at 40 mM Si (Figure 3.10B). However, the formation rate decreased faster with ageing for the more concentrated (500 mM Si) nanosilica dispersion. These results are consistent with previous studies that have shown that the rate of silicate polymerization increases with total Si concentration (Kinrade and Swaddle, 1988). Figure 3.10C shows the area under the absorbance curves (from 0-5 h, Abs (400 nm) \times h) for each of the dispersions tested. The area under the curve is proportional to the relative amount of silicic acid that was released in 5 h, and it can be correlated to relative condensation of a dispersion. The plot shows that the area under the curves decreases with time and with Si concentration. Whether the decrease in the area under the curves (*i.e.*, an increase in condensation) is due to Ostwald ripening or agglomeration of the insoluble materials is unknown.

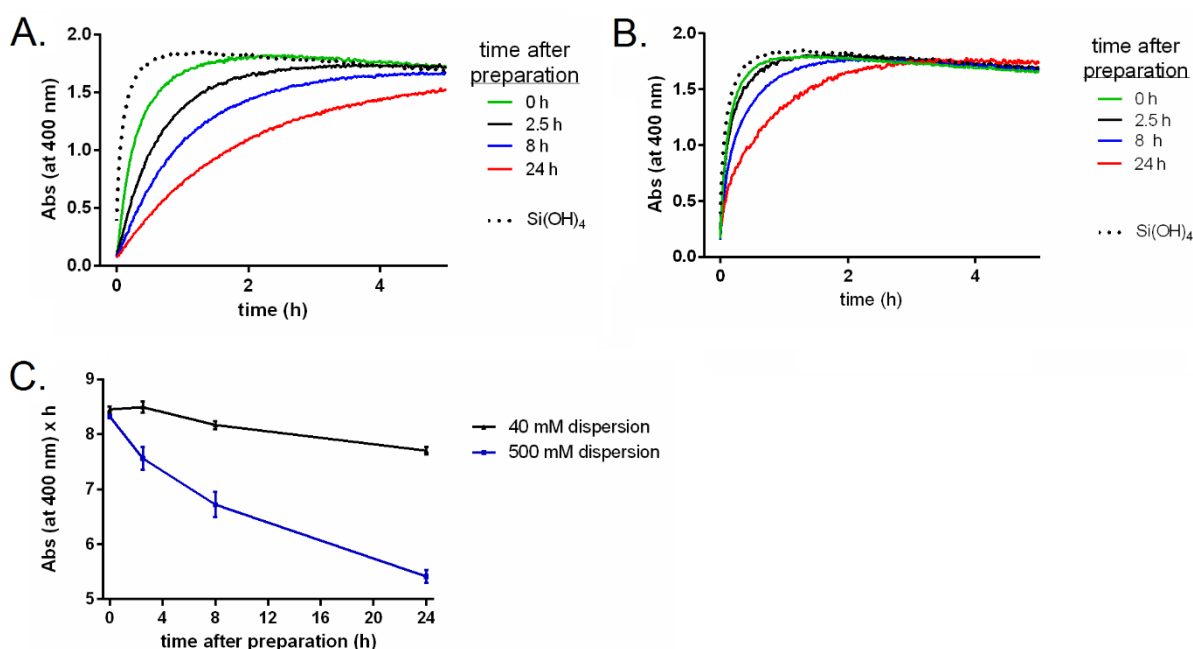


Figure 3.10. Formation of the β -silicomolybdate complex over time, as measured by the absorbance at 400 nm, following dilution of aged 500 mM (A.) and 40 mM (B.) nanosilica dispersions (prepared at pH 1) to 1 mM Si in a molybdic acid solution (pH \sim 0.8). The area under the absorbance curves (in A. and B.) was determined and plotted against age of the dispersion (C.), showing an increase in condensation with ageing. Data are means of 3 replicate measurements per dispersion.

The effect of pH on silicate condensation and stability was investigated next. Figure 3.11A shows silicic acid release, as determined by the formation of the β -silicomolybdate complex and represented as areas under the curves, from 40 mM silicate dispersions prepared at pH 1, 7.4 and 9. Area under the curve decreased rapidly after pH adjustment to 7.4 and 9, indicating that silicate condensation occurs rapidly at these pHs. It reached its minimum at 2.5 h, after which only the soluble silicic acid fraction present in the dispersions was complexed by molybdic acid. The difference in solubility of silicic acid at pH 7.4 and 9, ca. 1.7 and 4 mM, respectively (Jugdaohsingh et al., 2008), most likely explains the slight difference in the area under the curves after 2.5 h. However, although a minimum was reached at 2.5 h, condensation of the particles continues after this time (Figure 3.11B and Figure 3.04); the low pH conditions of the assay prevent highly condensed particles from releasing silicic acid. The large difference in silicic acid release (*i.e.*, condensation rates) between dispersions at low (*i.e.*, pH 1) and physiological pH corroborate studies that show nanosilica particles are more stable (*i.e.*, have slower polymerization and agglomeration rates) below pH 5 compared to pH 6-9 (Bergna and Roberts, 2005).

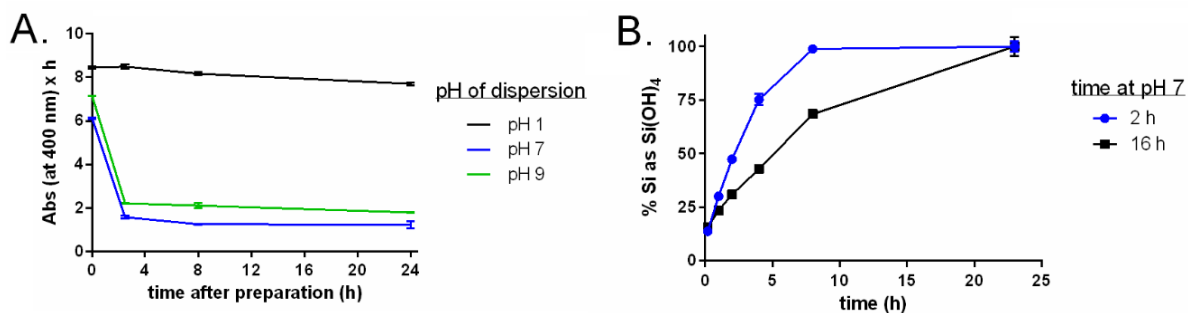


Figure 3.11. A. The area under the absorbance curve (measured at 400 nm between 0 and 5 h), corresponding to the formation of the β -silicomolybdate complex, after dilution of aged 40 mM nanosilica dispersions (prepared at pH 1, 7.4 and 9) to 1 mM Si in a molybdic acid solution. **B.** The effect of incubation time at pH 7 on dissolution rate of nanosilica dispersions after dilution to ca. 1 mM in HEPES buffer (pH 7.0-7.3). Data are means and SD of 3 replicate measurements per dispersion.

As nanosilicates were shown to condense at a slower rate at low pH, the suspensions were adjusted to low pH as to prolong shelf life. However, dispersions stored at low pH require a neutralization step prior to use. The effect of neutralization on particle size was investigated here.

Figure 3.12 shows the effect of neutralization on the phase distribution and particle size of a nanosilica dispersion (3-4 nm in diameter, stored at pH 1.5) after adjustment to pH 7.4. The proportion of silicon <50 kDa in size (4 nm average pore size (Guo and Santschi, 2007)) decreased significantly after pH adjustment (Figure 3.12A). DLS measurements also showed a slight increase in particle size immediately after neutralization (Figure 3.12B). The particles continued to agglomerate after 10 min, reaching a median particle size of 9 nm at 2 h. These results corroborate those that show that condensation and agglomeration rates increase at physiological pH.

Next, the effect of dilution on a neutralized nanosilica dispersion was investigated. Figure 3.12C shows the phase distribution of the dispersions after dilution in PBS and incubation for 10 min. Despite having significantly different phase distributions upon neutralisation (Figure 3.12A), there was no difference in phase distribution upon immediate dilution below 1 mM Si. These results would suggest that the growth immediately after pH adjustment is due to weak agglomeration. These agglomerates break apart if diluted immediately thereafter.

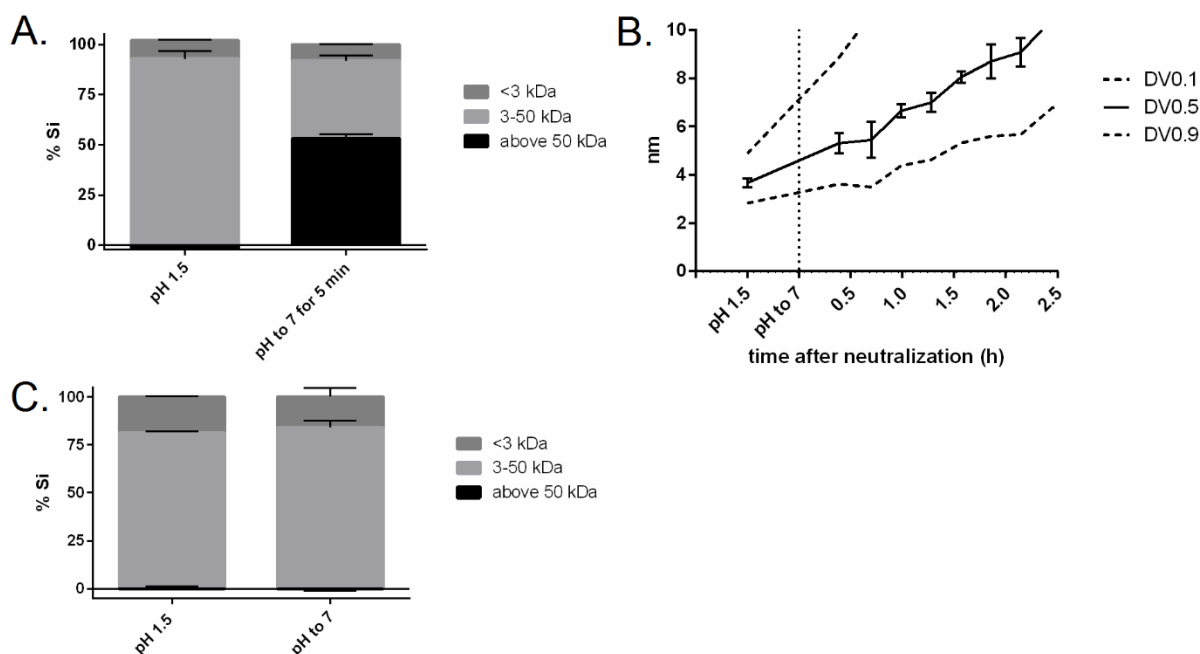


Figure 3.12. A. Percentage of silicon in a nanosilica dispersion (40 mM, pH 1.5) that passed through 3 and 50 kDa ultrafilters (*ca.* 1.5 and 4 nm respectively (Guo and Santschi, 2007)) before and after adjustment to pH 7. Data are means and SD of 2 independent replicates. **B.** Particle size distribution (by DLS) of the nanosilica dispersion after pH adjustment to 7. Data are means and SD of 3 replicate measurements. **C.** Percentage of silicon in the nanosilica dispersion (40 mM, pH 1.5, as shown in A.) that passed through 3 and 50 kDa ultrafilters (*ca.* 1.5 and 4 nm respectively (Guo and Santschi, 2007)) after dilution to 0.4 mM Si and incubation for 10 min. Data are means and SD of 2 independent replicates.

3.2.3 Preparation and characterization of control particles

In this section, investigations were conducted to find non-silica nanoparticles of similar size to those used here (in this thesis), as a control for in cellular investigations. Commercially, a number of different particles are available, though most are not appropriate. Many dispersions 1-5 nm in size are supplied at low concentrations (1-2 mM), making it not possible to match the concentrations of silica used in the biological assays. Other materials, characterized by electron microscopy, have core particle sizes between 1 and 5 nm but when the stabilizer and hydrodynamic shell are accounted for, the particles are too large for comparison. For example, Figure 3.13 shows the aqueated size of (11-mercaptoundecyl)tetra(ethylene glycol) functionalized gold nanoparticles. The core particle size is 3-4 nm by TEM (Sigma-Aldrich, #687863) but in suspension (in water) the median particle size is *ca.* 10 nm, more than double that of the nanosilica particles used in the majority of the biological investigations herein.

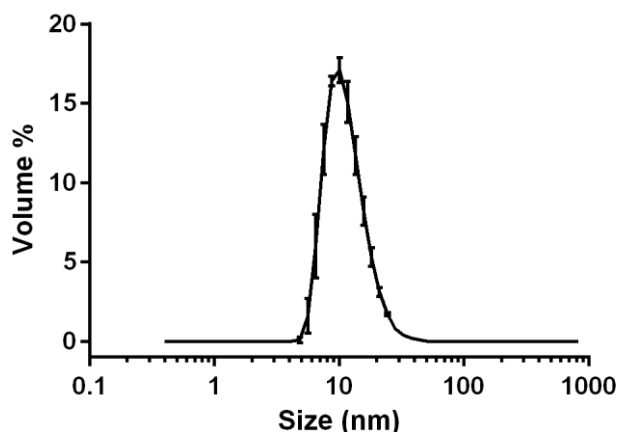


Figure 3.13. Particle size distribution of (11-mercaptoundecyl)tetra(ethylene glycol) functionalized gold nanoparticles (Sigma-Aldrich, 687863)

Whether aluminium clusters could be used as control particles was investigated next. Aluminium clusters can be formed by increasing the pH of an acidic aluminium chloride solution with NaOH (Fu et al., 1991). Figure 3.14A shows the size of an aluminium hydroxide dispersion prepared by adjusting a 100 mM Al chloride solution to pH 4.2 with NaOH and incubating for 24 h. The size of the Al hydroxide clusters was similar to that of the 1-2 nm nanosilica particles but the proportion of Al contained within the dispersion, versus soluble Al, is not known. Attempts were made to increase particle size above 2 nm, a size where 3 kDa ultrafilters (1-2 nm average pore size (Guo and Santschi, 2007)) could be used to separate and determine the portion of soluble Al. However, every attempt to increase particle size resulted in either no particle growth or full agglomeration. Despite not knowing the distribution of Al in the dispersion, investigations were carried out to determine whether the clusters agglomerate after dilution in cell growth media. Figures 3.14B and C show the phase distribution of the Al dispersion after addition to either complete growth media or BSS media (balanced salt solution, a minimal salt solution used to decrease the rate of nanoparticle agglomeration (Pereira et al., 2015)). The aluminium clusters agglomerated rapidly after addition to cell culture media and the majority (>90%) of Al did not pass through the 1,000 kDa ultrafilter (11 nm average pore size (Guo and Santschi, 2007)) at 0.5 h. Due to their rapid rate of agglomeration, Al dispersions are not suitable for comparison to the nanosilica dispersions.

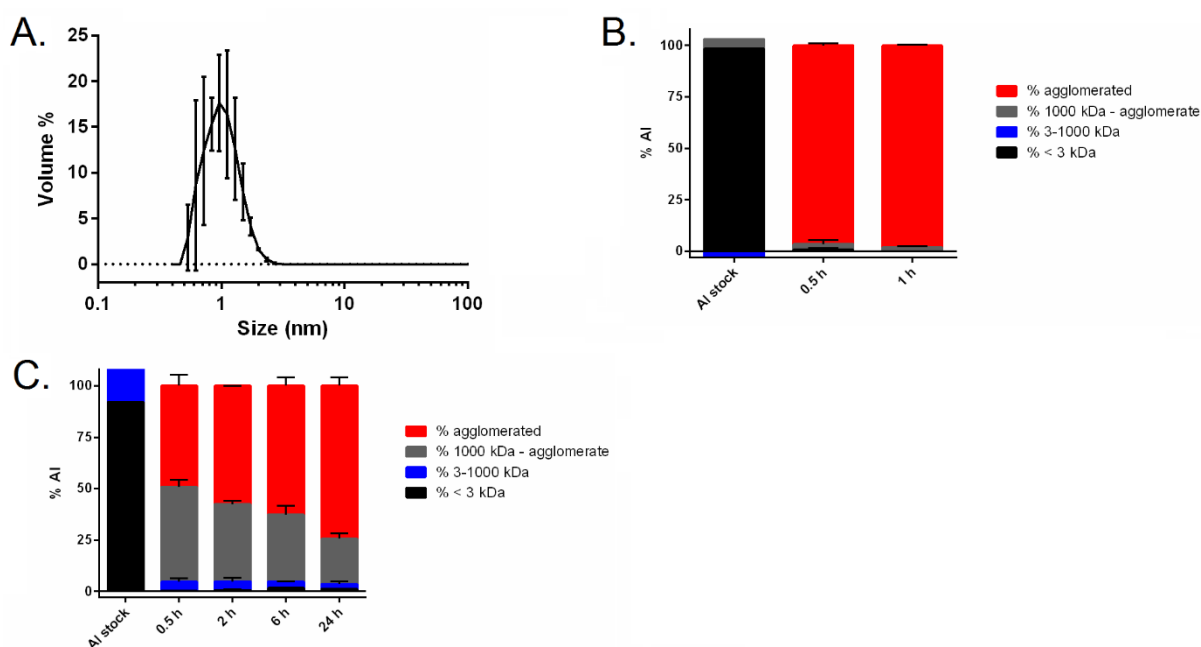


Figure 3.14. A. Particle size distribution of an aluminium hydroxide dispersion (100 mM Al at pH 4.2). Data are means and SD of 3 measurement replicates. Percentage of aluminium that passed through 3 and 1,000 kDa ultrafilters (1-2 and 10-11 nm respectively (Guo and Santschi, 2007)) after addition to BSS (B.) and complete growth media (RPMI+10% FBS, C.) at 1 mM Al. Data are means and SD of 2 independent replicates.

An iron hydroxide nanoparticle coated with adipate and tartrate was selected as a control particle due to its similar size distribution to that of nanosilica. This material, which was fully characterized by Pereira *et al.* (Pereira *et al.*, 2015), maintains its size in BSS media and therefore is suitable for comparison to nanosilica in cell assays.

3.3 Conclusions

In this chapter, a range of nanosilica particles were generated and characterized for use in cell based assays (as described in the subsequent chapters of this thesis). The nanosilica particles generated here were predominantly less than 10 nm in size and dissolved completely within 48 h after dilution below 1 mM Si. The effect of these labile nanosilica dispersions on cells was investigated in the following chapters.

The relationship between particle dissolution and physicochemical properties was also investigated. Particles with a greater persistence in the dilute conditions were found to consist of a greater percentage of fully condensed silicate centres (Q^4). The materials investigated here were less condensed than those investigated in the literature (Kalia *et al.*, 2016). Condensation, within the limited range investigated here, was found to have no effect on the zeta-potential of the particles.

In the following chapters, the effect of nanosilica particles on cells was investigated.

Chapter 4 – The effects of nanosilica on cell viability and function

4.1 Introduction

As noted above, due to its recent use in biomedical applications and the resulting intravenous administration route, the effect of nanosilica on peripheral immune cells has been investigated. Cells of the innate immune system were the focus for most of these studies as many innate immune cell types, including monocytes, phagocytose and clear foreign materials from circulation (Murray and Wynn, 2011). Amorphous nanosilica has been shown to be cytotoxic to monocytic cell lines, both of human and murine origin (Malugin et al., 2011; Mohamed et al., 2011; Nabeshi et al., 2011; Park and Park, 2009; Park et al., 2011; Sandberg et al., 2012; Waters et al., 2009). Nanosilica particles were also shown to decrease viability in peripheral blood mononuclear cell (PBMC) cultures (Fedeli et al., 2013; Mendoza et al., 2014). Lymphocytes were more resistant to the particles compared to monocytes and macrophages, where the overall resistance to the particles was correlated to phagocytic capabilities of the cell (Fedeli et al., 2013).

Although many have studied the effects of particulate silica on cells, little is known as amorphous nanosilica consists of a large range of particles with an even larger range in properties. In these investigations, the effect of nanosilica particles under 10 nm in size on peripheral immune cells (primary, transformed, and cancerous) was investigated. This may infer upon their safety for their therapeutic use.

4.2 Results and discussion

4.2.1 EBV transformed B cells.

B cells virally infected with Epstein-Barr virus, a virus in the herpesvirus family, were used in the initial *in vitro* investigations. These cells are in a constant state of stimulation and have a high risk of developing cancer (Chen, 2011; Saha and Robertson, 2011). Due to their chronic stimulated state, they proliferate quickly which makes them inexpensive and ideal for easy primary cell screening of nanosilica toxicity. CFDA-SE based flow cytometric assays were utilized to test the effect of silicic acid and a 3.6 nm nanosilica dispersion on cell proliferation. Figures 4.01A and B show their effect on the proliferation of the transformed B cells after 24 and 48 h, respectively. Silicic acid had no effect on cell proliferation below 1 mM Si while the cells treated with 3.6 nm nanosilica above 200 μ M Si showed a significant reduction in proliferation from that of the control, an effect that was greatest at 48 h. The nanosilica dispersion also decreased cell viability. Figure 4.01C shows the effect of nanosilica on cell viability and on the proliferation of the viable cells after 48 h incubation. The decrease in proliferation was lower when only the viable cells were considered, which may suggest that growth inhibition was occurring through a cellular damage/toxicity based mechanism. To ensure that the reduction in proliferation was not specific to a certain donor, EBV transformed

B cells from another donor were tested. Figure 4.01D shows the effect of 3.6 nm nanosilica on the proliferation of 2 transformed B cell lines. At the highest concentration of nanosilica, there was significant variability between the two cell lines but growth inhibition by nanosilica was observed in both. Further investigations using this assay (EBV B cell line 1, at 48 h incubation) were conducted to better understand how the nanosilica was interacting with these cells.

Figure 4.02 shows the effect of nanosilica size on the inhibition of transformed B cell proliferation. An increase in median particle size (by volume, DV0.5) from 3.6 nm to 4.7 nm resulted in a 30% decrease in proliferation inhibition. As particle size was increased further the effect on proliferation decreased and, at a median particle size of 25 nm, its effect was no longer statistically different to silicic acid or to micron-sized silica particles which were used as a control. The dissolution rates of the nanosilica particles in simple media were very similar (Figure 3.02A), which may suggest that the larger particles were aggregates of the 3.6 nm particle. However, the significant decrease in proliferation inhibition with size would suggest that aggregates remain intact and do not break up into the smaller particles that they are composed of. Whether the presence of cells or the complexity of media is preventing the large particles from breaking up is unknown.

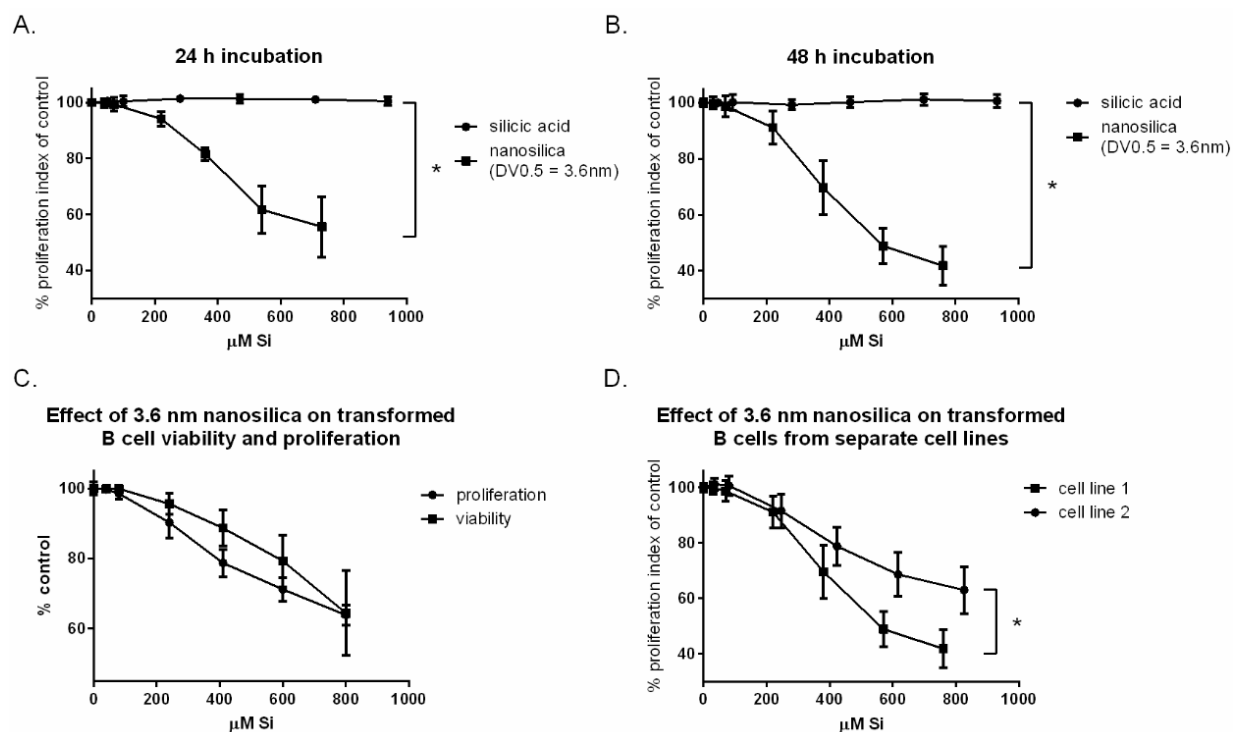


Figure 4.01. The effect of silicic acid and 3.6 nm nanosilica on transformed B cell proliferation after 24 h (A.) and 48 h (B.) incubation at 37 °C. C. The effect of 3.6 nm nanosilica on cell viability and proliferation of viable cells. D. The effect of 3.6 nm nanosilica on transformed B cells from separate donors. (*denotes $p < 0.001$, two-tailed T test, unpaired. Individual percent controls averaged between A. 2 experiments with 3 replicates, B-D. 3 experiments with 3 replicates). (A, B, D) EBV B cells were selected based on FSC versus SSC profiles through a B cell gate also which excluded debris. (C) EBV B cells were first selected based on FSC versus SSC profiles through a B cell gate also which excluded debris, followed by a viability gate (Violet LIVE/DEAD^{LOW}).

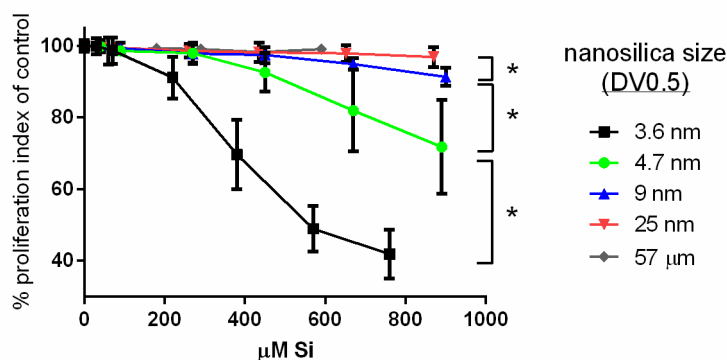


Figure 4.02. The effect of nanosilica size on transformed B cell proliferation. (*denotes $p < 0.001$, two-tailed T test, unpaired. Individual percent controls averaged between 3 experiments with 3 replicates. Size and concentration averaged from the 3 experiments. EBV B cells were selected based on FSC versus SSC profiles through a B cell gate also which excluded debris.

Figure 4.03A shows the effect of nanosilica particles below 2 nm in size on transformed B cell proliferation. Only at concentrations of silicon approaching its solubility limit (polymerization boundary) did the small nanosilica particles have any effect on proliferation. Figure 4.03B shows that the particles below 2 nm in size dissolve much more rapidly than that of the 3.6 nm particles, where complete dissolution was reached before 2 h and 24 h, respectively. It is not known whether the decreased effect of the small nanosilica dispersion on transformed B cells is due to reduced size or increased dissolution rate. Attempts were made to decrease the dissolution rate of the small nanosilica dispersion while maintaining particle size, including doping with metals (Al, Ca, Fe, Zn) and the use of heat, but none were successful (data not shown).

To test the effect of nanosilica dissolution on transformed B cell activity, two nanosilica stocks with median diameters (by volume) of ca. 4.6 nm and varying dissolution profiles were tested. Despite having vastly different dissolution rates (Figure 4.04A), there was little difference in the inhibition of cell proliferation between the two nanosilica dispersions (Figure 4.04B). This would suggest that the decreased activity of the nanosilica dispersion below 2 nm in size is due to size and not due to the dissolution rate. It also would suggest that the effect of nanosilica at 48 h is a result of its interactions with the cells immediately after addition to media, as the lifetime of material A below its solubility is less than 4 h at room temperature.

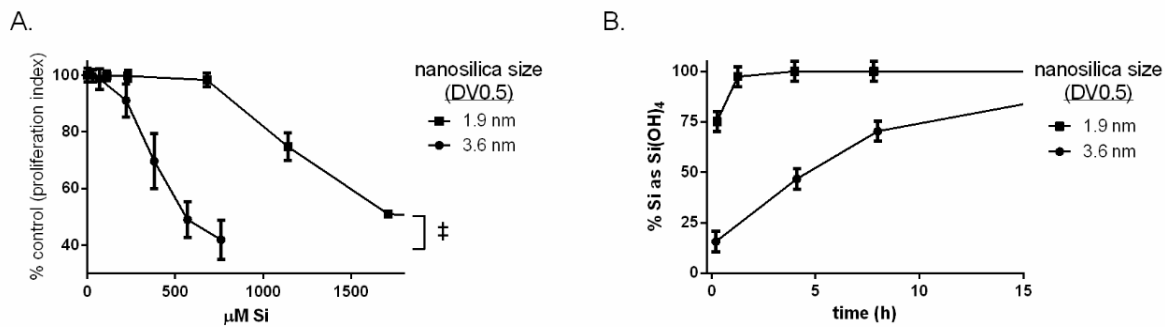


Figure 4.03. A. The effect of 1.9 nm and 3.6 nm nanosilica on the proliferation of transformed B cells. **B.** Dissolution of the nanosilica particles after dilution to ca. 1 mM Si in HEPES buffer (pH 7.0-7.3). (‡ denotes $p < 0.005$, two-tailed T test, unpaired. A. Average of 3 experiments with 3 replicates each). EBV B cells were selected based on FSC versus SSC profiles through a B cell gate also which excluded debris.

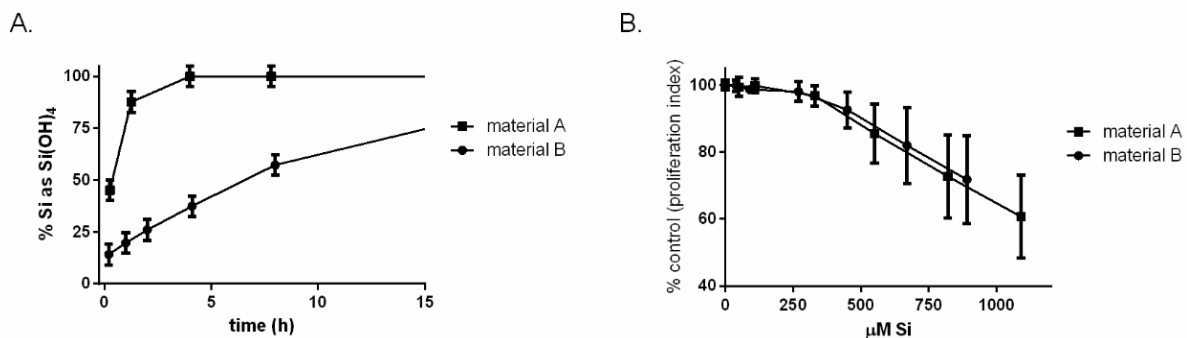


Figure 4.04. A. The dissolution of nanosilica particles ca. 4.6 nm in size prepared at different pHs after dilution to ca. 1 mM Si in HEPES buffer (pH 7.0-7.3). **B.** The effect of these particles on transformed B cell proliferation. (B The % control, size and concentration averaged between 3 independent experiments, each with 3 replicates. EBV B cells were selected based on FSC versus SSC profiles through a B cell gate also which excluded debris.

In summary, the effect of nanosilica on EBV transformed B cells was investigated. Nanosilica was found to decrease the proliferation and induce significant cell death of the virally transformed cells. It is suspected that the decrease in cell proliferation is through a cellular-damage/toxicity based mechanism, as there was a decrease in proliferation inhibition when only viable cells were considered versus all cells. A nanosilica dispersion with a median particle size of 3.6 nm induced greatest inhibition of proliferation, and increasing or decreasing size reduced particle activity. Lastly, the dissolution rate was shown to have little effect on particle activity.

4.2.2 Leukemic monocytic cell line – THP-1

Phagocytic cell lines have been used to assess the safety of nanoparticles. Amorphous silica nanoparticles 20-400 nm in size have been shown to induce cell stress pathways, increase levels of reactive oxygen species and induce cell death of leukemic macrophages and

monocytes (Malugin et al., 2011; Mohamed et al., 2011; Nabeshi et al., 2011; Park and Park, 2009; Park et al., 2011; Sandberg et al., 2012; Waters et al., 2009). Here, the effect of labile nanosilica particles below 10 nm in size on the viability of the leukemic human monocytic cell line THP-1 was investigated.

Figure 4.05 shows the effect of silicic acid and 3.6 nm nanosilica particles on THP-1 viability. Cell viability decreased slightly over time in the control cultures, which may be due to the decrease in available nutrients. Silicic acid had no effect on viability compared to that of the untreated cell culture. Nanosilica, at 800 μM Si, significantly decreased cell viability at 48 and 72 h, though more than 90% of the cells remained viable. Lower concentrations of nanosilica had no effect on viability. Indeed, the toxicity of 3.6 nm nanosilica was similar to nanosilica particles of 20-400 nm in size, where doses below 0.5 mg/mL (ca. 830 μM Si) did not induce significant cell death (Mohamed et al., 2011). These results would suggest that this immortalized cell line is quite resistant to nanosilica, even compared to the transformed B cells. As cell lines are known not to mimic primary cell cultures (Kaur and Dufour, 2012), further investigations using primary peripheral immune cell cultures were employed to assess the safety of the nanosilica particles below 10 nm in size.

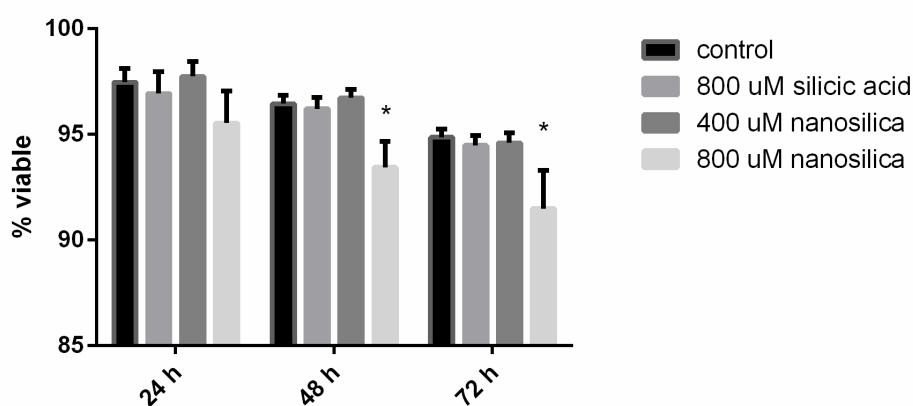


Figure 4.05. The effect of 3.6 nm nanosilica and silicic acid on THP-1 viability (* denotes $p < 0.05$, two-tailed T test, unpaired, averaged between 3 independent experiments, each with 3 replicates). THP-1 cells were first selected based on FSC versus SSC profiles through a THP-1 cell gate also which excluded debris.

4.2.3 Primary peripheral immune cells

Next, the effect of nanosilica particles on primary cells was investigated. Peripheral blood mononuclear cells (PBMCs), which consist of a mixed population of B cells, T cells, NK cells and monocytes, were isolated from blood, treated with nanosilica and analysed using flow cytometry. Monocytes, B cells and T cells were the primary focus of these investigations. Monocytes were identified by the CD11c receptor, which is expressed on monocytes, granulocytes and dendritic cells as it binds various ligands including bacterial components (lipopolysaccharide) (Wu et al., 2009). B cells were identified by the CD19 receptor, which is involved in numerous B cell functions including B cell differentiation (Del Nagro et al., 2005). T cells were identified by the CD3 receptor, which is a component of the T cell receptor complex and is essential in signal transduction during T cell activation (Wang et al., 2009b).

Figure 4.06 shows the effect of nanosilica on monocyte (CD11c⁺), B cell (CD19⁺) and T cell (CD3⁺) viability, as determined using an Invitrogen live-dead stain. The representative histograms show two distinct populations for each cell type, corresponding to viable cells, *i.e.*, those with intact cell membranes which have a lesser fluorescent intensity, and non-viable cells, *i.e.*, those with compromised cell membranes which have a greater fluorescent intensity. The viability decreased after nanosilica treatment. There was also a decrease in the number of cells present in each histogram after nanosilica treatment, which is a result of a significant forward scatter-side scatter (FS-SS) profile shift. Cells that have been treated with nanosilica shift into the region corresponding to cellular debris and, as debris can give false positive signals for viability, it is not possible to incorporate these events in the analysis. Figures 4.07A-F show the combined toxicity of nanosilica towards monocytes, B cell and T cells, represented as both percentage viable and viable cell counts. There was a significant decrease in both monocyte viability and viable monocyte counts after nanosilica treatment, where the counts decreased to <10% of the control after treatment with nanosilica at concentrations >400 μ M Si. Similarly, B cells and T cells also showed significant reductions in both the percentage viable and viable counts after nanosilica treatment, though the decrease in viable counts for these cell types was less than that of monocytes. T cells were most resistant to nanosilica, where its viability remained above 40% after nanosilica treatment at 800 μ M Si. The non-phagocytic nature of T cells is likely related to their increased resistance to the nanoparticulate. Specifically, T cell death would likely rely on membrane nanosilica accumulation rather than intracellular nanosilica overload due to phagocytosis. These results corroborate previous studies, which showed that nanosilica particles were >10 times more toxic towards monocytes and macrophages than towards endothelial cells and lymphocytes (Fedeli et al., 2013), a response assigned to the phagocytic nature of the cells.

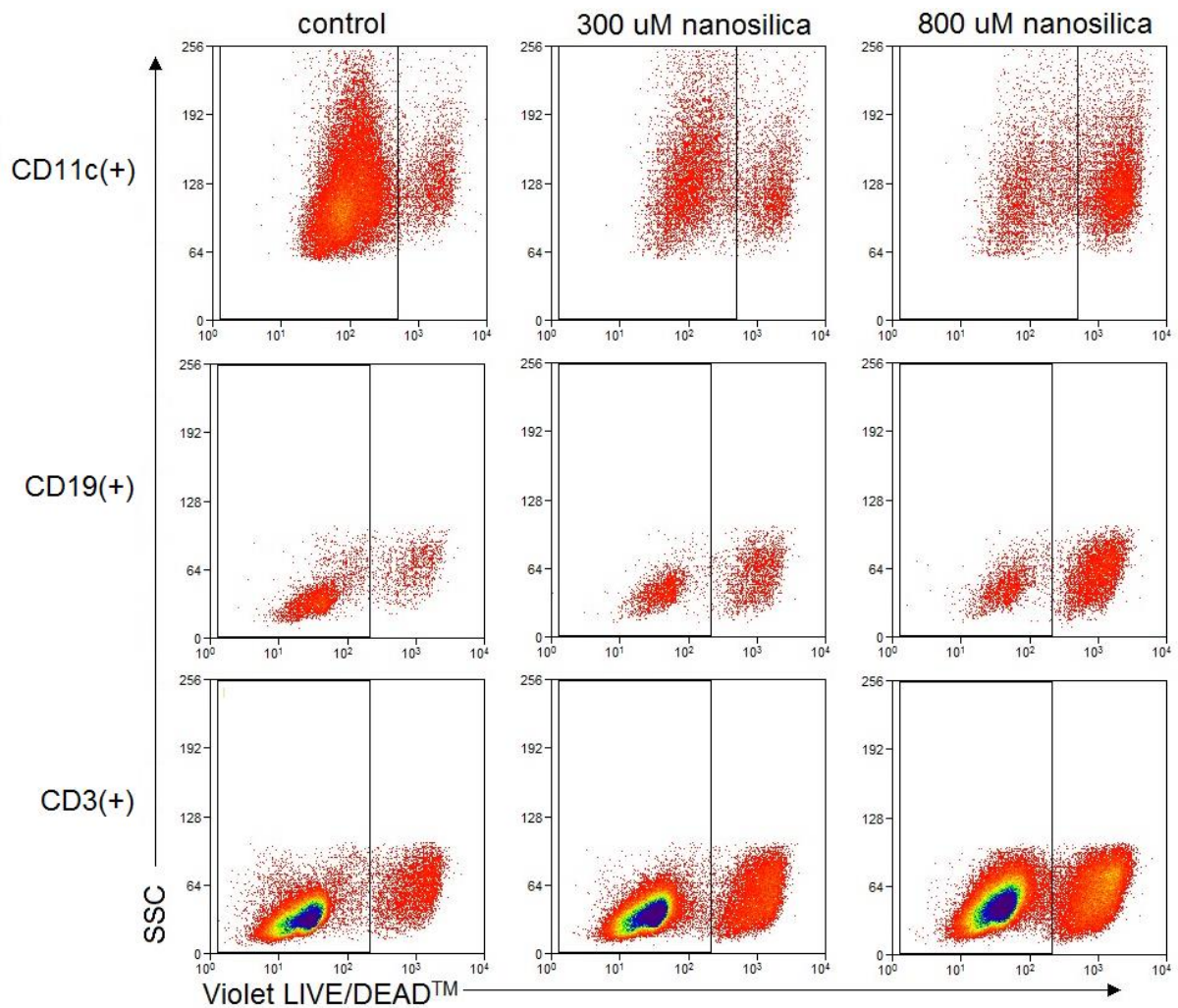


Figure 4.06. Representative FACS plots showing the effect of 3.6 nm nanosilica on monocyte, B cell and T cell viability in PBMC culture at 24 h. Cells were gated through a generous FS-SS gate to exclude debris followed by respective CD11c, CD19 and CD3 gates. Monocytes were first selected based on FSC versus SSC profiles through a monocyte gate which also excluded debris, followed by a CD11c(+) gate. T cells and B cells were first selected based on FSC versus SSC profiles through a lymphocyte gate which also excluded debris, followed by CD3(+) and CD19(+) gate, respectively.

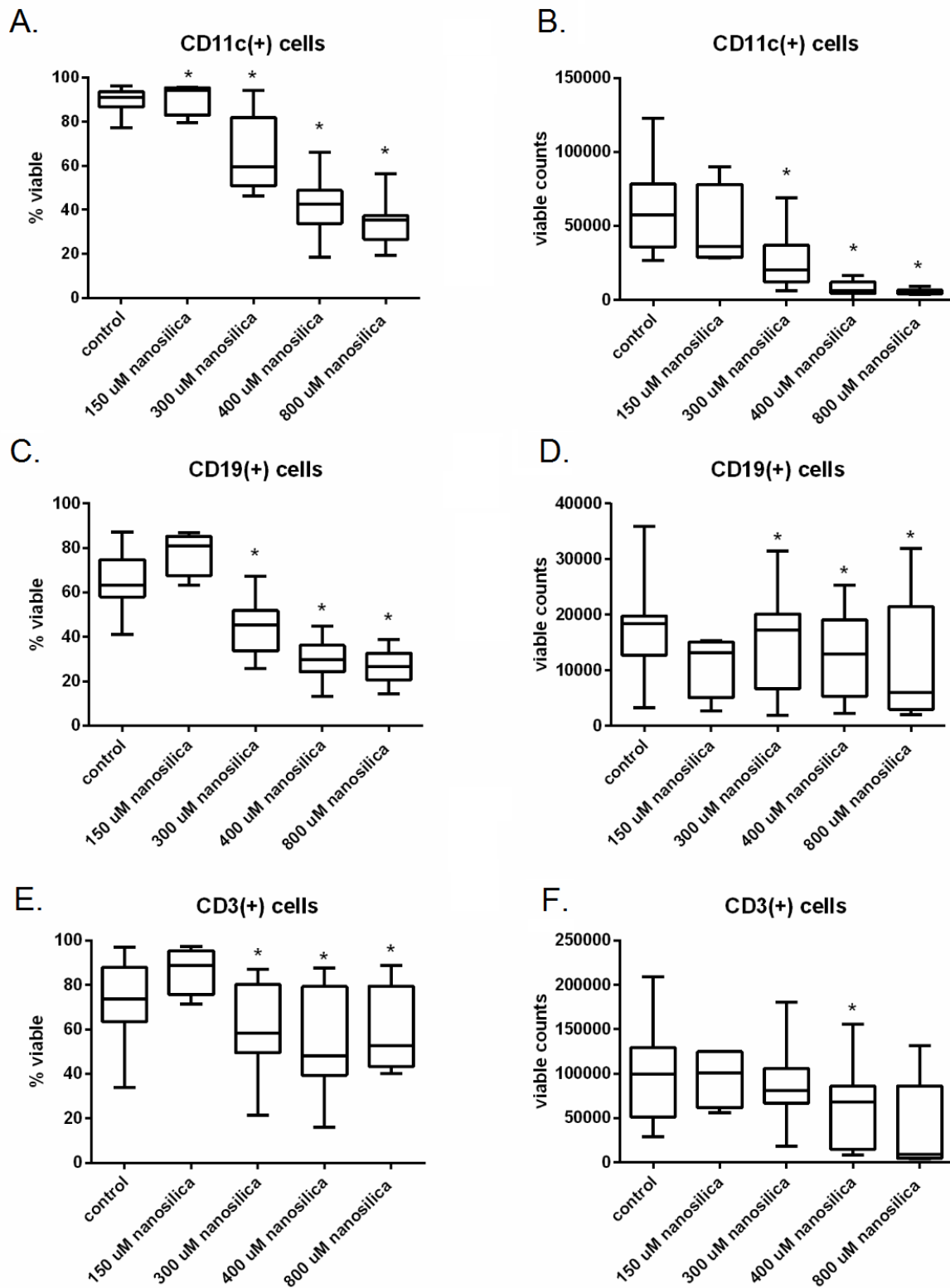


Figure 4.07. The effect of 3.6 nm nanosilica on percent viability and the viable cell counts of CD11c, CD19, and CD3 cells in PBMC culture at 24 h. The data is represented as the averages of 4-18 donors (* denotes a significance compared to the control, two-tailed paired T test, $p < 0.05$). Monocytes were first selected based on FSC versus SSC profiles through a monocyte gate which also excluded debris, followed by a CD11c(+) gate. T cells and B cells were first selected based on FSC versus SSC profiles through a lymphocyte gate which also excluded debris, followed by CD3(+) and CD19(+) gate, respectively.

Next, the mechanism of nanosilica induced cell death was investigated using the Annexin V flow cytometric assay (Biosciences, 2011). In these assays, apoptotic cells were identified through the surface expression of phosphatidylserine (PS, by the Annexin V stain), a protein that translocates from inner to outer cell membrane during apoptosis, and a fully intact membrane, as determined by a lack of intracellular DNA staining. Necrotic cells are also positive for PS but their cellular membranes are permeable to intracellular DNA stains. Cells that have undergone pyroptosis, another inflammatory mode of cell death, are also positive for both intracellular DNA stains and surface PS (Miao et al., 2011). Therefore, it is not possible to distinguish between necrosis and pyroptosis using this assay. Crystalline silica was used as a positive control as it has been previously shown to induce monocyte apoptosis (Joshi and Knecht, 2013).

Figure 4.08 shows the effect of crystalline silica and nanosilica on monocyte (CD11c) apoptosis and necrosis/pyroptosis. The representative histograms (Figure 4.08A) show the intracellular DNA stain (7-AAD) against the Annexin V stain after treatment for 8 h. The majority of monocytes in the untreated cultures were negative for both 7-AAD and Annexin V, indicating that they were viable. After treatment with crystalline silica, the majority of monocytes became Annexin V positive and 7-AAD negative, which would indicate apoptosis was induced. Nanosilica increased the number of cells positive for both Annexin V and 7-AAD, indicating that necrosis/pyroptosis was induced. Figures 4.08B and C show the percentage of monocytes that were apoptotic and necrotic/pyroptotic, respectively, from 0.5 to 24 h. Crystalline silica induced significant apoptosis of monocytes from 2 to 24 h, peaking at 8 h. These results corroborate those that show the majority of macrophages undergo apoptosis after exposure to crystalline particles (Joshi and Knecht, 2013). At 24 h, there was an increase in the percentage of necrotic/pyroptotic monocytes, which likely correspond to cells in late stage apoptosis or those that have completed apoptosis (Poon et al., 2010). There was a significant increase in the percentage of necrotic/pyroptotic monocytes after exposure to nanosilica for 4 to 24 h. Nanosilica only induced significant monocyte apoptosis 8 h after treatment. These results would suggest the majority of monocytes are dying through either necrosis or pyroptosis. Fedeli *et al.* showed that amorphous nanosilica particles can induce both necrosis and pyroptosis of monocytes, where the mechanism of cell death is dependent on the protein concentration (Fedeli et al., 2014). Specifically, pyroptosis is induced by nanosilica in media containing 10% FBS and necrosis is induced by the particulate in protein free conditions. These results would suggest that pyroptosis was induced in the investigations conducted here, as media containing 10% FBS was used. Pyroptosis is regulated through the same caspases that also regulate the production of IL-1 β and IL-18 (Jorgensen and Miao, 2015). To determine whether monocyte cell death occurs through necrosis or pyroptosis, the levels of IL-1 β in cell supernatants was assessed. Figure 4.09 shows the levels of IL-1 β in cell supernatants after 24 h. Low nanosilica concentrations were used to avoid complete cell death. Nanosilica

induced low levels of IL-1 β production, which may suggest that some cells are dying through pyroptosis. However, the induction of monocyte necrosis cannot be ruled out.

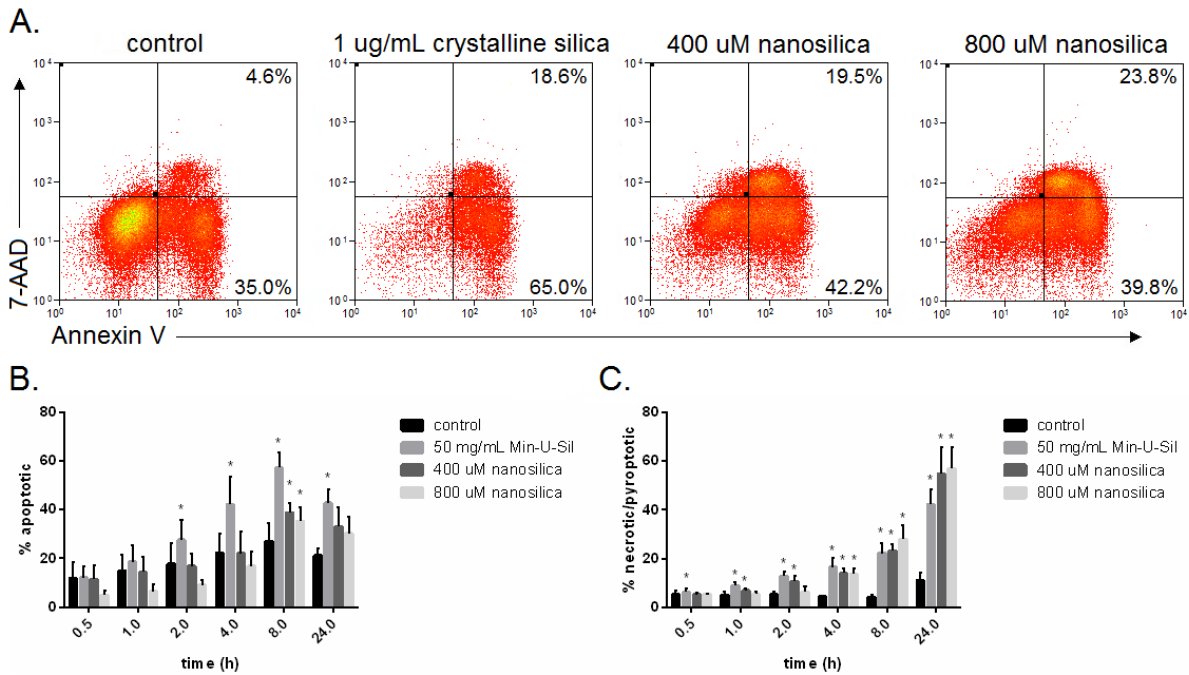
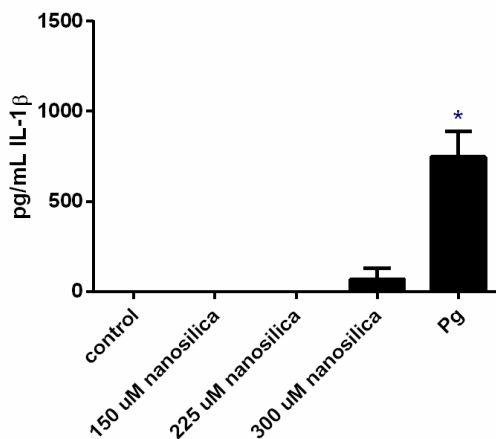


Figure 4.08. The effect of 3.6 nm nanosilica on monocyte apoptosis and necrosis. A. Representative histogram plots showing the effect of nanosilica treatment CD11c⁺ monocyte Annexin V and 7-AAD positivity at 8 h. The percentage of CD11c cells that are apoptotic (**B.**) or necrotic/pyroptotic (**C.**). Tabulated data represents the means \pm standard deviation for 4 donors (* denotes a significance compared to the control, two-tailed paired T test, $p < 0.05$). Monocytes were first selected based on FSC versus SSC profiles through a monocyte gate which also excluded debris, followed by a CD11c(+) gate.



Next, the mode of T cell death induced by nanosilica was investigated. Attempts were made to first identify the T cells by the T cell receptor (TCR), which recognises cognate antigen in an MHC receptor on an antigen presenting cells or infected/stressed cells. However, nanosilica inhibited staining of the TCR $\alpha\beta$ antibody from 0-2 h (example shown in Figure 4.10A). Further studies showed that nanosilica also inhibited staining of the CD3 ϵ antibody during that same time window (this was explored in more detail in Chapter 6). As the unbound nanosilica was washed from the system prior to staining the cells and that other T cell stains were not inhibited, it is possible that nanosilica directly interacts with the receptor. Indeed, studies conducted in Chapters 5 and 6 would confirm this interaction and show the consequences of it. For the studies of cell death conducted here, a specialized gating strategy was employed to analyse the data, where the TCR $\alpha\beta$ stain was ignored. Instead, cells were identified by the CD4 and CD8 co-receptors, which are expressed on helper and cytotoxic T cells, respectively, and bind the TCR:MHC complex during antigen presentation. The two T cell subsets have varying functions, where helper T cells mediate an immune response (by releasing cytokines and through expression of surface receptors) and cytotoxic T cells execute the immune response (by directly engaging unhealthy cells and releasing factors to induce their death). Figure 4.10B shows the gating strategy to select the CD4 and CD8 cells. As monocytes are known to express CD4 and CD8 (Gibbings et al., 2007; Kazazi et al., 1989; Zhen et al., 2014), they were excluded from the analyses using a CD11c stain.

The effect of crystalline silica and nanosilica on CD4(+) and CD8(+) cell apoptosis and necrosis/pyroptosis is shown in Figure 4.10C (representative histograms) and Figure 4.11 (percentage positive). Crystalline silica had little effect on CD4(+) cells as neither apoptosis (Figure 4.11A) nor necrosis/pyroptosis (Figure 4.11B) was significantly induced after exposure to the particles. On CD8(+) cells, there was a significant induction of necrosis/pyroptosis (Figure 4.11D) 1-2 h after treatment with crystalline silica. In the literature, the short term effects of these particles on T cell apoptosis and necrosis are not known. However, chronic exposure to crystalline silica has been shown to increase T cell expression of the Fas death receptor that, when engaged, induces cell apoptosis (Hayashi, 2010).

Nanosilica induced significant apoptosis of CD4(+) cells from 0.5 to 24 h. The induction of apoptosis was greatest at 24 h, which might suggest that nanosilica is inducing apoptosis indirectly. For example, nanosilica may be inducing T cell death via the activation induced cell death (AICD) pathway. This process can be initiated by numerous signals and is mediated by the expression of death receptors, such as the Fas (CD95) death receptor (Arakaki et al., 2014; Tummers and Green, 2017). Further studies (Chapter 5) showed that the percentage of CD4 T cells positive for CD95 increased after nanosilica treatment. Nanosilica also significantly increased the percentage of necrotic/pyroptotic CD4(+) cells at 24 h, likely corresponding to cells in late stage apoptosis or those that have completed apoptosis (Poon et al., 2010).

Nanosilica induced significant apoptosis and necrosis/pyroptosis of CD8(+) cells. As with the CD4(+) cells, the induction of apoptosis may occur through AICD as the levels of CD95 on CD8 T cells increased (non-significantly) after nanosilica treatment. It is unknown whether the 7-AAD, Annexin V double positive cells correspond to those that have undergone necrosis or pyroptosis. Whether the IL-1 β present in supernatant was produced by T cells is unknown. Therefore, it is not possible to determine which inflammatory mode of cell death the cells are following.

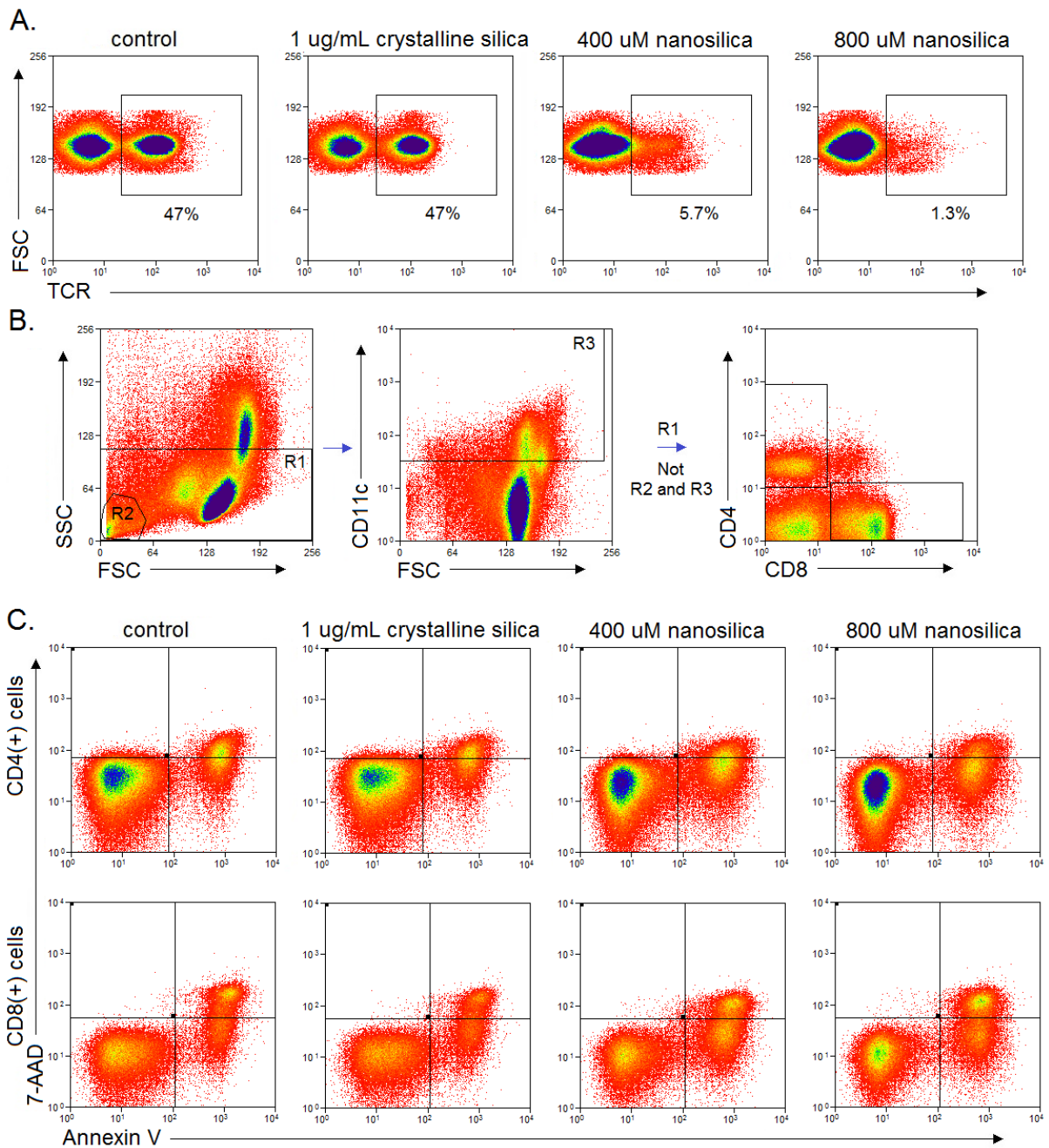


Figure 4.10. A. Representative histograms showing the effect of 3.6 nm nanosilica on TCR $\alpha\beta$ cell staining within a T cell FS-SC selection gate at 0.5 h. **B.** Gating strategy for selection of CD4 and CD8 cells. **C.** Representative histogram plots showing the effect of nanosilica treatment on CD4 and CD8 cell Annexin V and 7-AAD positivity at 8 h. T cells were first selected based on FSC versus SSC profiles through a lymphocyte gate, followed by negatively gating out debris and monocytes (CD11c(+)). Helper and cytotoxic T cells were then selected with respective CD4(+) and CD8(+) gates

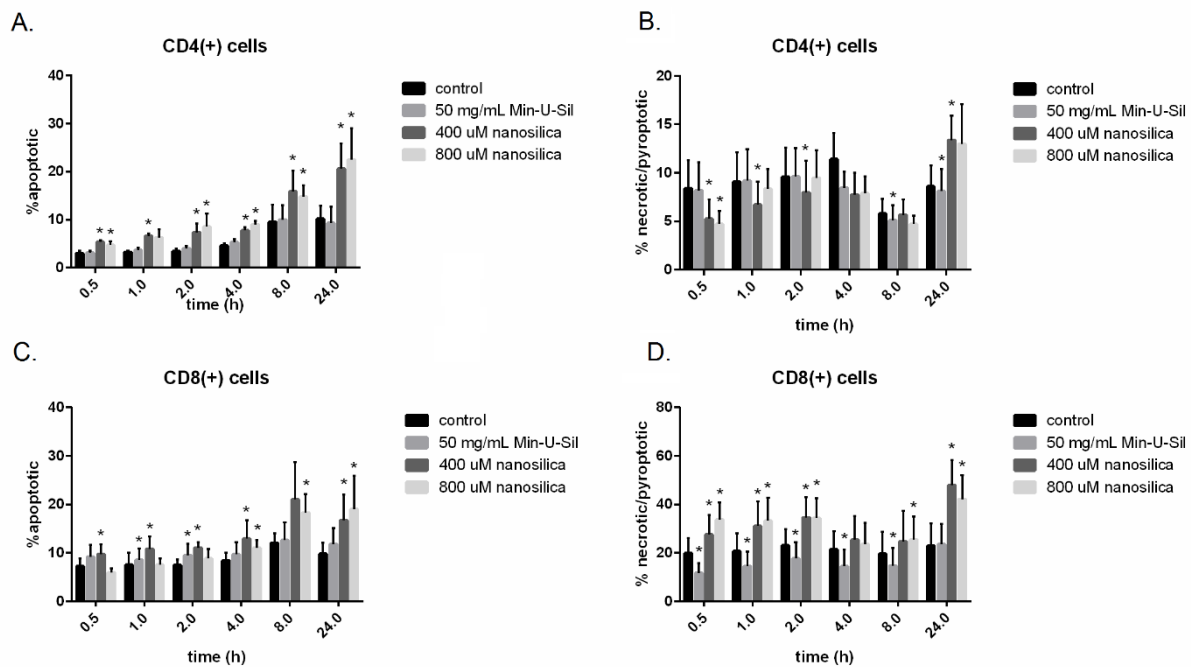


Figure 4.11. The effect of 3.6 nm nanosilica on CD4 (A, B) and CD8 (C, D) cells apoptosis and necrosis/pyroptosis. Tabulated data represents the means \pm standard deviation for 4 donors (* denotes a significance compared to the control, two-tailed paired T test, $p < 0.05$). T cells were first selected based on FSC versus SSC profiles through a lymphocyte gate, followed by negatively gating out debris and monocytes (CD11c(+)). Helper and cytotoxic T cells were then selected with respective CD4(+) and CD8(+) gates

The effect of nanosilica on monocyte function

Though there are studies that show the negative effects of nanosilica on phagocyte function (Fedeli et al., 2014; Fedeli et al., 2013; Mendoza et al., 2014), there are contradicting reports which show that nanosilica enhances antigen presenting cell (APC) activity. Nanosilica particles have been found to increase cross presentation of antigens by APCs (Hirai et al., 2012) and, consequently, have also been shown to increase T cell response to antigen (Brandenberger et al., 2013; Chen et al., 2014; Marzaioli et al., 2014). The nanosilica particles used in the literature were larger and more persistent than those tested here. Thus, whether nanosilica particles under 5 nm in size also alter monocyte function was investigated here. Again, low doses were used to avoid significant cell death.

First, the effect of nanosilica on the phagocytosis of other foreign materials by monocytes was investigated. Figures 4.12A-C show the effect of nanosilica on fluorescent bead uptake by monocytes. The representative histograms shows 2 populations with high CD11c positivity, corresponding to bead negative and positive cells. At the highest concentration of nanosilica used, there was a decrease in number of monocytes present in the histograms and, therefore, these concentrations should be considered toxic. After 1 h, more than half of the monocytes in the control groups were positive for the fluorescent beads. Increasing the incubation time further had little effect on cell positivity, as shown in the Figures 4.12B-C. Treating the cells

with low dose nanosilica decreased bead phagocytosis, both in the percentage of cells positive for beads and the fluorescent intensity of cells bead positive, *i.e.*, the number of beads the cell phagocytosed. These results would suggest that nanosilica has negative effects on monocyte phagocytosis of foreign materials, even at concentrations under 150 μM Si. The effect of orthosilicic acid on bead phagocytosis was investigated to ensure that these responses were due to nanosilica, and not its degradation product. Figure 4.12C-D shows the effect of silicic acid on bead uptake. Unlike the particles, orthosilicic acid did not affect bead phagocytosis.

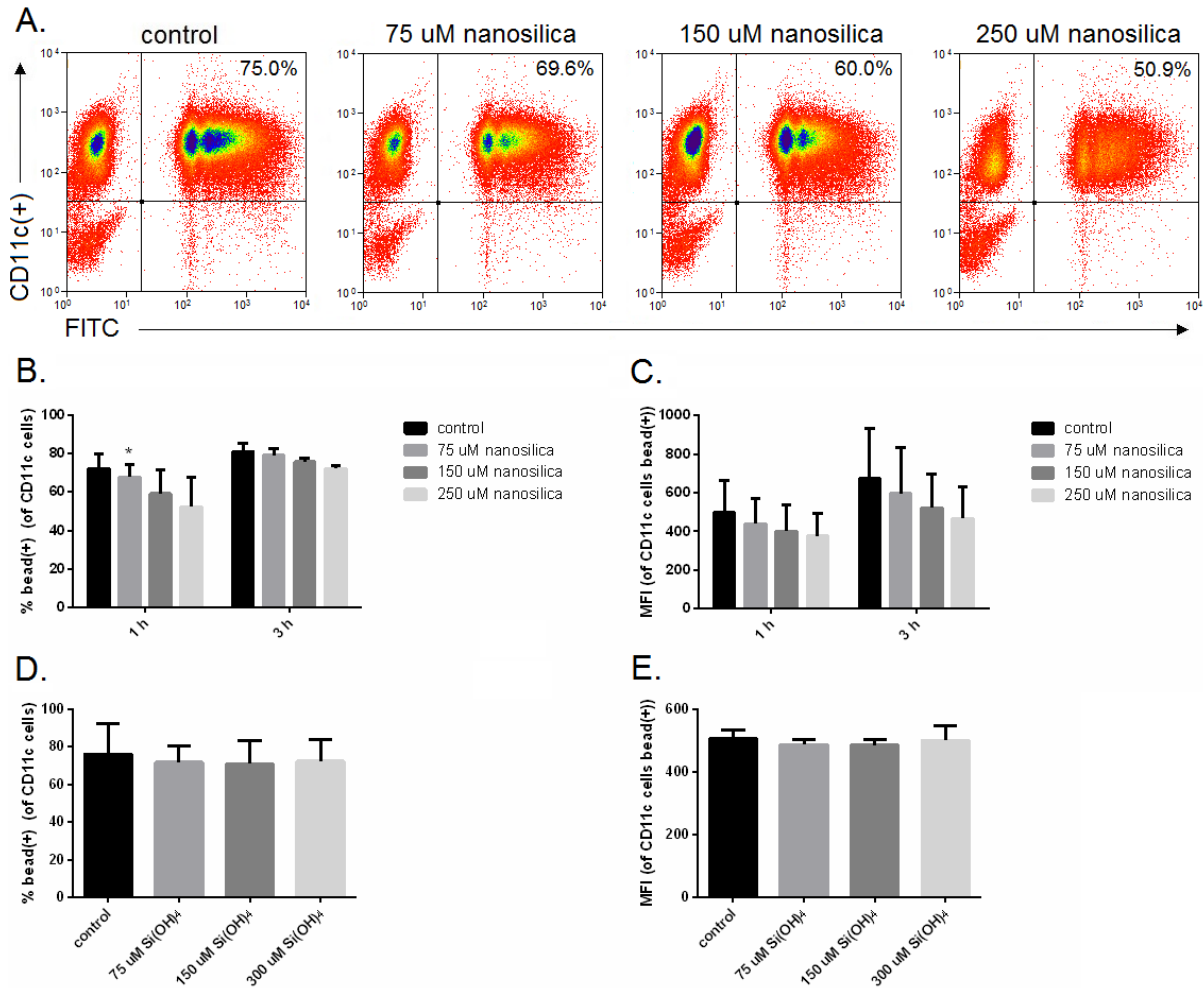


Figure 4.12. The effect of 3.6 nm nanosilica and silicic acid on the phagocytosis of polystyrene fluorescent beads by monocytes. **A.** Representative FACS plots showing the CD11c cells positive for fluorescent beads after 1 h incubation. The percentage of CD11c cells positive for fluorescent beads (**B.**) and the mean fluorescent intensity of the bead positive cells (**C.**) after nanosilica treatment for 1 and 3 h. The percentage of CD11c cells positive for fluorescent beads (**D.**) and the mean fluorescent intensity of the bead positive cells (**E.**) after silicic acid treatment for 1 h. Tabulated data represents the means \pm standard deviation for 3 donors (* denotes a significance compared to the control, two-tailed paired T test, $p < 0.05$). Monocytes were first selected based on FSC versus SSC profiles through a monocyte gate, followed by a monocyte gate (CD11c(+)) and a viability gate (Violet LIVE/DEAD^{LOW}).

As confirmation, the effect of nanosilica on bacterial uptake by monocytes was investigated, using fluorescent (non-viable) *Staphylococci aureus*. Figures 4.13A-B show the effect of nanosilica on monocyte bacterial uptake. Similar to the investigations with the fluorescent beads, nanosilica decreased the percentage of cells positive for bacteria, though mean fluorescent intensity only decreased at 3 h. These results would suggest that nanosilica, at subtoxic doses, has negative effects on monocyte function. Indeed, when the previous data was combined, nanosilica (at 150 μ M Si) significantly decreased the percentage of cells positive for beads or bacteria (1 h, $p = 0.0190$ and 3h, $p = 0.0090$, two-tailed paired T test). To ensure that decreased bead and bacterial positivity was not due to enhanced degradation of the fluorescent material, flow imaging analyses were conducted in parallel (Appendix 3). There was no evidence that nanosilica enhanced degradation of the fluorescent materials, which would suggest that nanosilica decreases monocyte phagocytosis of foreign materials.

In addition to the processing and presentation of antigen to T cells via the MHC receptors, blood derived monocytic cells also provide secondary signals. These signals can be stimulatory, e.g., CD80/86-CD28 signalling, or inhibitory, e.g., PD-L1-PD-1 signalling (Chen and Flies, 2013). Inhibitory signals, such as PD-L1, serve as checkpoint inhibitors and limit the immune response (Keir et al., 2008). If PD-L1 expression was altered so would the immune response. The effect of nanosilica pre-treatment on monocyte PD-L1 expression in response to peptidoglycan (PG), which has been shown to induce its expression on healthy monocytes (Hewitt et al., 2012), was investigated. Figure 4.14 shows the effect of nanosilica pre-treatment on monocyte PD-L1 expression. As with the previous analysis, the number of monocytes present in the histograms decreased after nanosilica treatment. Nanosilica pre-treatment at near-toxic doses decreased PD-L1 expression in a dose dependant manner, both in the percentage of cells positive for PD-L1 and the intensity of its expression (data not shown). It is likely that the decrease in PD-L1 expression is associated with cell death, as only at concentrations in which there was a significant decrease in monocyte cell counts was there a significant decrease in PD-L1 expression. Sub-toxic dose of nanosilica (150 μ M) had no effect on monocyte PD-L1 expression.

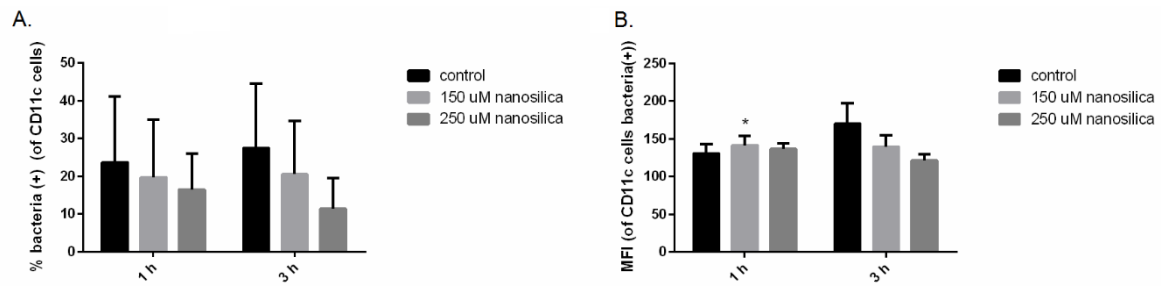


Figure 4.13. The effect of 3.6 nm nanosilica on the phagocytosis of fluorescent *S. aureus* by monocytes. The percentage of CD11c cells positive for fluorescent bacteria and the mean fluorescent intensity of the bacteria positive cells after nanosilica treatment for 1 and 3 h. Tabulated data represents the means \pm standard deviation for 3 donors (* denotes a significance compared to the control, two-tailed paired T test, $p < 0.05$). Monocytes were first selected based on FSC versus SSC profiles through a monocyte gate, followed by a monocyte gate (CD11c(+)) and a viability gate (Violet LIVE/DEAD^{LOW}).

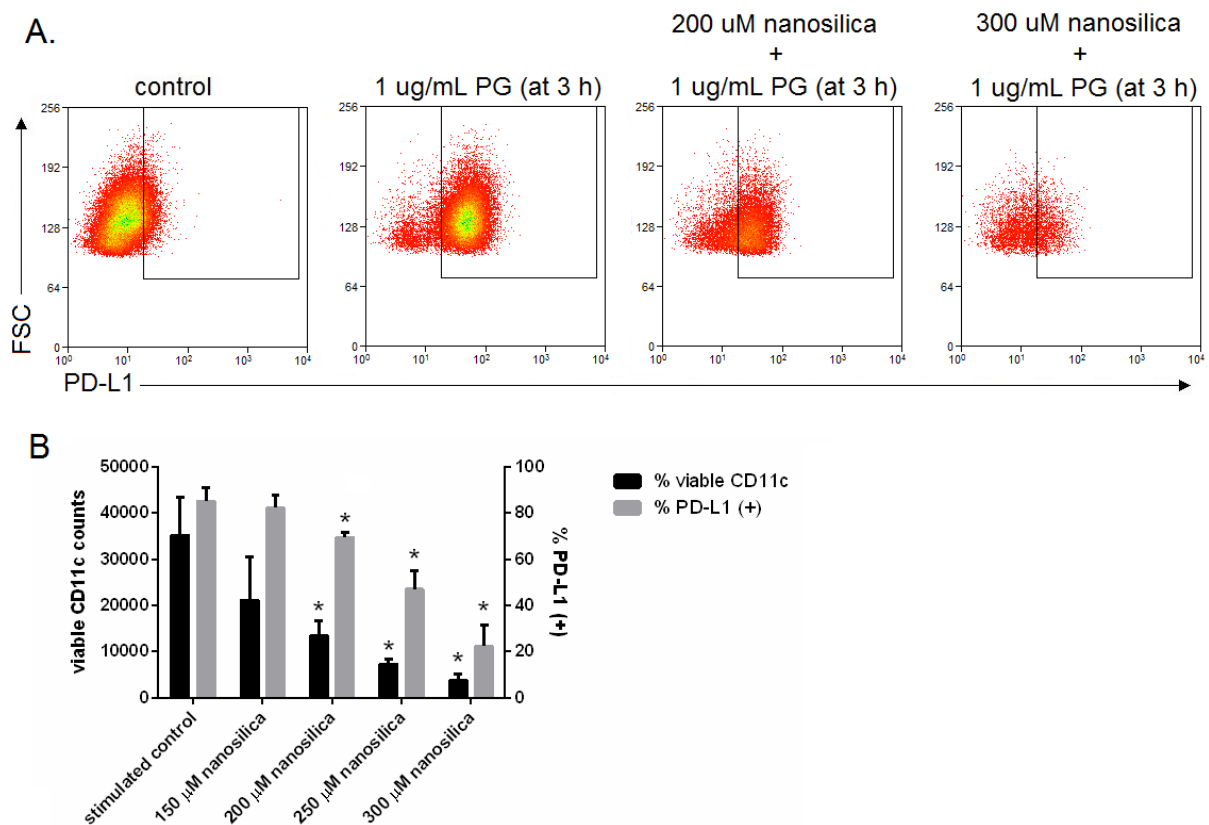


Figure 4.14. The effect of 3.6 nm nanosilica on PD-L1 expression by monocytes. **A.** Representative FACS plots showing the CD11c cells positive for PD-L1. **B.** The percentage of CD11c cells positive for PD-L1 and the viable CD11c counts. Tabulated data represents the means \pm standard deviation for 3 donors (* denotes a significance compared to the control, two-tailed paired T test, $p < 0.05$). Monocytes were first selected based on FSC versus SSC profiles through a monocyte gate, followed by a monocyte gate (CD11c(+)) and a viability gate (Violet LIVE/DEAD^{LOW}).

4.2.4 Gene array analysis

A microarray was conducted to better understand the effects of nanosilica on cell function. Three cell culture types, EBV transformed B cells, THP-1 cells, and PBMCs, were treated with a nanosilica dispersion 3.6 nm in size (at 150 μ M Si, to avoid significant cell death) and incubated for 4 h prior to RNA collection for gene assays performed by Dr Mark Boekschoten (Wageningen University, Netherlands). The expression of genes most significantly affected by nanosilica, and other genes of interest, were presented here.

First, the effect of nanosilica on EBV transformed B cell gene expression was investigated. Earlier in this chapter, nanosilica was shown to inhibit proliferation and induce death of the transformed cells, though these effects were only evident at concentrations higher than those used here. Table 4.01 shows the genes for which their expression was significantly altered by nanosilica treatment compared to that of the control. Nanosilica significantly increased expression of the gene corresponding to CCL3 (Macrophage inflammatory protein 1 α , MIP-1 α). MIP-1 α is a chemotactic cytokine (chemokines) that is released during cellular injury or infection for the recruitment of proinflammatory immune cells (Maurer and Von Stebut, 2004; Menten et al., 2002). Similarly, the gene corresponding to CCL4 (MIP-1 β), a chemokine in the same family of inflammatory proteins as CCL3, was more highly expressed after nanosilica treatment, though to a lesser extent. These results may suggest that nanosilica is inducing an inflammatory response in the EBV transformed B cells, potentially through nanosilica induced cell damage (injury). Nanosilica has previously been shown to induce expression of these genes in the leukemic murine macrophage RAW 264.7 cell line with nanosilica particles 10 and 500 nm in size (Waters et al., 2009).

The expression of many genes associated with cholesterol biosynthesis were also significantly increased after nanosilica treatment. The most highly up-regulated gene pathways involved cholesterol biosynthesis (Table 4.02). These results corroborate studies that have shown nanosilica particles 100-400 nm in size increase cholesterol biosynthesis (Chatterjee et al., 2016). As particles with a greater surface area are known to alter cholesterol biosynthesis to a greater extent (Chatterjee et al., 2016), it is not surprising that the 3.6 nm nanosilica particles used here induced the expression of these genes at concentrations 10 times lower than those previously employed.

Pathways associated with NF- κ B and inflammation were also significantly up-regulated after nanosilica treatment (Table 4.03). NF- κ B signalling is a key regulator of the immune system, initiated in response to infection or injury, and is also associated with inflammation (Hoesel and Schmid, 2013; Napetschnig and Wu, 2013; Oeckinghaus et al., 2011). As with the induction of the CCL3 and CCL4 genes, nanosilica may be inducing cellular damage thus initiating NF- κ B signalling. Other gene groups shown in Table 4.03 are associated with poor tumour prognosis and autoimmunity. TWEAK and TNFR2 signalling pathways, both of which are linked to NF- κ B

signalling, can lead to cell survival and proliferation instead of apoptosis (Faustman and Davis, 2010; Winkles, 2008).

Table 4.01. Individual genes in EBV transformed B cells whose expression was significantly altered by 3.6 nm nanosilica compared to that of the control

gene name	description	Limma Fold	
		Change	q
HMGCS1	3-hydroxy-3-methylglutaryl-CoA synthase 1 (soluble)	1.396	0.000
LDLR	low density lipoprotein receptor	1.286	0.000
HILPDA	hypoxia inducible lipid droplet-associated	-1.583	0.000
CCL3	chemokine (C-C motif) ligand 3	1.813	0.001
SQLE	squalene epoxidase	1.354	0.001
PFKFB4	6-phosphofructo-2-kinase/fructose-2,6-biphosphatase 4	-1.476	0.001
EGLN3	egl-9 family hypoxia-inducible factor 3	-1.421	0.001
MYLIP	myosin regulatory light chain interacting protein	-1.299	0.003
HMGCR	3-hydroxy-3-methylglutaryl-CoA reductase	1.277	0.003
INSIG1	insulin induced gene 1	1.282	0.003
MSMO1	methylsterol monooxygenase 1	1.395	0.003
DUSP10	dual specificity phosphatase 10	1.328	0.005
DHCR24	24-dehydrocholesterol reductase	1.219	0.005
ANKRD37	ankyrin repeat domain 37	-1.740	0.005
ZC3H6	zinc finger CCCH-type containing 6	-1.428	0.005
RGS1	regulator of G-protein signaling 1	1.317	0.005
CD86	CD86 molecule	1.199	0.016
SSTR2	somatostatin receptor 2	1.308	0.016
DHCR7	7-dehydrocholesterol reductase	1.212	0.021
NRROS	negative regulator of reactive oxygen species	1.248	0.029
SNORD14E	small nucleolar RNA, C/D box 14E	1.492	0.033
DNTTIP2	deoxynucleotidyltransferase, terminal, interacting protein 2	1.132	0.048

Table 4.02. Gene pathways in EBV transformed B cells whose expression was significantly altered by 3.6 nm nanosilica compared to that of the control, showing the number of genes in the pathway (size), normalized enrichment scores (NES) and q-values

name	size	NES	q
CHOLESTEROL.BIOSYNTHESIS	22	2.760	0.00000
WP1795.CHOLESTEROL.BIOSYNTHESIS	19	2.657	0.00000
WP197.CHOLESTEROL.BIOSYNTHESIS	17	2.630	0.00000
ACTIVATION.OF.GENE.EXPRESSION.BY.SREBF.SREBP.	40	2.600	0.00000
KEGG_STEROID.BIOSYNTHESIS	20	2.484	0.00000
WP2706.ACTIVATION.OF.GENE.EXPRESSION.BY.SREBP.SREBF.	38	2.459	0.00000
REGULATION.OF.CHOLESTEROL.BIOSYNTHESIS.BY.SREBP.SREBF.	53	2.451	0.00000
KEGG_RIBOSOME.BIOGENESIS.IN.EUKARYOTES	73	2.226	0.00044
WP1982.SREBP.SIGNALLING	63	2.176	0.00167
WP2710.NONSENSE.MEDIATED.DECAY	118	2.171	0.00174
WP2011.SREBF.AND.MIR33.IN.CHOLESTEROL.AND.LIPID.HOMEOSTASIS	17	2.162	0.00190

Table 4.03. Gene pathways associated with apoptosis in EBV transformed B cells whose expression was significantly altered by 3.6 nm nanosilica compared to that of the control

name	size	NES	q
BIOC_TNFR2PATHWAY	18	2.134	0.003
BIOC_STRESSPATHWAY	25	2.116	0.003
BIOC_NFKBPATHWAY	22	2.003	0.009
KEGG_NF.KAPPA.B.SIGNALING.PATHWAY	86	1.906	0.023
WP2036.TWEAK.SIGNALING.PATHWAY	41	1.817	0.036
P75NTR.SIGNALS.VIA.NF.KB	15	1.837	0.037
WP254.APOPTOSIS	84	1.804	0.040

The response of THP-1 cell, a leukemic monocyte cell line, to nanosilica was investigated next. Table 4.04 shows the genes whose expression was up- or down-regulated 4 h after treatment with nanosilica compared to that of the control. There were very few genes whose expression was affected by nanosilica treatment. Nanosilica induced expression of genes corresponding to proteins with varying functions, such as negative regulation of cytoskeletal organization (RND3), cancerous cell growth delay (GPNMB), and breakdown of serine. Most of the genes whose expression was altered by nanosilica were unrelated as only one gene pathway showed a difference in overall expression after treatment with nanosilica. Gene group WP2739 amyloids was significantly increased after nanosilica treatment (NES 2.1266, FDR q value 0.015685). Amyloids, which are protein aggregates, are associated with many diseases such as Alzheimer's and diabetes (Knowles et al., 2014). These results might suggest nanosilica increases amyloid production. The decreased genomic response of the monocytic cell line investigated here compared to the macrophagic cell line investigated in the literature (Waters et al., 2009), could be due to reasons such as concentration (150 μ M vs 800 μ M), the cancerous cell state and/or origin of the cells (human vs mouse).

Table 4.04. Individual genes in THP-1 cells whose expression was significantly altered by 3.6 nm nanosilica compared to that of the control

gene name	description	Limma Fold Change	q
SDS	serine dehydratase	2.157	0.0066
SGK1	serum/glucocorticoid regulated kinase 1	1.474	0.0066
TBC1D30	TBC1 domain family, member 30	-1.482	0.0066
MYLIP	myosin regulatory light chain interacting protein	-1.345	0.0066
HMOX1	heme oxygenase (decycling) 1	1.641	0.0433
RND3	Rho family GTPase 3	1.570	0.0433
NUPR1	nuclear protein, transcriptional regulator, 1	1.377	0.0433
GPNMB	glycoprotein (transmembrane) nmb	1.252	0.0480

The response of primary cells to nanosilica was investigated next. PBMC cultures, a mixed cell culture consisting of monocytes, B cells, T cells and other lymphocytes, were used. Table 4.05 shows the genes of interest whose expression was significantly altered after nanosilica treatment. A number of genes associated with T cell function were more highly expressed after nanosilica treatment. Specifically, the expression of the genes corresponding to the Ly9 protein, a member of the signalling lymphocytic activation marker (SLAM) family, and CRTAM, a CD8 T cell and natural killer T cell (NKT) activation marker, increased in cultures exposed to nanosilica (Patiño-Lopez et al., 2006; Schwartzberg et al., 2009). The expression of other genes associated with T cell activation also increased, including iCOS, CD69, IFN- γ , and IL-10 (Geginat et al., 2015; Radulovic et al., 2013; Wikenheiser and Stumhofer, 2016). Whether these responses are related to the inhibition of T cell receptor staining shown in Figure 4.10 was investigated in Chapters 5 and 6. Table 4.06 shows the gene groups whose expression was significantly up or down regulated after nanosilica treatment. As with the transformed B cells, nanosilica induced expression of genes associated with cholesterol biosynthesis, inflammation (WP530 cytokine and inflammatory response) and NF- κ B signalling (P75NTR. Signals via NF- κ B) in primary cell culture. There were also some lysosomal and endosomal genes induced after exposure to nanosilica, potentially suggesting that nanosilica is being phagocytosed by monocytes.

Table 4.05. Individual genes in PBMC culture whose expression was significantly altered by 3.6 nm nanosilica compared to that of the control

gene name	description	Limma Fold Change	q
SPINK1	serine peptidase inhibitor, Kazal type 1	11.329	0.016
NRIP3	nuclear receptor interacting protein 3	4.049	0.022
FNIP2	folliculin interacting protein 2	6.181	0.022
CSTB	cystatin B (stefin B)	2.126	0.031
TMEM38B	transmembrane protein 38B	2.140	0.031
ASAH1	N-acylsphingosine amidohydrolase (acid ceramidase) 1	2.375	0.031
CRISPLD2	cysteine-rich secretory protein LCCL domain containing 2	-2.428	0.031
LRRK2	leucine-rich repeat kinase 2	-2.822	0.031
CD79B	CD79b molecule, immunoglobulin-associated beta	-2.412	0.031
LY9	lymphocyte antigen 9	2.409	0.034
NR4A3	nuclear receptor subfamily 4, group A, member 3	2.221	0.034
CCRL2	chemokine (C-C motif) receptor-like 2	2.797	0.034
DUSP3	dual specificity phosphatase 3	2.063	0.034
PTGFRN	prostaglandin F2 receptor inhibitor	-3.506	0.038
GAS2L3	growth arrest-specific 2 like 3	2.985	0.038
BRI3	brain protein I3	1.792	0.048
NRP2	neuropilin 2	2.240	0.048
CRTAM	cytotoxic and regulatory T cell molecule	2.666	0.048
BMF	Bcl2 modifying factor	-2.185	0.048
CD72	CD72 molecule	2.129	0.048

Table 4.06. Gene pathways in PBMC culture whose expression was significantly altered by 3.6 nm nanosilica compared to that of the control

name	size	NES	q
KEGG Lysosome	122	2.41	0
Transferrin endocytosis and recycling	29	2.34	0
KEGG Collection duct acid secretion	27	2.33	0
Iron uptake and transport	43	2.30	0
WP2670 Iron uptake and transport	11	2.27	0
WP2700 Latent infection of homo sapiens with <i>Mycobacterium tuberculosis</i>	30	2.27	0
Latent infection of homo sapiens with <i>Mycobacterium tuberculosis</i>	33	2.21	2.09 x 10 ⁻⁴
Phagosomal maturation early endosomal stage	33	2.23	2.35 x 10 ⁻⁴
Insulin receptor recycling	26	2.23	2.69 x 10 ⁻⁴
Sphingolipid metabolism	69	2.15	3.84 x 10 ⁻⁴
KEGG Sphingolipid metabolism	47	2.03	6.82 x 10 ⁻³
Glycosphingolipid metabolism	38	2.01	7.86 x 10 ⁻³
KEGG <i>Vibrio cholerae</i> infection	54	2.00	8.83 x 10 ⁻³
WP516 Hepertrophy model	20	1.98	0.0107
KEGG Synaptic vesicle cycle	63	1.98	0.0108
P75NTR Signals via NK-KB	15	1.93	0.0175
WP197 Cholesterol biosynthesis	17	1.94	0.0180
WP1912 Signalling by insulin receptor	73	1.92	0.0189
WP2788 Sphingolipid metabolism	45	1.90	0.0235
KEGG Rheumatoid arthritis	86	1.86	0.0348
WP530 Cytokines and inflammatory response	23	1.85	0.0434
Peroxisomal lipid metabolism	21	-2.05	0.0421
KEGG Peroxisome	79	-2.03	0.0385
HDACS Deacetylate histones	56	-2.01	0.0324

4.3 Conclusions

In this chapter, the effect of nanosilica on toxicity and cell function was investigated. First, its effect on cell lines was assessed. The nanoparticulate decreased the proliferation of an EBV transformed B cell line in a dose and size dependant manner. Nanosilica was also shown to induce significant death of these cells. Immortalized phagocytic cells, specifically the cancer derived monocytic cell line THP-1, were more resistant to the silica nanoparticles, where the viability only decreased by 5% after treatment with high doses and long incubation periods (48 and 72 h).

The effect of nanosilica on primary peripheral immune cells was investigated next. The nanoparticulate induced significant cell death in all cell types analysed in PBMC cultures. Compared to the cancerous and, to a lesser extent, transformed cell lines, the primary cells were more susceptible to nanosilica induced cell death. Additionally, it was shown that phagocytic cells in primary culture were more susceptible to the cytotoxicity induced by the nanoparticulate than non-phagocytes, corroborating studies in the literature which used larger nanosilica particles (Fedeli et al., 2013). Investigations on the mode of nanosilica induced cell death would suggest that pyroptosis or necrosis is induced in primary monocytes, once again corroborating studies with larger nanosilica particles (Fedeli et al., 2014). CD4 and CD8 T cells were shown to undergo both apoptosis and necrosis after nanosilica treatment.

Microarray analyses showed that gene expression of proteins associated with inflammation, cell injury/infection and cholesterol biosynthesis were induced after nanosilica treatment in primary and transformed cells, corroborating studies in the literature which employed larger particles (Chatterjee et al., 2016; Waters et al., 2009). As with toxicity, the genomic response of the cancerous cell line to the nanoparticulate was small.

The results in this chapter may suggest that nanosilica effects primary T cell function. In the apoptosis/necrosis studies, nanosilica inhibited TCR, not CD4 or CD8, staining 0.5-2 h after treatment. This may suggest nanosilica is interacting with the T cell receptor. Additionally, the induction of T cell apoptosis was greatest 8-24 h after treatment, which may suggest that the mechanism of induced apoptosis is indirect and potentially through a process such as activation induced cell death. Lastly, nanosilica was found to increase the expression of genes associated with T cell activation. Given these results, along with the lack of studies which have investigated the effects of nanosilica on T cell function, further investigations on the effect of amorphous silica nanoparticles on T cells were warranted.

Chapter 5. Effect of nanosilica on T cell activation

5.1 Introduction

In the previous chapter, there was evidence that would suggest nanosilica might be inducing T cell activation. The nanosilica dispersions were found to induce T cell apoptosis, a process that can be initiated by activation induced cell death (AICD) (Arakaki *et al.*, 2014). Additionally, when PBMC cultures were treated with nanosilica, there was an increase in the expression of multiple genes associated with T cell activation, including iCOS, IFN- γ , Ly9 and CRTAM (Geginat *et al.*, 2015; Patiño-Lopez *et al.*, 2006; Schwartzberg *et al.*, 2009; Wikenheiser and Stumhofer, 2016).

In this chapter, the effect of nanosilica on T cell function was investigated by assessing expression of activation markers, measuring cell proliferation and analysing cell supernatants for cytokines. A nanosilica dispersion with a median particle diameter of 3.4-3.8 nm was used throughout this chapter. *Staphylococcal enterotoxin B*, a superantigen known to induce chronic T cell activation, was used as a positive control.

5.2 Results and discussion

5.2.1 The effect of nanosilica on CD4 T cells

5.2.1.1 General markers of activation

The ability of nanosilica to induce T cell activation was first assessed on helper T cells by monitoring the expression of the CD25 and CD69 surface activation markers, which are expressed after T cell encounter with cognate antigen presented on an APC (Broere *et al.*, 2011; Létourneau *et al.*, 2009; Malek and Castro, 2010; Radulovic *et al.*, 2013). T helper cells were identified by the CD3 receptor and the CD4 co-receptor (Chakraborty and Weiss, 2014).

Figure 5.01 shows CD25 and CD69 expression on CD4 T cells after PBMC cultures were treated with SEB, silicic acid and nanosilica. The fluorescent intensity (Figure 5.01A) and the percentage of cells positive (Figure 5.01B) for CD25 and CD69 was low in the control cultures. In cultures treated with the SEB positive control, the fluorescent intensity increased significantly and approximately half of the CD4 T cells were positive for the activation markers. These results indicate that the CD4 T cells in the PBMC cultures employed here were unstimulated and, upon addition of SEB, they were chronically activated (*i.e.*, respond appropriately to SAg). The percentage of cells positive for the activation markers in the negative and positive control cultures was consistent with those reported in the literature (Reddy *et al.*, 2004; Sancho *et al.*, 1999). The expression of the activation markers on CD4 T cells in cultures treated with silicic acid were similar to those in the untreated control. These results would suggest that soluble silica does not activate resting T helper cells. In cultures treated with nanosilica, which was produced from the same stock solutions (sodium silicate, HCl and H₂O) as the silicic acid control, the CD4 T cells expressed significant levels of the

activation markers. The levels of CD25 and CD69 induced by nanosilica were comparable to those induced by SEB, both in fluorescent intensity (Figure 5.01B) and in percentage positive (Figure 5.01C). These results would suggest that nanosilica induces activation of CD4 T cells. As the silicate treatments were both prepared from the same stock solutions, it is highly unlikely that a contaminate in the nanosilica stock (*e.g.*, an endotoxin) was responsible for the induction of the activation markers. The high percentage of cells positive for the activated markers would suggest that nanosilica, like SEB, is inducing activation regardless of the T cell antigenic specificity (*i.e.*, TCR clonotype). Whether the nanosilica induced activation shown here is similar to the one eluded to by Chen *et al.* is unknown (Chen *et al.*, 2014).

Figure 5.02 shows the effect of nanosilica concentration on the expression of CD25 and CD69 on T helper cells. At 150 μM Si, nanosilica increased CD69 positivity on CD4 T cells, but had no effect on CD25 levels. At higher concentrations (300 μM), nanosilica induced significant expression of both activation markers. Interestingly, the concentrations which induced significant T cell activation were the same as those that induced significant cell death (Chapter 4). Whether monocyte and B cell death is involved in the activation of T cells was investigated in Chapter 6.

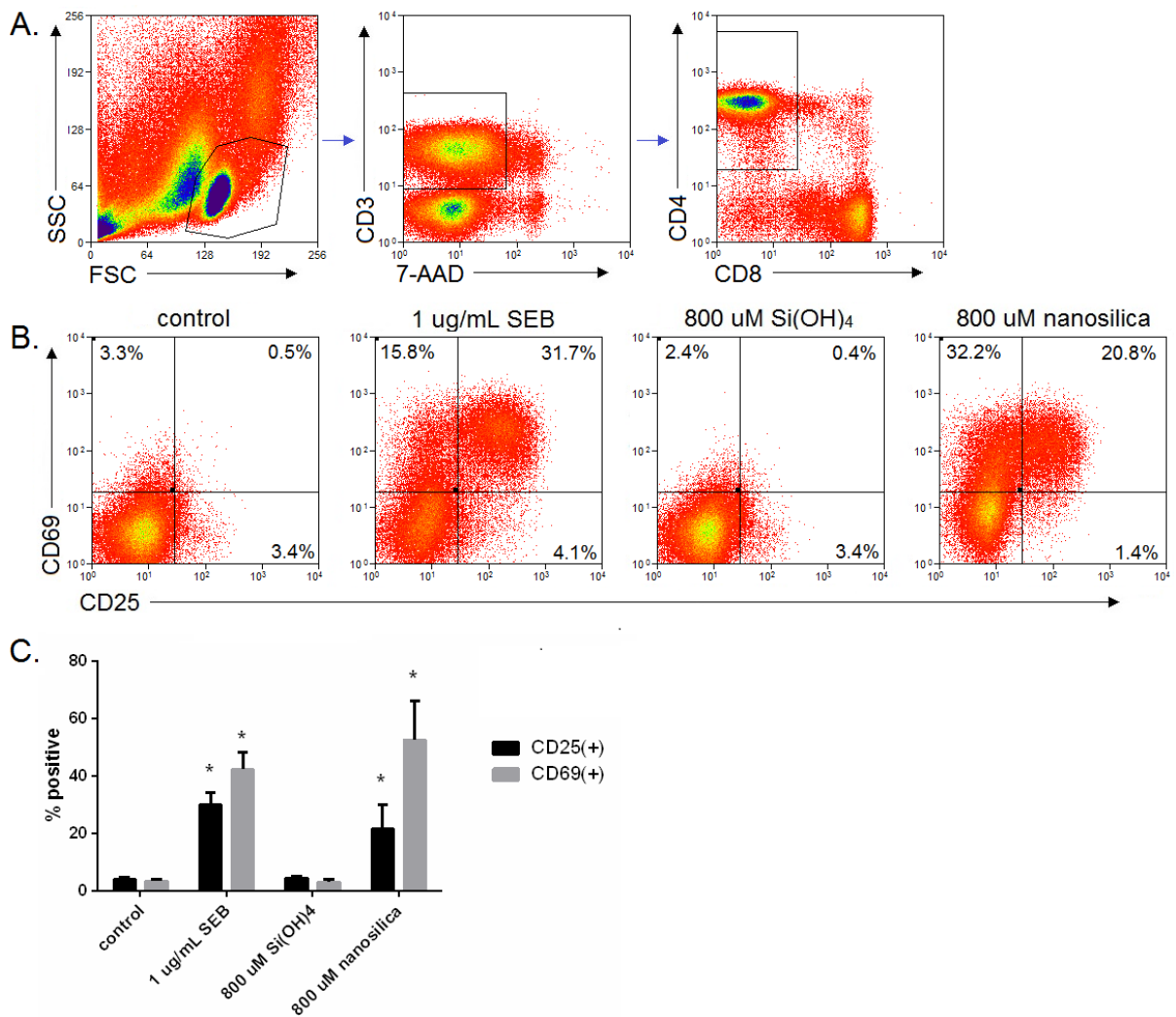


Figure 5.01. The effect of SEB, silicic acid and nanosilica on the expression of CD25 and CD69 on CD4 T cells in PBMC culture after 24 h. **A.** Flow cytometric gating strategy for selecting CD4 T cells within PBMC. T cells were first selected based on FSC versus SSC profiles through a T cell gate also which excluded debris, followed by a viable T cell gate (7-AAD(-)CD3(+)) and a CD4(+) gate. **B.** Representative dot plots showing the expression of CD25 and CD69 on CD4 T cells. **C.** The percentage of CD4 T cells positive for CD25 and CD69. Tabulated data represent the mean \pm standard deviation for 7 donors (* denotes a significance compared to the control, two-tailed paired T test, $p < 0.05$).

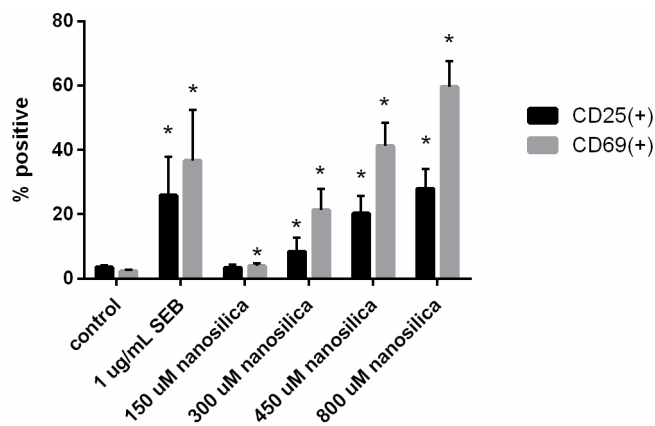


Figure 5.02. The effect of nanosilica concentration on the percentage of CD4 T cells positive for CD25 and CD69 in PBMC culture after 24 h. Tabulated data represent the mean \pm standard deviation for 7 donors (* denotes a significance compared to the control, two-tailed paired T test, $p < 0.05$). T cells were first selected based on FSC versus SSC profiles through a T cell gate which also excluded debris, followed by a viable T cell gate (7-AAD(-)CD3(+)) and a CD4(+) gate

The expression of CD25 and CD69 on T cells can be induced by antigen stimulation alone (Reddy *et al.*, 2004; Sprent *et al.*, 1997). Other markers of T helper cell activation, like proliferation, require secondary signals supplied by APCs for their induction (Chen and Flies, 2013). Whether nanosilica induces T cell proliferation was investigated using CFDA-SE flow cytometric assays (Chapter 2). In these assays, resting T cells were stained with CFDA-SE, treated, and incubated for 3-5 days. Figure 5.03A shows representative flow cytometric dot plots of T cell proliferation after 3 days. In the control cultures, there was a single population at high fluorescent intensity, corresponding to undivided CD4 T cells. In the flow cytometric dot plot of the SEB treated cultures, there were two populations of lesser CFDA-SE intensity to the parent cells. These populations correspond to T cells that have undergone cell division, as the CFDA-SE from the parent cell is split between the two daughter cells (thus fluorescence decreases by 50%). A high percentage of the helper T cells in cultures treated with SEB underwent 1 or 2 rounds of division, indicating that complete T cell activation was induced by the superantigen. There was no distinct daughter cell population in flow cytometric dot plot of the culture treated with nanosilica, which would suggest that nanosilica does not induce T cell proliferation. Figure 5.03B shows the percentage of CD4 T cells that had undergone 1 or more rounds of division. Although a distinct population was not present in the flow cytometric dot plots, there was significant induction of CD4 T cell proliferation in cultures treated with nanosilica. However, the low percentage of T helper cells that had undergone proliferation would suggest that the T cells are not completely activated by nanosilica. The reason for the low levels of T cell proliferation was investigated in Chapter 6.

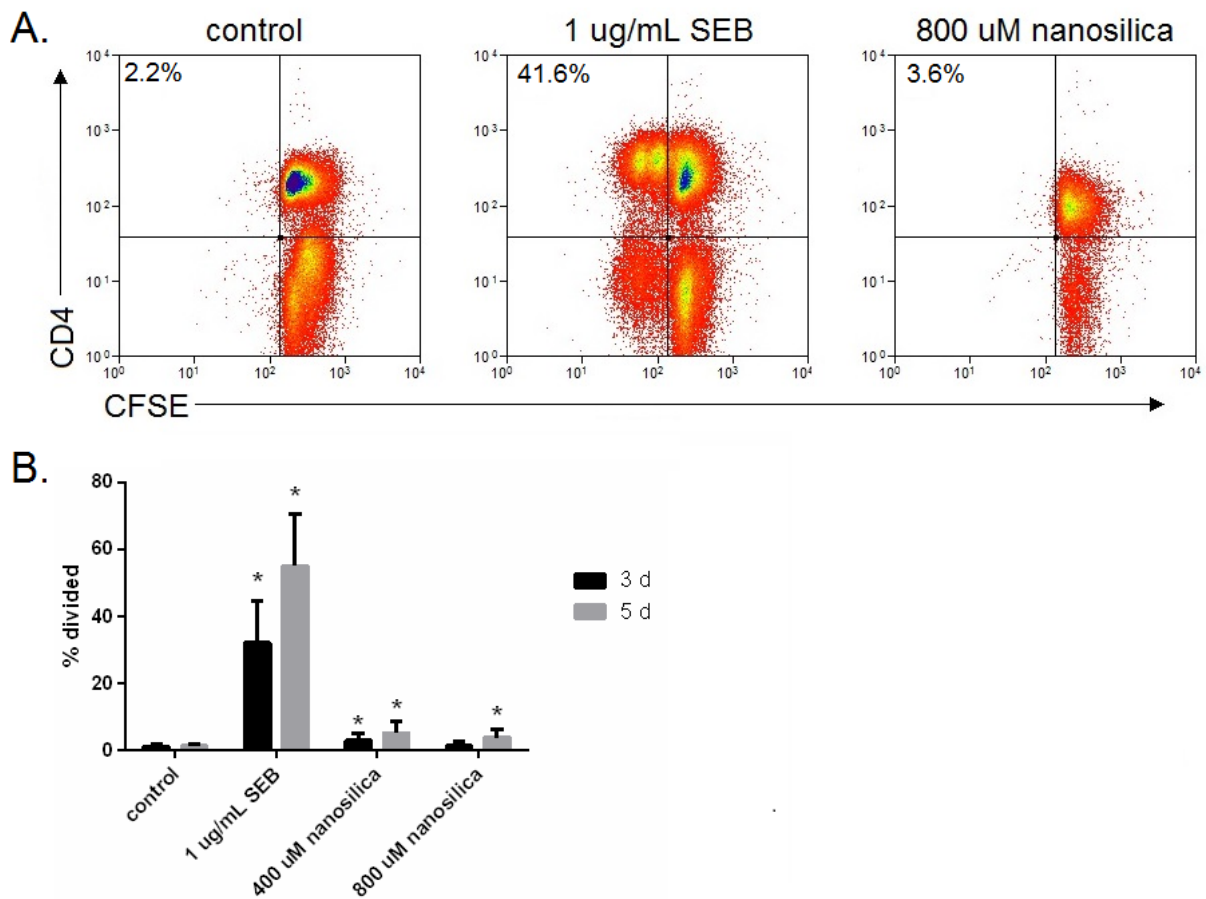


Figure 5.03. The effect of nanosilica on CD4 T cell proliferation in PBMC culture after 3 and 5 d. **A.** Representative dot plots showing the CFSE proliferation profile of CD4 T cells. Percentages correspond to divided CD4(+) cells. **B.** The percentages of CD4 T cells that had undergone 1 or more rounds of division. Tabulated data represent the mean \pm standard deviation for 7 donors (* denotes a significance compared to the control, two-tailed paired T test, $p < 0.05$). T cells were first selected based on FSC versus SSC profiles through a T cell gate which also excluded debris, followed by a viable T cell gate (7-AAD(-)CD3(+)) and a CD4(+) gate

In Chapter 4, nanosilica was found to induce apoptosis of CD4 and CD8 T cells. T cells can undergo apoptosis through a process called activation induced cell death (AICD) (Arakaki *et al.*, 2014). AICD is initiated when the CD95 (Fas) receptor is engaged by the CD178 ligand (FasL). Upon engagement, CD95 trimerizes and downstream signalling is initiated, which leads to the release of intracellular caspases and apoptosis. The engagement of CD95 receptor on T cells does not always initiate AICD, as it also acts as a co-stimulatory receptor. In this co-stimulatory role, the magnitude of signalling will dictate its effect on T cell response, where low levels of signalling through CD95 enhances the T cell response while high levels of signalling inhibits/decreases T cell response (Paulsen and Janssen, 2011). Consequently, the expression of CD95 increases after T cell activation, as it involved in the modulation of the T cell response (McLeod *et al.*, 1998; Paulsen and Janssen, 2011). Whether nanosilica effects the expression of Fas was investigated here.

Figure 5.04 shows the levels of Fas on CD4 T cells after treatment with nanosilica. The baseline levels of CD95 on CD4 T cells was high, >50% Fas(+), despite low expression of other activation markers (CD25, data not shown). This may suggest that the CD95 antibody is detecting both the monomeric and trimeric (activated) forms of the receptor. The SEB treatment significantly increased the expression of CD95 on the surface of CD4 T cells, which is consistent with studies in the literature (McLeod *et al.*, 1998). Silicic acid did not alter the expression of CD95, further indicating that soluble silica has no effect on T cell function. Nanosilica significantly increased CD95 expression on CD4 T cells, which provides further evidence that nanosilica induces T cell activation. These results might suggest that CD4 T cells treated with nanosilica are more susceptible to AICD, potentially indicating a mechanism for the nanosilica induced T cell apoptosis shown in Chapter 4.

In this section, it was shown that nanosilica induces T cell activation. The expression of CD25, CD69 and CD95 were induced on CD4 T cells. The lack of T cell proliferation after nanosilica treatment would suggest that complete activation is not induced. Next, the responses specific to T helper cell lineages were investigated.

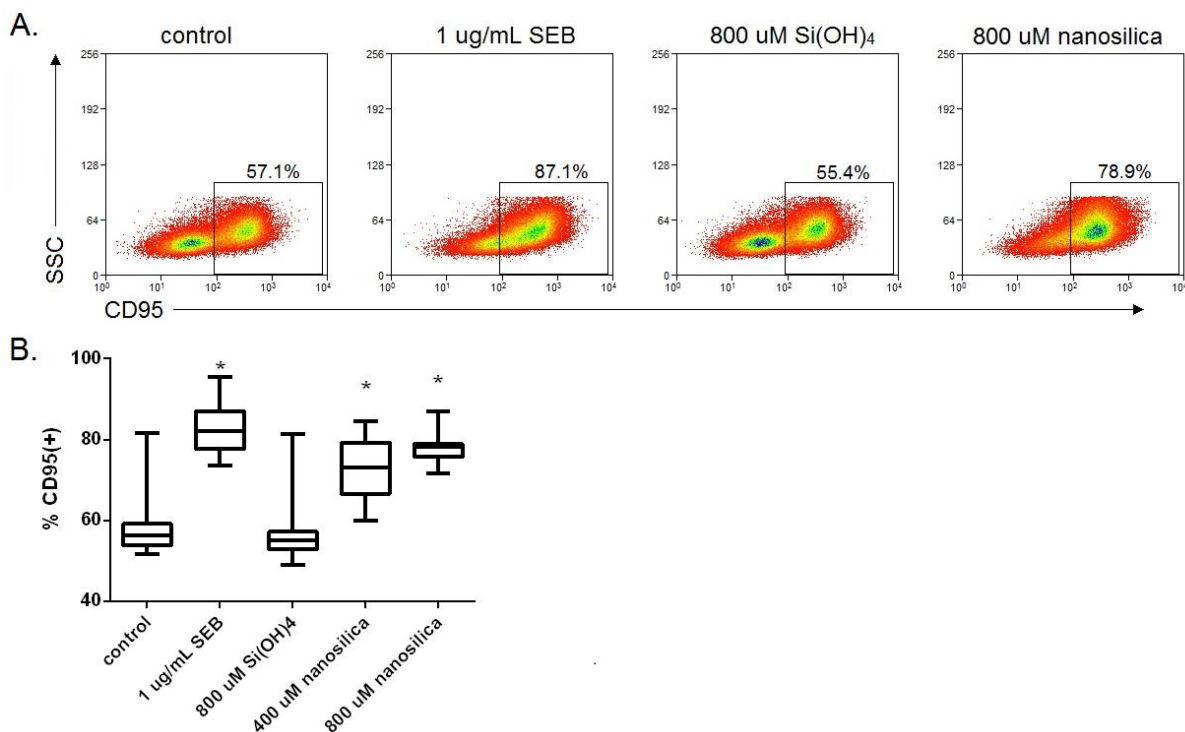


Figure 5.04. The effect of nanosilica on the expression of CD95 on CD4 T cells in PBMC culture after 24 h. A. Representative dot plots showing the expression of CD95 on CD4 T cells. **B.** The percentage of CD4 T cells positive for CD95. Tabulated data represent the mean values for 8 donors (* denotes significance compared to the control, two-tailed paired T test, $p < 0.05$). T cells were first selected based on FSC versus SSC profiles through a T cell gate which also excluded debris, followed by a viable T cell gate (7-AAD(-)CD3(+)) and a CD4(+) gate

5.2.1.2 The effect of nanosilica on helper (CD4(+)) T cells lineage

As CD4 T cells can take on a number of different Th lineages upon their activation (Geginat *et al.*, 2015), the polarization of the CD4 T cells to specific helper cell lineages in response to nanosilica was investigated here.

Regulatory T cells

Regulatory T cells (Treg) are responsible for suppressing immune responses. During inflammation, Tregs release cytokines to inhibit further activation, thus limiting damage to the surrounding tissues and preventing autoimmunity (Arpaia *et al.*, 2015). There are two types of regulatory T cells, natural (nTreg), which can be identified by the foxhead box P3 (FoxP3) protein and CD25, and inducible (iTreg), which can be identified by CD25 but can be both FoxP3 positive and negative (Mellanby *et al.*, 2009). FoxP3 is a regulator of development and maintenance for this T cell subset in humans (Sakaguchi *et al.*, 2010). Whether nanosilica induces a Treg lineage was first investigated by determining the levels of FoxP3 in CD4(+)CD25(+) T cells. These analyses therefore excluded inducible FoxP3(-) Tregs. Figure 5.05 shows the levels of intracellular FoxP3 in activated (CD25(+)) CD4 T cells. There were few T cells in the flow cytometric dot plot of untreated cultures due to the low baseline activation levels, where approximately 5% of the CD4 T cells were CD25(+). Of the activated cells, approximately 5-10% were positive for the FoxP3 protein, corroborating the peripheral CD25 and FoxP3 levels reported in the literature (Finney *et al.*, 2010; Olkowska-Truchanowicz *et al.*, 2013; Valmori *et al.*, 2005). The SEB positive control increased the number of cells positive for FoxP3, but the proportion of activated cells FoxP3 positive did not significantly change compared to that of the control. The percentage of activated CD4 T cells positive for FoxP3 increased significantly after treatment with nanosilica. Approximately 25% of the CD4(+)CD25(+) T cells were also positive for intracellular FoxP3 after treatment with high dose nanosilica. These results might suggest that nanosilica is inducing a Treg phenotype on a portion of the Th cells. The percentage of CD4 T cells that have a regulatory phenotype and are CD25(+)FoxP3(-) is unknown.

Next, the expression of latency-associated peptide (LAP) and glycoprotein A repetitions predominant (GARP) on activated CD4 T cells was assessed. LAP and GARP are proteins associated with the latent-TGF- β complex, which is only expressed on regulatory T cells (Gauthy *et al.*, 2013; Stockis *et al.*, 2009). This complex is responsible for releasing the immunosuppressive cytokine TGF- β . Figure 5.06 shows the expression of LAP and GARP on activated (CD25(+)) CD4 T cells. As with the FoxP3 analysis, low baseline activation levels in the untreated cultures resulted in few cells being present in the flow cytometric dot plots. Also similar to the other Treg marker, SEB increased the number of activated CD4 T cells positive for LAP and GARP but it did not increase the overall percentage of activated cells positive for these markers. The percentage of activated CD4 T cells positive for LAP and GARP

significantly increased after treatment with 800 μM nanosilica. Indeed, nanosilica induced similar levels of FoxP3, LAP and GARP on activated CD4 T cells. These results would suggest that a fraction of activated CD4(+) T cells have a regulatory phenotype.

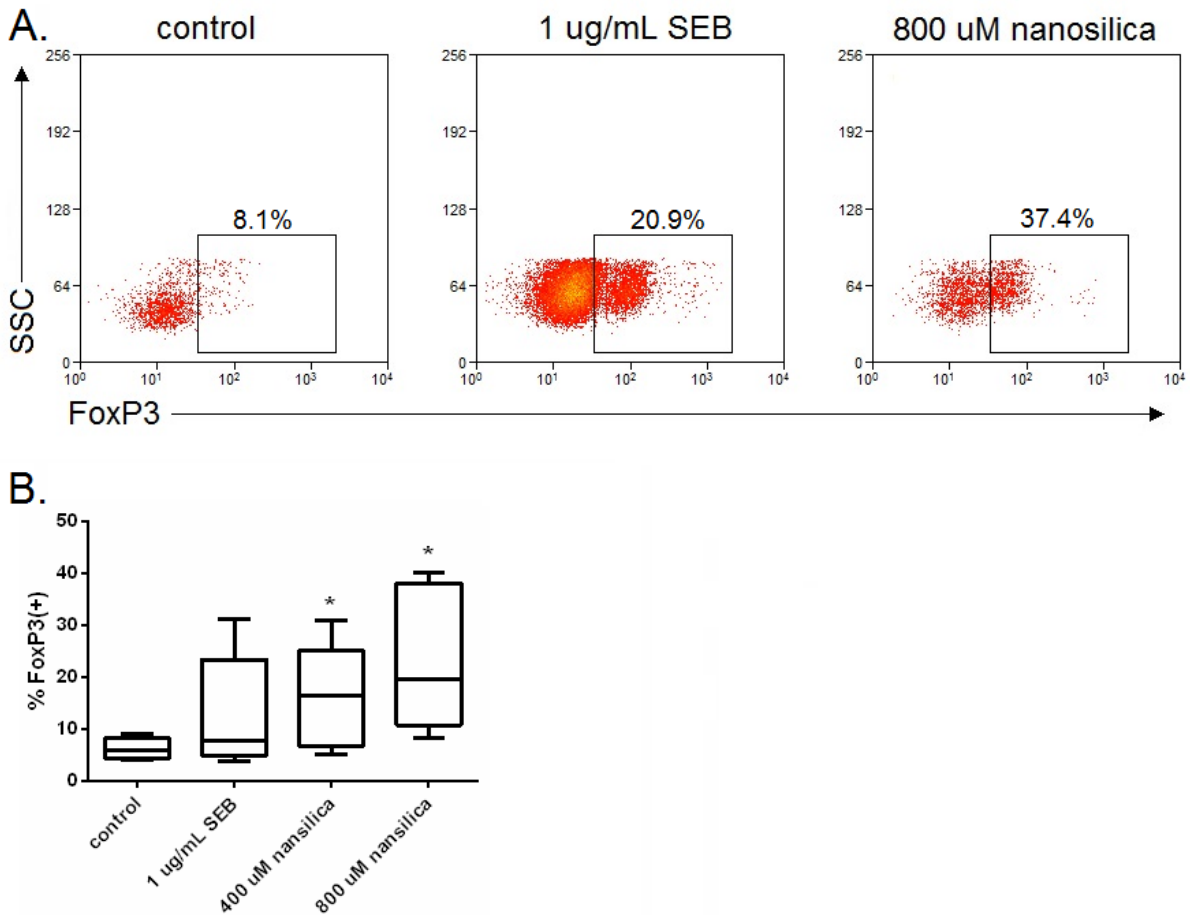


Figure 5.05. The effect of nanosilica on intracellular FoxP3 levels in activated CD4 T cells in PBMC culture after 24 h. **A.** Representative flow cytometric dot plots showing the levels of FoxP3 in activated (CD25(+)) CD4 T cells. **B.** The percentage of activated CD4 T cells positive for FoxP3. Tabulated data represent the mean values for 6 donors (* denotes a significance compared to the control, two-tailed paired T test, $p < 0.05$). T cells were first selected based on FSC versus SSC profiles through a T cell gate which also excluded debris, followed by a viable T cell gate (7-AAD(-)CD3(+), a CD4(+) gate and a CD25(+) gate

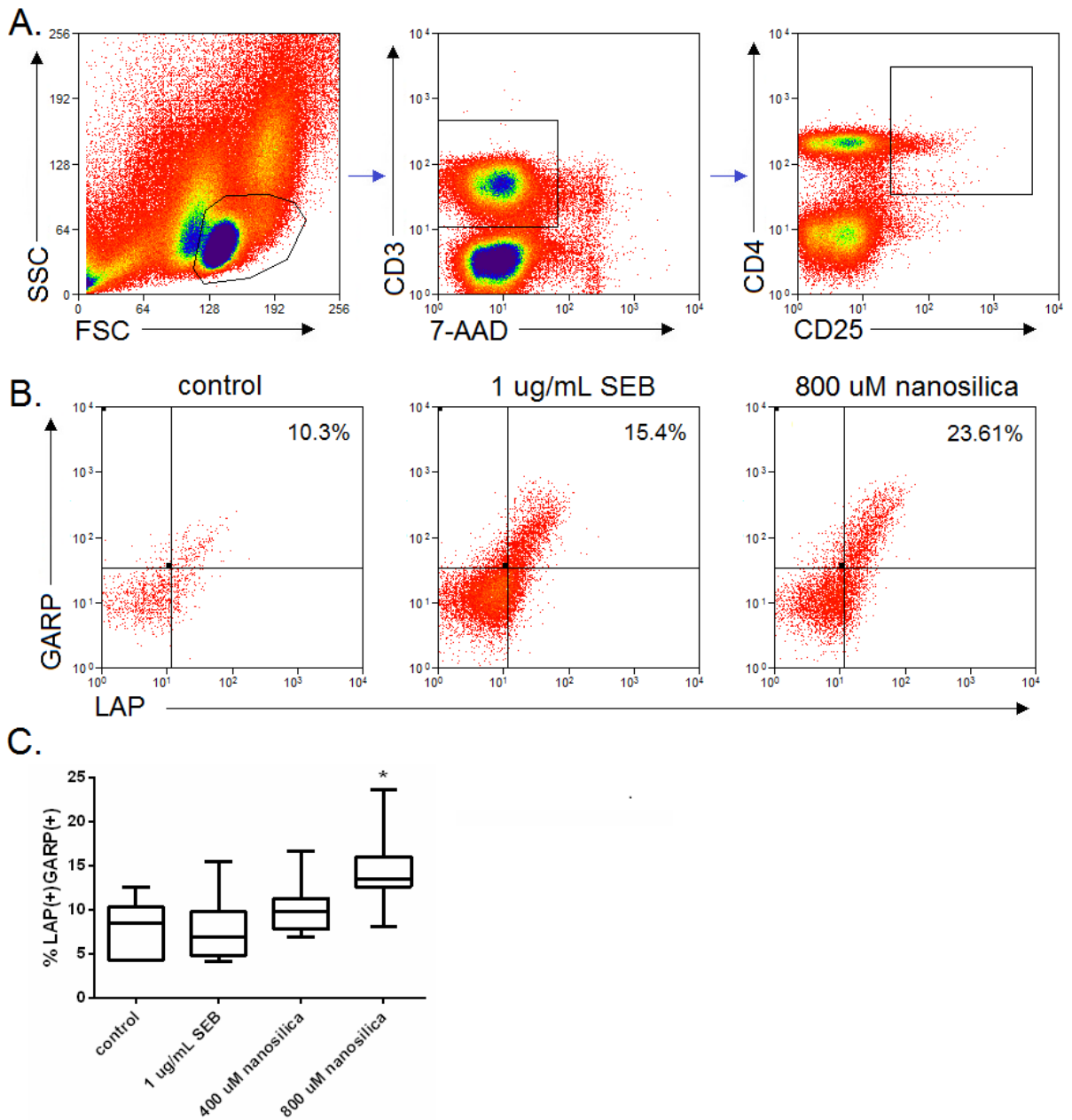


Figure 5.06. The effect of nanosilica on LAP and GARP expression on activated CD4 T cells in PBMC culture after 24 h. **A.** Flow cytometric gating strategy for selecting activated CD4 T cells within PBMC. T cells were first selected based on FSC versus SSC profiles through a T cell gate which also excluded debris, followed by a viable T cell gate (7-AAD(-)CD3(+)) and a CD4(+)/CD25(+) gate. **B.** Representative dot plots showing the expression of LAP and GARP on activated CD4 T cells. **C.** The percentage of activated CD4 T cells double positive for LAP and GARP. Tabulated data represent the mean values for 7 donors (* denotes a significance compared to the control, two-tailed paired T test, $p < 0.05$).

Regulatory T cells can inhibit immune responses by releasing immunosuppressive cytokines. IL-10 is a cytokine released by Tregs to inhibit an inflammatory response (Couper *et al.*, 2008). Whether nanosilica induces IL-10 production was investigated. Figure 5.07 shows the levels of IL-10 present in the supernatants collected 24 h after nanosilica treatment. There was only detectable IL-10 in the supernatants from the SEB treated cultures. The levels of IL-10 in untreated and nanosilica treated cultures remained below the limit of detection (< 30 pg/mL). These results would suggest that although certain regulatory markers (FoxP3 levels, LAP/GARP) are induced by nanosilica, a full regulatory response is not.

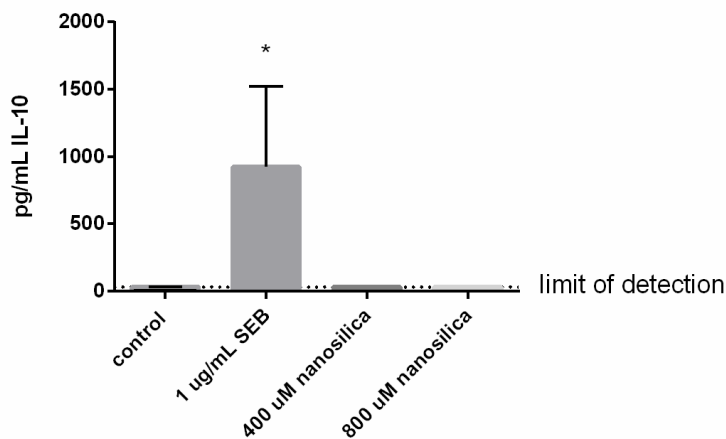


Figure 5.07. The effect of nanosilica on IL-10 levels in PBMC culture supernatants after 24 h. Tabulated data represent the means \pm standard deviation for 10 donors. * denotes a significance compared to the control, two-tailed paired T test, $p < 0.05$)

Th1 T cells

CD4 T cells with a Th1 lineage mediate a cytotoxic T cell response and activate monocytes (Geginat *et al.*, 2015). They are characterized by the production of IFN- γ , though other cell subsets have also been shown to produce this cytokine (Thäle and Kiderlen, 2005). The ability of nanosilica to induce a Th1 response was investigated by assessing supernatant IFN- γ levels. Figure 5.08 shows the levels of IFN- γ in cell supernatants after 24 h. There was no detectable IFN- γ in the supernatants from untreated and silicic acid treated cultures. The supernatants from cultures treated with nanosilica contained ca. 2 ng/mL IFN- γ . These results would suggest that nanosilica is inducing a Th1 response. However, direct evidence that CD4 T cells are producing IFN- γ is still required as other cell types in culture are capable of producing this cytokine (Thäle and Kiderlen, 2005).

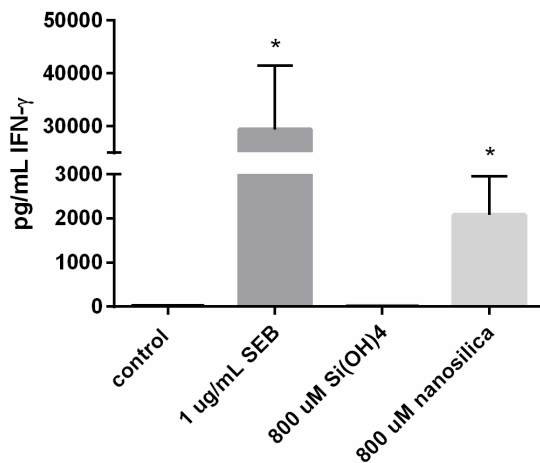


Figure 5.08. The effect of silicic acid and nanosilica on IFN- γ levels in PBMC culture supernatants after 24 h. Tabulated data represent the means \pm standard deviation for 7 donors. (* denotes a significance compared to the control, two-tailed paired T test, $p < 0.05$)

Th2 T cells

CD4 T cells with a Th2 lineage are responsible for mediating B cell responses. The type of B cell response is dependent on the signals Th2 cells provide (Crotty, 2015; Sahoo *et al.*, 2016). Whether nanosilica induces a Th2 response was investigated.

CD40L (CD154) is expressed on Th2 cells and, when it engages the CD40 receptor on B cells, it induces B cell proliferation and survival (Crotty, 2015; Elgueta *et al.*, 2009; Janeway Jr *et al.*, 2001; Jenkins *et al.*, 2008). Figure 5.09 shows the effect of nanosilica on CD40L expression. The percentage of CD4 T cells positive for CD40L was low in the control and silicic acid treated cultures, and was similar to the levels reported in the literature (Desai-Mehta *et al.*, 1996). SEB significantly increased the levels of CD40L positive cells, consistent with its non-specific activation of T cells. Indeed, SAGs are known to induce responses from all Th phenotypes simultaneously (Terman *et al.*, 2013), which explains the induction of Treg, Th1 and Th2 responses shown in this chapter. Nanosilica was also found to significantly increase CD40L expression on CD4 T cells. These results might suggest that nanosilica, like SEB, is inducing non-specific CD4 T cell activation as at least one activation marker from each Th lineage was induced.

Whether nanosilica induces other Th2 responses was investigated by assessing the expression of inducible T cell costimulator (iCOS). iCOS is expressed on Th2 cells and is involved in the induction of antibody and cytokine production by B cells (Sahoo *et al.*, 2016; Wikenheiser and Stumhofer, 2016; Yong *et al.*, 2009). Figure 5.10 shows the effect of nanosilica on iCOS expression. As with CD40L, the levels of iCOS on CD4 T cells in the untreated and silicic acid treated cultures were low and similar to those reported in the literature (Chen *et al.*, 2009a). The expression of iCOS significantly decreased after nanosilica treatment, contradicting the results that show nanosilica increases the expression of the gene corresponding to iCOS (Chapter 4). It remains unclear whether nanosilica induces a full Th2 response.

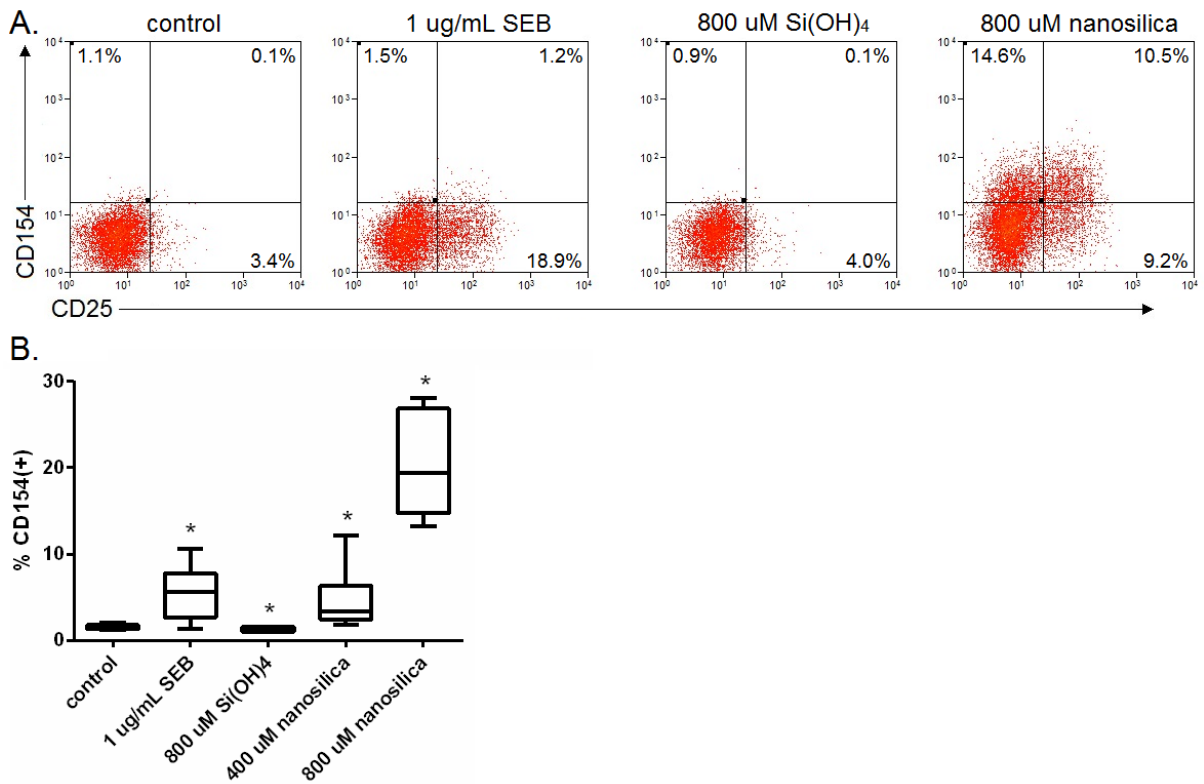


Figure 5.09. The effect of nanosilica on CD40L (CD154) expression on CD4 T cells in PBMC culture after 24 h. A. Representative dot plots showing the expression of CD25 and CD154 on CD4 T cells. **B.** The percentage of CD4 T cells positive for CD154. Tabulated data represent the mean values for 7 donors (* denotes a significance compared to the control, two-tailed paired T test, $p < 0.05$). T cells were first selected based on FSC versus SSC profiles through a T cell gate which also excluded debris, followed by a viable T cell gate (7-AAD(-)CD3(+)) and a CD4(+) gate. Note – only 4 of replicates were tested for silicic acid in B.

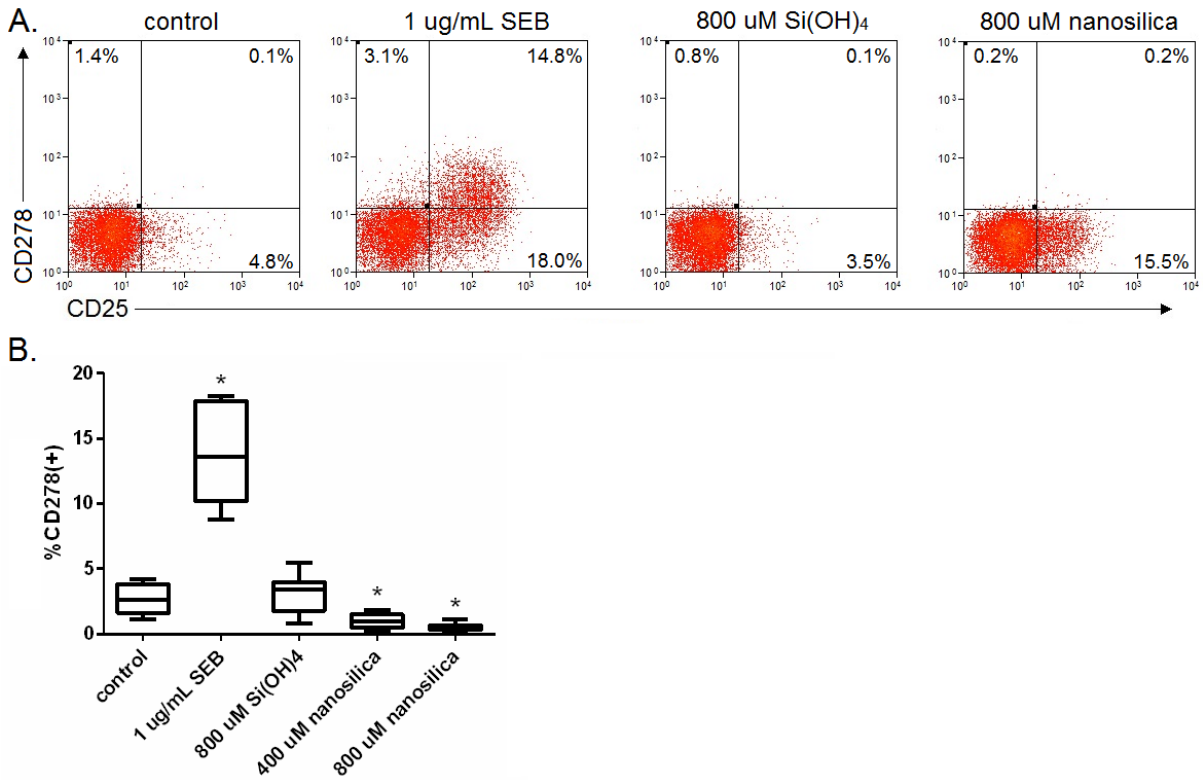


Figure 5.10. The effect of nanosilica on iCOS (CD278) expression on CD4 T cells in PBMC culture after 24 h. **A.** Representative dot plots showing the expression of CD25 and CD278 on CD4 T cells. **B.** The percentage of CD4 T cells positive for CD278. Tabulated data represent the mean values for 8 donors (* denotes a significance compared to the control, two-tailed paired T test, $p < 0.05$). T cells were first selected based on FSC versus SSC profiles through a T cell gate which also excluded debris, followed by a viable T cell gate (7-AAD(-)CD3(+)) and a CD4(+) gate

The presence of IL-4 in nanosilica treated cultures was assessed to determine whether a complete Th2 response was induced. IL-4 is produced by Th2 cells and further supports development of this Th phenotype (Geginat *et al.*, 2015; Jiang and Dong, 2013; Silva-Filho *et al.*, 2014). Figure 5.11 shows the levels of IL-4 in cell supernatants after 24 h. The levels of IL-4 were below the limit of detection (15 pg/mL) in the supernatants of the untreated, silicic acid and nanosilica treated cultures. These results would suggest that nanosilica is not inducing a Th2 response in cell culture.

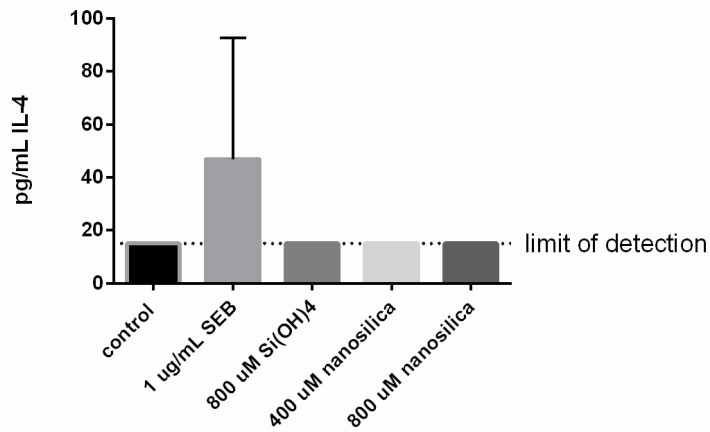


Figure 5.11. The effect of nanosilica on IL-4 levels in PBMC culture supernatants after 24 h. Tabulated data represent the means \pm standard deviation for 8 donors.

In this section, the effect of nanosilica on the polarization of CD4 T cells to specific lineages was investigated. The results would suggest that nanosilica likely induces a Th1 phenotype, as there was significant levels of IFN- γ present in cell supernatants after nanosilica treatment. Cytokines of Th2 and Treg phenotypes (IL-4 and IL-10, respectively) were not detected in cell supernatants after nanosilica treatment, though activation markers of these Th subsets were induced. These results would suggest that nanosilica is non-specifically inducing CD4 T cell activation.

5.2.2 The effect of nanosilica on cytotoxic lymphocytes

5.2.2.1 The effect of nanosilica on CD8 T cells

The effect of nanosilica on cytotoxic T cell activation was investigated next. Cytotoxic T cells (CTLs) are an essential part of the adaptive immune system as they eliminate stressed, abnormal, and infected cells (Barry and Bleackley, 2002). As with the CD4 T cells, activated CTLs express the CD25 and CD69 activation markers. Cytotoxic T cells were identified by the CD3 receptor, which flanks the TCR, and the CD8 co-receptor, which binds the TCR:pMHC class I complex.

Figure 5.12 shows CD25 and CD69 expression on cytotoxic T cells after PBMC cultures were treated with SEB, silicic acid and nanosilica. The control cultures show the baseline expression levels of CD25 and CD69, where the majority of cells were negative for the activation markers. The percentage of resting cells positive for CD25 and CD69 was consistent with levels reported in the literature (Reddy *et al.*, 2004; Sancho *et al.*, 1999). Adding SEB to culture resulted in significant expression of the activation markers, indicating that the CTLs responded appropriately in culture. As with the T helper cells, soluble silica (silicic acid) did not alter the expression of CD25 or CD69 on cytotoxic T cells, indicating that the nanosilica degradation product has no effect on T cell activation. Nanosilica induced significant expression of the activation markers on CD8 T cells. The levels of CD25 and CD69 induced by nanosilica were

less than those induced by SEB, both in fluorescent intensity (Figure 5.12A) and in percentage positive (Figure 5.12B), but they were still significantly greater than that of the control. The high percentage of cells positive for the activated markers and the activation of both CD4 (Section 5.2.1) and CD8 T cells would suggest that nanosilica is inducing activation regardless of the T cell antigenic specificity and co-receptor.

Figure 5.12C shows the effect of nanosilica concentration on the expression of CD25 and CD69 on CTLs. Nanosilica increased CD69 positivity on CD8 T cells but had no effect on CD25 levels at 150 μ M Si. At higher concentrations (300 μ M), nanosilica induced significant expression of both activation markers. As indicated in Section 5.2.1, the concentrations which induced significant activation were the same that induced significant cell death.

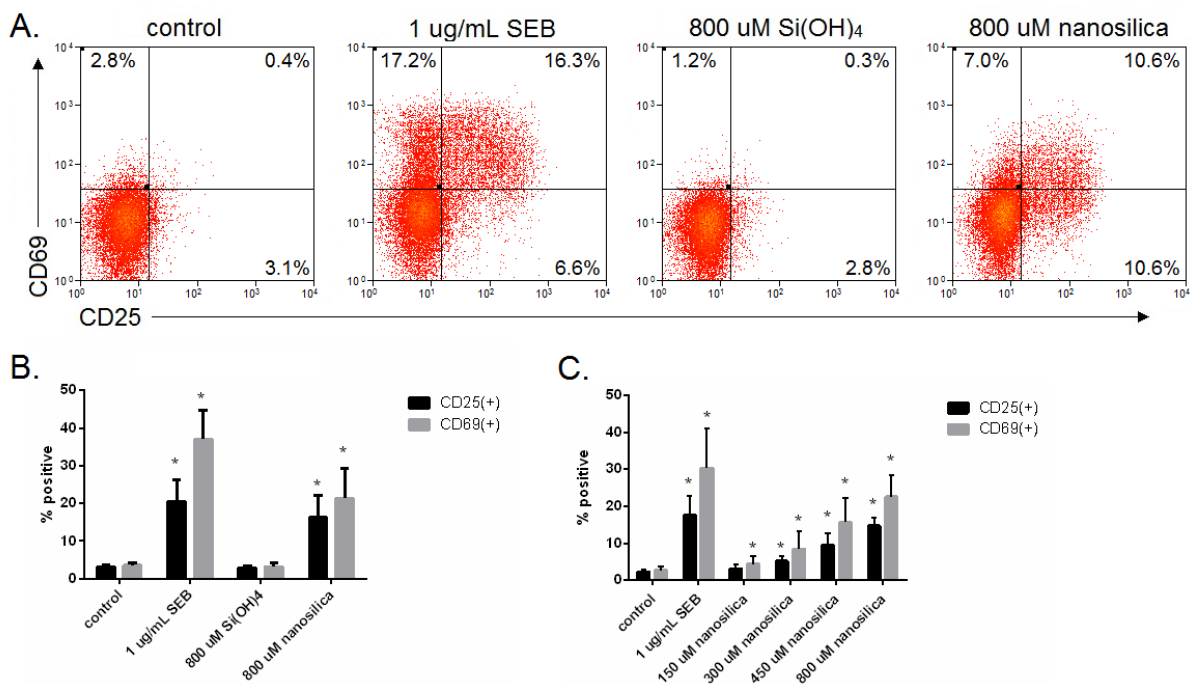


Figure 5.12. The effect of SEB, silicic acid and nanosilica on the expression of CD25 and CD69 on CD8 T cells in PBMC culture after 24 h. **A.** Representative dot plot showing the expression of CD25 and CD69 on CD8 T cells. **B.** The effect of silicic acid and nanosilica on the percentage of CD8 T cells positive for CD25 and CD69. **C.** The effect of nanosilica concentration on the percentage of CD8 T cells positive for CD25 and CD69. Tabulated data represent the mean \pm standard deviation for 7 donors (* denotes a significance compared to the control, two-tailed paired T test, $p < 0.05$). T cells were first selected based on FSC versus SSC profiles through a T cell gate which also excluded debris, followed by a viable T cell gate (7-AAD(-)CD3(+)) and a CD8(+) gate

The effect of nanosilica on cytotoxic T cell proliferation was investigated next, using CFDA-SE flow cytometric assays (same as those used in the CD4 T cell assays). Figure 5.13A shows representative flow cytometric dot plots of CD8 T cell proliferation after 3 days. The dot plot of the control culture showed one population of high CFDA-SE intensity, corresponding to resting (parent) CD8 T cells. The dot plot of the culture treated with SEB showed an additional two populations of lesser fluorescent intensity, which correspond to CD8 T cells that had undergone 1 and 2 rounds of division. These populations were not evident in the dot plots of the cultures treated with nanosilica, indicating that nanosilica does not induce CD8 T cell proliferation. Figure 5.13B shows the percentage of CD8 T cells that had undergone 1 or more rounds of division. As with the CD4 T cells, there were significant levels of CD8 T cell proliferation in cultures treated with nanosilica after 5 days, despite a lack of a discernible population in the flow cytometric dot plots. The low levels of induced proliferation would suggest that nanosilica does not induce complete T cell activation.

In Section 5.2.1, nanosilica was found to induce CD95 expression on CD4 T cells, potentially suggesting that the apoptosis shown in Chapter 4 was through Fas mediated AICD. CD8 T cells can also proceed through AICD via the Fas death receptor (Arakaki *et al.*, 2014). CD95 also acts a co-stimulatory receptor, modulating the T cell response depending on the magnitude of CD95 ligation and the activation state of the T cell during its ligation (Paulsen and Janssen, 2011). Whether nanosilica could be inducing CD95 expression on CTLs was investigated here. Figure 5.14 shows the levels of Fas on CD8 T cells after treatment with nanosilica. As with the CD4 T cells, there was a high CD95 baseline on CD8 T cells in untreated cultures, potentially suggesting that the CD95 antibody is detecting both the monomeric and trimeric forms of the receptor. Despite the high baseline levels, the SEB treatment significantly increased the expression of CD95. The silicate treatments, both nanosilica and the soluble silica control, did not significantly affect receptor expression, though nanosilica inconsistently increased CD95 on CD8 T cells. The slight increase in CD95 expression after nanosilica treatment further indicates that the nanoparticulate activates CD8 T cells, and can induce expression of ligands which can further modulate the T cell response.

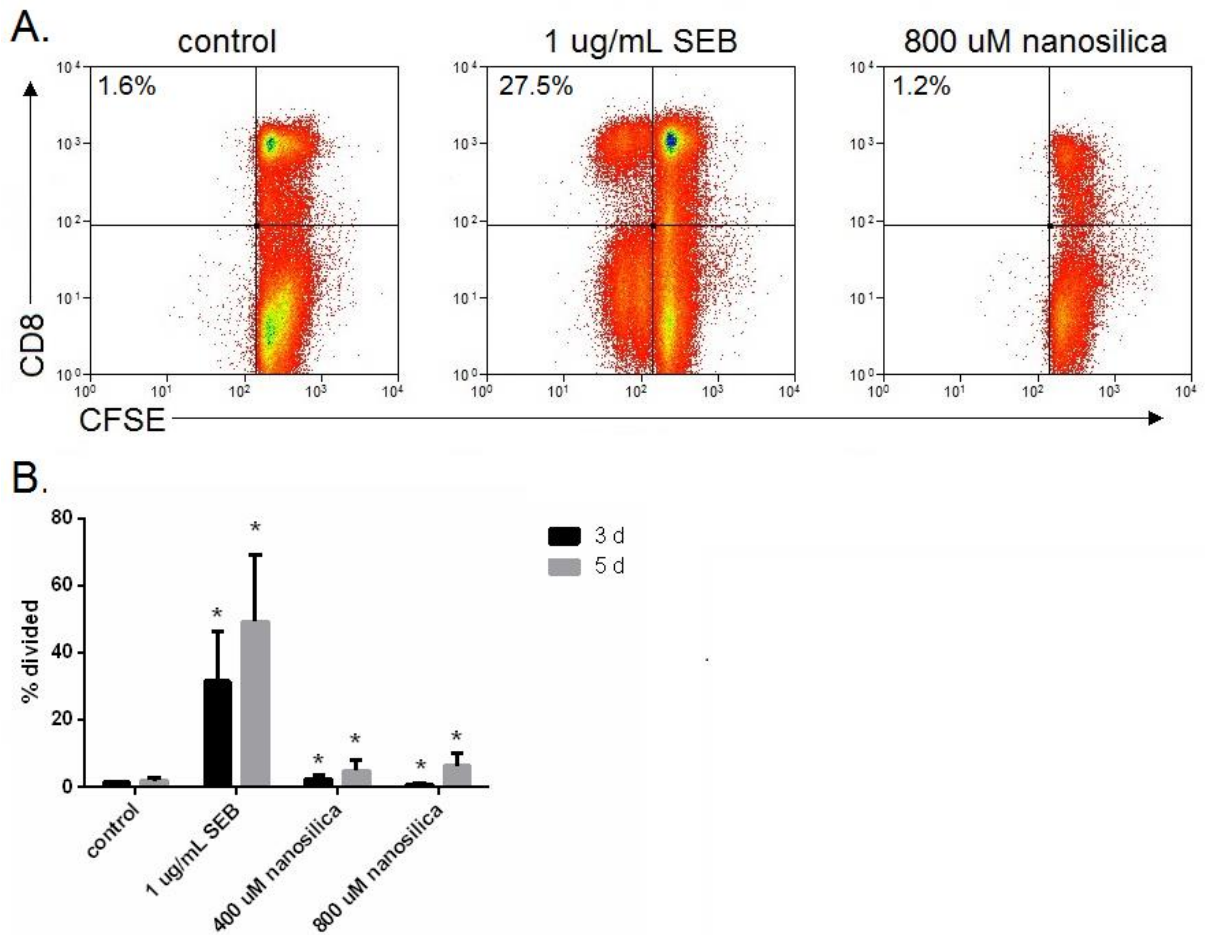


Figure 5.13. The effect of nanosilica on CD8 T cell proliferation in PBMC culture after 3 and 5 d. A. Representative dot plots showing the CFSE proliferation profile of CD8 T cells at 3 d. Percentages correspond to divided CD8(+) cells. **B.** The percentages of CD8 T cells that had undergone 1 or more rounds of division. Tabulated data represent the mean \pm standard deviation for 7 donors (* denotes a significance compared to the control, two-tailed paired T test, $p < 0.05$). T cells were first selected based on FSC versus SSC profiles through a T cell gate which also excluded debris, followed by a viable T cell gate (7-AAD(-)CD3(+)) and a CD8(+) gate

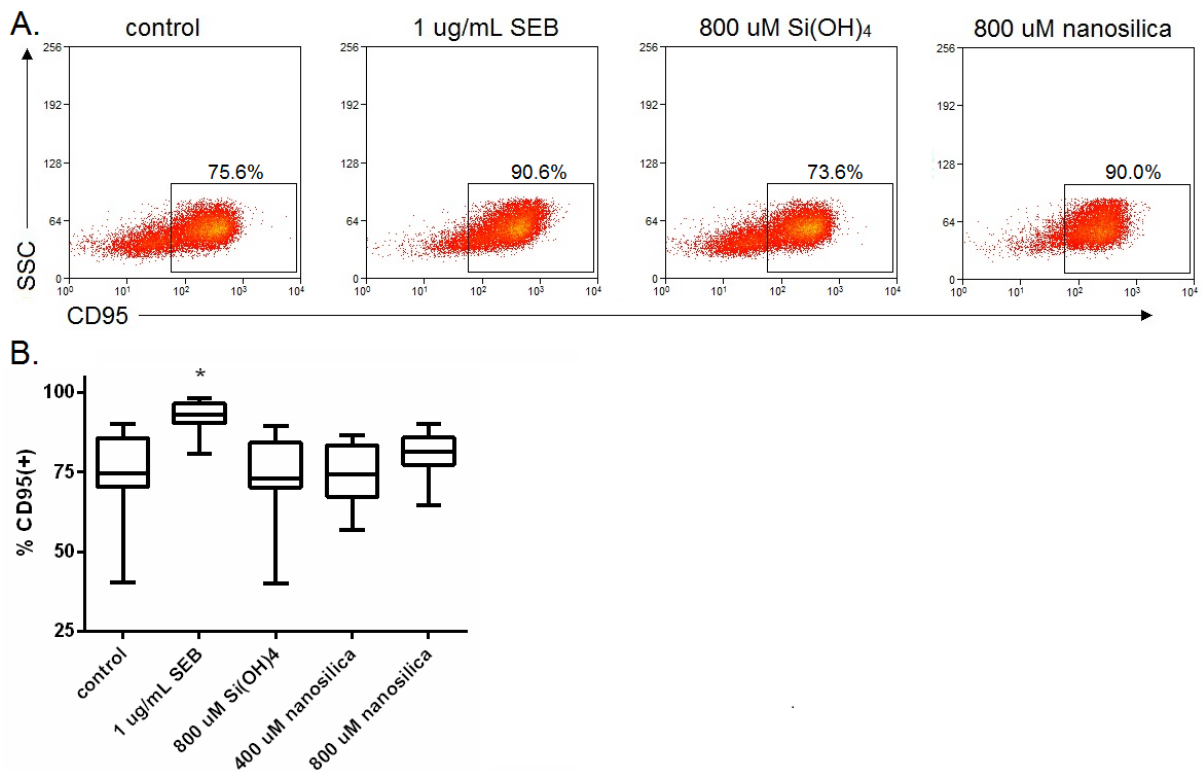


Figure 5.14. The effect of nanosilica on the expression of CD95 on CD8 T cells in PBMC culture after 24 h. A. Representative dot plots showing the expression of CD95 on CD8 T cells. **B.** The percentage of CD8 T cells positive for CD95. Tabulated data represent the mean values for 8 donors (* denotes a significance compared to the control, two-tailed paired T test, $p < 0.05$). T cells were first selected based on FSC versus SSC profiles through a T cell gate which also excluded debris, followed by a viable T cell gate (7-AAD(-)CD3(+)) and a CD8(+) gate

5.2.2.2 The effect of nanosilica on $\gamma\delta$ T cells and NK/NKT cells

There are other lymphocyte subsets with cytotoxic capabilities present in the periphery. The effect of nanosilica on these cell subsets was also investigated.

$\gamma\delta$ T cells are a low frequency T cell subset with a T cell receptor (TCR) consisting of γ and δ chains rather than the more common α and β TCR chains. $\gamma\delta$ T cells comprise 1-5% of the T cells in the periphery and are known for their anti-tumour properties (Silva-Santos *et al.*, 2015). Structurally, the $\gamma\delta$ TCR has a much smaller angle between the constant and variable domain compared to that of the $\alpha\beta$ TCR (Allison *et al.*, 2001). $\gamma\delta$ T cells do not recognize antigen presented in MHC receptors but instead recognize soluble antigens, CD1 receptors (MHC-like) and other proteins expressed on cell surfaces (Dar *et al.*, 2015; Vantourout and Hayday, 2013; Wiest, 2016; Wu *et al.*, 2014). Whether $\gamma\delta$ T cells are activated by nanosilica was investigated.

Figure 5.15 shows the effect of nanosilica on the expression of CD25 and CD69 on $\gamma\delta$ T cells. The decreased frequency of this T cell subset, compared to $\alpha\beta$ T cells, is evident in the flow cytometric dot plots. The SEB positive control induced significant expression of the activation

markers, indicating that the cells responded appropriately in culture. Superantigens are thought to activate $\gamma\delta$ T cells in a similar fashion to $\alpha\beta$ T cells (Ramesh *et al.*, 1995; Rust and Koning, 1993). Soluble silica showed similar CD25 and CD69 levels to that of the untreated control, both of which similar to those reported in the literature (Kunzmann *et al.*, 2000). As with $\alpha\beta$ T cells, nanosilica induced significant expression of CD25 and CD69 on $\gamma\delta$ T cells. These results further support that nanosilica induced T cell activation is non-specific. The mechanism in which nanosilica is inducing $\gamma\delta$ T cell activation was investigated in Chapter 6.

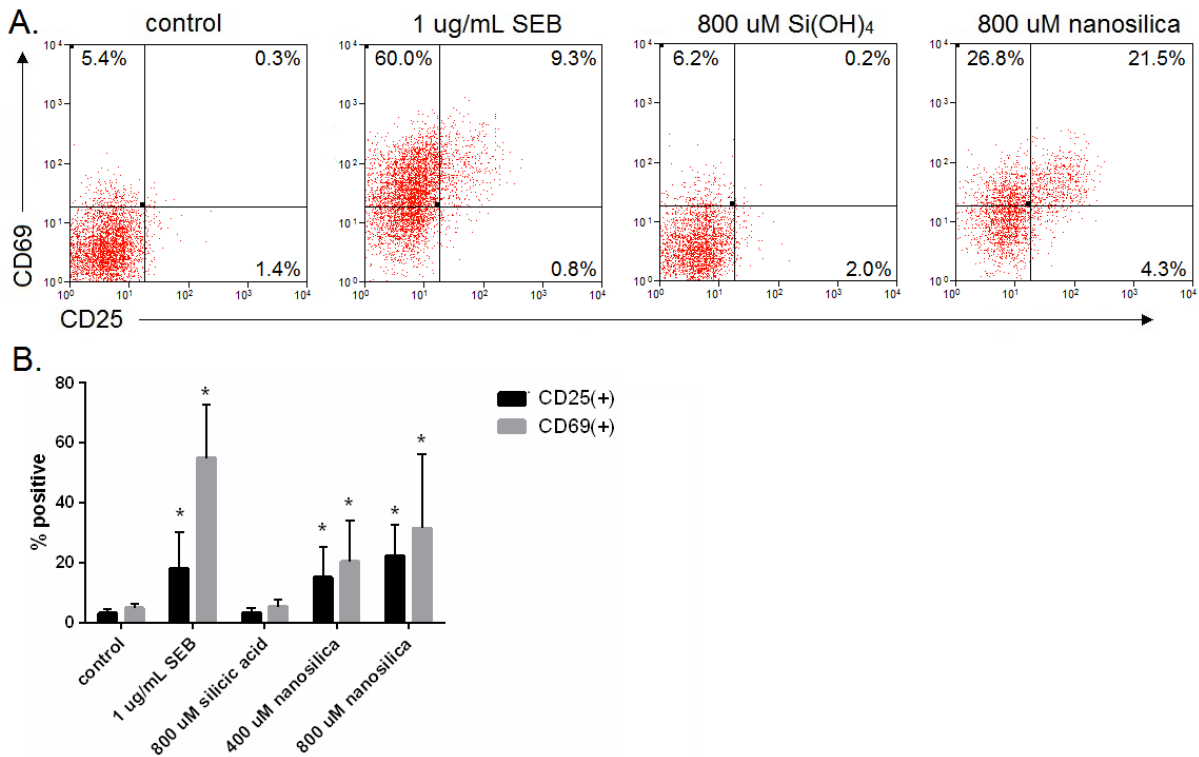


Figure 5.15. The effect of nanosilica on CD25 and CD69 expression on $\gamma\delta$ T cells in PBMC culture after 24 h. **A.** Representative dot plots showing the expression of CD25 and CD69 on $\gamma\delta$ T cells. **B.** The percentage of $\gamma\delta$ T cells positive for CD25 and CD69. Tabulated data represent the mean \pm standard deviation for 8 donors (* denotes a significance compared to the control, two-tailed paired T test, $p < 0.05$). T cells were first selected based on FSC versus SSC profiles through a T cell gate which also excluded debris, followed by a viability (7-AAD(-)) and a $\gamma\delta$ TCR(+) gate.

Natural killer (NK) cells are another lymphocyte subset that have cytotoxic capabilities. Unlike T cells, NK cells are a part of the innate immune system. NK cells do not have a TCR to recognize antigen but instead are activated through a number of different receptors, including NKp30, NKp44, and CD160 (Long *et al.*, 2013; Vivier *et al.*, 2008) and cytokines, including IL-2, IL-12, and IFN- γ (Zwirner and Domaica, 2010). There is a T cell subset that also expresses NK cell markers. These cells, referred to as natural killer T (NKT) cells, have an invariant TCR that recognises the MHC-like CD1b receptor (Vivier *et al.*, 2012). Whether nanosilica induces NK/NKT cell activation was investigated here. NK and NKT cells were identified by the CD57 receptor (Leong *et al.*, 2003).

Figure 5.16 shows the effect of nanosilica on the expression of CD25 and CD69 on NK/NKT cells. The SEB positive control induced the expression of CD25 and CD69 on these cells, corroborating studies in the literature which show that both NK and NKT cells are activated by superantigens (Chen *et al.*, 2009b; D'Orazio *et al.*, 1995). Nanosilica also induced significant expression of CD25 and CD69 on NK/NKT cells, while the soluble silicic acid control did not. The mechanism of nanosilica-induced NK/NKT cell activation is unknown. However, it is possible that nanosilica induces stress markers on other cell types, thus leading to NK/ NKT cell activation. Indeed, gene expression of the stress receptor MHC class I polypeptide-related sequence A (MICA) was increased in PBMC and EBV transformed B cell cultures after nanosilica treatment (Chapter 4). The recognition of MICA by the NKG2D receptor on NK/NKT cells can induce their activation (Chan *et al.*, 2014). Therefore, it is plausible that NK/NKT cell activation occurs through nanosilica induced cell stress.

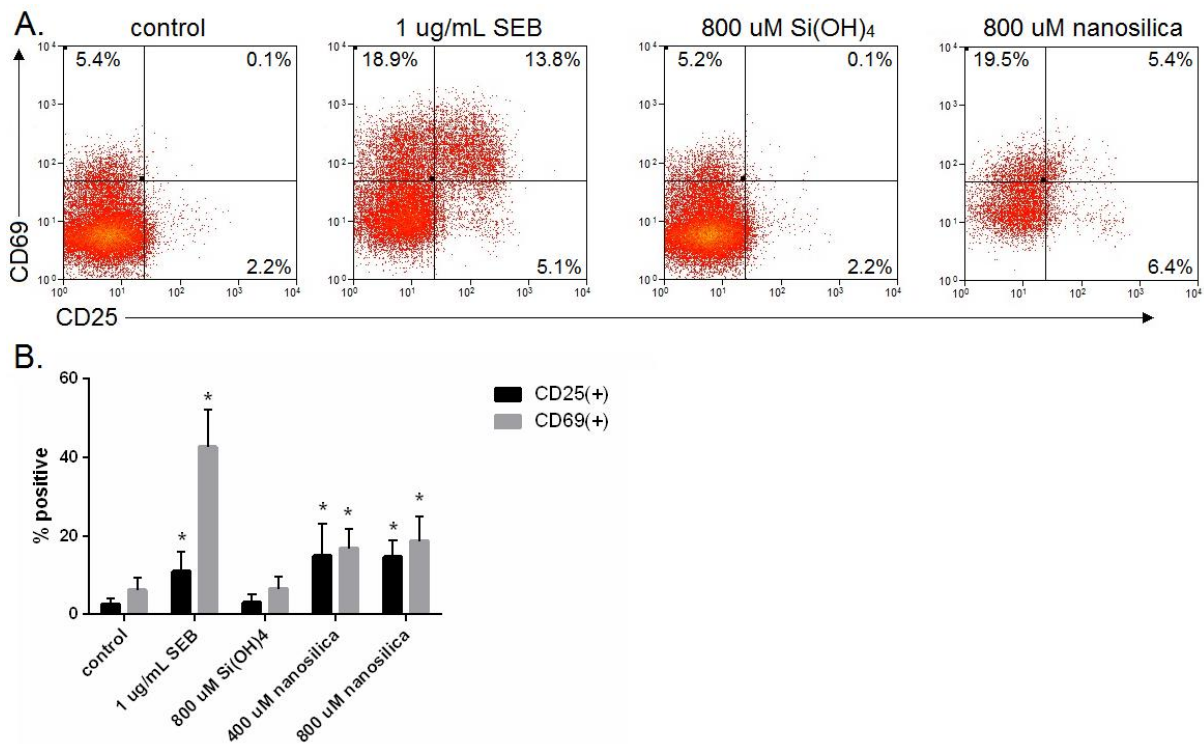


Figure 5.16. The effect of nanosilica on CD25 and CD69 expression on NK/NKT (CD57(+)) cells in PBMC culture after 24 h. A. Representative dot plots showing the expression of CD25 and CD69 on NK/NKT cells. **B.** The percentage of NK/NKT cells positive for CD25 and CD69 after nanosilica treatment. Tabulated data represent the mean \pm standard deviation for 8 donors (* denotes a significance compared to the control, two-tailed paired T test, $p < 0.05$). NK/NKT cells were first selected based on FSC versus SSC profiles through a T cell gate which also excluded debris, followed by a viability (7-AAD(-)) and a CD56(+) gate

In summary, the effect of nanosilica on activation of cytotoxic lymphocytes was investigated. The expression of CD25 and CD69 was induced by nanosilica on all cytotoxic lymphocyte subsets, including CTLs, $\gamma\delta$ T cells, and NK/NKT cells.

5.3 Conclusions

In this chapter, the effect of nanosilica on T cell activation was investigated. Previously (in Chapter 4), it was shown that labile nanosilica particles, 3-4 nm in diameter, induce significant cell death in PBMC cultures. Of the cells tested in PBMC, T cells were most resistant to death upon exposure to the particles, though a significant portion of both CD4 and CD8 T cells did undergo cell apoptosis. It was later found that a number of genes associated with T cell activation were more highly expressed after nanosilica treatment. These results, along with the complete lack of published work in the subject area, warranted a full investigation on the response of T cells to nanosilica.

Nanosilica, 3-4 nm in diameter, was found to activate T cells. The expression of the T cell activation markers CD25 and CD69 increased significantly on both CD4 and CD8 T cells after nanosilica treatment, while soluble silicon did not increase their expression. Other T cell

subsets, including $\gamma\delta$ T cells and NK/NKT cells, also expressed high levels of these activation markers after nanosilica treatment. The amorphous particles did not induce $\alpha\beta$ T cell proliferation, which would suggest that it does not induce complete T cell activation.

Investigations on the polarization of T helper cells were also conducted. Supernatants from PBMC cultures treated with nanosilica contained significant levels of the cytokine IFN- γ , which would suggest that a Th1 phenotype is induced. However, phenotypic markers of Tregs (FoxP3, LAP/GARP) were also induced by nanosilica, though its corresponding cytokine was not. Similarly, Th2 cytokines were not induced. These results, along with the activation of the various cytotoxic T cell subsets, would suggest that nanosilica is inducing significant non-specific T cell activation.

In the next chapter, the T cell response to nanosilica was further investigated. The mechanism of nanosilica-induced T cell activation, the effect of nanosilica on T cell recognition of cognate antigen and the effect of particle characteristics on induced activation were all studied.

Chapter 6 – Investigations into the mechanism of T cell activation by nanosilica

6.1 Introduction

As shown previously, nanosilica particles 3.6 nm in diameter were found to activate T cells. The expression of activation markers on both CD4 and CD8 T cells and the production of IFN- γ was induced by the nanoparticulate. Exposure to nanosilica did not result in complete T cell activation, as T cell proliferation was not induced. In this chapter, the mechanism of nanosilica induced T cell was investigated using immunoblot and flow cytometry based assays, by using various cell lines, enriched cell cultures and cells from transgenic mice, and by using a range of nanoparticles.

6.2 Results and discussion

6.2.1 Role of antigen-presenting cells (APCs)

Investigations were conducted to determine whether the activation of CD4 T cells by nanosilica is APC dependant. CD4 T cells require APCs for activation as they only recognise cognate antigen in the context of an MHC class II receptor, which are predominately expressed on APCs (Kambayashi and Laufer, 2014). By removing APCs from culture, it is possible to determine whether nanosilica requires MHC class II receptors for CD4 T cell activation. The MHC class I receptor, which presents antigen to CD8 T cells, is expressed on all mammalian cells (including T cells) and therefore cannot be removed from culture (Tourdot and Gould, 2002).

T cells from PBMC cultures were enriched using monocyte adherence or T cell isolation kits (through negative selection). Figure 6.01A shows the cell distribution of the enriched T cell cultures. The percentage of cells positive for CD3 ϵ in the enriched cultures was >88%, increased from that of 50-70% in PBMC cultures (data not shown). The percentage of cells positive for CD11c (monocytes, the professional APCs) was <3% in the enriched T cell cultures, down from 10-35% in PBMC cultures. The enriched T cell cultures were treated and the expression of the CD25 and CD69 activation markers, which are expressed on activated T cells (D'Souza and Lefrançois, 2003; Mackay et al., 2015; Malek and Castro, 2010; Radulovic et al., 2013), were assessed.

Figure 6.01B shows the effect of nanosilica on the expression of CD25 and CD69 on CD4 and CD8 T cells in enriched T cell cultures. SEB induced significant expression of CD25 and CD69 on both T cell subsets. However, the percentage of CD4 T cells positive for the activation markers was much lower in enriched T cell cultures compared to that in full PBMC cultures. Figure 6.01C shows the difference in activation which was induced in enriched T cell cultures versus that which was induced in PBMC cultures, as determined by the following equation:

$$\% \text{ difference} = (\% \text{ CDXX}(+)_{\text{EN T cells}} - \% \text{ CDXX}(+)_{\text{PBMC}}) / \% \text{ CDXX}(+)_{\text{PBMC}} \times 100\%$$

CD25 and CD69 induced on CD4 T cells by SEB decreased by *ca.* 50% in the enriched cultures while the percentage of CD8 T cells positive for the activation markers remained relatively unchanged. Superantigens induce T cell activation by crosslinking MHC receptors to TCRs (Arad *et al.*, 2011; Fraser, 2011; Li *et al.*, 1998). The activation of CD4 T cells decreased in enriched T cell cultures as there were fewer MHC class II receptors for the SA_g to crosslink. The activation of CD8 T cells in enriched cultures did not significantly decrease as its MHC receptor (class I) is expressed on all mammalian cells types including T cells (Tourdot and Gould, 2002).

Nanosilica induced significant expression of CD25 and CD69 on CD4 and CD8 T cells in enriched T cell cultures (Figure 6.01B). The percentage of CD4 T cells positive for the activation markers in the enriched T cell cultures was similar to that found in PBMC cultures (Figure 6.01C). These results would suggest that the nanosilica does not require MHC class II receptors (APCs) to induce CD4 T cell activation. Interestingly, the percentage of CD8 T cells positive for CD25 and CD69 in enriched T cell cultures was significantly greater than that found in PBMC cultures. It is possible that the interaction (phagocytosis) of nanosilica with APCs in full PBMC cultures decreases its potential for interaction with CD8 T cells.

To confirm that nanosilica induced CD4 T cell activation is APC independent, the effect of nanosilica on Jurkat T cells was investigated. Jurkat cells are a leukemic T cell line that are CD4(+), CD8(-) and MHC class II(-) (Holling *et al.*, 2004; Sandberg *et al.*, 2007). Jurkat cells therefore require an APC, *i.e.*, a cell expressing an MHC class II receptor, for antigen presentation. As APCs were not added to Jurkat T cell cultures, the effect of nanosilica on T cell activation was investigated in a culture completely deplete of MHC class II receptors. Figure 6.02 shows the effect of nanosilica on the induction of CD25 and CD69 on Jurkat T cells. The SA_g control did not induce expression of the activation markers, as wildtype Jurkat T cells do not have a TCR sequence in which SEB can bind (Fleischer *et al.*, 1996; Hayworth *et al.*, 2009). Nanosilica increased CD69 expression on Jurkat T cells but did not induce significant expression of CD25. The lack of CD25 induction is not a defect in this cell line, as it can be induced with PHA and PdBu (Shatrova *et al.*, 2015). The reason nanosilica does not induce CD25 expression is not known. However, the induction of CD69 on Jurkat T cells would suggest that APCs, and therefore MHC class II receptors, are not required for the activation of CD4 T cells by nanosilica.

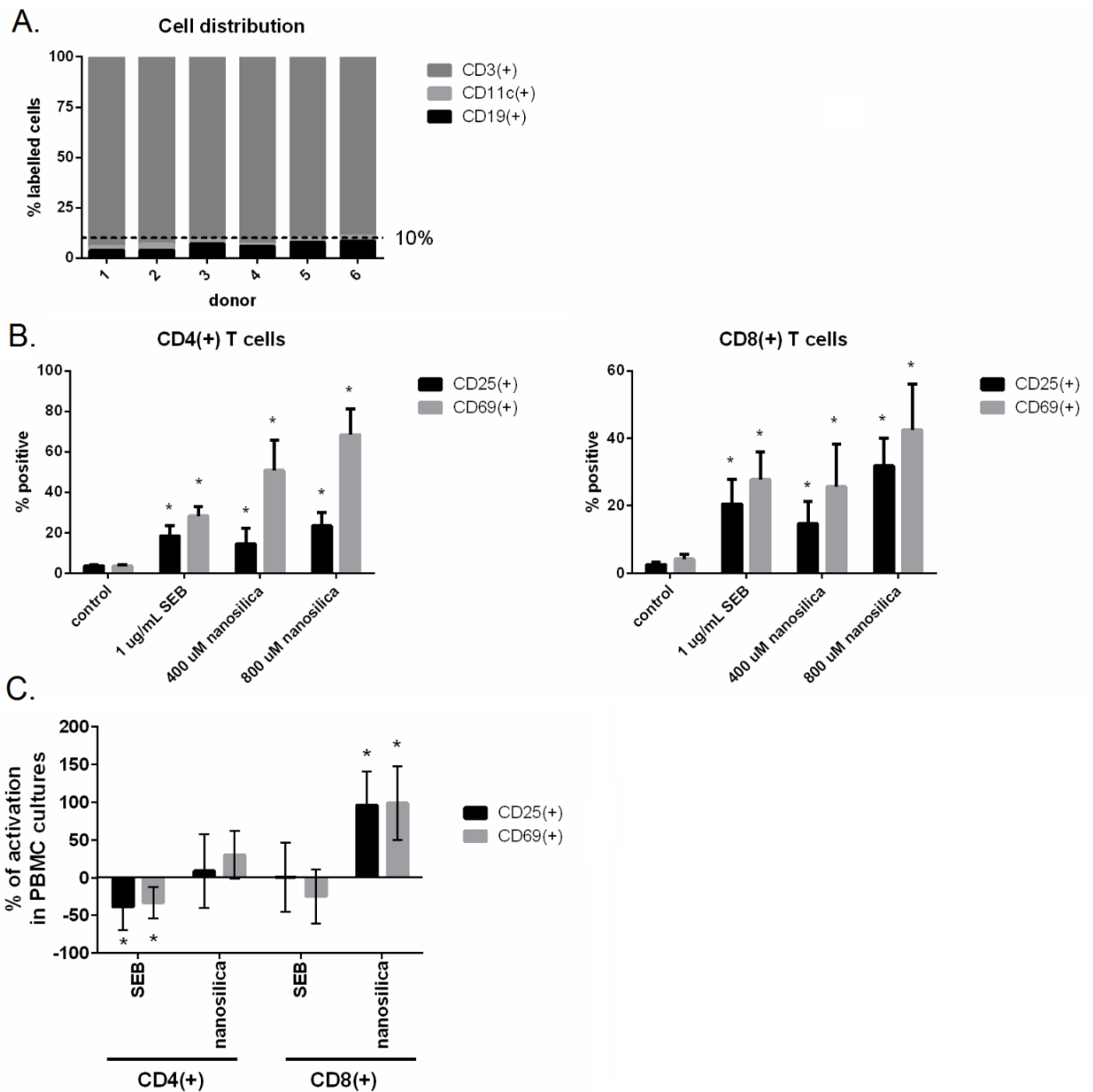


Figure 6.01. The effect of nanosilica on CD25 and CD69 expression on CD4 and CD8 T cells in enriched T cell cultures. A. The cell distribution in the cultures tested after T cell enrichment. **B.** The effect of nanosilica on the percentage of CD4 and CD8 T cells positive for CD25 and CD69. Tabulated data represent the means \pm standard deviation for 6 donors (* denotes significance compared to the control, paired T test, $p < 0.05$). T cells were first selected based on FSC versus SSC profiles through a T cell gate which also excluded debris, followed by a viable T cell gate (7-AAD(-)CD3(+)) and a CD4(+) or a CD8(+) gate. **C.** The percentage difference in the induction of the CD25 and CD69 activation markers in enriched T cell cultures and in PBMC culture (* denotes significance compared to that in PBMC culture, unpaired T test, $p < 0.05$. PBMC activation data from Figure 5.01 was used for the calculations)

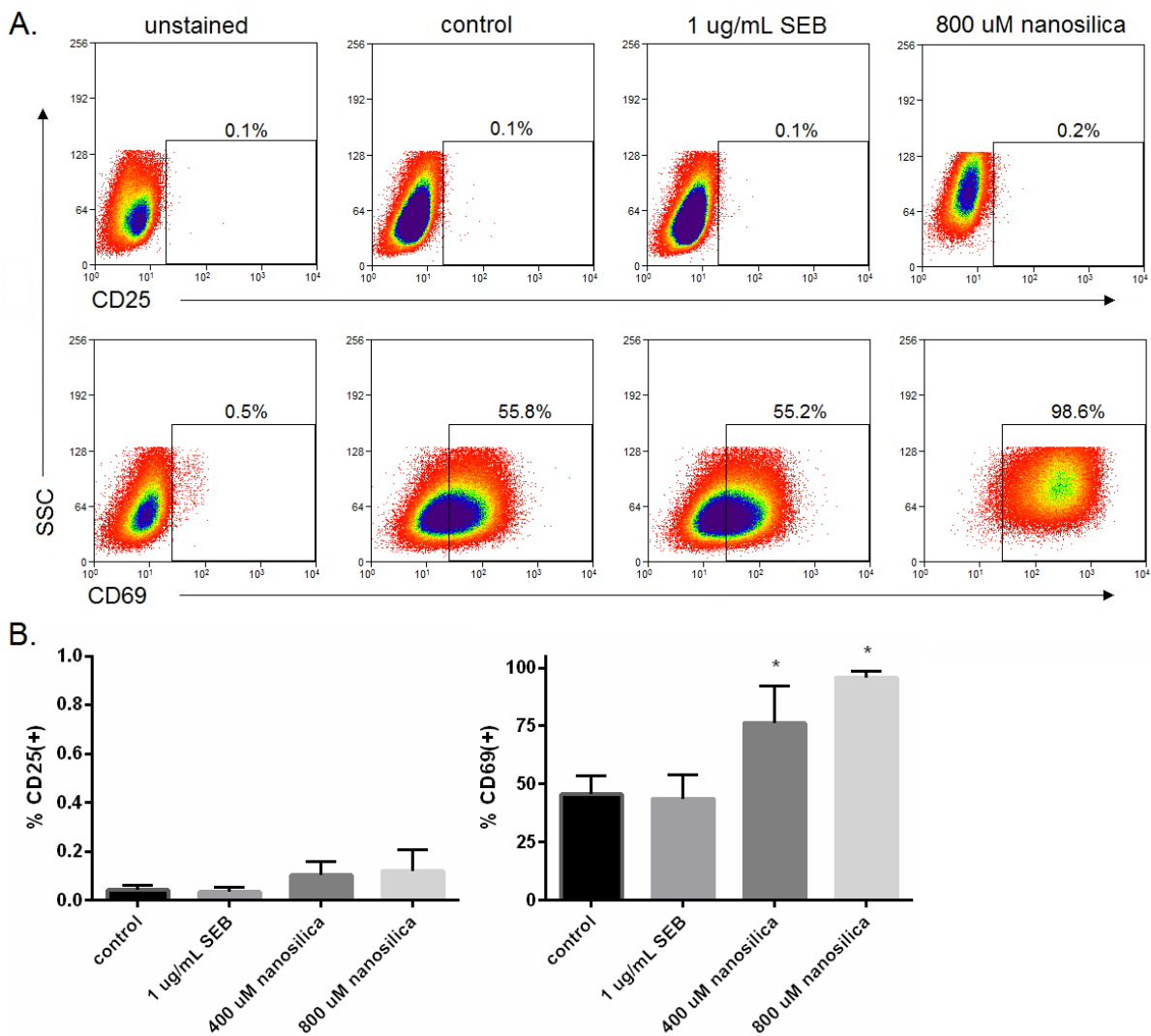


Figure 6.02. The effect of nanosilica on Jurkat T cell CD25 and CD69 expression. A. Representative dot plots showing the expression of CD25 and CD69 on Jurkat T cells. **B.** The percentage of Jurkat T cells positive for CD25 and CD69. Tabulated data represent the means \pm standard deviation for 3 independent replicates (* denotes significance compared to the control, unpaired T test, $p < 0.05$). Jurkat cells were first selected based on FSC versus SSC profiles to exclude debris followed by a viable T cell gate (7-AAD(-)CD3(+)).

The requirement of the TCR/CD3 complex in nanosilica induced T cell activation was investigated next. Karpas 299 cells, a lymphomic T cell line lacking the TCR/CD3 complex, were employed in these investigations. Figure 6.03 shows the effect of SEB and nanosilica on the expression of CD25 and CD69 on Karpas 299 cells. Over 95% of the untreated Karpas 299 cells were positive for CD25. These results corroborate studies which have shown that Karpas 299 cells have a regulatory T cell phenotype (Sandberg *et al.*, 2007). Regulatory T cells require IL-2 for homeostasis and therefore constitutively express the IL-2 receptor, in which CD25 is a component (Létourneau *et al.*, 2009; Malek and Castro, 2010). The baseline levels of CD69 were low, and treatment with SEB or nanosilica did not increase its expression. These results would suggest that the TCR/CD3 complex is required for T cell activation by nanosilica.

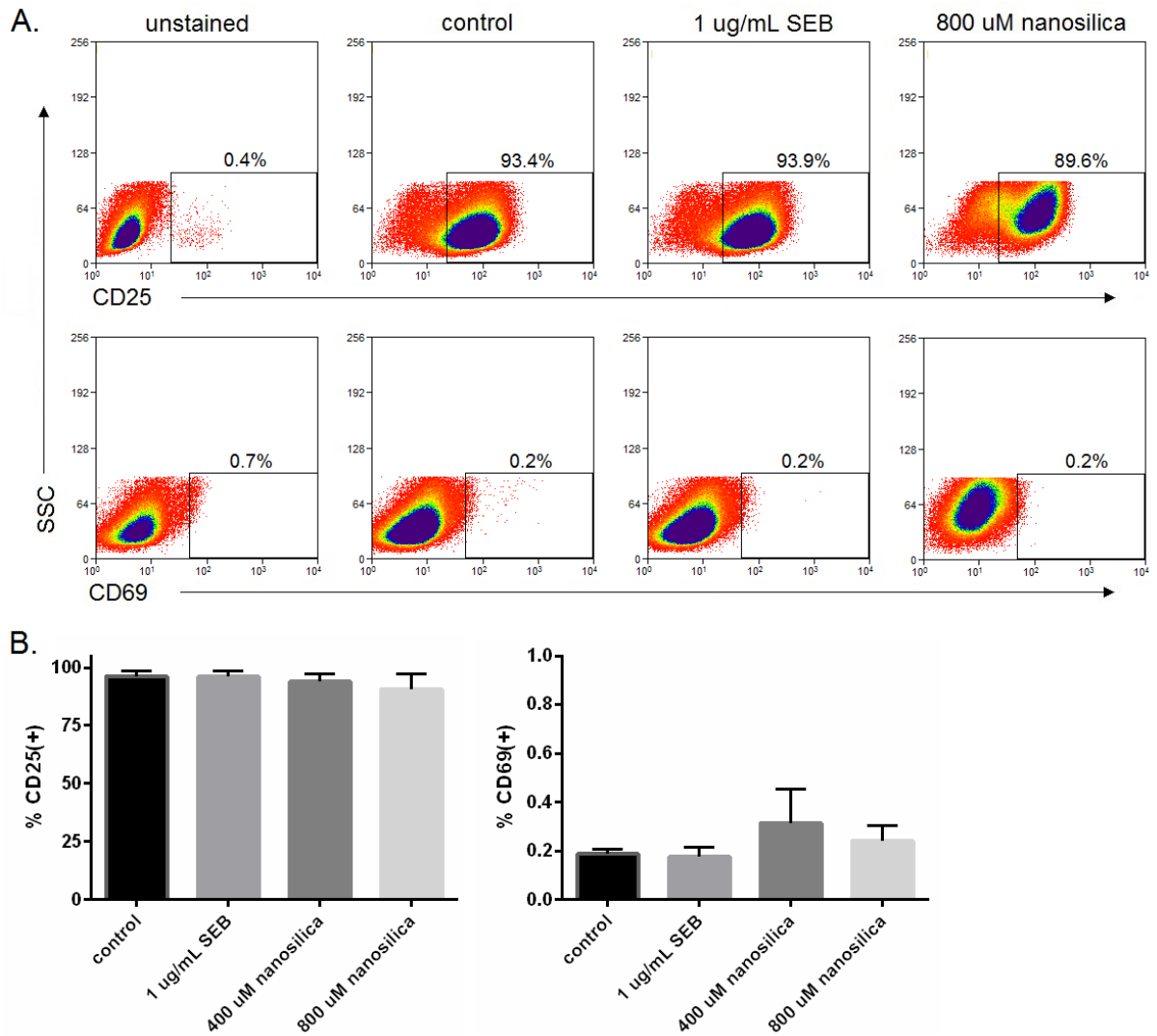


Figure 6.03. The effect of nanosilica on Karpas 299 cell CD25 and CD69 expression. A. Representative dot plots showing the expression of CD25 and CD69 on viable Karpas 299 cells. **B.** The percentage of Karpas 299 cells positive for CD25 and CD69. Tabulated data represent the means \pm standard deviation for 3 independent replicates (* denotes significance compared to the control, unpaired T test, $p < 0.05$). Karpas 299 cells were first selected based on FSC versus SSC profiles to exclude debris followed by a viability gate (7-AAD(-))

6.2.2 Induction of intracellular signalling pathways

The mechanism of nanosilica induced T cell activation was further investigated by assessing intracellular signalling pathways. Upon TCR engagement, downstream signalling is initiated through the phosphorylation of ITAMs, Zap70 and LAT (Brownlie and Zamoyska, 2013). Whether nanosilica is inducing signalling downstream of the TCR complex was first investigated by assessing the phosphorylation of Zap70 in enriched T cells from PBMC using western blot analyses.

Figure 6.04A shows an immunoblot, which was stained for vinculin and phosphorylated Zap70 (pZap70), of enriched T cell lysates after cultures were treated with nanosilica. The bands at *ca.* 130 kDa correspond to the vinculin protein. Vinculin is a cell membrane protein involved in cell adhesion and is commonly used as an immunoblot loading control (An *et al.*, 2012; Solan *et al.*, 2003). The band at *ca.* 70 kDa corresponds to pZap70. The control and the PHA treated cells did not contain significant levels of pZap70. Known T cell activators (superantigens, anti-CD3, PHA) are not commonly used as positive controls in phosphorylation studies as specific incubation steps, unlike those used here, are required to get an appropriate phosphorylation response (Watson and Lee, 2006). Instead hydrogen peroxide is commonly used, but was avoided here due to the long incubation times. Studies using Jurkat T cells with a hydrogen peroxide positive control showed significant levels of pZap70 (data not shown). The lysates of cells treated with nanosilica were positive for pZap70, indicating that nanosilica induces signalling downstream of the TCR. Figure 6.04B shows the normalized levels of pZap70 (compared to the internal control) in cell lysates after nanosilica treatment of cultures for 0.2 to 6 h. pZap70 was present in all cell lysates of cultures treated with nanosilica for 0.2-6 h, but its concentration was highest between 0.2 and 2 h. These results would suggest that nanosilica is inducing persistent signalling downstream of the TCR/CD3 complex. The concentration of pZap70 is approximately inversely proportional to the dissolution of nanosilica over time, potentially suggesting that nanosilica induces signalling as long as it is present in culture, corroborating studies shown later on in this section (Figure 6.10).

Investigations assessing the phosphorylation of LAT after nanosilica treatment were also conducted using enriched T cells from PBMC. The LAT protein is essential in T cell activation and is involved in a number of signalling pathways, including one leading to CD69 expression (Balagopalan *et al.*, 2010). It is phosphorylated by pZap70 after TCR engagement (Chakraborty and Weiss, 2014). Figure 6.05A shows an immunoblot of enriched T cell lysates after cultures were treated with nanosilica, staining for vinculin and phosphorylated LAT (pLAT). The levels of the pLAT protein (*ca.* 35 kDa in size) were low in the control culture lysates, where no distinct bands were evident. Bands corresponding to the pLAT protein were present in the lysates of cultures treated with nanosilica for 0.2 h. Figure 6.05B shows the normalized levels of pLAT (compared to the internal control) in cell lysates of cultures treated

with nanosilica. Nanosilica significantly increased the levels of the pLAT protein in lysates of enriched T cell cultures, corroborating the previous studies with pZap70 which show that nanosilica is inducing signalling downstream of the TCR complex.

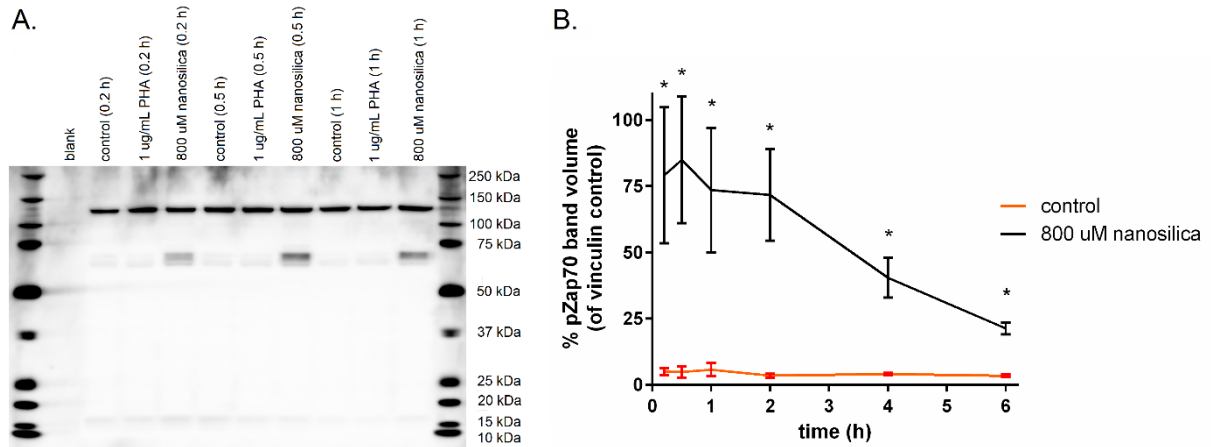


Figure 6.04. Effect of nanosilica on the phosphorylation of Zap70 in enriched T cell cultures. **A.** A representative immunoblot of lysates from cultures stimulated for 0.2-1 h. Blots were probed with antibodies to detect pZap70 (at Tyr319, protein ca. 70 kDa) and vinculin (protein ca. 128 kDa). **B.** Percentage of pZap70 band volume compared to the vinculin band (internal control). Tabulated data represent the means \pm standard error for 6 donors (* denotes significance compared to the control, paired T test, $p < 0.05$)

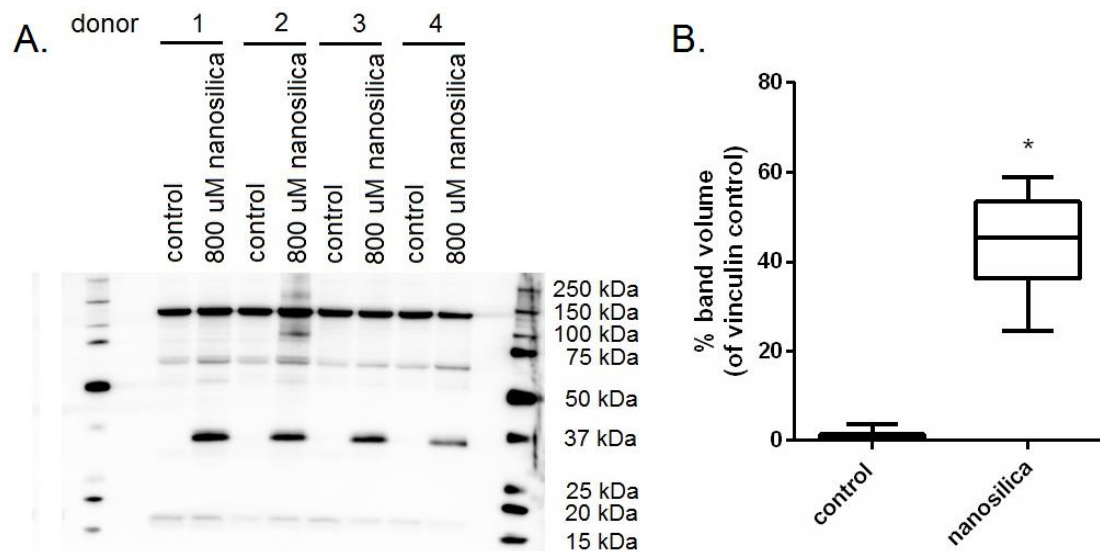


Figure 6.05. Effect of nanosilica on the phosphorylation of LAT in enriched T cell cultures. **A.** A representative immunoblot of lysates from cultures stimulated for 0.2 h. Blots were probed with antibodies to detect pLAT (at Tyr191, protein ca. 37 kDa) and vinculin (protein ca. 128 kDa). **B.** Percentage of pLAT band volume compared to the vinculin band (internal control). Tabulated data represent the means \pm standard deviation for 6 donors (* denotes significance compared to the control, paired T test, $p < 0.05$)

6.2.3 Incomplete signalling in nanosilica induced T cell activation

In the previous section, it was shown that nanosilica induces signalling downstream of the TCR complex. It was also shown, in Chapter 5, that nanosilica did not induce T cell proliferation. These results may provide a clue to the mechanism of T cell activation. T cell proliferation requires a secondary signal, *i.e.*, costimulation, supplied by the cell presenting antigen if the stimulation through the TCR is inefficient (Chen and Flies, 2013; Csencsits and Bishop, 2003). In this section, the effect of costimulatory signals on nanosilica induced T cell activation was investigated.

Chemical inducers were employed to understand the signalling initiated by nanosilica. Phorbol 12, 13-dibutyrate (PdBu) is a chemical compound known to induce signalling through MAPK, which, in a healthy interaction, is induced after engagement of the CD28 receptor (Macián *et al.*, 2002). Calcium ionophores, such as ionomycin, increase intracellular levels of calcium and induce signalling through NFAT which, in a healthy interaction, is induced after TCR engagement (Macian, 2005; Macián *et al.*, 2002). Extended incubation periods with these chemical inducers, like those used to measure proliferation, led to significant cell death (data not shown). Therefore, instead of assessing T cell proliferation directly, the production of the cytokine IL-2 was used as an early surrogate marker. IL-2 is required in late stage T cell proliferation, which makes its production an indirect measure of the potential for clonal expansion (D'Souza and Lefrançois, 2003). Figure 6.06 shows the IL-2 levels in supernatants of cultures treated with nanosilica, PdBu, and/or ionomycin. PdBu and ionomycin individually did not significantly induce production of IL-2, as signalling through both pathways (MAPK and NFAT, respectively) is required for complete activation. When both chemical inducers were added to cell cultures, high levels of IL-2 were present in the cell supernatants. Therefore, IL-2 production indicates whether downstream signalling of both TCR and CD28 is induced. There were low levels of IL-2 in the supernatants after treatment with 400 μ M nanosilica, which corroborates the results showing only a very small amount of T cell proliferation (Chapter 5). The addition of PdBu to the nanosilica treated cultures resulted in significant production of IL-2. A similar response was not evident with the addition of ionomycin. These results confirm that nanosilica is inducing signalling downstream of the TCR complex (which corroborates the immunoblot assays shown previously), but it does not induce signalling through pathways downstream of costimulatory receptors. As both these pathways can be induced by efficient TCR antigenic stimulation alone (Csencsits and Bishop, 2003), these results would also suggest that TCR stimulation by nanosilica is inefficient.

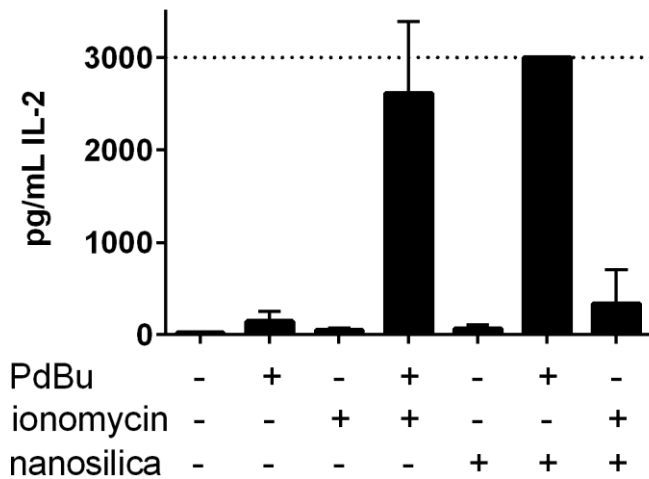


Figure 6.06. The effect of 400 μ M nanosilica, 0.5 μ g/mL ionomycin and 0.2 μ g/mL PdBu on IL-2 levels in PBMC culture supernatants at 24 h. Tabulated data represent the means \pm standard deviation for 4 replicates.

The effect of a costimulatory antibody, specifically anti-CD28, on T cell proliferation was next investigated, using CFDA-SE based flow cytometric assays. Figure 6.07 shows the effect of nanosilica and anti-CD28 on CD4 and CD8 T cell proliferation after 3 days. Neither the nanosilica nor anti-CD28 treatments induced significant T cell proliferation. There was a modest, but significant, increase in CD4 and CD8 T cell proliferation when cultures were treated with both nanosilica and anti-CD28 compared to all controls. These results would suggest that TCR signalling induced by nanosilica is inefficient and costimulatory signalling is required for a full T cell response, corroborating the studies with the chemical inducers. These results might also suggest that treatment with nanosilica alone can induce T cell anergy. Anergy is an activated T cell state in which the cells are hyporesponsive (Schwartz, 2003). It can be induced with chronic TCR stimulus without the appropriate costimulatory signals (Macian, 2005; Wells, 2009; Zheng *et al.*, 2008). Indications that nanosilica is inducing T cell anergy include the lack of proliferation and the lack of significant IL-2 production.

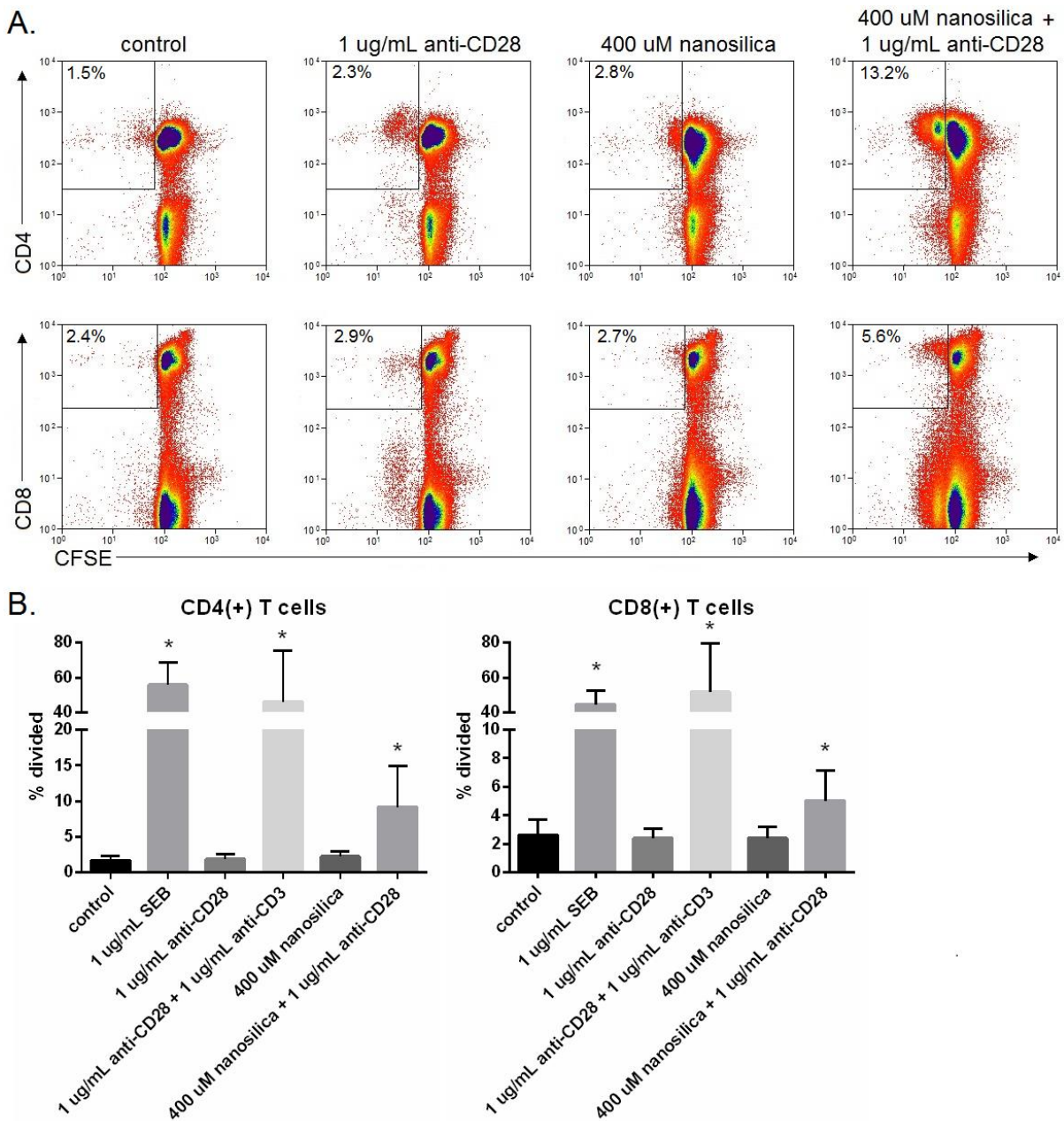


Figure 6.07. The effect of nanosilica and anti-CD28 on CD4 and CD8 T cell proliferation at 3 d. **A.** Representative dot plots showing CD4 and CD8 T cell proliferation. Although the CD4(-) and CD8(-) cells were shown in CD4 and CD8 plots, respectively, they were not included in the analysis. Therefore, percentages correspond to divided CD4(+) or CD8(+) T cells. **B.** The percentage of CD4 and CD8 T cells that have proliferated. T cells were first selected based on FSC versus SSC profiles through a T cell gate which also excluded debris, followed by a viable T cell gate (7-AAD(-)CD3(+)) and a CD4(+) or a CD8(+) gate. Tabulated data represent the means \pm standard deviation for 8 donors (* denotes significance compared to the negative controls (*i.e.*, control, anti-CD28, nanosilica), paired T test, $p < 0.05$)

In the above section, the inability of nanosilica to high amounts of T cell proliferation was investigated. Previous investigations have shown that nanosilica induces signalling downstream of the TCR complex. Here, it was shown that nanosilica does not induce signalling downstream of a co-stimulatory receptor, specifically CD28. When treated in combination with

the anti-CD28 antibody or PdBu (an inducer of the same pathway), nanosilica induced T cell proliferation and IL-2 production.

6.2.4 Nanosilica-T cell interactions

6.2.4.1 Primary screening

In the previous sections, nanosilica was shown to induce signalling downstream of the TCR complex and induce CD4 T cell activation in cultures deplete of APCs (MHC class II receptors). It was not able to induce activation of a T cell line lacking the TCR/CD3 complex. Taken together, these results might suggest that nanosilica is interacting directly with the TCR/CD3 complex. The effect of nanosilica on T cell staining with fluorescently conjugated antibodies was investigated to determine whether a direct interaction with the receptor is plausible. PBMC cultures were treated with nanosilica, incubated on ice for 5 min, and washed with PBS+BSA prior to staining for various T cell receptors. Figure 6.08 shows representative dot plots of TCR $\alpha\beta$, CD3 ϵ , CD4 and CD8 staining of cells within a T cell selection gate based off FSC versus SSC profiles after nanosilica treatment. The control group shows the typical proportion of cells positive for the T cell antibodies. The cells negative for the fluorescently conjugated TCR $\alpha\beta$ and CD3 ϵ antibodies correspond to B cells and monocytes that have bled into the T cell selection gate, along with NK cells that are not positive for the T cell markers. The SEB positive control had no effect on antibody staining. This would suggest that the TCR binding domain of SEB differs from than that of the fluorescently conjugated antibody used in this assay. Nanosilica was found to have a large effect on T cell antibody staining, where only a fraction of the cells were positive for TCR and CD3. This inhibition of staining might suggest that nanosilica is binding these receptors in a similar region as the TCR $\alpha\beta$ and CD3 ϵ antibodies. Nanosilica also affected CD4 and CD8 antibody staining. There was a large reduction in the mean fluorescent intensity of their expression when exposed to nanosilica (Figure 6.08). It is possible that the CD4 and CD8 receptors attempt to bind the TCR complex after engagement by nanosilica (as they would for a healthy pMHC-TCR interaction), thus becoming less susceptible to antibody staining. Figure 6.09 shows the effect of nanosilica pretreatment on TCR $\alpha\beta$, CD3 ϵ , CD4 and CD8 positivity within a T cell selection gate based off FSC versus SSC profiles. The consistent inhibition of TCR $\alpha\beta$ and CD3 ϵ antibody staining might suggest that nanosilica is interacting with the TCR-CD3 complex at the binding sites of the antibodies. Commercial fluorescent antibodies come with limited information regarding their binding site (and companies will not provide further details), so it is not possible identify exactly where they, and potentially nanosilica, are binding. Studies have extensively modelled the extracellular end of the TCR-CD3 complex, determining that the approximate size is 8 nm x 5.8 nm for the TCR $\alpha\beta$ unit, 4 nm x 5 nm for CD3 $\epsilon\delta$ unit, and 4 nm x 5.5 nm for CD3 $\epsilon\gamma$ unit (Sun *et al.*, 2004). It is unlikely that a single nanosilica particle (with a hydrodynamic diameter of 3.6 nm) is blocking both the TCR $\alpha\beta$ and CD3 ϵ antibodies, especially as there are two CD3 ϵ chains

flanking each side of the TCR unit. This might suggest that nanosilica is inducing receptor internalization and/or multiple particles are associating to the TCR receptor complex.

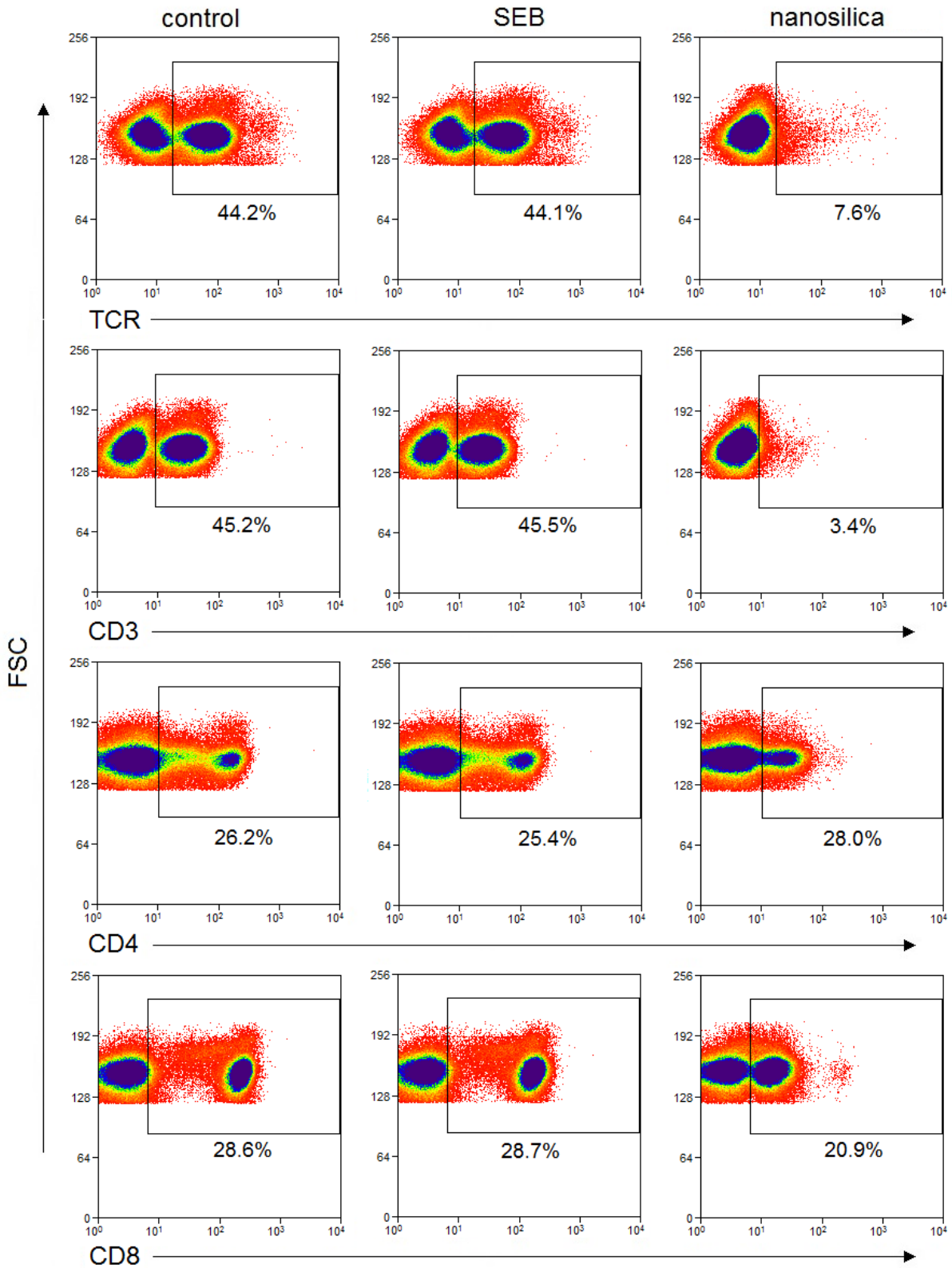


Figure 6.08. Representative dot plots showing the expression of TCR $\alpha\beta$, CD3 ϵ , CD4 and CD8 in cultures exposed to SEB and nanosilica for 5 min. T cells were selected based on FSC versus SSC profiles through a T cell gate which also excluded debris

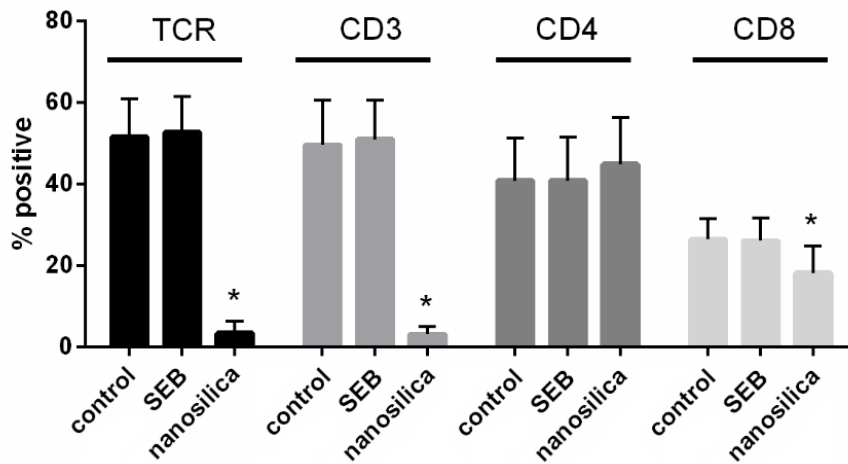


Figure 6.09. Percentage of the cells positive for TCR $\alpha\beta$, CD3 ϵ , CD4 and CD8 in cultures exposed to SEB and nanosilica for 5 min. Tabulated data represent the means \pm standard deviation for 4 donors (* denotes significance compared to the control, paired T test, $p < 0.05$). T cells were selected based on FSC versus SSC profiles through a T cell gate which also excluded debris

During healthy activation, the TCR complex is internalized after disengagement from the pMHC complex and is either recycled back to the surface or broken down (Finetti *et al.*, 2015). By permeabilizing the membrane and staining for CD3 and TCR, receptor internalization can be assessed. Figure 6.10 shows the percentage of cells positive for internal TCR and CD3 after treatment with nanosilica. Intracellular CD3 levels increased after nanosilica treatment, while levels of intracellular TCR did not. It is unclear whether the lack of intracellular TCR staining was due to the degradation of the TCR receptor. However, the results showing CD3 internalization would suggest that nanosilica is inducing receptor internalization, likely contributing to the lack of surface TCR and CD3 staining.

To explore whether the lack of staining shown in Figure 6.09 is solely due to receptor internalization, the effect of nanosilica on antibody staining in fixed cell cultures was investigated. Figure 6.11 shows the effect of nanosilica on TCR $\alpha\beta$, CD3 ϵ , CD4 and CD8 staining in cultures that were pre-treated with PBS+2% paraformaldehyde for 2 h. There was still a significant reduction in antibody staining after nanosilica treatment in the fixed cell cultures. This might suggest that nanosilica is directly binding the TCR/CD3 complex, thus inhibiting antibody staining. It is unknown where the nanosilica is binding but, as noted above, the size of the receptor, as modelled by Sun *et al.* (Sun *et al.*, 2004), versus the size of the particle (3.6 nm) would suggest multiple particles are involved. Additionally, the ability of nanosilica to inhibit CD3 ϵ staining might suggest that the particles are not interacting with the variable region of the TCR but instead a constant region on the TCR or CD3 receptor.

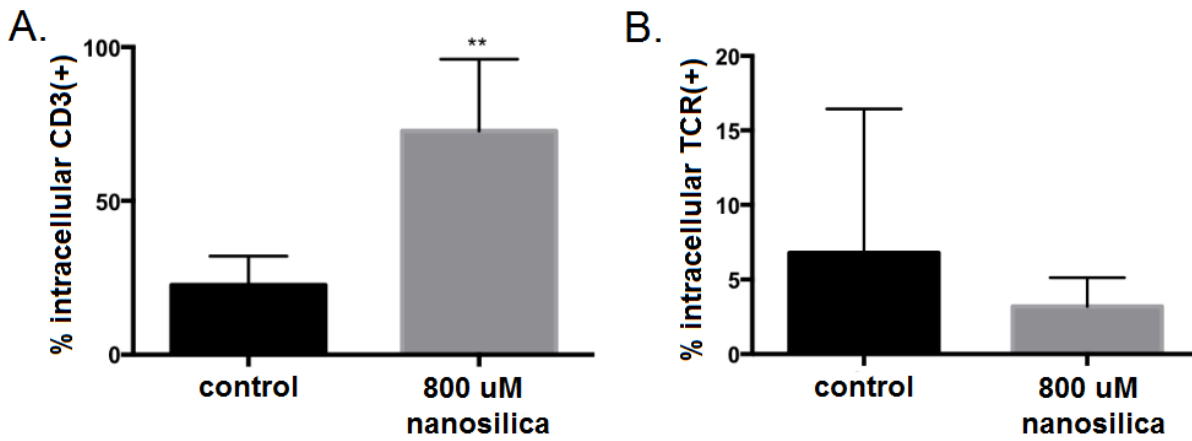


Figure 6.10. Percentage of the T cells positive for internal TCR and CD3 after treatment with nanosilica for 30 min. Tabulated data represent the means \pm standard deviation (* denotes significance compared to the control, paired T test, $p < 0.05$). Studies (experimental and analysis) conducted by C. Fairbairn.

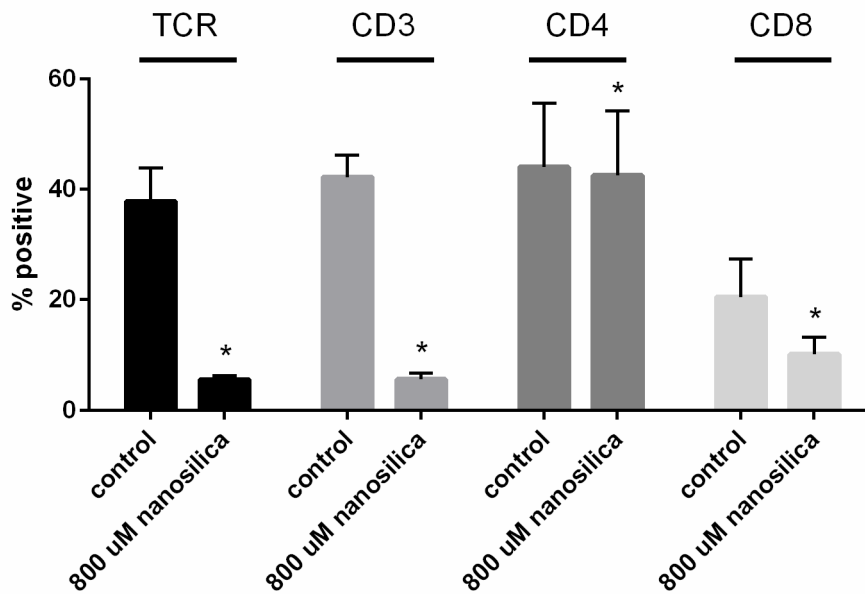


Figure 6.11. Percentage of the cells positive for TCR $\alpha\beta$, CD3 ϵ , CD4 and CD8 in fixed cell cultures exposed to nanosilica (800 μ M) for 10 min. The cells were incubated in 2% paraformaldehyde prior to treatment with nanosilica/staining. Tabulated data represent the means \pm standard deviation for 4 donors (* denotes significance compared to the control, paired T test, $p < 0.05$). T cells were selected based on FSC versus SSC profiles through a T cell gate which also excluded debris

Next, the inhibition of TCR and CD3 antibody staining by nanosilica was investigated over time. Figure 6.12 shows the effect of nanosilica on TCR $\alpha\beta$ and CD3 ϵ staining over 4 h, representing the data as percent inhibition calculated using the following equation (using TCR as an example).

$$\% \text{ inhibition of antibody staining} = \frac{(\% \text{TCR}(+)_{\text{control}} - \% \text{TCR}(+)_{\text{nanosilica}})}{\% \text{TCR}(+)_{\text{control}}} \times 100\%$$

There was significant inhibition of antibody staining up to 2 h after nanosilica treatment. At 4 h, nanosilica no longer had an effect on antibody staining, where the percentage of cells positive for TCR $\alpha\beta$ and CD3 ϵ was no different than that of the control. This trend is inversely proportional to the dissolution rate of nanosilica (shown in the red dashed line). Approximately 75% of the nanosilica is considered soluble (*i.e.*, < 3 kDa (1-2 nm) in size) after 4 h in cell culture media, as explained in Chapter 3. These results further confirm that nanosilica, not soluble silicon, interacts with the TCR/CD3 complex. Further investigations showed that orthosilicic acid did not affect TCR or CD3 antibody staining (data not shown). These results are also similar to those from the western blot analyses, which showed that TCR downstream signalling (*i.e.*, phosphorylation of Zap70) was greatest from 0.2 to 2 h after nanosilica treatment, and it decreased thereafter. Both western blot analyses and antibody staining inhibition would indicate that either the interaction between nanosilica and the TCR complex is persistent (*i.e.*, an irreversible interaction) or that this interaction is transient and nanosilica (which is in great excess) is in constant exchange with the receptor. Whichever the case, the interaction between nanosilica and the TCR complex not natural. The half-life between an MHC-foreign antigen complex and a TCR is typically 2-10 s and is even shorter when the MHC complex is presenting self-antigen (Acuto *et al.*, 2008). If the nanosilica:TCR/CD3 interaction is persistent, it could last up to 2 h, which is approximately 3,000 times longer than a healthy interaction. Alternatively, if the nanosilica is in constant exchange with the TCR/CD3 complex, it would transiently mimic an environment of infection which contains high antigen concentrations.

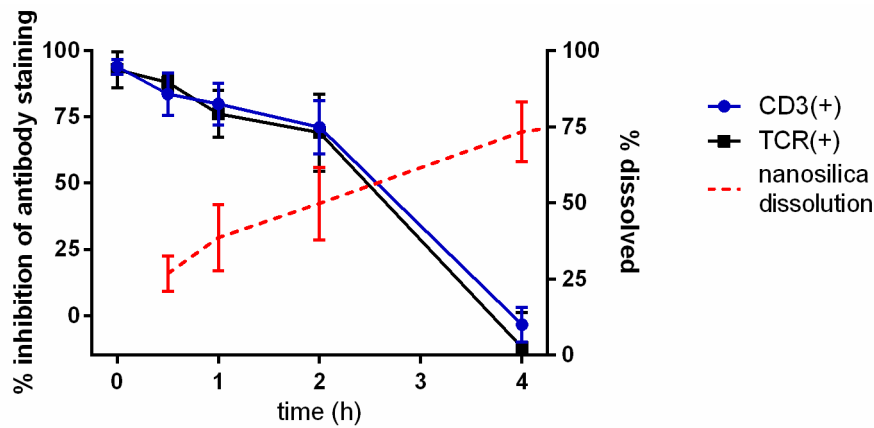


Figure 6.12. (Left y-axis) Percentage of the cells positive for TCR $\alpha\beta$, CD3 ϵ , CD4 and CD8 in cultures exposed to nanosilica (800 μ M) for 0.1-4 h. Tabulated data represent the means \pm standard deviation for 4 donors. T cells were selected based on FSC versus SSC profiles through a T cell gate which also excluded debris **(Right y-axis) Dissolution of nanosilica in cell-free growth media.** The percentage of dissolved silica as determined through ultrafiltration (see Chapter 3).

In the Chapter 5, nanosilica was found to activate $\gamma\delta$ T cells. The TCR of this less common T cell subset is comprised of γ and δ chains, rather than the more common α and β TCR chains. There are structural differences between the TCRs, as the angle between the constant and variable domain is smaller for the $\gamma\delta$ TCR than it is for the $\alpha\beta$ TCR (Allison *et al.*, 2001). Whether nanosilica inhibits the staining of a $\gamma\delta$ TCR antibody was investigated. Figure 6.13 shows the effect of nanosilica pretreatment on $\gamma\delta$ TCR positivity within a T cell selection gate based on FSC versus SSC profiles. As with the $\alpha\beta$ TCR antibody, nanosilica inhibited staining of the $\gamma\delta$ TCR antibody. The tabulated values show the inter-individual variance in $\gamma\delta$ T cell population size, which is consistent with that of the literature (Girardi, 2006). Despite inter-donor variance, the percentage of cells positive for $\gamma\delta$ TCR decreased after nanosilica treatment. The location of the nanosilica-TCR interaction remains unknown, but it is clear that nanosilica inhibits constant domain staining of the TCR complex. Whether the variable region of the receptor is also blocked is not known.

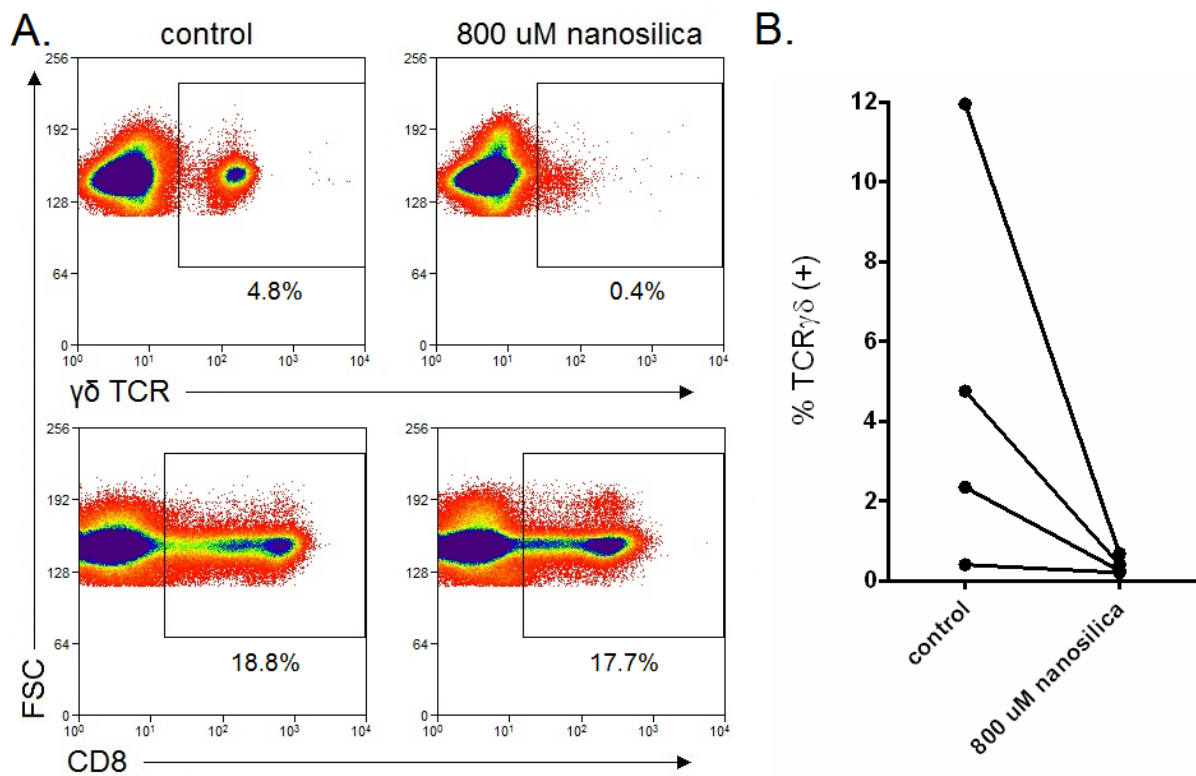


Figure 6.13. Effect of nanosilica on $\gamma\delta$ TCR and CD8 antibody staining. **A.** Representative dot plots showing the expression of $\gamma\delta$ TCR and CD8 on cells exposed to nanosilica (800 μ M) for 10 min. **B.** Percentage of the cells positive for $\gamma\delta$ TCR and CD8. No significance compared to the control (paired T test, $p < 0.05$), likely due to the inter-donor variance in $\gamma\delta$ T cell numbers. T cells were selected based on FSC versus SSC profiles through a T cell gate which also excluded debris

In the above sections, the mechanism of T cell activation induced by nanosilica was investigated. The activation of CD4 T cells by nanosilica was shown to be APC (MHC class II receptor) independent. Nanosilica did not induce activation of a T cell line lacking the TCR complex and was later found to inhibit TCR $\alpha\beta$, TCR $\gamma\delta$, and CD3 ϵ antibody staining. Additionally, the nanoparticulate was found to induce signalling downstream of the TCR complex. These results would suggest that nanosilica interacts directly with the TCR/CD3 complex. The data would also suggest that nanosilica is not interacting with the variable region of the TCR/CD3 complex but instead the constant domain or a conserved section of the variable region as 1) the variable region of TCRs vary significantly (Laydon *et al.*, 2015; Warren *et al.*, 2011), 2) nanosilica non-specifically activates >50% of T cells in PBMC culture, and 3) nanosilica non-specifically inhibits both TCR and CD3 antibody staining.

6.2.4.2 Particle specificity for inducing T cell activation

In the previous investigations (including those in Chapter 5), a nanosilica dispersion with a median diameter of 3.4-3.8 nm and specific dissolution rate was employed. The effect of particle characteristics, *i.e.*, size, condensation and composition, on T cell activation was investigated next as it may provide further insight towards nanoparticle-T cell interactions.

First, the effect of particle size on the induction of CD25 and CD69 was investigated. Figure 6.14A shows the particle size distribution of the nanosilica dispersions employed in the investigations. Although the median particle size differed between the dispersions, there was significant overlap in the size distribution of the materials. Many of the dispersions contained particles of the same diameter, though the proportion of these particles differed.

Figure 6.14B shows the effect of nanosilica particle size on the expression of CD25 and CD69 on CD4 and CD8 T cells after 24 h. There were significant differences in the induction of the activation markers between the materials tested, as shown in Table 6.01 for clarity. The greatest expression of CD25 and CD69 was induced by dispersions with median particle diameters of 3.6 ± 0.5 nm and 5.1 ± 0.6 nm (by volume, DV0.5). At a median particle size of 7.8 ± 0.7 nm, there was a significant decrease in the percentage of T cells positive for the activation markers compared that induced by the 3.6 ± 0.5 nm and 5.1 ± 0.6 nm dispersions. There was no significant induction of CD25 or CD69 on CD4 and CD8 T cells in cultures treated with the particles 16 ± 1.3 nm in size. The induction of the activation markers by particles 1.8 ± 0.7 nm in size was also significantly lower than that induced by 3.6 ± 0.5 nm and 5.1 ± 0.6 nm dispersions. However, this response cannot be solely assigned to particle size, as the dissolution profile between these dispersions differ greatly. Nanosilica dispersions > 3.6 nm in size have similar dissolution rates (Figure 3.01). The dispersions 1.8 ± 0.7 nm in size dissolve much more rapidly than the larger particles (Figure 3.05). Therefore, it is not possible to assign the decreased induction of CD25 and CD69 by the 1.8 ± 0.7 nm dispersion to size, as particle lifetime is also likely involved. Nonetheless, these results would suggest that the ability of nanosilica to induce T cell activation decreases as median particle size increases above 5 nm.

There are a number of possibilities to explain this size dependency. It is possible that T cells only interact with particles of a specific size range (likely between 1-5 nm). The induction of T cell activation by larger (>5 nm) particles could therefore be due to their change in size after dilution and incubation in cell culture media. The change in size can be achieved through dissolution or the breaking of large particle agglomerates. Alternatively, the size dependant T cell response could be due to particle affinity for the receptor. It is possible that the large nanosilica particles have a lower affinity for the receptor and therefore have decreased efficacy. Additionally, the particle concentration for larger dispersions is significantly lower than the smaller dispersions, potentially shifting the equilibrium away from TCR:nanosilica complex.

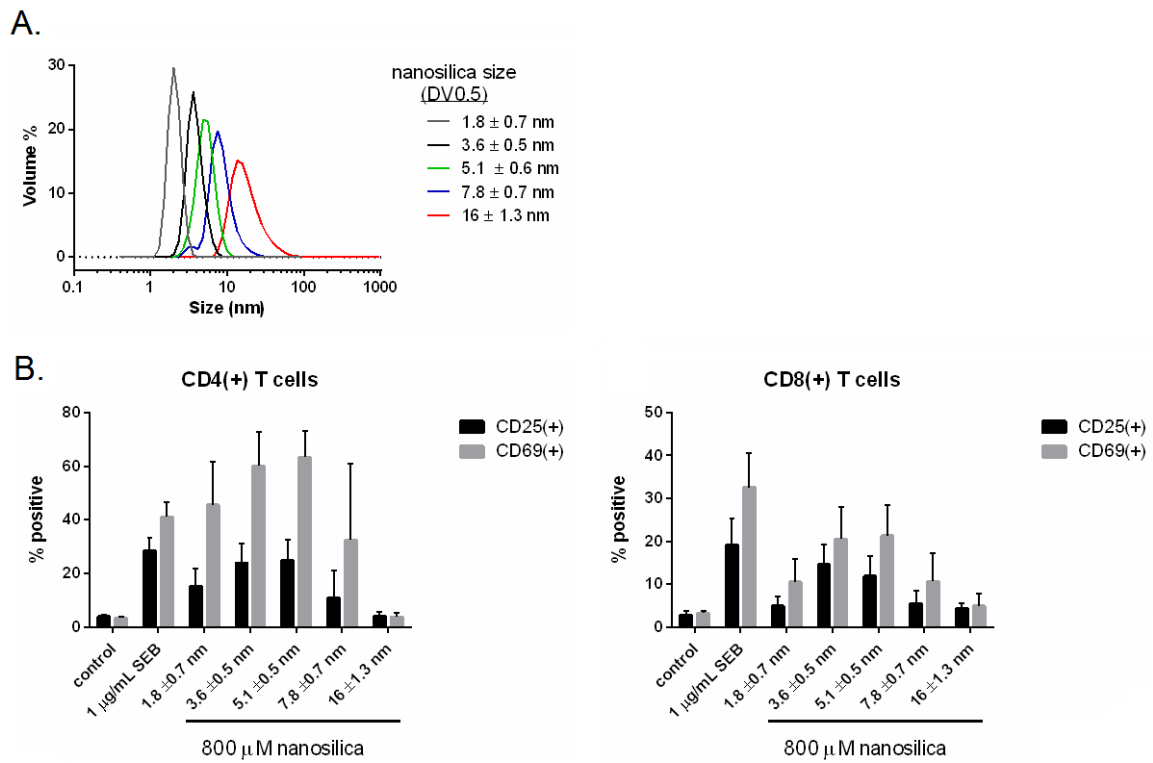


Figure 6.14. Effect of nanosilica particle size on expression of CD25 and CD69 on CD4 and CD8 T cells. **A.** The particle size distribution of the stock nanoparticle dispersions tested in cell assays. **B.** The effect of the dispersions (at 800 μ M Si) on CD25 and CD69 expression on CD4 and CD8 T cells. Tabulated data represent the means \pm standard deviation for a minimum of 8 donors. T cells were first selected based on FSC versus SSC profiles through a T cell gate which also excluded debris, followed by a viable T cell gate (7-AAD(-)CD3(+)) and a CD4(+) or a CD8(+) gate. Statistical analyses of cellular data is shown on the next page.

Table 6.01. Statistical analysis of the induction of CD25 and CD69 on CD4 and CD8 T cell between nanosilica dispersions of different sizes (shown in Figure 6.14). Green denotes significant, red denotes non-significant Two-way Anova, $p < 0.05$, $n = 8-12$

		median particle diameter				
		1.8 ± 0.7 nm	3.6 ± 0.5 nm	5.1 ± 0.6 nm	7.8 ± 0.7 nm	16 ± 1.3 nm
control	CD4-CD25	Red	Green	Green	Red	Red
	CD4-CD69	Green	Green	Green	Green	Red
	CD8-CD25	Red	Green	Green	Red	Red
	CD8-CD69	Green	Green	Green	Green	Red
1.8 ± 0.7 nm	CD4-CD25	Grey	Red	Red	Red	Red
	CD4-CD69	Grey	Green	Green	Red	Green
	CD8-CD25	Grey	Green	Green	Red	Red
	CD8-CD69	Grey	Green	Green	Red	Red
3.6 ± 0.5 nm	CD4-CD25	Grey	Grey	Red	Green	Green
	CD4-CD69	Grey	Grey	Red	Green	Green
	CD8-CD25	Grey	Grey	Red	Green	Green
	CD8-CD69	Grey	Grey	Red	Green	Green
5.1 ± 0.6 nm	CD4-CD25	Grey	Grey	Grey	Red	Green
	CD4-CD69	Grey	Grey	Grey	Green	Green
	CD8-CD25	Grey	Grey	Grey	Red	Green
	CD8-CD69	Grey	Grey	Grey	Green	Green
7.8 ± 0.7 nm	CD4-CD25	Grey	Grey	Grey	Grey	Red
	CD4-CD69	Grey	Grey	Grey	Grey	Green
	CD8-CD25	Grey	Grey	Grey	Grey	Red
	CD8-CD69	Grey	Grey	Grey	Grey	Red

Condensation is another important property of amorphous nanosilica particles. Condensation refers to the connectivity within the particles and it correlates with dissolution rate in dilute conditions (see Chapter 3). Particles with a slower dissolution rate were shown to have a greater percentage of fully condensed (Q^4) silicate centres and fewer partially condensed (Q^2 and Q^3) silicate centres. Whether particle dissolution rate affects nanosilica induced T cell activation was investigated.

Figures 6.15A and B show the size of the nanosilica dispersions and their dissolution rate in simple media at room temperature. For simplicity, the nanosilica dispersions were denoted as materials A and B. The particle size distribution of the materials was identical but their dissolution rates in dilute conditions differed, where material A dissolved more rapidly than

material B. All attempts made to prepare a more condensed particle resulted in increased particle sizes. This study was therefore limited to 2 materials.

Figure 6.15C shows the effect of the materials on CD25 and CD69 expression on CD4 and CD8 T cells. Both materials induced significant expression of the activation markers on both T cell subsets. The percentage of cells positive for the activation markers on CD4 T cells was significantly lower in cultures treated with material A compared to those treated with material B (shown in Figure 6.15D for clarity). A similar response was evident with CD25, not CD69, on CD8 T cells. The decreased response of T cells towards material A could potentially be explained by the increased dissolution rate. Alternatively, the particles could have varying affinities for the TCR/CD3 complex. To determine which is more plausible, the effect of nanosilica dissolution rate on the inhibition of fluorescent antibody staining was investigated.

Figure 6.16 shows the effect of material A and B on fluorescently conjugated antibody staining. Materials A and B both inhibited TCR and CD3 antibody staining to a similar extent. These results would suggest that both materials are rapidly engaging the TCR/CD3 receptor and have approximately the same affinity. Therefore, it is plausible that the decreased activation shown in Figure 6.15 is due to dissolution rate not affinity for the receptor. The increased dissolution rate would decrease the contact time with the receptor complex, thus decreasing induced activation.

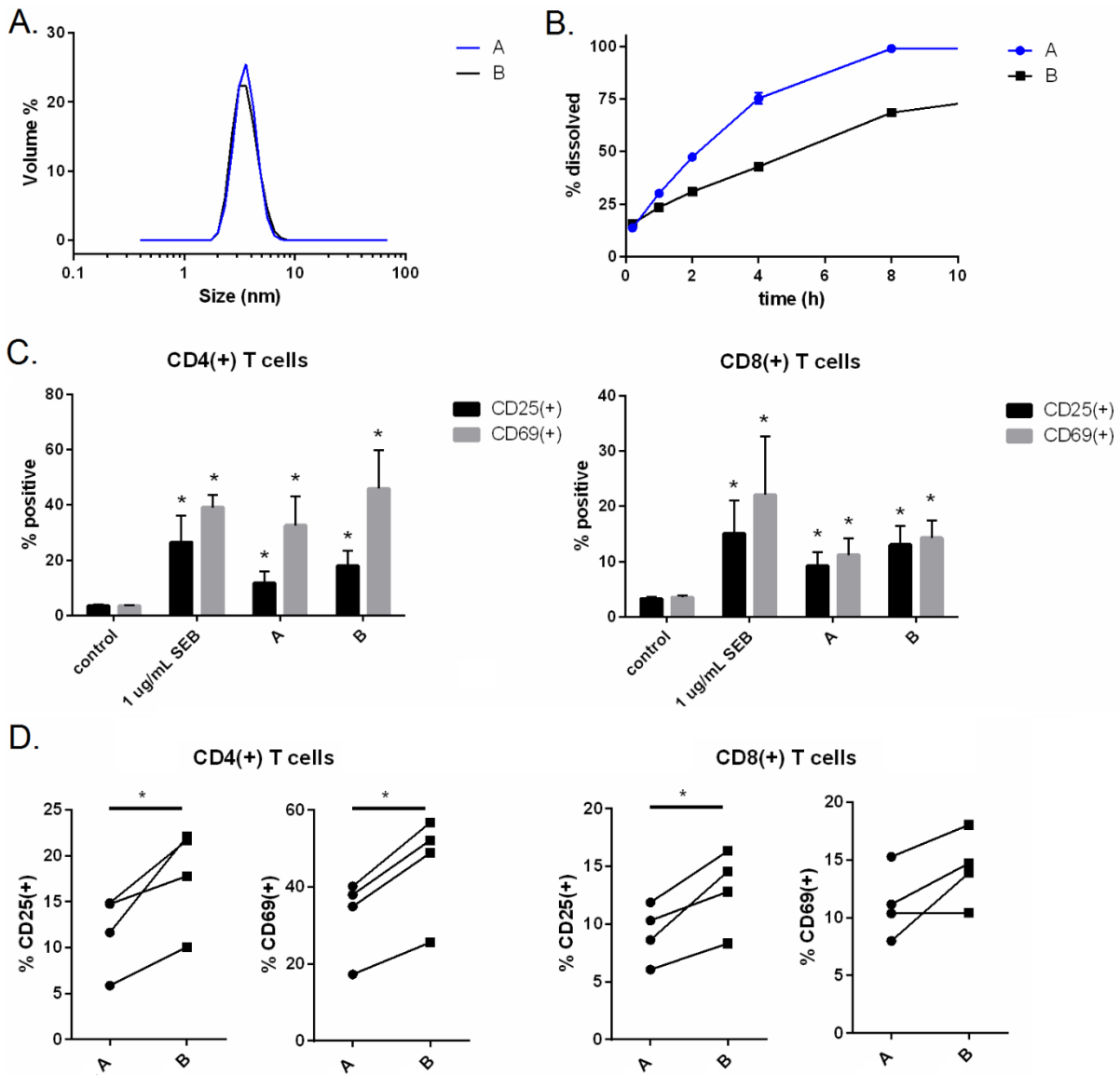


Figure 6.15. Effect of nanosilica particle lifetime in dilute conditions on expression of CD25 and CD69 on CD4 and CD8 T cells. **A.** The particle size distribution of the stock nanoparticle dispersions tested in cell assays. **B.** The dissolution rate of the nanosilica particles after dilution to 1 mM Si in HEPES (pH 7.4) at room temperature. **C.** The effect of the dispersions (at 800 μ M Si) on CD25 and CD69 expression on CD4 and CD8 T cells. Tabulated data represent the means \pm standard deviation for 4 donors (* denotes significance compared to the control, paired T test, $p < 0.05$). **D.** Comparison of the induction of activation markers by materials A and B on CD4 and CD8 T cells. (* denotes significance, paired T test, $p < 0.05$). T cells were first selected based on FSC versus SSC profiles through a T cell gate which also excluded debris, followed by a viable T cell gate (7-AAD(-)CD3(+)) and a CD4(+) or a CD8(+) gate

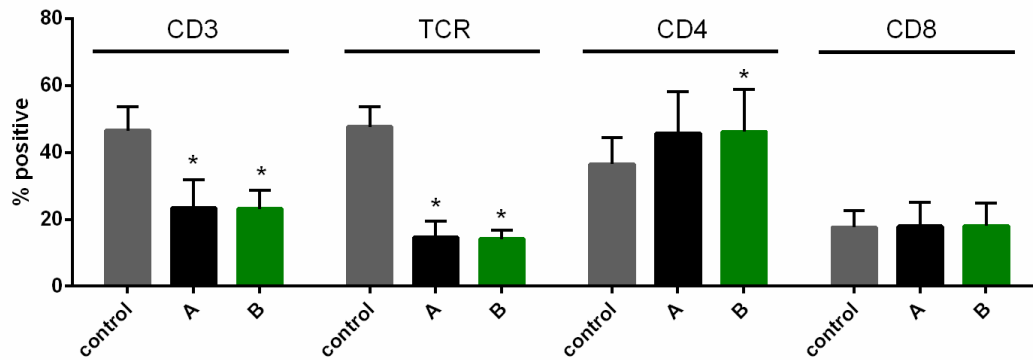


Figure 6.16. Percentage of the cells positive for TCR $\alpha\beta$, CD3 ϵ , CD4 and CD8 within a T cell selection gate (based on FSC versus SSC profiles) after treatment with 400 μ M nanosilica (materials A and B, as defined in Figure 6.20) for 10 min. Tabulated data represent the means \pm standard deviation for 4 donors (* denotes significance compared to the control, paired T test, $p < 0.05$)

The effect of iron nanoparticles on T cell activation was investigated to determine whether the response is limited to silica. Figure 6.17 shows the effect of nanoiron and nanosilica (sizes shown in A) on T cell activation. In addition to treatment in complete growth media, cells were also exposed to the nanoparticles in a basic salt solution (BSS) which was designed specifically to prevent nanoiron agglomeration (Pereira *et al.*, 2015). Nanosilica induced significant CD25 and CD69 expression on CD4 and CD8 T cells in full growth media and BSS media. Interestingly, nanosilica induced greater expression of the activation markers in BSS media than in full growth media. This may suggest that protein may interact with nanosilica, thus preventing it from interacting with the T cell. Protein has been shown to interact and form a corona with nanosilica, even at the low protein concentrations used in complete growth media (Clemments *et al.*, 2015; Lehman *et al.*, 2016). In BSS, the iron nanoparticles induced significant CD69 expression on CD4 T cells, but had no effect on CD25 expression. It also did not affect CD25 and CD69 expression on CD8 T cells in BSS media or either T cell subset in full growth media. Similar to nanosilica, iron nanoparticles are known to interact with protein in sera (Safi *et al.*, 2011), thus explaining the decreased response in the complete growth media. These results would suggest that the activation of T cells by nanoparticles is not completely restricted to silica, though the magnitude of the response to each material can vary significantly. In the literature there are studies that might suggest that other nanoparticles alter T cell function, as cobalt nanoparticles, ZnO nanoparticles and fullerenes have been shown to induce IFN- γ production in T cell containing cultures (Hanley *et al.*, 2009; Liu *et al.*, 2009; Petrarca *et al.*, 2005). Further investigations are required to investigate the effect of nanoparticle composition on T cell activation.

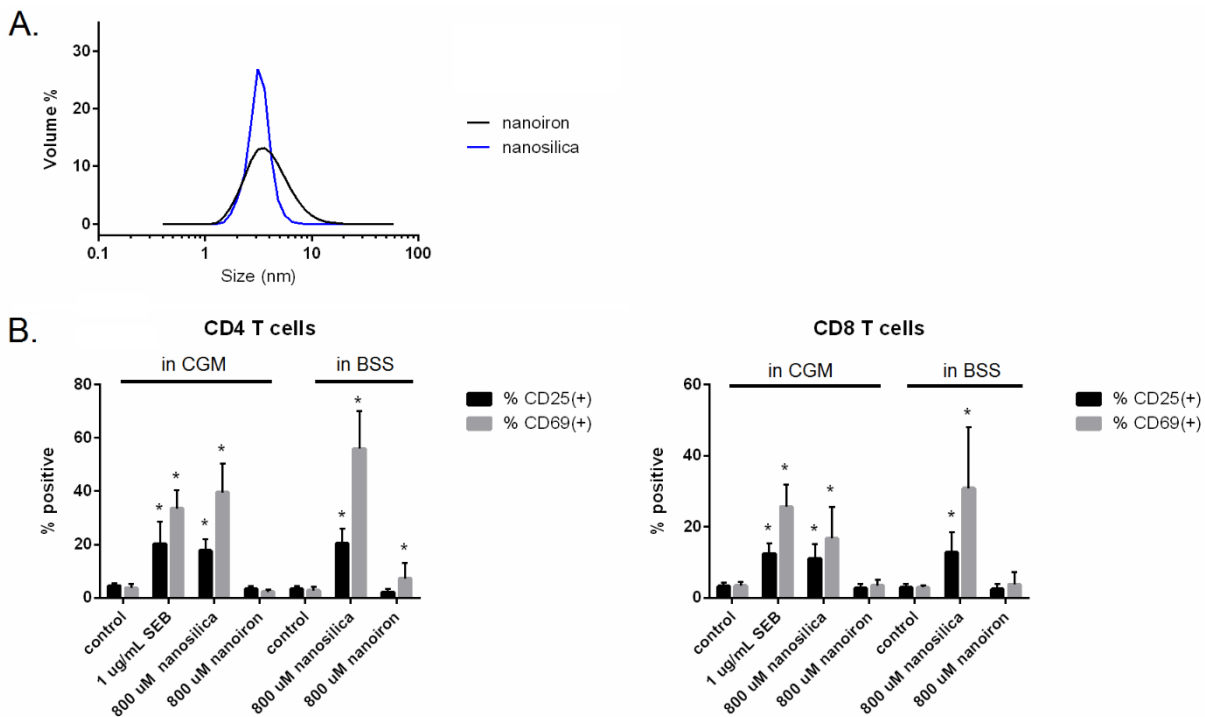


Figure 6.17. The effect of nanosilica and iron nanoparticles on expression of CD25 and CD69 on CD4 and CD8 T cells after 24 h. **A.** The particle size distribution of the stock nanoparticle dispersions tested in cell assays. **B.** The effect of the dispersions (800 uM Si or Fe) on CD25 and CD69 expression on CD4 and CD8 T cells. In CGM, the particles were added to culture followed by incubation for 24 h. In BSS media, the particles were added to culture, incubated for 3 h, resuspended in CGM, and incubated for 21 h. Tabulated data represent the means \pm standard deviation for 8 donors (* denotes significance compared to the control, paired T test, $p < 0.05$). T cells were first selected based on FSC versus SSC profiles through a T cell gate which also excluded debris, followed by a viable T cell gate (7-AAD(-)CD3(+)) and a CD4(+) or a CD8(+) gate

In this section, it was shown that nanosilica size has a large effect on the induction of T cell activation. Further analyses, e.g., theoretical modelling, high resolution imaging (SuperSTEM, neutron scatter) or plasma resonance analyses, are required to better understand the nanosilica-TCR/CD3 interaction. Iron nanoparticles were shown to induce CD4 T cell activation, though the response was much less significant than that induced by nanosilica.

6.3 Conclusions

In this chapter, the mechanism of nanosilica induced T cell activation was investigated. Previously, it was shown that nanosilica induces T cell activation, inducing expression of surface activation markers and cytokine production. Nanosilica did not induce complete T cell activation, as most T cells had not divided in cultures treated with the nanoparticulate. Investigations into the mechanism of activation were warranted, as activation of T cells by uncoated nanoparticles has never been documented.

First, it was determined that nanosilica does not require APCs for induction of CD4 T cell activation, suggesting that the effect is MHC class II independent. Next, it was shown that

nanosilica induces signalling downstream of the TCR/CD3 complex. In the previous chapter, it was shown that silica nanoparticles did not induce high levels of T cell proliferation, suggesting that it does not induce complete activation. Here, it was shown that full activation, *i.e.*, production of IL-2 and proliferation, can be induced by nanosilica in the presence secondary signals, *i.e.*, phorbate esters or anti-CD28.

Nanosilica was found to inhibit both TCR and CD3 antibody staining, which would suggest that nanosilica induces T cell activation by directly engaging the TCR/CD3 complex. A particle size range for maximum T cell response to nanosilica was determined, where particles 3.6-5.1 nm in size induced greatest expression of CD25 and CD69. T cell activation decreased significantly as size increased above 7 nm. Lastly, it was found that the induction of T cell activation was not specific to nanosilica, as low levels of CD69 were induced on CD4 T cells after nanoiron treatment.

In the next chapter, the ability of nanosilica to induce activation in whole blood was investigated. These studies may infer to the safety of the amorphous silica used in biomedical applications (Bitar *et al.*, 2012).

Chapter 7 – Effect of nanosilica on peripheral cells in whole blood and *in vivo*

7.1 Introduction

In Chapters 5 and 6, it was shown that amorphous silica nanoparticles induced T cell activation in isolated PBMC cultures. Nanosilica engaged the T cell receptor (TCR) complex, regardless of its antigenic peptide specificity, and induced downstream signalling leading to induction of activation markers (*e.g.*, CD25, CD69 and, to a lesser extent, CD95) and cytokine production (*i.e.*, IFN- γ and, to a lesser extent, IL-2). Nanosilica did not induce high levels of T cell proliferation and was later found not to induce signalling through MAPK, which can be induced through sufficient TCR signalling or engagement of the costimulatory receptor CD28 (Chen and Flies, 2013; Csencsits and Bishop, 2003).

Previous investigations of T cell activation and cell viability were conducted in isolated peripheral blood mononuclear cell (PBMC) and cell line cultures, suspended in complete growth media (CGM). Whole blood is a more complex matrix than CGM as it contains plasma, platelets, higher protein concentrations, red blood cells and polymorphonuclear cells, including neutrophils. Amorphous silica has been shown to interact with each of these components (Clemments *et al.*, 2015; Gryshchuk and Galagan, 2016; Lehman *et al.*, 2016; Zhang *et al.*, 2012; Zimmerman *et al.*, 1986). These interactions could potentially alter the dynamic of nanosilica in culture. In this chapter, the effect of nanosilica on T cell activation and cell viability was assessed in whole blood, as it may infer towards the safety of these particles *in vivo* after, for example injection for use in biomedical applications (Bitar *et al.*, 2012; Meddahi-Pellé *et al.*, 2014; Scaramuzzi *et al.*, 2016; Skrastina *et al.*, 2014). Additionally, whether these particles have therapeutic effects *in vivo* was investigated.

7.2 Results and discussion

7.2.1 Activation and toxicity in whole blood – preliminary investigations

First, the ability of nanosilica to induce T cell activation in whole human blood was investigated. As with the previous chapters, T cell activation was assessed using the CD25 and CD69 activation markers. These activation markers are expressed on T cells after recognition of cognate antigenic peptide (presented in a MHC receptor) (D'Souza and Lefrançois, 2003; Malek and Castro, 2010; Radulovic *et al.*, 2013) and have been shown to be induced by nanosilica (Chapters 5 and 6). Here, T cells were identified by the CD3 receptor, which is a part of the T cell receptor complex and is involved in T cell activation and signalling (Wang *et al.*, 2009b).

Figure 7.01 shows the effect of nanosilica on CD3 T cell activation in whole blood after 24 h. In the untreated control, the expression of CD25 and CD69 was low, in both the intensity of its expression (fluorescence, Figure 7.01A) and in the percentage of cells positive for the

receptors (Figure 7.01B). The percentage of T cells positive for the activation markers were similar to those reported in the literature for peripheral T cells (Reddy *et al.*, 2004; Sancho *et al.*, 1999). The *Staphylococcal enterotoxin B* (SEB) positive control significantly increased the expression CD25 and CD69 on CD3 T cells. These results would indicate that T cells in whole blood culture respond appropriately to stimulation. SAGs are known to induce chronic T cell activation in the periphery, which can lead to a number of symptoms (vomiting, fever, rash) and even lethal shock (Fraser, 2011). A soluble silica (silicic acid) control was not used in these investigations due to the low solubility of Si at physiological pH. The addition of a neutral silicic acid stock would result in significant dilution of the blood and therefore would alter the whole blood environment. Nanosilica, at a concentration of 400 μM Si, did not significantly affect the expression of CD25 or CD69 on CD3 T cells. At the same concentrations in PBMC culture, there was significant induction of these activation markers (Chapter 5). These results would suggest that the effects of nanosilica are significantly attenuated in whole blood. At a concentration of 800 μM Si, nanosilica significantly induced the expression of CD69 on CD3 T cells in whole blood, though only *ca.* 2% of the T cells were positive for this marker. At 2 mM Si, a concentration which surpasses the solubility limit of amorphous silica at blood pH (*ca.* 1.7 mM Si at pH 7.4 (Jugdaohsingh *et al.*, 2008; Mosby, 2016)), the effect of nanosilica on T cell activation was still low. In these conditions, the particles would not be able to dissolve completely, meaning a fraction of the particles would be persistent throughout the incubation period. The phase of these particles is unknown, though in a complex matrix such as whole blood it is very likely that, for the particles not phagocytosed by monocytes and neutrophils, agglomerates would form with itself or with other components contained in blood. The response of nanosilica is significantly attenuated in whole blood. Whole blood is a much more complex matrix than cell culture media, with higher protein content (upwards of 4 g/L albumin (Don and Kaysen, 2004)) and other factors such as platelets and red blood cells that can and have been shown to interact with silica (Clemments *et al.*, 2015; Gryshchuk and Galagan, 2016; Lehman *et al.*, 2016; Zhang *et al.*, 2012; Zimmerman *et al.*, 1986). Additionally, whole blood contains polymorphonuclear cells, such as neutrophils (commonly 40-80% of peripheral cells, cell counts shown in Figure 7.05), which are not present in isolated peripheral blood mononuclear cell (PBMC) cultures. The interaction of nanosilica with these components would limit its exposure to T cells and thereby decrease the cellular response.

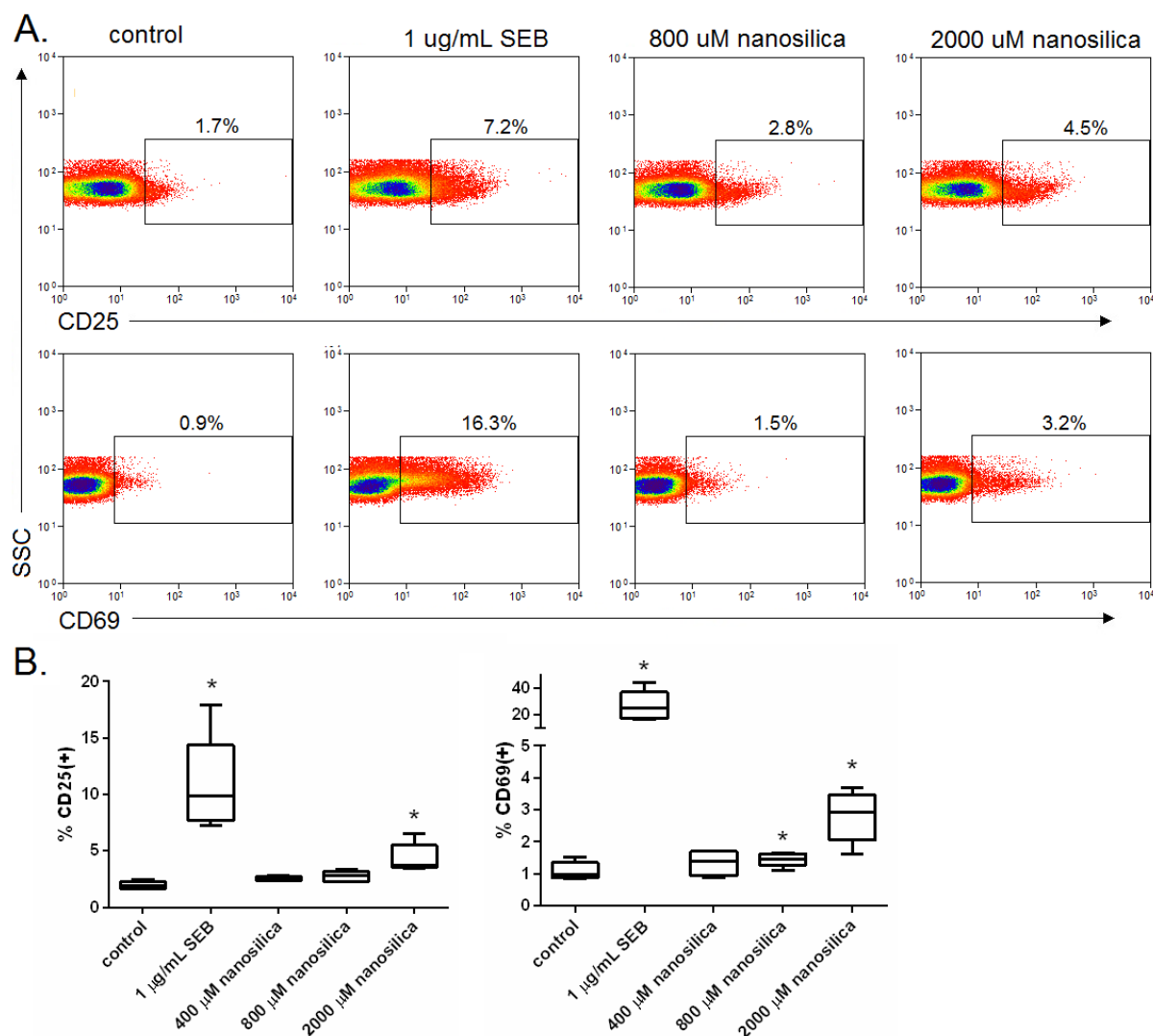


Figure 7.01. The effect of nanosilica on the percentage of CD3 T cells positive for CD25 and CD69 in whole blood culture after 24 h. A. Representative dot plots showing the expression of CD25 and CD69 on CD3 T cells. **B.** Tabulated data represent the averages for 5 donors (* denotes a significance compared to the control, two-tailed paired T test, $p < 0.05$). T cells were first selected based on FSC versus SSClog profiles through a T cell gate which also excluded debris, followed by a singlets gate (FSClin vs FSCarea), a T cell gate (CD3(+)) and a viability gate (Invitrogen LIVE/DEAD, Violet^{LOW}).

Next, investigations were conducted using nanosilica dispersions with varying properties. In Chapter 6, the effect of nanosilica size on the induction of T cell activation was conducted in PBMC culture. In this simple matrix, it was found that the particles with a median diameter of 3.6-5.1 nm induced greatest expression of CD25 and CD69 on CD4 and CD8 T cells, while particles both larger and smaller had decreased efficacy. However, it was not wholly established whether the decreased efficacy of the smaller particles was due to size or particle dissolution rate. In whole blood, the dispersion which induces greatest T cell activation could differ from that in PBMC cultures, as there are a greater number of components with which nanosilica can interact and higher concentrations of nanosilica are required to induce activation (thus normalizing for particle dissolution rate). Therefore, investigations were conducted to

assess the effect of 1-2 nm and 3.6 nm nanosilica dispersions on T cell activation in whole blood. In these investigations, additional markers were used to identify helper and cytotoxic T cells. Helper T cells, which can be identified by their CD4 co-receptor, mediate immune responses by releasing cytokines and expressing various surface receptors after recognition of cognate antigen (DuPage and Bluestone, 2016; Geginat *et al.*, 2015; Meddahi-Pellé *et al.*, 2014). Cytotoxic T cells (CTLs), which can be identified by the CD8 co-receptor, execute an immune response by directly engaging a target cell and releasing factors to induce its death (Aktas *et al.*, 2009; Alter *et al.*, 2004; Chakraborty and Weiss, 2014). Upon activation, both helper and cytotoxic T cells are known to express the CD25 and CD69 activation markers (Broere *et al.*, 2011; Létourneau *et al.*, 2009; Malek and Castro, 2010; Radulovic *et al.*, 2013).

Figures 7.02A and B show the representative sizes and dissolution rates of the materials employed in the whole blood investigations. Material A, which has a median diameter of 3.5 nm, is a concentrated mimic of the dispersion tested in Figure 7.01. This material was originally developed for translation into *in vivo* studies, as more concentrated dispersions were required due to limited dose volumes. Material B is a nanosilica dispersion 1-2 nm in diameter. It is prepared at low pH and it dissolves rapidly when diluted below the solubility limit of amorphous silica. Figure 7.03 shows the effect of the materials, at a concentration of 4 mM Si, on the expression of CD25 and CD69 on CD4 and CD8 T cells in whole blood. The baseline expression levels were low in the control, indicating a contamination free environment, and exposure to SEB lead to the induction of the activation markers. The effect of the nanosilica particles on T cell activation was low, even at a concentration of 4 mM Si. These results further emphasize the attenuated responses present in whole blood cultures. At these concentrations more than half of the Si would remain insoluble for the entire incubation period (Jugdaohsingh *et al.*, 2008; Mosby, 2016). However, it is likely that a large portion of the nanosilica would be phagocytosed and, the particles that were not, would likely agglomerate with itself and other components of blood. Given the low activation levels at 24 h, it is highly plausible that nanosilica does not stay in a form capable of inducing T cell activation. The nanosilica particles induced similar levels of CD25 and CD69 expression on both CD4 and CD8 T cells, regardless of particle properties. Given the complex matrix and the unknown form of nanosilica after its addition, it is difficult to interpret these results. For example, the exact form of the particle inducing activation is unknown, as it could be induced by the specific particle added into the blood or an agglomerate that is formed in blood. Nonetheless, these results would suggest that it is possible for nanosilica to induce T cell activation in whole blood.

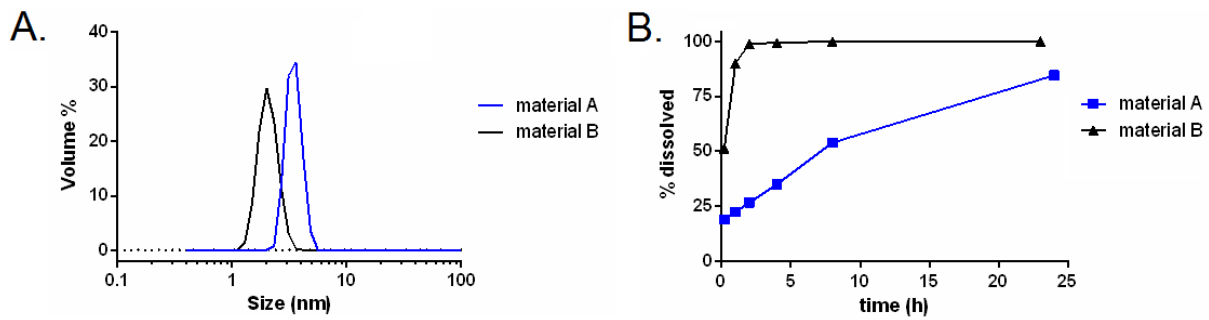
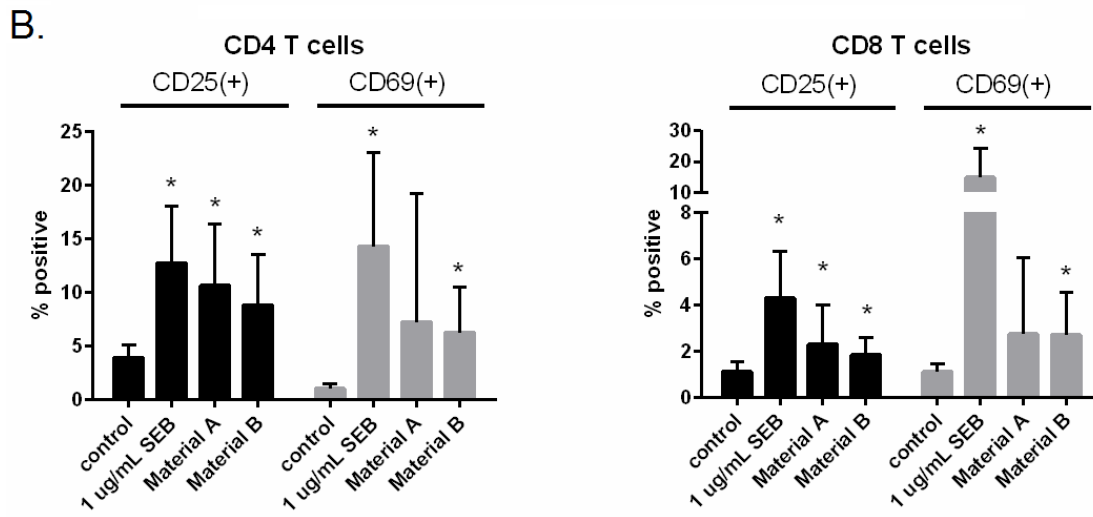
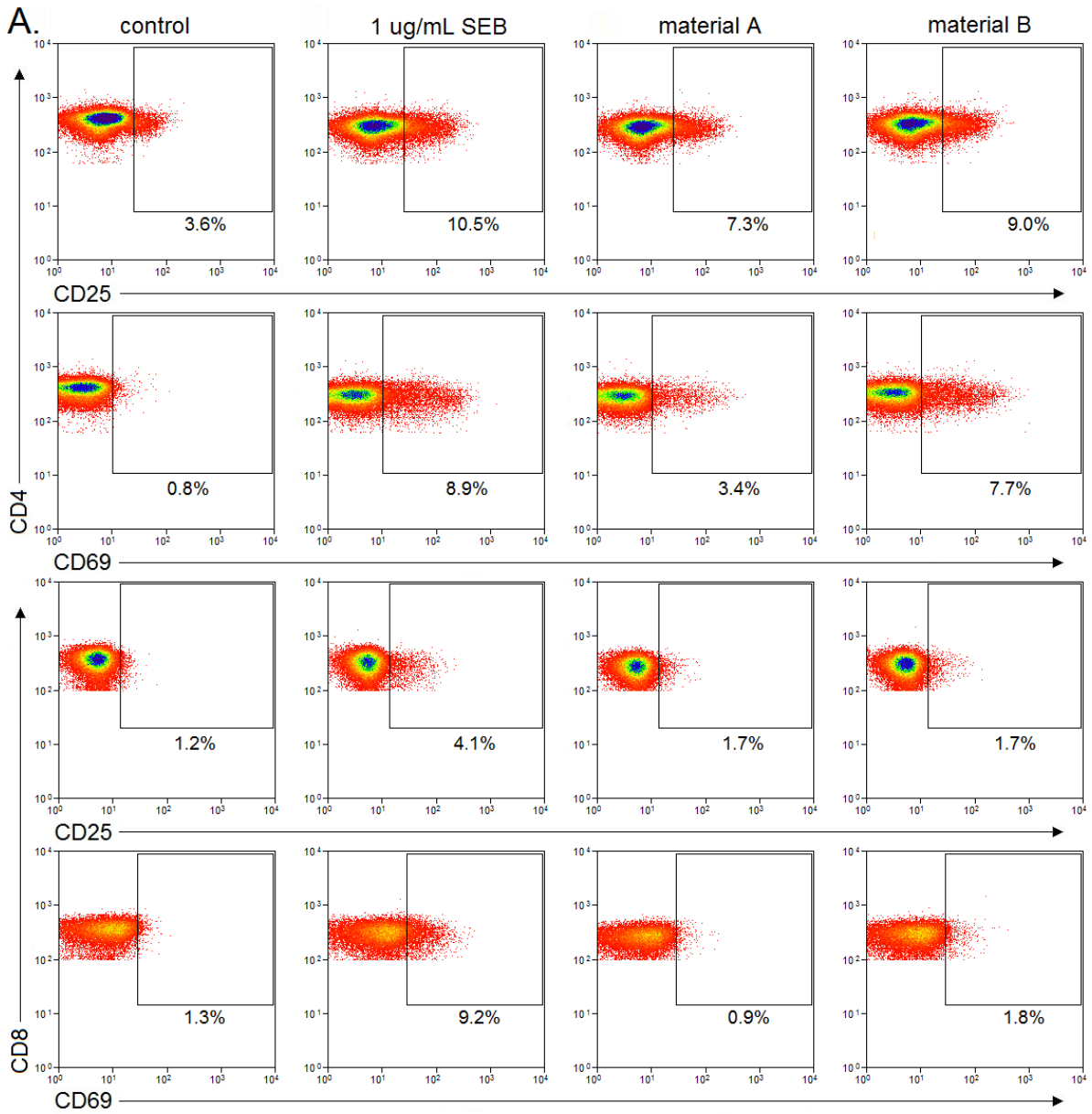


Figure 7.02. Representative size (A.) and dissolution rate (B.) of nanosilica dispersions (40 mM Si, various formulations denoted as materials A and B) employed in the whole blood assays (Figure 7.03)

Figure 7.03 The effect of nanosilica on the percentage of CD4 and CD8 T cells positive for CD25 and CD69 in whole blood culture after 24 h (overleaf). A. Representative dot plots showing the expression of CD25 and CD69 on CD4 and CD8 T cells. B. Tabulated data represent the means \pm standard deviation for 11 donors (* denotes a significance compared to the control, two-tailed paired T test, $p < 0.05$). T cells were first selected based on FSC versus SSClog profiles through a T cell gate which also excluded debris, followed by a singlets gate (FSClin vs FSCarea), a T cell gate (CD3(+)), and a CD4(+) or CD8(+) gate.

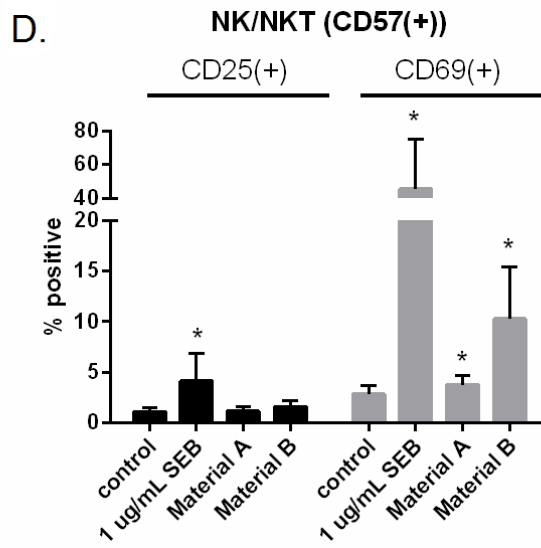
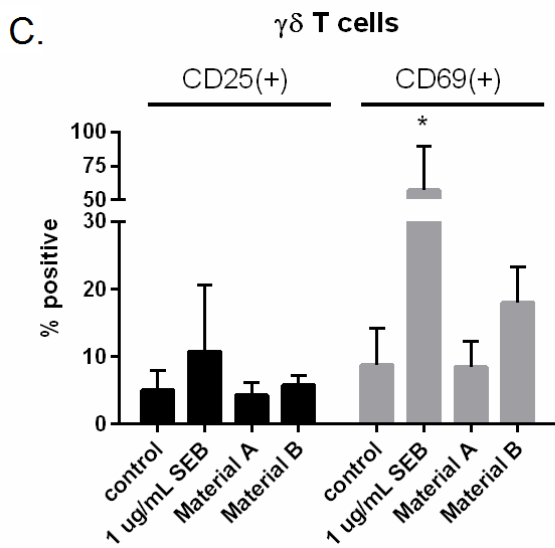
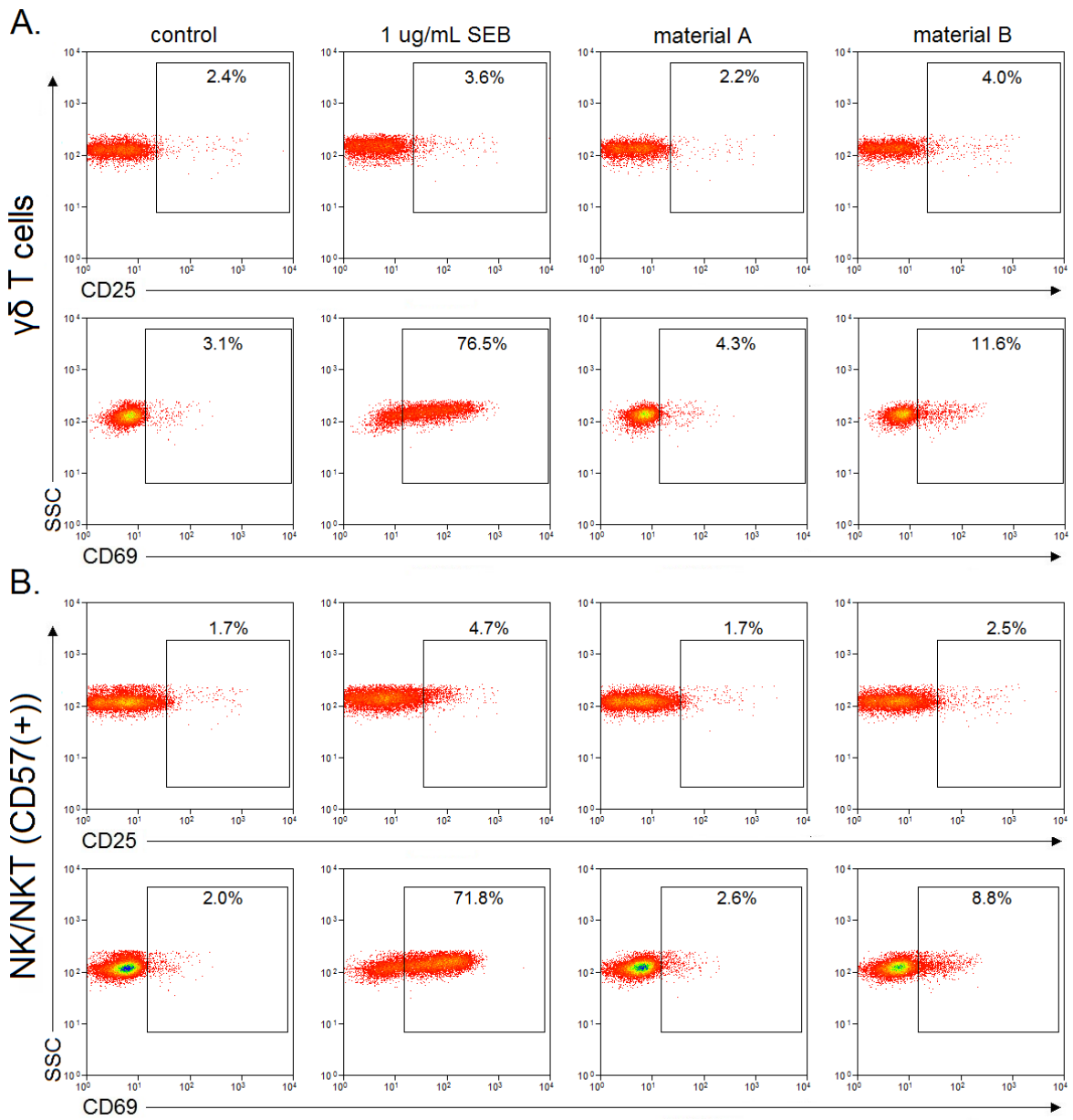


Next, the effect of nanosilica on $\gamma\delta$ T cells and NK/NKT cells in whole blood was investigated. These lymphocyte subsets are activated differently than $\alpha\beta$ T cell subsets. Instead of recognising antigenic peptide presented on an MHC receptor via a TCR, these cells are activated by the recognition of antigens on MHC-like CD1 receptors ($\gamma\delta$ T cells and NKT cells), soluble antigens ($\gamma\delta$ T cells) or stress receptors on expressed on the surface of cells (NK/NKT cells) (Dar *et al.*, 2015; Long *et al.*, 2013; Vantourout and Hayday, 2013; Vivier *et al.*, 2008; Vivier *et al.*, 2012; Wiest, 2016; Wu *et al.*, 2014) . Nanosilica was previously shown to induce activation of these lymphocyte subsets in PBMC cultures (Chapter 5). Whether activation is also induced in whole blood was investigated here. $\gamma\delta$ T cells were identified by its $\gamma\delta$ TCR and NK/NKT cells were identified by the CD57 receptor (Leong *et al.*, 2003).

Figure 7.04 shows the effect of nanosilica (as characterized in Figure 7.02) on CD25 and CD69 expression on $\gamma\delta$ T cells and NK/NKT cells. The baseline activation levels of the lymphocyte subsets was low and the superantigen induced significant expression of CD69 on $\gamma\delta$ T cells and both CD25 and CD69 on NK/NKT cells. After SEB treatment, upwards of 50% of these cytotoxic lymphocytes were positive for CD69, corroborating studies which show superantigens induce chronic activation of these cell subsets (Chen *et al.*, 2009b; D'Orazio *et al.*, 1995; Ramesh *et al.*, 1995; Rust and Koning, 1993). The nanosilica dispersions did not induce significant expression of CD25 or CD69 on $\gamma\delta$ T cells, though low levels of CD69 were induced by material B. As with the decreased responses of $\alpha\beta$ T cells to nanosilica, the complex matrix of whole blood is likely responsible for the attenuated responses present here. CD69 was significantly induced on NK/NKT cells after treating with nanosilica (both materials). As discussed in Chapter 5, the mechanism of induced NK/NKT cell activation by nanosilica is unknown. It is possible that nanosilica induces the expression of stress markers on other cells in whole blood, thus leading to NK/NKT cell activation upon their recognition.

Overall, these results would suggest that nanosilica is capable of inducing activation of lymphocytes in whole blood.

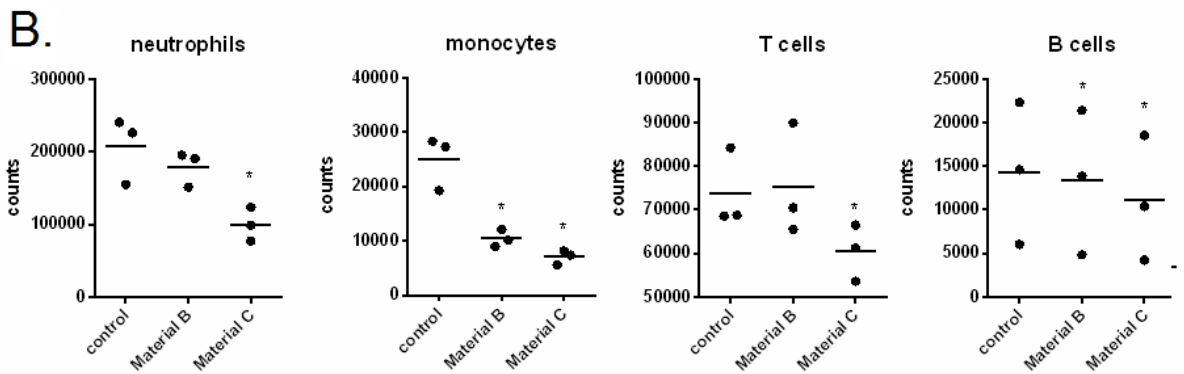
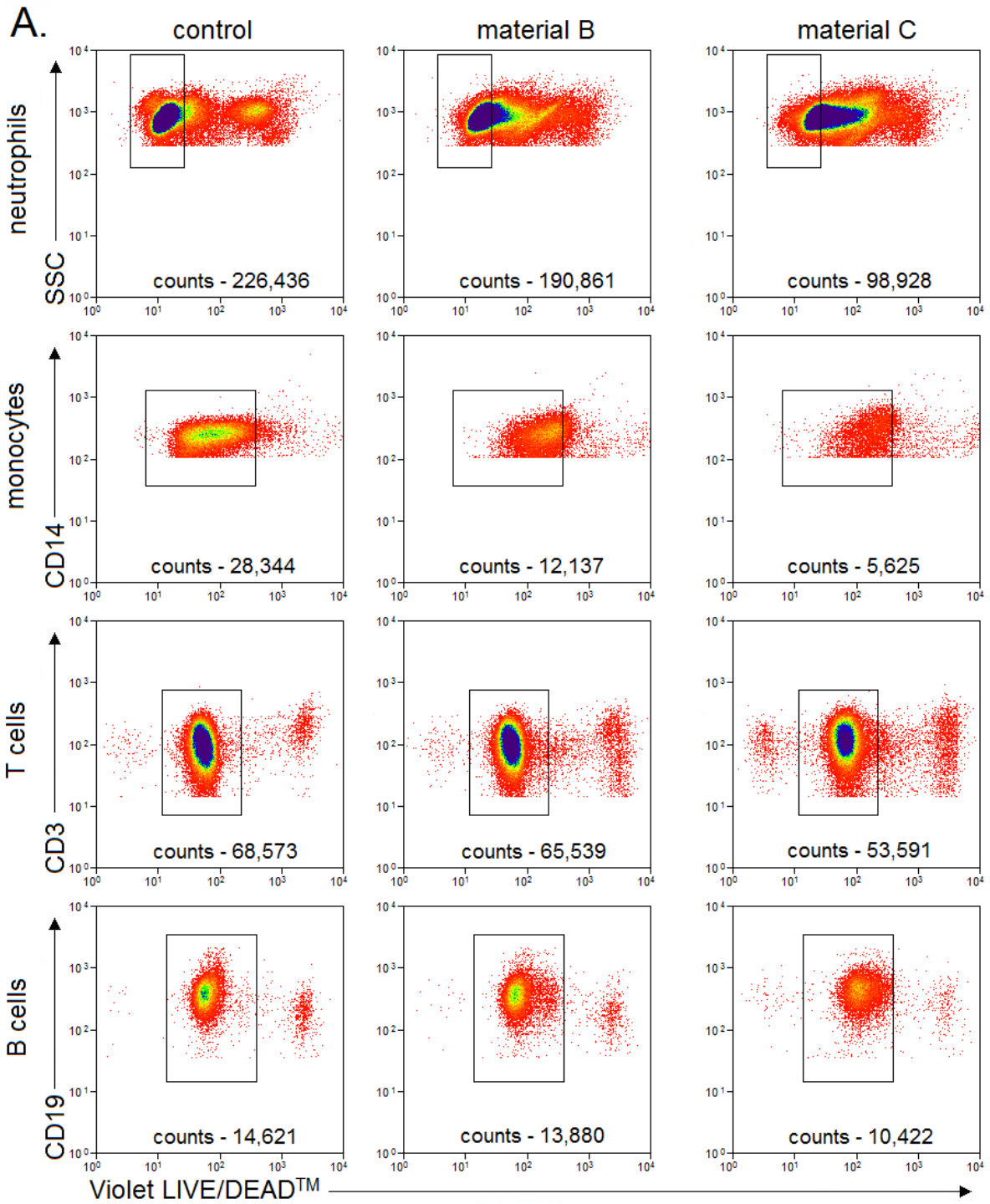
Figure 7.04. The effect of nanosilica on the percentage of $\gamma\delta$ T cells and NK/NKT cells (CD57(+)) positive for CD25 and CD69 in whole blood culture after 24 h (overleaf). Representative dot plots showing the expression of CD25 and CD69 on $\gamma\delta$ TCR(+) (A.) and CD57(+) (B.). Tabulated data for $\gamma\delta$ TCR(+) cells (C.) and CD57(+) cells (D.) represent the means \pm standard deviations for 5 donors (* denotes a significance compared to the control, two-tailed paired T test, $p < 0.05$). $\gamma\delta$ T cells and NK/NKT cells first selected based on FSC versus SSClog profiles through a lymphocyte cell gate which also excluded debris, followed by a singlets gate (FSClin vs FSCarea), and a $\gamma\delta$ TCR(+) or CD57(+) gate



Next, the cytotoxicity of nanosilica towards cells in whole blood was investigated. In PBMC cultures, nanosilica was found to be toxic to monocytes, B cells and T cells at concentrations above 300 μM Si (Chapter 4). Whether whole blood also attenuates nanosilica toxicity was assessed. The viability was represented as viable cell counts. The flow cytometric analyses of the whole blood samples conducted in this chapter employed a high FSC threshold, as to eliminate the residual RBC remaining after the RBC lysis step and the increased amount of debris. Dead cells shift below this high threshold and skew the total percentage of viable cells, thereby making viable cell counts a more accurate way of representing cytotoxicity.

Figure 7.05 shows the effect of nanosilica (as defined in Figure 7.02) on neutrophil, monocyte, B cell and T cell counts. The representative dot plots show two populations for each cell type corresponding to viable cells, *i.e.*, those of low fluorescent intensity (intact membrane), and non-viable cells, *i.e.*, those of high fluorescent intensity (compromised cell membrane). Decreased event numbers in the dot plots and an increased percentage of non-viable cells were evident after treatment with both nanosilica materials. Material B was found to be more toxic than material A, as it significantly reduced counts for all cell types tested. Material A significantly decreased B cell and monocyte counts but had no significant effect on neutrophil or T cell counts. On a percentage basis, monocytes were most susceptible to nanosilica induced cell death. However, on a per number basis, neutrophils showed the largest loss in cell numbers after nanosilica treatment, where *ca.* 10^5 neutrophils, which was greater than the whole monocyte population, were lost after treatment. The lymphocytes were most resistant to the nanosilica particles, corroborating reports that show phagocytes are the more susceptible to the cytotoxicity of nanosilica than cells with lesser phagocytic capabilities (Fedeli et al., 2013)

Figure 7.05. The effect of 4 mM nanosilica on neutrophil, monocyte (CD14), T cell (CD3) and B cell (CD19) in whole blood culture after 24 h (overleaf). **A.** Representative dot plots showing viability on neutrophils, monocytes, T cells and B cells. **B.** Tabulated data show the counts for 3 donors (* denotes a significance compared to the control, two-tailed paired T test, $p < 0.05$). Neutrophils were first selected based on FSC versus SSClog profiles followed by a CD14(-)/CD14^{low} gate. Monocytes were first selected based on FSC versus SSClog profiles followed by a CD14^{high} gate. T cells and B cells were first selected based on FSC versus SSClog profiles followed by a CD3(+) or a CD19(+) gate.



In this section, it was shown that nanosilica is capable of activating helper T cells, cytotoxic T cells and NK/NKT cells in whole blood. In order to demonstrate this, the concentration of nanosilica had to be increased above the solubility limit of silicic acid. At these concentrations, nanosilica was significantly toxic towards all cell types, especially the phagocytes, corroborating studies in literature (Fedeli *et al.*, 2013). *In vivo*, it is unlikely that these concentrations would be maintained as investigations have shown that nanosilica is rapidly cleared from the periphery and excreted (Jugdaohsingh, Appendix 2). To determine whether nanosilica induced T cell activation *in vivo* is actually plausible, the effect of nanosilica in more applicable conditions was assessed.

7.2.2 Activation and toxicity in whole blood – dynamic whole blood environment

It was previously established that nanosilica particles can induce T cell activation in whole blood, though the conditions used were distant from an *in vivo* situation. After intravenous injection of a nanosilica dispersion, the particles would be continuously diluted and cleared from circulation quite rapidly. Indeed, it has been shown that most Si is removed from circulation hours after injection (Jugdaohsingh, Appendix 2). *In vitro*, it is not possible to mimic nanosilica clearance but continuous dilution is possible. By continuously diluting with untreated whole blood, information regarding the dynamics of nanosilica in blood after intravenous administration may be learned and may help narrow the materials to be used in future translational *in vivo* investigations (See Section 7.2.4).

In these investigations, the effect of high nanosilica doses followed by continuous dilution on T cell activation and monocyte cell death in whole blood was investigated. Initial investigations employed a simplified dilution schedule, specifically a 4 mM Si incubation step for 1 h followed by 2 mM Si for 3 h and finally 1 mM Si for 20 h. As little is known of the dynamics of dilution immediately after intravenous administration, the effect of a concentrated pulse was also investigated. It can be speculated that at the site of injection of the *in vivo* studies conducted below (Section 7.2.4), nanosilica could reach a concentration upwards of 16 mM Si before it is evenly diluted throughout the periphery. Therefore, the effect of a 16 mM nanosilica pulse (for 25 s) followed by the dilution schedule outlined above on T cell activation and leukocyte viability was assessed. Figure 7.06 shows the effect of a high nanosilica pulse on the expression of CD25 and CD69 on CD4 and CD8 T cells. In these investigations, a nanosilica dispersion of 1-2 nm in size, with a rapid dissolution rate (when below Si solubility limit, rate exceeding that of material B in Figure 7.02)) was employed and is referred to as material C. In the cultures not treated with a 16 mM Si pulse, there was only significant induction of CD69 on CD4 T cells. The expression of CD25 on CD4 T cells did not significantly increase, neither did the activation markers on CD8 T cells. In the cultures pulsed with 16 mM nanosilica, CD69 was significantly induced on CD4 and CD8 T cells and CD25 was induced on CD4 T cells. These results would suggest that a highly concentrated pulse has a large effect on T cell activation. As the only

difference between the 2 treatment schedules was the 16 mM Si pulse, it is possible that the T cells present in the pulse are those that are expressing the activation markers. To determine the approximate percentage of cells activated during the pulse, the following equation was used (using CD69 as an example):

$$\% \text{ activated in pulse} = ((\% \text{CD69}(+)_{\text{nanosilica}} - \% \text{CD69}(+)_{\text{control}})_{\text{+pulse}} - (\% \text{CD69}(+)_{\text{nanosilica}} - \% \text{CD69}(+)_{\text{control}})_{\text{-pulse}}) \times 27.3$$

where 27.3 is the ratio final blood volume (390 μL) over pulse blood volume (14.3 μL). Table 7.01 shows the percentage of the T cells activated (with respect to the various activation markers) in the 16 mM Si, 25 s pulse. The majority of the CD4 T cells were activated, approximately 50% being positive for CD25 and CD69. Upwards of 20% of the CD8 T cells present in the concentrated pulse became positive for CD69. These results would suggest that the intravenous injection rate would dictate the amount of T cell activation induced by nanosilica *in vivo*. For example, a rapid intravenous injection rate could create a high transient, localized concentration. The data shown here would suggest that the T cells present in this localized, concentrated environment would likely become activated. A highly concentrated localized environment would not be present if a slow injection rate was used, likely resulting in a lack of significant T cell activation.

The effect of a 16 mM Si, 25 s pulse on monocyte counts was also assessed. For simplicity, the only monocyte counts were shown as they were previously demonstrated to be the most susceptible to nanosilica induced cell death. Here, the monocyte counts were represented as a percentage of the total cell distribution (neutrophils, monocytes, B cells, T cells), which better normalizes the cell numbers to account for varying cell losses during the staining protocol and sample transfers. Figure 7.07 shows the percentage of the monocytes within the cell distribution after nanosilica treatment. There was a decrease in monocyte cell counts after nanosilica treatment according to both dosing schedules. The concentrated pulse (16 mM Si, 25 s pulse) did not seem to enhance the toxicity of nanosilica. These results might suggest that a rapid intravenous injection rate (*i.e.*, the formation of a highly concentrated localized environment intravenously) does not enhance the toxicity of nanosilica to monocytes. Diluting the nanoparticulate to levels below its solubility (*ca.* 1.7 mM Si at pH 7.4 (Jugdaohsingh *et al.*, 2008; Mosby, 2016)) after 4 h did not attenuate all of its cytotoxicity towards monocytes. These results would indicate that even short term exposure (up to 4 h) to nanosilica above its solubility can result in monocyte death.

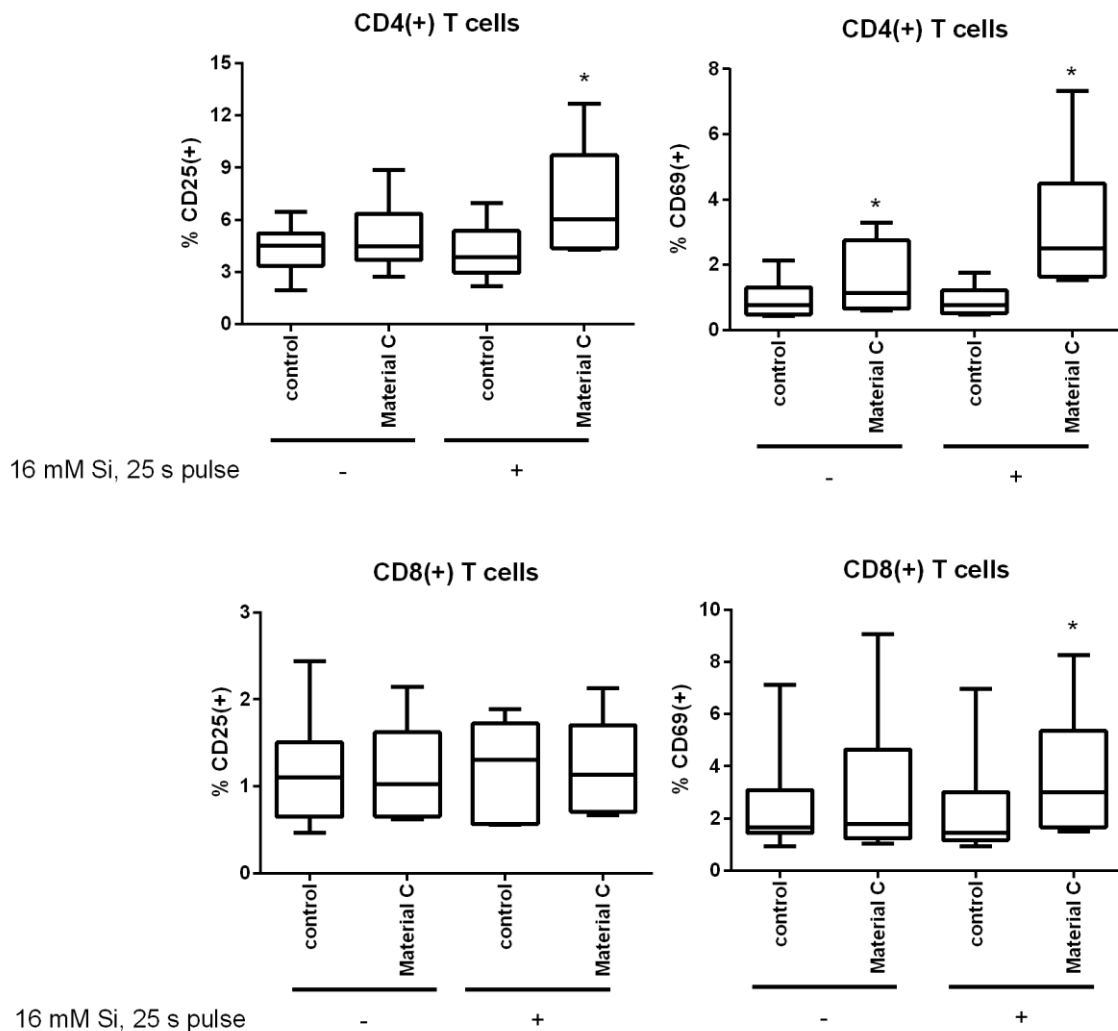


Figure 7.06. The effect of nanosilica on the percentage of CD4 and CD8 T cells positive for CD25 and CD69 in whole blood culture. Whole blood was treated with (+) or without (-) 16 mM Si 25 s pulse, followed by a 4 mM Si incubation step for 1 h, 2 mM Si incubation for 3 h and finally a 1 mM Si incubation for 20 h. Tabulated data represent the averages for 6 donors (* denotes a significance compared to their respective control, two-tailed paired T test, $p < 0.05$). T cells were first selected based on FSC versus SSClog profiles through a T cell gate which also excluded debris, followed by a singlets gate (FSClin vs FSCarea), a T cell gate (CD3(+)), and a CD4(+) or CD8(+) gate.

Table 7.01. The percentage of T cells activated (expressing CD25 and CD69) in the 16 mM Si, 25 s nanosilica pulse.

	CD4(+) T cells		CD8(+) T cells	
	CD25	CD69	CD25	CD69
Average +/- SEM	60.5 ± 20.1	45.4 ± 11.8	0.6 ± 5.5	21.4 ± 23.4

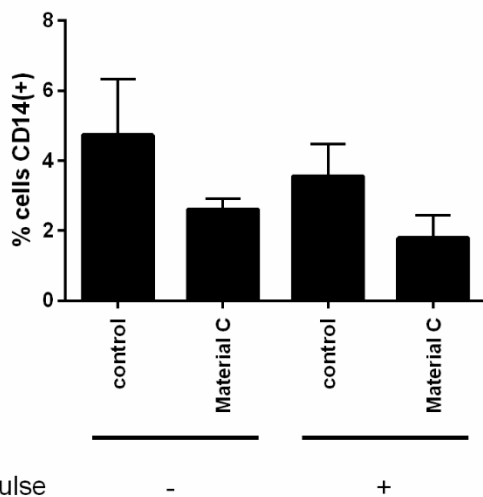


Figure 7.07. The effect of nanosilica on the percentage of monocytes within the cell distribution in whole blood culture. Whole blood was treated with (+) or without (-) 16 mM Si 25 s pulse, followed by a 4 mM Si incubation step for 1 h, 2 mM Si incubation for 3 h and finally a 1 mM Si incubation for 20 h. Tabulated data represent the averages for 3 donors (* denotes a significance compared to the control, two-tailed paired T test, $p < 0.05$)

After intravenous injection, the dilution of the nanosilica likely occurs faster than the dilution schedule used above. For example, blood flow rate is approximately 2 mL/s on the right upper limb (Zhang *et al.*, 2014) and, at the heart, blood is pumped at a rate of 4.7-6.6 L/min (Clayman, 1995). Assuming that there would be sufficient mixing (*e.g.*, at the heart or at vein/arterial intersections), the nanosilica dispersion would likely be diluted below its solubility quite rapidly. To better simulate this, the effect of a high nanosilica pulse (16 mM Si, 25 s) followed by immediate dilution to 1 mM Si (referred to a treatment schedule A) on T cell activation at 24 h was tested and is shown in Figure 7.08. As a point of comparison, the previous dilution schedule was tested in parallel (referred to as treatment schedule B (*i.e.*, 16 mM Si for 25s, 4 mM Si for 1 h, 2 mM Si for 3 h, 1 mM Si, for 20 h)). In cultures treated according to schedule A, there was significant induction of CD69 on CD4 and CD8 T cells, but CD25 was not significantly induced. In cultures treated according to schedule B, CD25 was also significantly increased on CD4 T cells. This would suggest that the dilution rate effects the ability of nanosilica to induce T cell activation. Indeed, the percentage of CD4 T cells positive for CD25 and CD69 was significantly higher in cultures treated according to schedule B compared to those treated according to schedule A. The increased dilution rate would likely result in a shorter nanosilica:TCR complex occupancy time (as explained in Chapter 6), either by increasing the rate in which nanosilica is dissolving or, if the nanosilica-TCR/CD3 interaction is in equilibrium with free nanosilica and TCR/CD3 (*i.e.*, it is a reversible reaction), shifting the equilibrium to the free species at a more rapid rate.

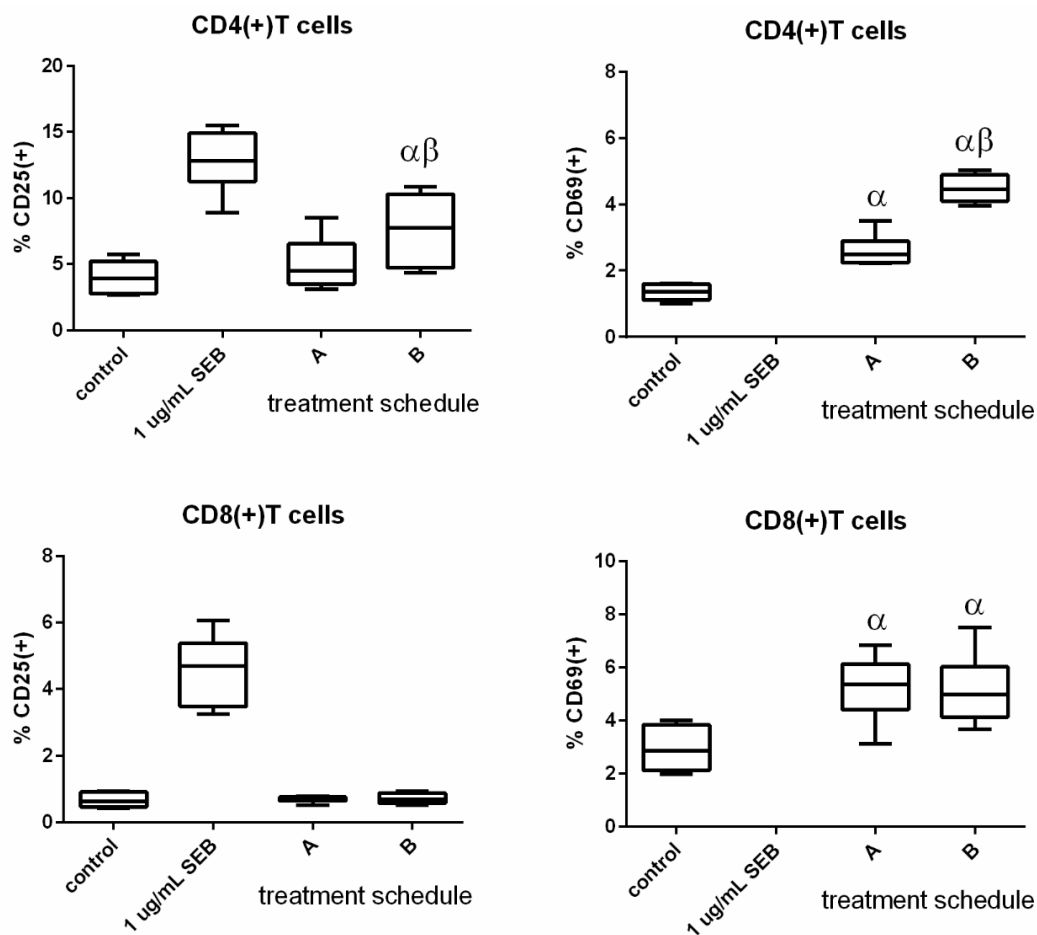


Figure 7.08. The effect of nanosilica and dilution schedule on the percentage of CD4 and CD8 T cells positive for CD25 and CD69 in whole blood culture. Whole blood was treated with material C at 16 mM Si for 25 s, followed either by a 1 mM Si incubation for 24 h (“treatment schedule A”) or a 4 mM Si incubation step for 1 h, 2 mM Si incubation for 3 h and a 1 mM Si incubation for 20 h (“treatment schedule B”). Tabulated data represent the averages for 6 donors (α denotes a significance compared to the control, β denotes a significance compared other treatment schedule, two-tailed paired T test, $p < 0.05$). The percentage of CD4 and CD8 T cells positive for CD69 after treatment with SEB exceeded 10%, but was left off scale to more clearly show activation induced by nanosilica. T cells were first selected based on FSC versus SSClog profiles through a T cell gate which also excluded debris, followed by a singlets gate (FSClin vs FSCarea), a T cell gate (CD3(+)), and a CD4(+) or CD8(+) gate.

Figure 7.09 shows the effect of the dilution schedule on the monocyte cell counts, once again shown as the percentage of monocytes in the cell distribution (B cells, T cells, monocytes and neutrophils). There was a greater reduction in monocyte counts when cultures were treated according to schedule B compared to those treated according to schedule A. There was no significant difference in monocyte counts between the control and the cultures treated with nanosilica according to schedule A. These results would suggest that if nanosilica dispersions are rapidly diluted below their solubility limit, most of their cytotoxicity is attenuated. However, the response of T cells is also greatly attenuated after rapid dilution, which might indicate that there is a proportional relationship between T cell activation and monocyte cell death.

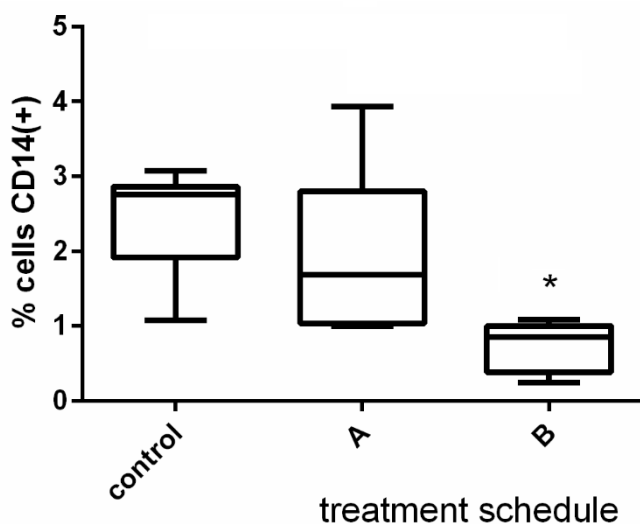


Figure 7.09. The effect of the nanosilica dilution schedule on the percentage of monocytes within the cell distribution in whole blood culture. Whole blood was treated with material C at 16 mM Si for 25 s, followed either by a 1 mM Si incubation for 24 h (“treatment schedule A”) or a 4 mM Si incubation step for 1 h, 2 mM Si incubation for 3 h and a 1 mM Si incubation for 20 h (“treatment schedule B”). Tabulated data represent the averages for 6 donors (* denotes a significance compared to the control, two-tailed paired T test, $p < 0.05$).

7.2.3 Assessing dispersions for use in future *in vivo* trials

The assays employed in Section 7.2.2 provide a closer mimic of the conditions after intravenous injection of nanosilicate and could provide information on which dispersions would be most efficacious *in vivo* (greatest T cell activation, minimal cell death). To identify possible candidates for *in vivo* trials, treatment schedule B (*i.e.*, 16 mM Si for 25s, 4 mM Si for 1 h, 2 mM Si for 3 h, 1 mM Si, for 20 h) was employed to test the effect of nanosilica formulation on T cell activation and monocyte cell death.

It was shown previously that 1-2 nm nanosilica particles activate T cells and induce significant monocyte cell death in whole blood. Whether there is a particle that induces significant activation in the absence of monocyte death was investigated here. In these studies, nanosilica dispersions prepared at low pH were employed as they are labile (*i.e.*, will dissolve into inert silicic acid rapidly after dilution) and would therefore be less likely to induce cell death.

Figure 7.10A shows the relative condensation of the materials used in these investigations, represented as area under the absorbance curves (Chapter 3). The area under the absorbance curve is proportional to the release of silicic acid from the nanoparticles at low pH. Upon Si(OH)_4 release, it is complexed by molybdic acid and it forms a complex that is absorbant at 400 nm. The rate of Si(OH)_4 release corresponds to the relative dissolution rate of the particles. For example, a distribution that has a large area under the curve would dissolve relatively faster than a dispersion that has a smaller area under the curve. There was a decrease in the area under the curve with an increase in particle age. This would suggest that the older dispersions would dissolve at a relatively slower rate than the fresher dispersions. Importantly,

the size of dispersions were all below 2 nm in median diameter (which is pushing the detection limits of the DLS device).

Figure 7.10B shows the effect of particle age on the induction of CD25 and CD69 on CD4 and CD8 T cells in whole blood cultures after treatment according to dosing schedule B. The data (3 independent studies, all n=6) was left separated due to the interdonor variance between the studies. The particles prepared 0.2 and 2 h prior to addition to whole blood did not induce significant T cell activation. The decreased efficacy may be due to the increased dissolution rate of the particles (which was also shown in Chapter 6), as it would decrease the contact time between the nanosilica particle and the TCR complex. Alternatively, the formation of these particles, which is a mechanism that is not well understood, may be responsible for the decreased induction of T cell activation. Immediately after preparation of these (and most other) dispersions, the size measurements are quite inconsistent. Specifically, some measurement replicates show particles below 2 nm in size while others do not detect any small particles. This might suggest that there are particles (or “oligomers”) below 1 nm in size (and the detection limits of the DLS equipment) that eventually agglomerate to form the particles 1-2 nm in size. It is possible that these ultrafine “oligomers” do not engage the TCR complex like the larger particles. Whatever the reason, what remains clear is that fresh, ultra-labile, dispersions do not induce T cell activation in whole blood. The particles that were aged 1-10 d induced significant expression of CD25 and CD69 on CD4 T cells and CD69 on CD8 T cells. Interestingly, the dispersions aged 10 days had decreased efficacy compared to the dispersions aged only 1 and 5 days. The reason for the reduced induction of the activation markers is unknown but it could relate to particle condensation. For example, there may be fewer particles present in the dispersion as a result of slight, undetectable, agglomeration. The particles aged 1 and 5 days induced the greatest expression of the activation markers. Whether these particles also induced significant monocyte cell death was also investigated. Figure 7.11 shows the percentage of monocyte counts with the cell distribution after treatment with 1 and 5 d old particles. As with the previous particles tested, both these dispersions induced significant monocyte cell death. It is quite plausible that the properties that nanosilica requires to induce significant T cell activation are the same as those that induce significant monocyte cell death.

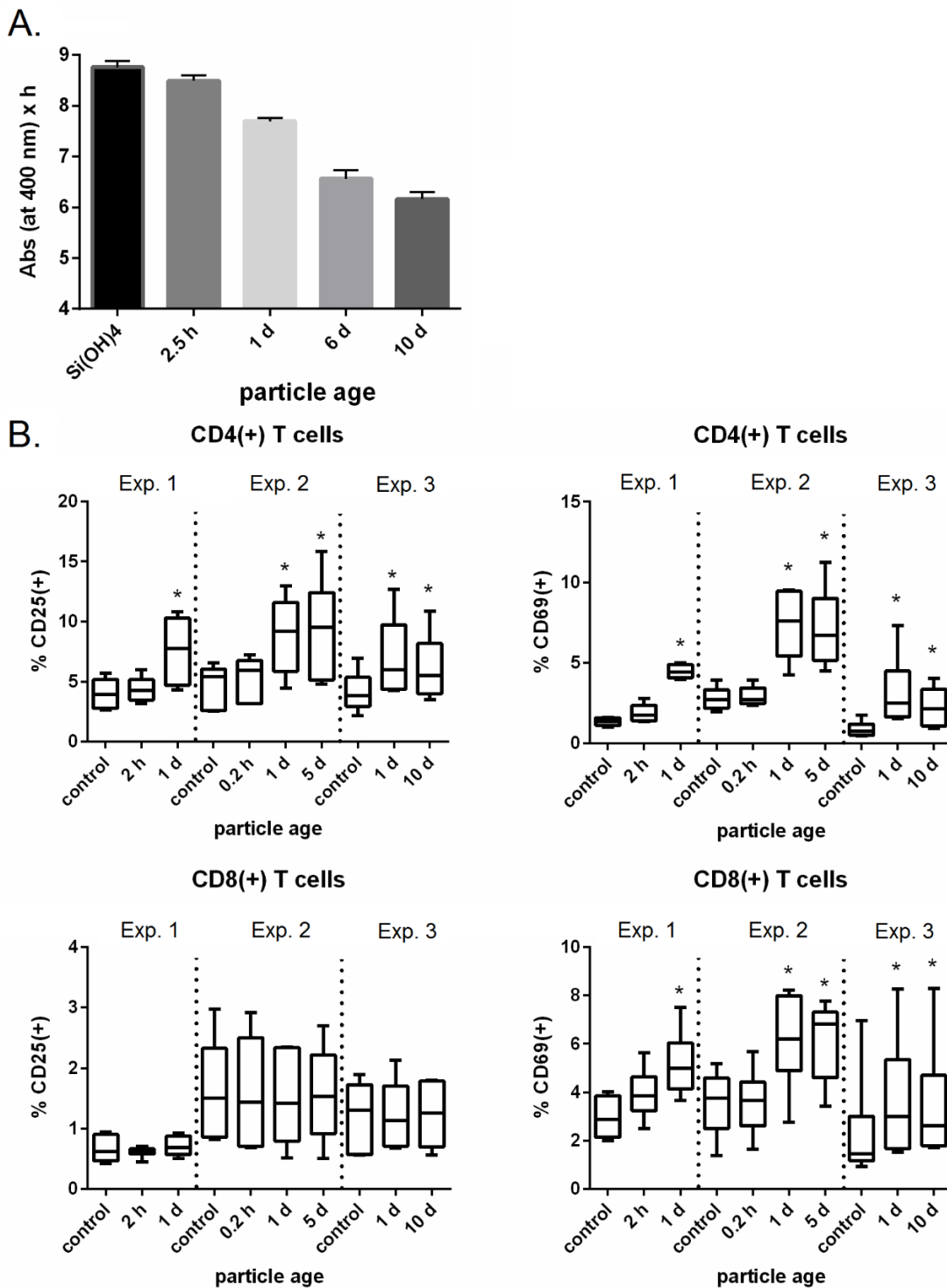


Figure 7.10. The effect of nanosilica particle age on the percentage of CD4 and CD8 T cells positive for CD25 and CD69 in whole blood culture. **A.** The area under the curve, corresponding to the formation of the β -silicomolybdate complex, as measured by absorbance at 400 nm from 0-5 h, after dilution of aged 40 mM nanosilica dispersions (pH 2.3) to 1 mM Si in a molybdic acid solution. **B.** Whole blood was treated with 16 mM Si 25 s pulse, followed by a 4 mM Si incubation step for 1 h, 2 mM Si incubation for 3 h and finally a 1 mM Si incubation for 20 h. Tabulated data represent the averages for 6 donors (* denotes a significance compared to their respective control, two-tailed paired T test, $p < 0.05$). T cells were first selected based on FSC versus SSClog profiles through a T cell gate which also excluded debris, followed by a singlets gate (FSClin vs FSCarea), a T cell gate (CD3(+)), and a CD4(+) or CD8(+) gate.

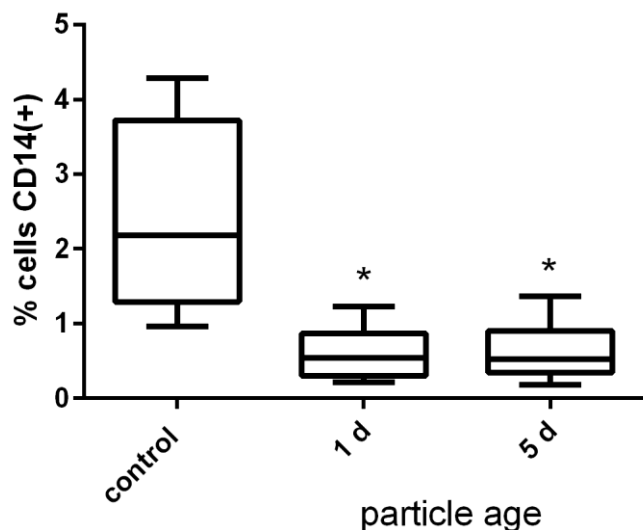


Figure 7.11. The effect of the particle age on the percentage of monocytes within the cell distribution in whole blood culture. Whole blood was treated with 16 mM Si 25 s pulse, followed by a 4 mM Si incubation step for 1 h, 2 mM Si incubation for 3 h and finally a 1 mM Si incubation for 20 h. Tabulated data represent the averages for 6 donors (* denotes a significance compared to their respective control, two-tailed paired T test, $p < 0.05$). Monocytes were first selected based on FSC versus SSClog profiles followed by a CD14^{high} gate.

Lastly, the effect of a nanosilica dispersion prepared through an alternative synthetic route was investigated. It was previously shown that most dispersions require a 24 h incubation period to become efficacious. If the particles are used immediately after preparation, they have no effect on T cell activation (Figure 7.10). This prolonged preparation (incubation) step inserts a degree of complexity for an *in vivo*/clinical situation (below). An alternative synthesis strategy was developed to simulate the 24 h aged materials (prepared at low pH) which were previously shown to be most efficacious in whole blood. This alternative synthetic strategy involved a 30 min incubation step at pH 5, generating a material, referred to as material D, with the same relative condensation (as determined through silicic acid release) and particle size (as determined by DLS) as the 1 d old material (Material C) (Bastos and Faria, unpublished). Figure 7.12 shows the effect of the nanosilicate particles produced as previous and through the alternative synthesis strategy. Both materials induced significant, similar levels of CD25 and CD69 on CD4 T cells and CD69 on CD8 T cells. Figure 7.13 shows the percentage of monocytes within the cell distribution after treatment with the materials. Both materials induced significant monocyte cell death. The alternative synthetic strategy successfully mimicked the material shown to induce greatest T cell activation in whole blood.

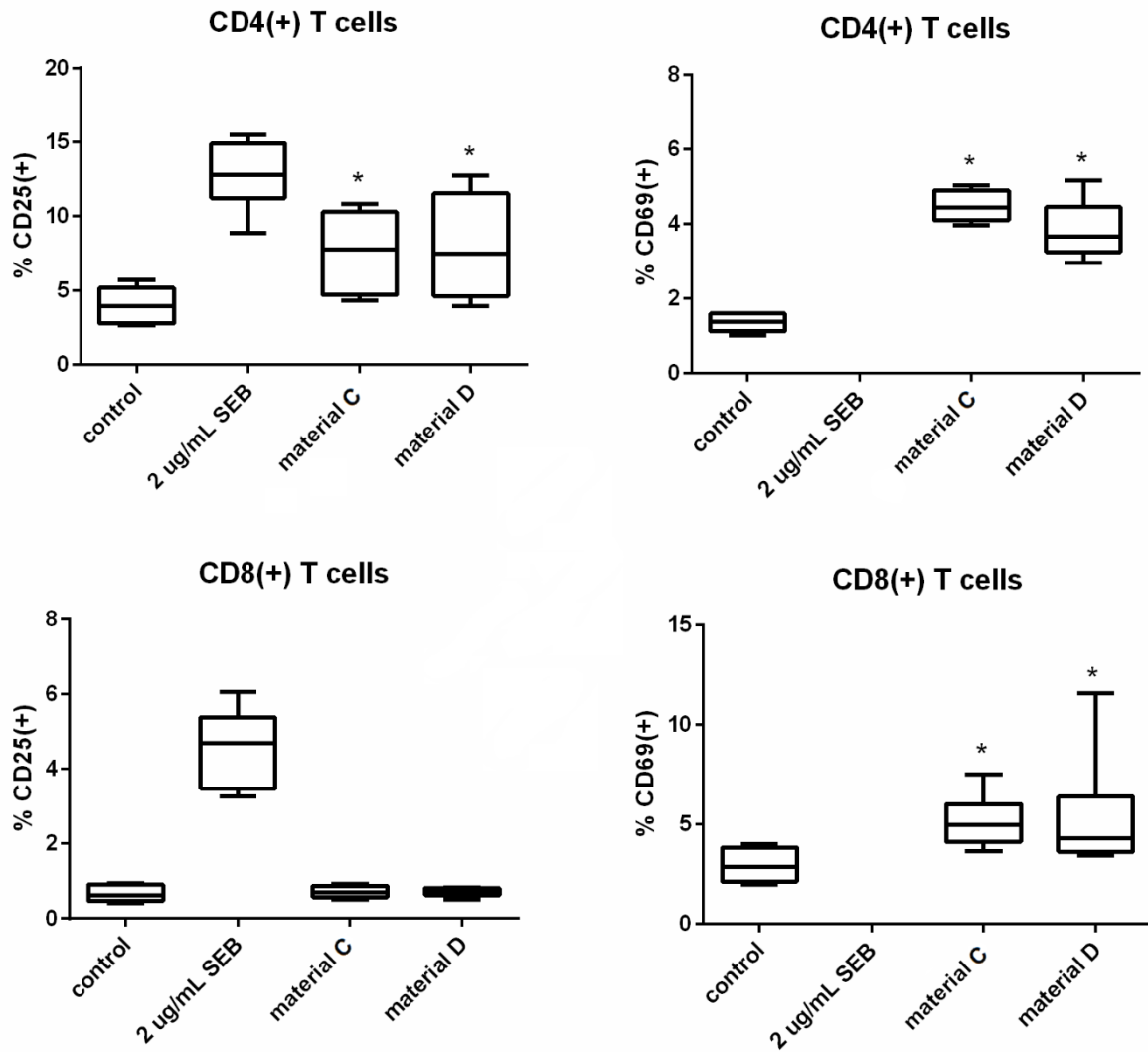


Figure 7.12. The effect of nanosilica (material C and D) on the percentage of CD4 and CD8 T cells positive for CD25 and CD69 in whole blood culture. Whole blood was treated with 16 mM Si 25 s pulse, followed by a 4 mM Si incubation step for 1 h, 2 mM Si incubation for 3 h and finally a 1 mM Si incubation for 20 h. Tabulated data represent the averages for 6 donors (* denotes a significance compared to their respective control, two-tailed paired T test, $p < 0.05$). The percentage of CD4 and CD8 T cells positive for CD69 after treatment with SEB exceeded 10%, but was left off scale to more clearly show activation induced by nanosilica. T cells were first selected based on FSC versus SSClog profiles through a T cell gate which also excluded debris, followed by a singlets gate (FSClin vs FSCarea), a T cell gate (CD3(+)), and a CD4(+) or CD8(+) gate.

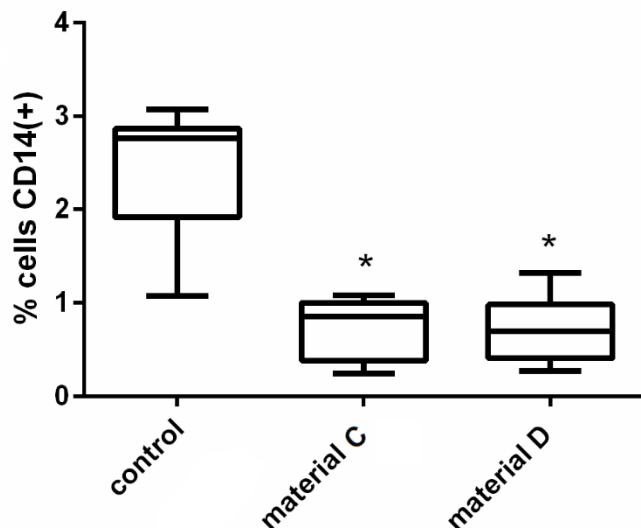


Figure 7.13. The effect of nanosilica (material C and D) on the percentage of monocytes in the cell distribution in whole blood culture. Whole blood was treated with 16 mM Si 25 s pulse, followed by a 4 mM Si incubation step for 1 h, 2 mM Si incubation for 3 h and finally a 1 mM Si incubation for 20 h. Tabulated data represent the averages for 6 donors (* denotes a significance compared to their respective control, two-tailed paired T test, $p < 0.05$). Monocytes were first selected based on FSC versus SSClog profiles followed by a CD14^{high} gate.

7.2.4 *In vivo* trials

7.2.4.1 Preliminary study and post termination studies

Prior to 2013, there were many unpublished investigations assessing whether nanosilica can effectively inhibit tumour growth rate. An example of these studies is shown (with permission) in Figure 7.14, where the effect of 3-84 nm nanosilica particles on the growth of an established subcutaneous tumour was assessed. It was found that particles less than 10 nm in size decreased tumour growth rate, while larger nanosilicates had little effect. The nanosilica particle 3.6 nm in size inhibited tumour growth as effectively as the temozolomide positive control. Interestingly, the size dependent decrease in tumour growth matches the size dependence for maximal T cell activation (Chapter 6). A number of post-termination studies were conducted to determine the possible mechanism of nanosilica induced tumour growth inhibition.

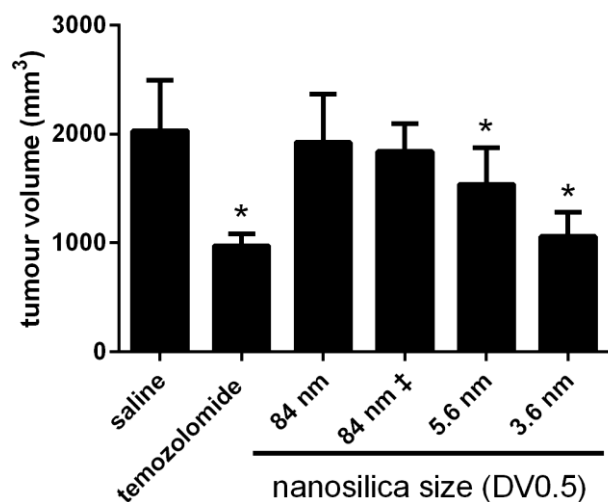


Figure 7.14. Tumour sizes after 14 d from mice injected subcutaneously with B16-F10 melanoma and treated daily with saline, temozolomide and nanosilica (23 mM Si, 400 μ L) for 10 d. Tumours were allowed to grow to ca. 100 mm³ before mice were treated. ‡ represents prophylactic treatment prior to tumour inoculation and treatment during initial tumour growth. * denotes difference ($p < 0.05$) from vehicle (with permission from HS Pharma, dispersions prepared by B Vis prior to start of thesis, animal work conducted by Translational Drug Development (TD2)).

First, the concentration of silicon in the excised tumours was assessed. These studies may infer to whether nanosilica, previously shown to be quite toxic to cells (Chapter 4), could infiltrate and directly interfere with tumour cell growth. Figure 7.15 shows the concentration of Si in the tumours. The concentration of silicon present in the tumours was higher in the nanosilica treated groups than in the vehicle control group. These results are unsurprising as nanosilica was injected daily at high volumes (ca. 23 mM Si, 400 μ L) and therefore increased Si levels in all tissues would be expected. The most effective nanosilica treatment (in terms of inhibition of tumour growth) had the lowest tumour silicon level. When tumour size was correlated against silicon level in the mice treated with 3.6 nm nanosilica, the larger tumours were found to have higher levels of silicon. This may suggest that the mechanism of tumour growth inhibition is not through a direct tumour infiltration/toxicity-based mechanism. In Chapter 4, the effect of nanosilica on viability of a cancerous cell line was investigated. It was found that the cancerous cells were resistant to nanosilica and high concentrations were required to significantly reduce cell viability. Considering the high concentration of nanosilica required to kill tumour cells directly, the low levels of silicon in the tumours and lack of correlation between tumour size and Si concentration, it is unlikely that nanosilica is inhibiting tumour growth through direct toxicity. The slight increase in Si levels in the tumours of the temozolomide treated group is likely due to contamination from the silica filler used in the tablets in which the temozolomide was extracted from.

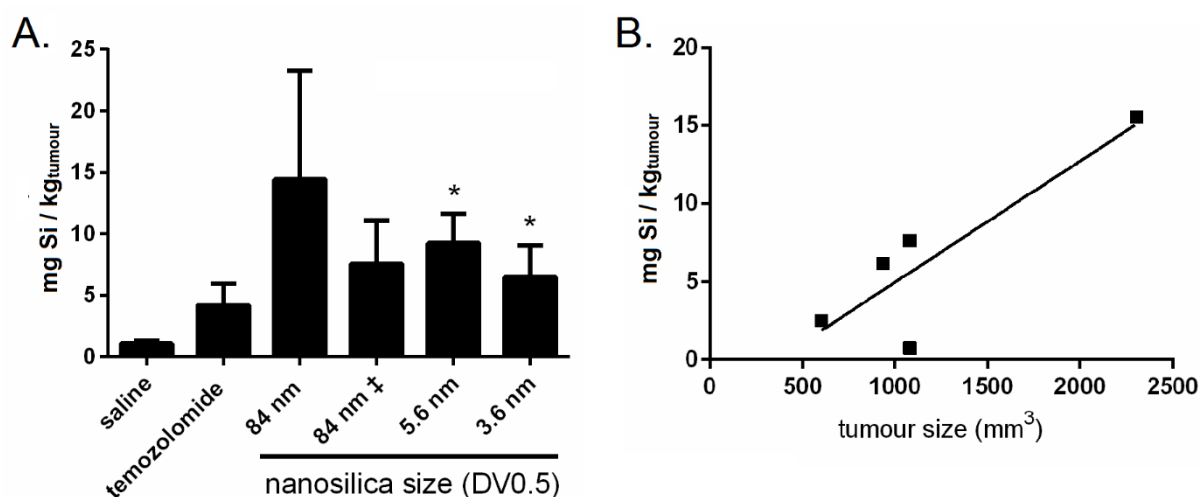


Figure 7.15. A. Concentration of Si in tumours from the murine melanoma model shown in Figure 7.14. Concentration are mg Si per kg dry tumour mass. Values determined from >5 different tumours from each treatment group. ‡ represents prophylactic treatment prior to tumour inoculation and during initial tumour growth. **B.** Correlation between tumour size and concentration of Si.

Next, the post termination studies assessing cytokine, chemokine and antibody levels in sera were conducted. The sera from the vehicle and 3.6 nm nanosilica treated mice was sent to Myriad RBM for a thorough assessment of serum analyte levels.

First, the levels of innate pro-inflammatory cytokines were assessed, mainly IL-1 β , IL-6 and TNF- α . IL-1 β is a cytokine released in response to pathogens or during pyroptosis to activate innate immune cells, mainly monocytes and neutrophils (Lopez-Castejon and Brough, 2011; Netea *et al.*, 2010). TNF- α , produced predominantly by monocytes but also by T cells, NK cells, B cells, neutrophils and endothelial cells, is involved in the recruitment of white blood cells to the site of the infection (Bradley, 2008). IL-6, whose production is stimulated by IL-1 β and TNF- α , is known to stimulate lymphocytes, contributes to both innate and adaptive immunity, and is involved in tissue homeostasis (Hunter and Jones, 2015). Together, the presence of these cytokines would indicate the induction of an innate inflammatory response. Figure 7.16 shows the sera analyte levels from the tumour bearing mice treated with nanosilica (3.6 nm), represented as a percentage of the saline control. Serum levels of IL-1 β and TNF- α were below the detection limits while the levels of IL-6 remained unchanged in the nanosilica treated mice compared to the saline control. These results would suggest that nanosilica is not inducing an innate inflammatory response. These results conflict with those in the literature that showed increased IL-1 β and TNF- α levels after intraperitoneal injection with 12 nm nanosilica particles (Park and Park, 2009). Whether particle characteristics (size and dissolution rate) or injection site (intravenous versus intraperitoneal) is responsible for the conflicting results is unknown.

Analytes associated with neutrophil recruitment and activation (macrophage inflammatory proteins (MIP) 1 β , myeloperoxidase (MPO), granulocyte chemoattractant protein 2(GCP-2) and MMP-9) (Linge *et al.*, 2008; Maurer and Von Stebut, 2004; Menten *et al.*, 2002; Nauseef, 2014; Parks *et al.*, 2004) were elevated in the sera of nanosilica treated mice. In addition to its association to neutrophil recruitment and activation, the analyte MIP-1 β is also known to be produced by cytotoxic lymphocytes upon their activation and it is present within their cytotoxic granules (Catalfamo *et al.*; Wooldridge *et al.*, 2010). These results would suggest that nanosilica is inducing a response from neutrophils and cytotoxic cells after intravenous administration.

An analyte associated with T cell recruitment and activation was also elevated after nanosilica treatment, specifically lymphotactin (Figure 7.17A). Lymphotactin is produced by CD4 T cells, CD8 T cells and NK cells, mediating Th1 and cytotoxic immune responses (Lei and Takahama, 2012). The levels of lymphotactin correlated with a decreased tumour size after treatment with nanosilica, but not saline (Figures 7.17B-C). These results may suggest that T cells may be involved in the decreased tumour growth rates present after nanosilica treatment. In PBMC culture, nanosilica was also shown to increase lymphotactin levels (Figure 7.17D). This may infer that nanosilica is inducing T cell activation *in vivo*.

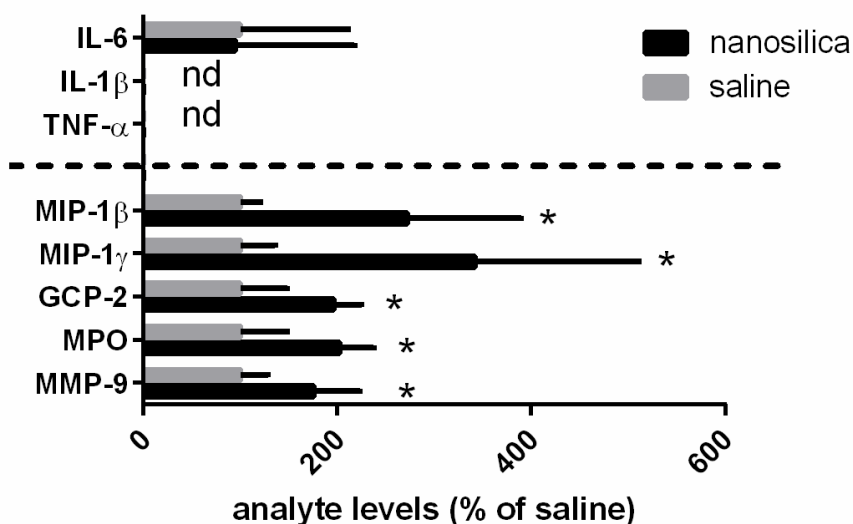


Figure 7.16. Serum cytokine levels from mice injected subcutaneously with B16-F10 melanoma and treated daily with saline and nanosilica (DV0.5 = 3.6 nm) for 10 d. Tumours were allowed to grow to ca. 100 mg before mice were treated. * denotes difference ($p < 0.05$) from vehicle

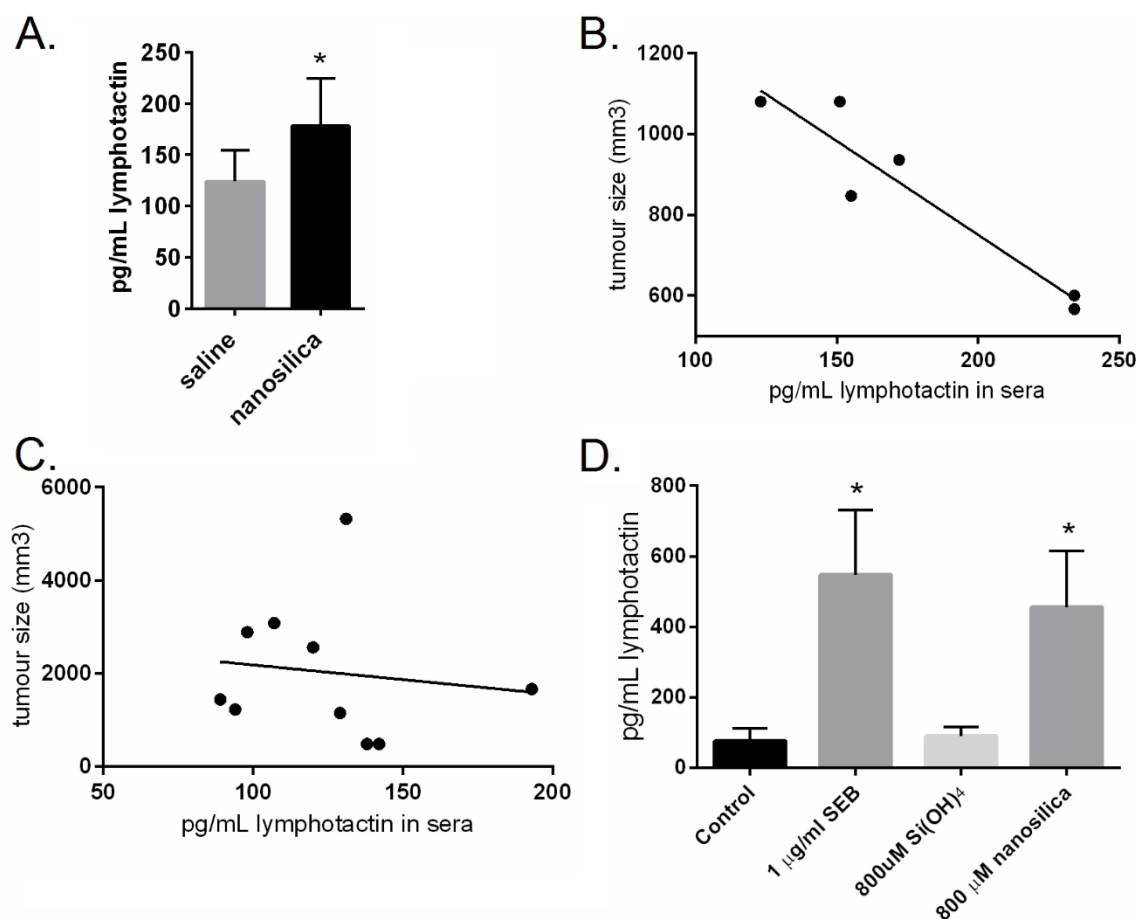


Figure 7.17. **A.** Serum lymphotactin levels from mice injected subcutaneously with B16-F10 melanoma and treated daily with saline and nanosilica (DV0.5 = 3.6 nm) for 10 d. Tumours were allowed to grow to ca. 100 mg before mice were treated (* denotes difference (two-tailed unpaired T test, $p < 0.05$) from vehicle). **B.** Correlation between tumour size and lymphotactin levels after nanosilica treatment **C.** Correlation between tumour size and lymphotactin levels after saline treatment. One data point for the nanosilica treated animals was ruled as an outlier and excluded (Grubbs' test, $\alpha = 0.05$). **D.** The effect of silicic acid and nanosilica on lymphotactin levels in PBMC culture supernatants after 24 h. Tabulated data represent the means \pm standard deviation for 7 donors. (* denotes a significance compared to the control, two-tailed paired T test, $p < 0.05$). ELISA analysis of supernatants for data shown in D were conducted by M. Miniter.

Lastly, antibody levels in the sera was investigated. Figure 7.18 shows the effect of nanosilica treatment on IgA, IgG and IgM antibody levels. The levels of IgA, as determined in the RBM analyte analysis, increased significantly after nanosilica treatment. Similarly, nanosilica treatment increased IgG levels, as determined by ELISA (Figure 7.18B). The particles which induced greatest IgG production were not the same those that significantly inhibited tumour growth inhibition. Nanosilica did not increase the levels of all antibodies, as there were decreased IgM levels in the sera of silica treated mice (Figure 7.18C). Interestingly, the increase in IgG levels and decrease in IgM levels correlated to tumour size (Figure 7.18D), where the mice which had the largest antibody switch also had the smallest tumours. IgG is known to have anti-cancer properties (Sapir and Shoenfeld, 2005), though it remains unknown whether the IgG is directly responsible for the decrease in tumour growth rate. Whether

nanosilica induced T cell activation is responsible for the class switch or whether nanosilica directly acts on B cells to induce an immunoglobulin class switch is also unknown. However, both CD40L and IFN- γ , which nanosilica has previously been shown to induce *in vitro* (Chapter 5), have been shown to effect immunoglobulin production (Kracker and Radbruch, 2004; Stavnezer, 1996). In the literature, there is evidence of other silicate particles effecting antibody production *in vivo*. Both crystalline and amorphous silica have been shown to increase antibody production in response to antigen (Brandenberger *et al.*, 2013; Pernis and Vigliani, 1960). Whether these responses relate to those shown here is unknown.

Overall, the effect of nanosilica on serum analyte and antibody levels would suggest that IV administered nanosilica is inducing an immunological response.

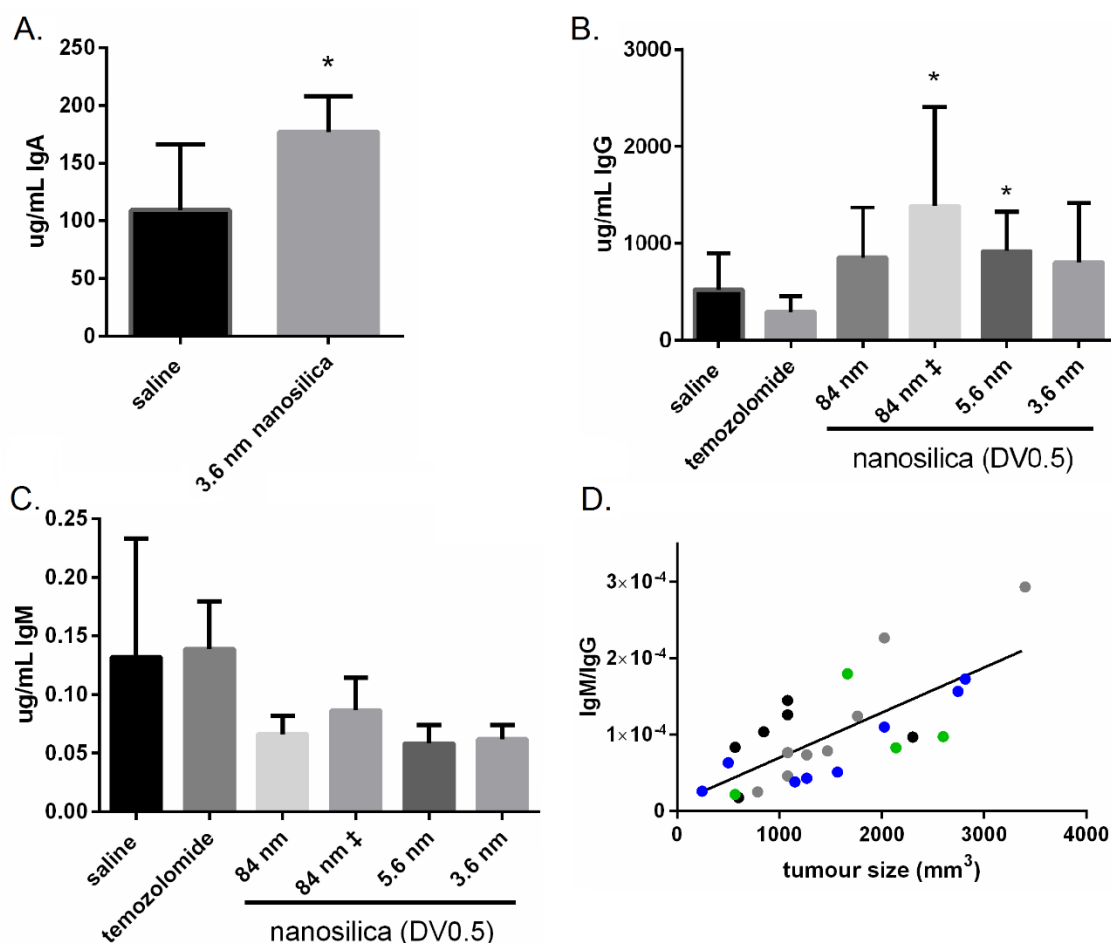


Figure 7.18. Serum IgA (A), IgG (B) and IgM (C) levels from mice injected subcutaneously with B16-F10 melanoma and treated daily with saline and nanosilica for 10 d. ‡ represents prophylactic treatment prior to tumour inoculation and treatment during initial tumour growth. Correlation between tumour size and IgM/IgG (D), Colour of the data points correlate to the different nanosilica dispersions where, black - 3.6 nm, blue - 5.6 nm, grey – 84 nm , and green – 84 nm ‡). Line was significantly different than zero (linear regression $p < 0.001$) One data point for the nanosilica treated animals was ruled as an outlier and excluded (Grubbs' test, $\alpha = 0.05$). Tumours were allowed to grow to ca. 100 mg before mice were treated. * denotes difference ($p < 0.05$) from vehicle. IgA levels were conducted by RBM.

7.2.4.2 Follow up investigations

Follow up investigations were conducted to replicate the tumour growth inhibition by nanosilica. Animal care regulations in the United Kingdom are more restrictive than those in the United States of America, where the previous *in vivo* investigation was conducted. Therefore, doses volumes needed to be reduced (to 200 μL from 400 μL), dose frequency was decreased (every 3 days vs every day), and the study was terminated at an earlier timepoint (tumour sizes at time of termination $<600 \text{ mm}^3$ vs 2000 mm^3). Figures 7.19A and B show the dosing schedule and the effect of nanosilica on subcutaneous tumour growth. As before, nanosilica significantly decreased subcutaneous tumour growth rate. However, the response to nanosilica was less pronounced in these studies than those conducted previously. The differences in efficacy are likely do to the differences in experimental design. In particular, it is suspected that nanosilica may have larger effect on more well established tumours. Cancer cells, like healthy cells, require oxygen and nutrients to survive. Larger tumours require greater vascular networks to obtain their nutrients than smaller tumours (Rieger and Welter, 2015). With a greater vascular network, nanosilica or nanosilica activated cells would have greater access to the tumour site. Previous studies (Figure 7.14) have shown that Si levels in the tumours increased with its size, potentially indicating a greater tumour vascular network and infiltration by nanosilica and/or nanosilica activated cells.

A metastatic cancer model mimics a situation of the dissemination and growth of cancer cells in metastatic sites from either cancer cell release from a primary tumour site, (Steeg, 2016) or escape during/after surgery (Tavare *et al.*, 2012). In fact, most cancer deaths are due metastatic (secondary) growths rather than the primary tumour site (Chambers *et al.*, 2002). After entering the periphery, cancerous cells frequently establish on the lungs, a site where nanosilica has also been found to accumulate (Steeg, 2016; Xie *et al.*, 2010). Here, the effect of nanosilica on the formation of tumour nodules on the lungs was assessed after intravenous injection of a melanoma cell line. Figures 7.19C and D show the dosing schedule and the number of surface nodules on the lungs upon study termination. Nanosilica was found to significantly decrease the number of nodules that formed, indicating that it has anti-metastatic properties. CD4 T cells, B cells, macrophages/monocytes, and neutrophils (though the involvement of neutrophils is still unclear/controversial) have been shown to contribute to the formation of metastases, immune cell populations which nanosilica has been shown to affect (Kitamura *et al.*, 2015). Post-termination studies on the immune populations within the blood, lymph nodes and lungs were inconclusive (for these and the solid tumour studies), leaving the mechanism behind the anti-metastatic properties of nanosilica unresolved.

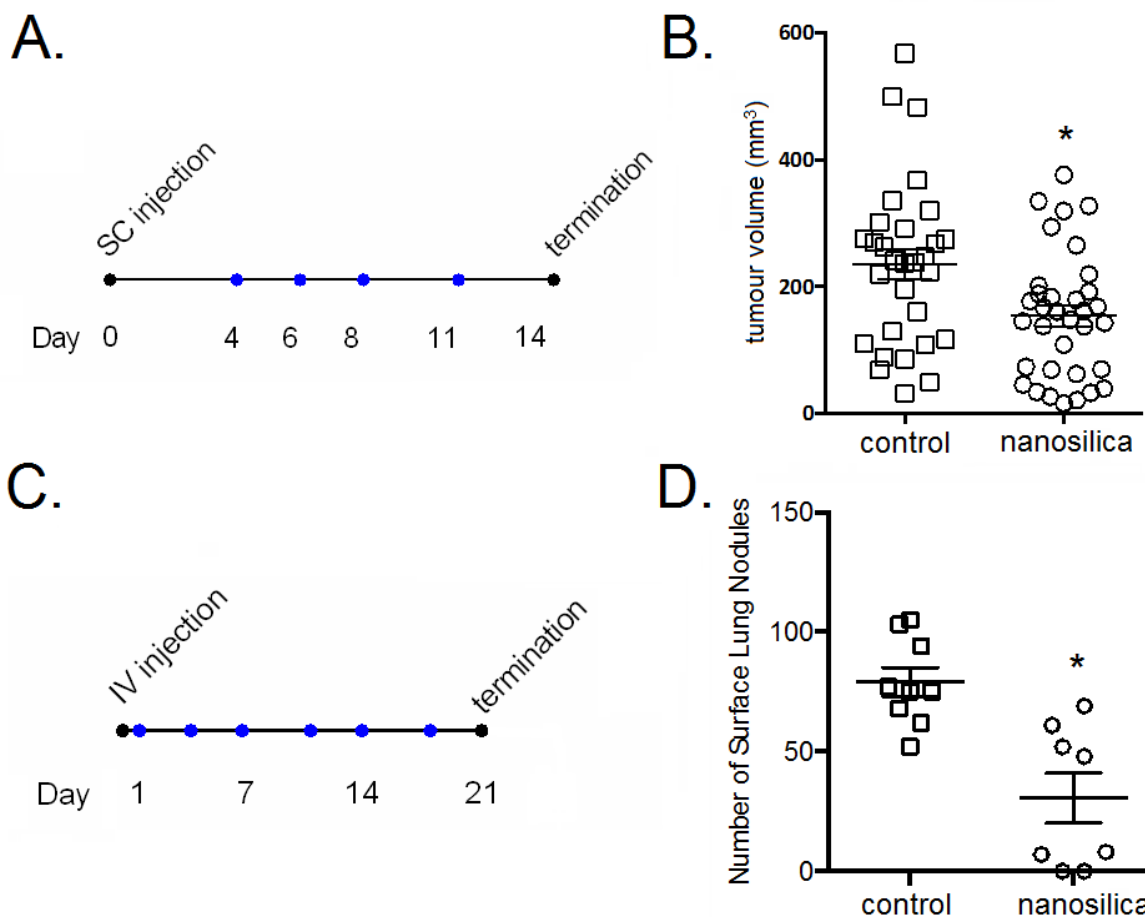


Figure 7.19. Treatment schedule (A.) and tumour sizes (B.) after 8-15 d of mice injected subcutaneously with B16-F10 melanoma and treated with saline and nanosilica. Blue dots represent treatment with saline/nanosilica. Treatment schedule (C.) and number of surface lung nodules (D.) 21 d after intravenous injection with B16-F10 melanoma and treated with saline and nanosilica. Blue dots represent treatment with saline/nanosilica. Studies were conducted by Drs J. Shields and L. Pedro.

7.3 Conclusions

In the previous chapters, it was shown that amorphous nanosilica particles less than 10 nm in size induced activation of T cells and significant cell death in PBMC cultures. Fresh PBMC were chosen for these assays because these cells are non-transformed and display behavioural, phenotypic and functional characteristics of peripheral blood cells *in vivo*. However, these assays lack many components of whole blood that would likely interact with nanosilica after intravenous injection. In this chapter, whole blood assays were conducted to better understand the *in vivo* safety of nanosilica.

T cell activation induced by nanosilica was significantly attenuated in whole blood cultures compared to that in PBMC cultures. There was more than a 50% decrease in the induction of the CD25 and CD69 activation markers in whole blood versus that in isolated cultures, despite using concentrations that were 5 times higher and that surpassed the Si solubility limit. The

attenuated effect is likely due to the increased complexity of whole blood, as it contains additional cells and components known to interact with silica (Clemments *et al.*, 2015; Don and Kaysen, 2004; Gryshchuk and Galagan, 2016; Lehman *et al.*, 2016; Zhang *et al.*, 2012; Zimmerman *et al.*, 1986). The cytotoxicity of nanosilica was also greatly attenuated in whole blood cultures. There was a relationship between the amount of T cell activation and monocyte cell death. Specifically, only in conditions in which there was significant monocyte cell death was there a large induction of T cell activation. There was also significant T cell activation and monocyte cell death induced by nanosilica in conditions that more closely mimicked an *in vivo* situation after intravenous injection (*i.e.*, short incubations at high nanosilica concentrations followed by continuous dilution).

Post-termination studies of a murine subcutaneous melanoma model where nanosilica was injected at high doses and was found to have mild anti-cancer properties were conducted. It was found that Si infiltration into the tumour was low, suggesting that the anti-cancer responses are not through direct toxicity. Analysis of analytes in the sera would suggest that nanosilica is inducing an immune response, as concentrations of many chemokines and antibodies were greater after nanosilica treatment. The increase in chemokine and antibody levels were also shown to correlate to decreased tumour sizes. Follow up investigations confirmed the mild anti-cancer responses of nanosilica in the subcutaneous tumour model and showed that nanosilica inhibits metastatic tumour formation. The precise mechanism of the mild anti-tumour and anti-metastatic properties of nanosilica remain unknown.

Chapter 8 – Conclusions

8.1 Summary of the project

Due to their highly tailorable properties, amorphous silica particles are used in a vast range of applications. Increasingly, they are being used in biomedical applications including as binding agents in tissue repair, drug and gene therapy delivery agents, coatings for medical contrast agents and as vaccine adjuvants (Bitar et al., 2012). Despite their increasing use, the safety of amorphous silica is not completely understood. In this thesis, the safety of amorphous nanosilica particles under 10 nm in size was assessed.

In Chapter 3, amorphous nanosilica particles were prepared and characterized. The particles, all less than 30 nm in diameter but predominately less than 10 nm, were highly resorbable, being completely dissolved within 48 h after dilution below the solubility limit of silica (< 2 mM Si). Particles with increased lifetimes under dilute conditions were also engineered. In general, particles generated and tested in this thesis were less condensed than most other particles reported in the literature, as determined by dissolution rate and by ²⁹Si NMR spectroscopy.

In Chapter 4, the toxicity of these engineered labile nanosilica particles was assessed using transformed, cancerous and primary peripheral blood mononuclear cells. Primary cells were most susceptible to nanosilica induced cell death and, particularly towards the phagocytes, corroborating studies in the literature (Fedeli et al., 2013). The engineered nanosilica particles were also found to induce pyroptosis/necrosis of primary monocytes, again corroborating published studies with larger nanosilica particles (Fedeli et al., 2014), and apoptosis of CD4 T cells. Further data collected suggested that the nanosilica particles have a unique effect on T cells (e.g., the nanosilica particles inhibited fluorescent TCR antibody staining, induced the expression of genes associated with T cell activation, and induced apoptosis possibly through activation induced cell death). Therefore, investigations were carried out looking specifically at T cell responses.

In Chapter 5, the nanosilica particles were found to non-specifically induce T cell activation. The T cell activation markers CD25, which is a component of the IL-2 receptor, and CD69, which is involved in T cell migration, were both significantly expressed on T cells after treatment with nanosilica. Helper T cells, cytotoxic T cells, $\gamma\delta$ T cells and NK/NKT cells all expressed significant levels of these receptors when exposed to nanosilica. The high percentage of cells expressing the activation markers would suggest that nanosilica induced T cell activation is independent of T cell antigenic specificity. Not all markers of T cell activation were induced by nanosilica, as only low levels of T cell proliferation was detected, which would suggest that complete activation was not induced.

Markers of activation from multiple T helper cell subsets were induced by nanosilica. Treatment with nanosilica was found to increase supernatant IFN- γ levels and surface LAP, GARP and FoxP3 expression, further indicating the non-specific nature of nanosilica induced activation.

In Chapter 6, the mechanism of nanosilica induced T cell activation was investigated. It was determined that APCs are not required for the induction of CD4 T cell activation by nanosilica, indicating an MHC class II receptor independent activation mechanism. After confirming the requirement of the TCR/CD3 complex for nanosilica induced activation, it was shown that nanosilica directly engages the TCR/CD3 complex (likely on the constant domain of the TCR or a CD3 chain) and induces downstream signalling. TCR ligation by amorphous nanosilica was inefficient, as complete T cell activation (as determined by proliferation) was not induced. Proliferative responses were induced when treated in combination with co-stimulatory signals (signal 2). These results were confirmed using chemical inducers which would indicate that nanosilica does not induce signalling through MAPK, which is downstream of the CD28 receptor. Figure 8.01 shows the proposed mechanism of amorphous nanosilica induced T cell activation.

Silica dispersions with mean diameters between 3.6 and 5.1 nm induced the greatest expression of CD25 and CD69 on CD4 and CD8 T cells in PBMC cultures. Induction of the activation markers decreased when particle size was either increased or decreased from a median diameter of 3.6 nm. A nanoiron dispersion, 3-5 nm in size and coated in adipate and tartrate, induced low levels of CD69 expression on CD4 T cells, which would indicate that the induction of T cell activation is not specific to nanosilica, though the magnitude of its induction is, *i.e.*, nanosilica is a more potent inducer of T cell activation.

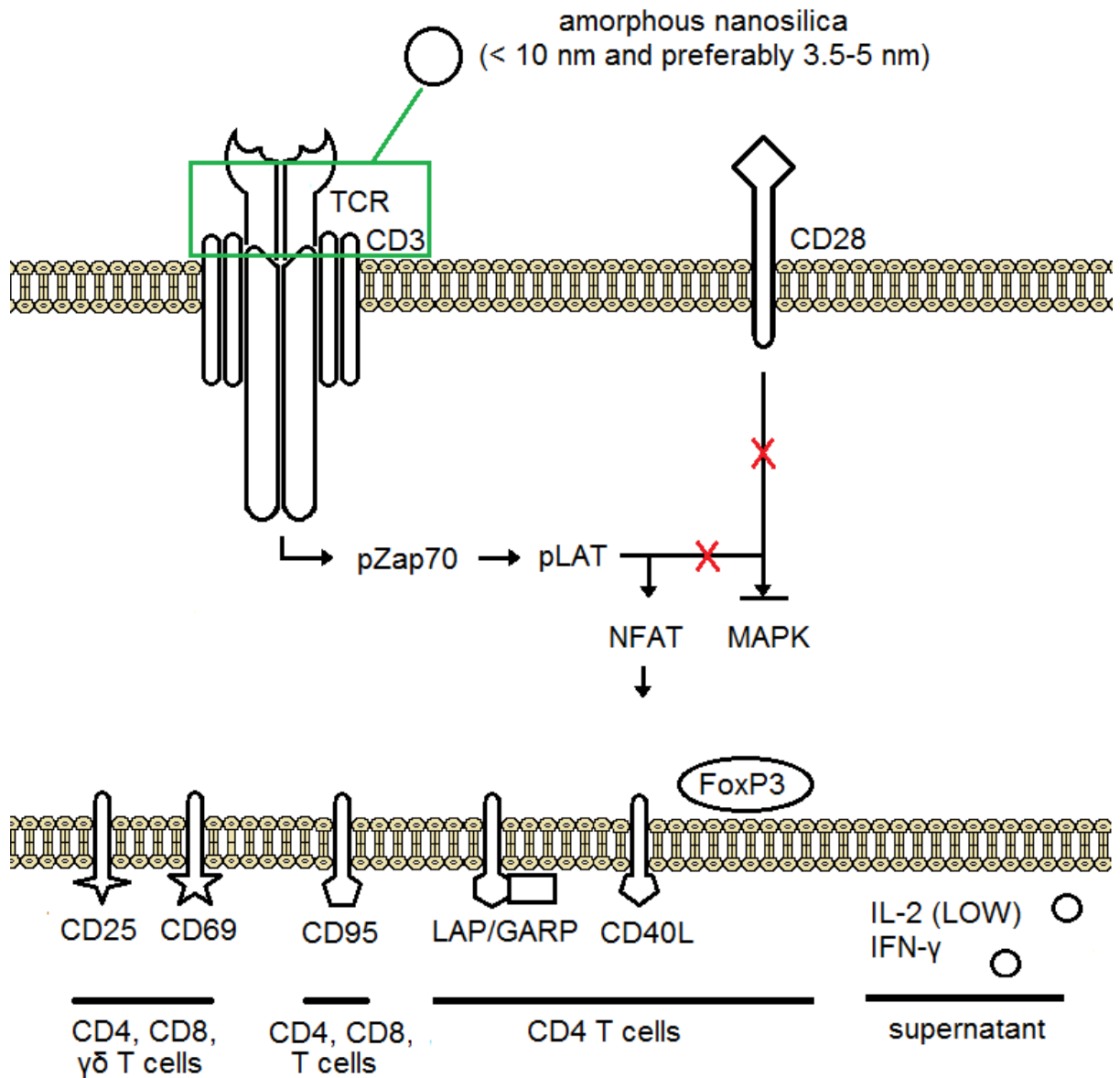


Figure 8.01. Proposed mechanism of nanosilica induction of T cell activation. Nanosilica is suspected to bind the constant domain of the TCR/CD3 complex (as determined by fluorescent antibody binding inhibition), inducing phosphorylation of Zap-70 and LAT (as determined by western blot analysis), and inducing signaling through NFAT, not MAPK (as determined by co-incubation with chemical inducers and antibodies), leading to induction of T cell activation markers. The cell signaling pathway was adapted from Acuto, Huehn, DuPage and Brownlie (Acuto et al., 2008; Brownlie and Zamoyska, 2013; DuPage and Bluestone, 2016; Huehn et al., 2009). Note – nanosilica particle size is not to scale.

In Chapter 7, investigations were conducted in freshly collected whole blood cultures as to better mimic the environment after intravenous injection of the nanosilica dispersions. There was significant attenuation of the induced T cell activation (expression of CD25 and CD69) in whole blood cultures compared to that in PBMC culture, likely due to the increased number of components present in whole blood and their known interactions with silica (Clemments et al., 2015; Don and Kaysen, 2004; Gryshchuk and Galagan, 2016; Lehman et al., 2016; Zhang et al., 2012; Zimmerman et al., 1986). Concentrations of nanosilica surpassing the solubility of silicic acid were employed, and significant T cell activation and decreases in peripheral cell counts were evident. It was also shown that nanosilica induced both significant T cell activation and monocyte cell death when using a dosing schedule that more closely mimicked an *in vivo* situation after intravenous injection (*i.e.*, short incubations at high nanosilica concentrations followed by continuous dilution).

Studies conducted prior to 2013 showed that a nanosilica dispersion can inhibit tumour growth rate in mice (HS Pharma, unpublished data). Post-termination studies conducted here showed that the mechanism of tumour growth inhibition is not likely through direct toxicity, as determined by Si infiltration into the tumour. The levels of analytes and antibodies in the serum increased after nanosilica treatment, which would suggest an immune response was induced. One of the analytes induced, lymphotactin, a chemokine for and produced by T cells, increased after nanosilica injection and it correlated to a decreased tumour size, potentially inferring to the mechanism of tumour growth inhibition. The mild anti-cancer properties of nanosilica were confirmed in a subcutaneous tumour model and a metastatic tumour model, though the mechanism behind these responses remains unknown.

8.2 Future perspectives

The results in this thesis show that amorphous nanosilica particles under 10 nm in diameter induce non-specific activation of T cells. Evidence would suggest that the nanoparticulate directly engages the TCR/CD3 complex, the first non-MHC coated nanoparticle found to do so, and induces numerous surface activation markers and cytokine production. Complete T cell activation was not induced (as determined by the low percentage of cells which proliferated), suggesting that TCR ligation by nanosilica is inefficient and that costimulatory receptors are not engaged. Further investigations pertaining to the signalling induced by nanosilica are required. In the literature, insufficient TCR ligation in the absence of co-stimulation can induce a hyporesponsive T cell state, specifically T cell anergy. Whether nanosilica induces T cell anergy is not known and would have an impact on its *in vivo* safety.

The effect of nanosilica on natural killer cells also requires further investigation. Nanosilica was shown to induce CD25 and CD69 expression on NK/NKT cells. Whether NK cells, which lack a TCR, are activated by nanosilica remains unclear.

The studies conducted in this thesis were predominately carried out using materials comprised of silica, where the only other particle tested was an iron hydroxide nanoparticle (coated in adipate and tartrate). Given the wealth of particles that humans are constantly exposed to (Lomer et al., 2002), further investigations are required to identify whether other particles induce similar responses. In the literature, fullerenes, cobalt nanoparticles and ZnO nanoparticles were shown to induce IFN- γ production (Hanley et al., 2009; Liu et al., 2009; Petrarca et al., 2005). Whether they induce the production of this cytokine through engagement of the TCR (like nanosilica) is unknown. Additionally, further investigations are also required to assess the effect of the silicate materials used in the biomedical applications on T cell activation.

The anti-tumour and anti-metastatic properties of nanosilica were confirmed and identified in this thesis, though the underlying mechanism remains unknown. Further investigations are required to determine whether these responses are due to nanosilica induced T cell activation. One way this could be accomplished is through isolating, labelling, and treating T cells with nanosilica (*ex vivo*) and administering the activated cells to cancer bearing mice. Whether treatment with nanosilica leads to greater tumour infiltration could then be identified. Further *in vivo* studies should include the effect of the high silica load on the animals and investigating the long term effects on the spleen, liver, and lungs.

References

- Acuto, O., V. Di Bartolo, and F. Michel. 2008. Tailoring T-cell receptor signals by proximal negative feedback mechanisms. *Nature Reviews Immunology*. 8:699-712.
- Ahmad, J., M. Ahamed, M.J. Akhtar, S.A. Alrokayan, M.A. Siddiqui, J. Musarrat, and A.A. Al-Khedhairi. 2012. Apoptosis induction by silica nanoparticles mediated through reactive oxygen species in human liver cell line HepG2. *Toxicology and Applied Pharmacology*. 259:160-168.
- Akhtar, M.J., M. Ahamed, S. Kumar, H. Siddiqui, G. Patil, M. Ashquin, and I. Ahmad. 2010. Nanotoxicity of pure silica mediated through oxidant generation rather than glutathione depletion in human lung epithelial cells. *Toxicology*. 276:95-102.
- Aktas, E., U.C. Kucuksezer, S. Bilgic, G. Erten, and G. Deniz. 2009. Relationship between CD107a expression and cytotoxic activity. *Cellular immunology*. 254:149-154.
- Al-Rawi, M., S. Diabaté, and C. Weiss. 2011. Uptake and intracellular localization of submicron and nano-sized SiO₂ particles in HeLa cells. *Archives of toxicology*. 85:813-826.
- Alberts, B. 2002. *Molecular Biology of the Cell*. Garland Science.
- Alexander, G. 1953. The reaction of low molecular weight silicic acids with molybdic acid. *Journal of the American Chemical Society*. 75:5655-5657.
- Allison, A., J. Harington, and M. Birbeck. 1966. An examination of the cytotoxic effects of silica on macrophages. *The Journal of experimental medicine*. 124:141-154.
- Allison, T.J., C.C. Winter, J.-J. Fournié, M. Bonneville, and D.N. Garboczi. 2001. Structure of a human $\gamma\delta$ T-cell antigen receptor. *Nature*. 411:820-824.
- Alter, G., J.M. Malenfant, and M. Altfeld. 2004. CD107a as a functional marker for the identification of natural killer cell activity. *Journal of immunological methods*. 294:15-22.
- Aminian, O., S. Akbar Sharifian, R. Mehrdad, K. Sadeghniyat Haghighi, and M. Mazaheri. 2009. Antinuclear antibody and rheumatoid factor in Silica-Exposed workers. *Arhiv za higijenu rada i toksikologiju*. 60:185-190.
- Amram, K., and J. Ganor. 2005. The combined effect of pH and temperature on smectite dissolution rate under acidic conditions. *Geochimica et Cosmochimica Acta*. 69:2535-2546.
- An, X., Y. Jin, M.J. Philbrick, J. Wu, A. Messmer-Blust, X. Song, B.L. Cully, P. He, M. Xu, and H.S. Duffy. 2012. Endothelial Cells Require Related Transcription Enhancer Factor-1 for Cell–Cell Connections Through the Induction of Gap Junction Proteins. *Arteriosclerosis, thrombosis, and vascular biology*. 32:1951-1959.
- Arad, G., R. Levy, I. Nasie, D. Hillman, Z. Rotfogel, U. Barash, E. Supper, T. Shpilka, A. Minis, and R. Kaempfer. 2011. Binding of superantigen toxins into the CD28 homodimer interface is essential for induction of cytokine genes that mediate lethal shock. *PLoS Biol*. 9:e1001149.
- Arakaki, R., A. Yamada, Y. Kudo, Y. Hayashi, and N. Ishimaru. 2014. Mechanism of activation-induced cell death of T cells and regulation of FasL expression. *Crit Rev Immunol*. 34:301-314.
- Arpaia, N., J.A. Green, B. Molledo, A. Arvey, S. Hemmers, S. Yuan, P.M. Treuting, and A.Y. Rudensky. 2015. A distinct function of regulatory T cells in tissue protection. *Cell*. 162:1078-1089.

- Arumugam, M.Q., D. Ireland, R.A. Brooks, N. Rushton, and W. Bonfield. 2006. The effect orthosilicic acid on collagen type I, alkaline phosphatase and osteocalcin mRNA expression in human bone-derived osteoblasts in vitro. *Key Engineering Materials*. 309:121-124.
- Avalos, A.M., and H. Ploegh. 2014. Early BCR events and antigen capture, processing, and loading on MHC class II on B cells. *Frontiers in immunology*. 5:92.
- Balagopalan, L., N.P. Coussens, E. Sherman, L.E. Samelson, and C.L. Sommers. 2010. The LAT story: a tale of cooperativity, coordination, and choreography. *Cold Spring Harbor perspectives in biology*. 2:a005512.
- Balamuralikrishnan, B., V. Balachandar, M.D. Subramaniam, K.K. Alagumuthu, S. Sureshkumar, M. Arun, S. Arun, K. Padmavathi, A.H. Razeena, and M. Gomathi. 2014. Assessment of genotoxic and humoral immune system alterations in silica exposed workers from pottery industries in South India. *Stochastic Environmental Research and Risk Assessment*. 28:1801-1814.
- Barry, M., and R.C. Bleackley. 2002. Cytotoxic T lymphocytes: all roads lead to death. *Nature Reviews Immunology*. 2:401-409.
- Bastos, C.A.P., J.J. Powell, N.J.R. Faria, and B.M. Vis. 2015. Materials and methods relating to stabilised polymeric silicate compositions. Patent application.
- Bechtold, M.F., and O.E. Snyder. 1951. Chemical processes and composition. US Patent 2,574,902.
- Bell, J. 2002. T-cell turn-off. *Nat Rev Immunol*. 2:460-460.
- Bellone, M. 2001. Autoimmune Disease: Pathogenesis. In eLS. John Wiley & Sons, Ltd.
- Belton, D.J., O. Deschaume, and C.C. Perry. 2012. An overview of the fundamentals of the chemistry of silica with relevance to biosilicification and technological advances. *FEBS Journal*. 279:1710-1720.
- Berghe, T.V., A. Linkermann, S. Jouan-Lanhouet, H. Walczak, and P. Vandenabeele. 2014. Regulated necrosis: the expanding network of non-apoptotic cell death pathways. *Nature reviews Molecular cell biology*. 15:135-147.
- Bergna, H.E., and W.O. Roberts. 2005. Colloidal silica: fundamentals and applications. CRC Press.
- Bergsbaken, T., S.L. Fink, and B.T. Cookson. 2009. Pyroptosis: host cell death and inflammation. *Nature Reviews Microbiology*. 7:99-109.
- Beshir, S., W.A. Shaheen, S. Elserougy, and H.M. Aziz. 2015. Serum autoantibodies in silicosis and non-silicosis cement workers. *American journal of industrial medicine*. 58:238-244.
- Biosciences, B. 2011. Detection of Apoptosis Using the BD Annexin V FITC Assay on the BD FACSVerser™ System.
- Bitar, A., N.M. Ahmad, H. Fessi, and A. Elaissari. 2012. Silica-based nanoparticles for biomedical applications. *Drug Discovery Today*. 17:1147-1154.
- Bluestone, J.A., H. Bour-Jordan, M. Cheng, and M. Anderson. 2015. T cells in the control of organ-specific autoimmunity. *The Journal of clinical investigation*. 125:2250-2260.

- Bolt, P., T. Beelen, and R. Van Santen. 1997. A small angle X-ray scattering study on high pH silica precipitations. *Colloids and Surfaces A: Physicochemical and Engineering Aspects*. 122:183-187.
- Boomer, J.S., and J.M. Green. 2010. An enigmatic tail of CD28 signaling. *Cold Spring Harbor perspectives in biology*. 2:a002436.
- Bradley, J. 2008. TNF-mediated inflammatory disease. *The Journal of pathology*. 214:149-160.
- Brandenberger, C., N.L. Rowley, D.N. Jackson-Humbles, Q. Zhang, L.A. Bramble, R.P. Lewandowski, J.G. Wagner, W. Chen, B.L. Kaplan, and N.E. Kaminski. 2013. Engineered silica nanoparticles act as adjuvants to enhance allergic airway disease in mice. *Particle and fibre toxicology*. 10:1.
- Broere, F., S.G. Apasov, M.V. Sitkovsky, and W. van Eden. 2011. A2 T cell subsets and T cell-mediated immunity. In *Principles of immunopharmacology*. Springer. 15-27.
- Bronder, S.R. 1999. Stabilized orthosilicic acid comprising preparation and biological preparation. Google Patents.
- Brown, J., A. Archer, J. Pfau, and A. Holian. 2003. Silica accelerated systemic autoimmune disease in lupus-prone New Zealand mixed mice. *Clinical & Experimental Immunology*. 131:415-421.
- Brownlie, R.J., and R. Zamoyska. 2013. T cell receptor signalling networks: branched, diversified and bounded. *Nature Reviews Immunology*. 13:257-269.
- Calomme, M., P. Geusens, N. Demeester, G. Behets, P. D'Haese, J. Sindambiwe, V. Van Hoof, and D.V. Berghe. 2006. Partial prevention of long-term femoral bone loss in aged ovariectomized rats supplemented with choline-stabilized orthosilicic acid. *Calcified tissue international*. 78:227-232.
- Cama, J., V. Metz, and J. Ganor. 2002. The effect of pH and temperature on kaolinite dissolution rate under acidic conditions. *Geochimica et Cosmochimica Acta*. 66:3913-3926.
- Carlisle, E.M. 1976. *In vivo* requirement for silicon in articular-cartilage and connective-tissue formation in chick. *Journal of Nutrition*. 106:478-484.
- Carlisle, E.M. 1982. The nutritional essentiality of silicon. *Nutrition Reviews*. 40:193-198.
- Carlisle, E.M. 1986. Silicon as an essential trace-element in animal nutrition. *Ciba Foundation Symposia*. 121:123-139.
- Carpenter, A.C., and R. Bosselut. 2010. Decision checkpoints in the thymus. *Nature immunology*. 11:666-673.
- Catalfamo, M., T. Karpova, J. McNally, S.V. Costes, S.J. Lockett, E. Bos, P.J. Peters, and P.A. Henkart. Human CD8⁺ T Cells Store RANTES in a Unique Secretory Compartment and Release It Rapidly after TcR Stimulation. *Immunity*. 20:219-230.
- Chakraborty, A.K., and A. Weiss. 2014. Insights into the initiation of TCR signaling. *Nature immunology*. 15:798-807.
- Chambers, A.F., A.C. Groom, and I.C. MacDonald. 2002. Metastasis: Dissemination and growth of cancer cells in metastatic sites. *Nat Rev Cancer*. 2:563-572.

- Chan, C., M. Smyth, and L. Martinet. 2014. Molecular mechanisms of natural killer cell activation in response to cellular stress. *Cell Death & Differentiation*. 21:5-14.
- Chang, J.-S., K.L.B. Chang, D.-F. Hwang, and Z.-L. Kong. 2007. In vitro cytotoxicity of silica nanoparticles at high concentrations strongly depends on the metabolic activity type of the cell line. *Environmental science & technology*. 41:2064-2068.
- Chatila, T., L. Silverman, R. Miller, and R. Geha. 1989. Mechanisms of T cell activation by the calcium ionophore ionomycin. *The Journal of Immunology*. 143:1283-1289.
- Chatterjee, N., J. Yang, R. Atluri, W. Lee, J. Hong, and J. Choi. 2016. Amorphous silica nanoparticle-induced perturbation of cholesterol homeostasis as a function of surface area highlights safe-by-design implementation: an integrated multi-OMICS analysis. *RSC Advances*. 6:68606-68614.
- Chen, H., C.I. Liakou, A. Kamat, C. Pettaway, J.F. Ward, D.N. Tang, J. Sun, A.A. Jungbluth, P. Troncoso, and C. Logothetis. 2009a. Anti-CTLA-4 therapy results in higher CD4+ ICOShi T cell frequency and IFN- γ levels in both nonmalignant and malignant prostate tissues. *Proceedings of the National Academy of Sciences*. 106:2729-2734.
- Chen, L., and D.B. Flies. 2013. Molecular mechanisms of T cell co-stimulation and co-inhibition. *Nature Reviews Immunology*. 13:227-242.
- Chen, M.-R. 2011. Epstein–Barr virus, the immune system, and associated diseases. *Frontiers in microbiology*. 2:5.
- Chen, W., W. Jin, N. Hardegen, K.-j. Lei, L. Li, N. Marinos, G. McGrady, and S.M. Wahl. 2003. Conversion of peripheral CD4+ CD25– naive T cells to CD4+ CD25+ regulatory T cells by TGF- β induction of transcription factor Foxp3. *The Journal of experimental medicine*. 198:1875-1886.
- Chen, W., Q. Zhang, B.L. Kaplan, G.L. Baker, and N.E. Kaminski. 2014. Induced T cell cytokine production is enhanced by engineered nanoparticles. *Nanotoxicology*. 8:11-23.
- Chen, Y., Y. Guo, and J. Zhong. 2009b. Morphology and differentiation pathway of superantigen SEB-activated NKT subsets. *Xi bao yu fen zi mian yi xue za zhi= Chinese journal of cellular and molecular immunology*. 25:596-599.
- Cho, M., W.-S. Cho, M. Choi, S.J. Kim, B.S. Han, S.H. Kim, H.O. Kim, Y.Y. Sheen, and J. Jeong. 2009. The impact of size on tissue distribution and elimination by single intravenous injection of silica nanoparticles. *Toxicology letters*. 189:177-183.
- Choi, H.-S., Y.-J. Kim, M. Song, M.-K. Song, and J.-C. Ryu. 2011. Genotoxicity of nano-silica in mammalian cell lines. *Toxicology and Environmental Health Sciences*. 3:7-13.
- Choi, M., W.-S. Cho, B.S. Han, M. Cho, S.Y. Kim, J.-Y. Yi, B. Ahn, S.H. Kim, and J. Jeong. 2008. Transient pulmonary fibrogenic effect induced by intratracheal instillation of ultrafine amorphous silica in A/J mice. *Toxicology Letters*. 182:97-101.
- Chu, Z., Y. Huang, L. Li, Q. Tao, and Q. Li. 2012. Physiological pathway of human cell damage induced by genotoxic crystalline silica nanoparticles. *Biomaterials*. 33:7540-7546.
- Chu, Z., Y. Huang, Q. Tao, and Q. Li. 2011. Cellular uptake, evolution, and excretion of silica nanoparticles in human cells. *Nanoscale*. 3:3291-3299.
- Clarke, F.W., and H.S. Washington. 1924. The composition of the earth's crust. US Government Printing Office.

- Clayman, C.B. 1995. *The Human Body: An Illustrated Guide to Its Structure, Function, and Disorders*. Dorling Kindersley Publishing, Incorporated.
- Clemments, A.M., P. Botella, and C.C. Landry. 2015. Protein Adsorption From Biofluids on Silica Nanoparticles: Corona Analysis as a Function of Particle Diameter and Porosity. *ACS applied materials & interfaces*. 7:21682-21689.
- Clogston, J.D., and A.K. Patri. 2011. Zeta potential measurement. *Characterization of nanoparticles intended for drug delivery*:63-70.
- Comber, J.D., and R. Philip. 2014. MHC class I antigen presentation and implications for developing a new generation of therapeutic vaccines. *Therapeutic Advances in Vaccines*. 2:77-89.
- Corbalan, J.J., C. Medina, A. Jacoby, T. Malinski, and M.W. Radomski. 2011. Amorphous silica nanoparticles trigger nitric oxide/peroxynitrite imbalance in human endothelial cells: inflammatory and cytotoxic effects. *Int J Nanomedicine*. 6:2821-2835.
- Couper, K.N., D.G. Blount, and E.M. Riley. 2008. IL-10: the master regulator of immunity to infection. *The Journal of Immunology*. 180:5771-5777.
- Crotty, S. 2015. A brief history of T cell help to B cells. *Nature Reviews Immunology*. 15:185-189.
- Csencsits, K.L., and D.K. Bishop. 2003. Contrasting alloreactive CD4+ and CD8+ T cells: there's more to it than MHC restriction. *American Journal of Transplantation*. 3:107-115.
- D'Orazio, J.A., G.W. Burke, and J. Stein-Streilein. 1995. Staphylococcal enterotoxin B activates purified NK cells to secrete IFN-gamma but requires T lymphocytes to augment NK cytotoxicity. *The Journal of Immunology*. 154:1014-1023.
- D'Souza, W.N., and L. Lefrançois. 2003. IL-2 is not required for the initiation of CD8 T cell cycling but sustains expansion. *The Journal of Immunology*. 171:5727-5735.
- Dar, A.A., R.S. Patil, and S.V. Chiplunkar. 2015. Insights into the relationship between toll like receptors and gamma delta T cell responses. *Pattern Recognition Receptors and Cancer*:15.
- Del Nagro, C.J., D.C. Otero, A.N. Anzelon, S.A. Omori, R.V. Kolla, and R.C. Rickert. 2005. CD 19 function in central and peripheral B-cell development. *Immunologic research*. 31:119-131.
- Desai-Mehta, A., L. Lu, R. Ramsey-Goldman, and S.K. Datta. 1996. Hyperexpression of CD40 ligand by B and T cells in human lupus and its role in pathogenic autoantibody production. *Journal of Clinical Investigation*. 97:2063.
- Desouky, M., J. Powell, R. Jugdaohsingh, K. White, and C. McCrohan. 2002. Influence of oligomeric silicic and humic acids on aluminum accumulation in a freshwater grazing invertebrate. *Ecotoxicology and environmental safety*. 53:382-387.
- Dobbie, J., and M.J. Smith. 1982. The silicon content of body fluids. *Scottish medical journal*. 27:17-19.
- Dobranskyte, A., R. Jugdaohsingh, E. Stuchlik, J. Powell, K. White, and C. McCrohan. 2004. Role of exogenous and endogenous silicon in ameliorating behavioural responses to aluminium in a freshwater snail. *Environmental Pollution*. 132:427-433.

- Doherty, G.J., and H.T. McMahon. 2009. Mechanisms of endocytosis. *Annual review of biochemistry*. 78:857-902.
- Doll, N.J., R.P. Stankus, J. Hughes, H. Weill, R.C. Gupta, M. Rodriguez, R.N. Jones, M.A. Alspaugh, and J.E. Salvaggio. 1981. Immune complexes and autoantibodies in silicosis. *Journal of Allergy and Clinical Immunology*. 68:281-285.
- Don, B.R., and G. Kaysen. 2004. Poor nutritional status and inflammation: serum albumin: relationship to inflammation and nutrition. *In Seminars in dialysis*. Vol. 17. Wiley Online Library. 432-437.
- Dorn, G.W. 2013. Molecular mechanisms that differentiate apoptosis from programmed necrosis. *Toxicologic pathology*. 41:227-234.
- Downs, R., and D. Palmer. 1994. The pressure behavior of α -cristobalite. *Am Mineral*. 79:9-14.
- Drescher, D., G. Orts-Gil, G. Laube, K. Natte, R.W. Veh, W. Österle, and J. Kneipp. 2011. Toxicity of amorphous silica nanoparticles on eukaryotic cell model is determined by particle agglomeration and serum protein adsorption effects. *Analytical and Bioanalytical Chemistry*. 400:1367.
- Duan, J., Y. Yu, Y. Li, Y. Yu, Y. Li, X. Zhou, P. Huang, and Z. Sun. 2013. Toxic effect of silica nanoparticles on endothelial cells through DNA damage response via Chk1-dependent G2/M checkpoint. *PloS one*. 8:e62087.
- DuPage, M., and J.A. Bluestone. 2016. Harnessing the plasticity of CD4+ T cells to treat immune-mediated disease. *Nature Reviews Immunology*.
- Edwardson, J., P. Moore, I. Ferrier, J. Lilley, J. Barker, J. Templar, and J. Day. 1993. Effect of silicon on gastrointestinal absorption of aluminium. *The Lancet*. 342:211-212.
- Eisinger, J., and D. Clairet. 1993. Effects of silicon, fluoride, etidronate and magnesium on bone mineral density: a retrospective study. *Magnesium research: official organ of the International Society for the Development of Research on Magnesium*. 6:247-249.
- Elgueta, R., M.J. Benson, V.C. De Vries, A. Wasiuk, Y. Guo, and R.J. Noelle. 2009. Molecular mechanism and function of CD40/CD40L engagement in the immune system. *Immunological reviews*. 229:152-172.
- Elmore, S. 2007. Apoptosis: a review of programmed cell death. *Toxicologic pathology*. 35:495-516.
- Exley, C., C. Schneider, and F.J. Doucet. 2002. The reaction of aluminium with silicic acid in acidic solution: an important mechanism in controlling the biological availability of aluminium? *Coordination Chemistry Reviews*. 228:127-135.
- Fairhurst, D., and R.W. Lee. 2008. Aggregation, Agglomeration-How to Avoid Aggravation When Formulating Particulate Suspensions. *Drug Delivery Tech*. 8.
- Fathman, C.G., and N.B. Lineberry. 2007. Molecular mechanisms of CD4+ T-cell anergy. *Nature Reviews Immunology*. 7:599-609.
- Faustman, D., and M. Davis. 2010. TNF receptor 2 pathway: drug target for autoimmune diseases. *Nature reviews Drug discovery*. 9:482-493.
- Fazekas De St. Groth, B., A.L. Smith, and C.A. Higgins. 2004. T cell activation: in vivo veritas. *Immunol Cell Biol*. 82:260-268.

- Fede, C., F. Selvestrel, C. Compagnin, M. Mognato, F. Mancin, E. Reddi, and L. Celotti. 2012. The toxicity outcome of silica nanoparticles (Ludox (R)) is influenced by testing techniques and treatment modalities. *Analytical and Bioanalytical Chemistry*. 404:1789-1802.
- Fedeli, C., D. Segat, R. Tavano, G. De Franceschi, P.P. De Laureto, E. Lubian, F. Selvestrel, F. Mancin, and E. Papini. 2014. Variations of the corona HDL: albumin ratio determine distinct effects of amorphous SiO₂ nanoparticles on monocytes and macrophages in serum. *Nanomedicine*. 9:2481-2497.
- Fedeli, C., F. Selvestrel, R. Tavano, D. Segat, F. Mancin, and E. Papini. 2013. Catastrophic inflammatory death of monocytes and macrophages by overtaking of a critical dose of endocytosed synthetic amorphous silica nanoparticles/serum protein complexes. *Nanomedicine*. 8:1101+.
- Fedeyko, J.M., J.D. Rimer, R.F. Lobo, and D.G. Vlachos. 2004. Spontaneous formation of silica nanoparticles in basic solutions of small tetraalkylammonium cations. *The Journal of Physical Chemistry B*. 108:12271-12275.
- Fesnak, A.D., C.H. June, and B.L. Levine. 2016. Engineered T cells: the promise and challenges of cancer immunotherapy. *Nat Rev Cancer*. 16:566-581.
- Finetti, F., A. Onnis, and C.T. Baldari. 2015. Regulation of vesicular traffic at the T cell immune synapse: lessons from the primary cilium. *Traffic*. 16:241-249.
- Finney, O.C., E.M. Riley, and M. Walther. 2010. Phenotypic analysis of human peripheral blood regulatory T cells (CD4⁺ FOXP3⁺ CD127^{lo/-}) ex vivo and after in vitro restimulation with malaria antigens. *European journal of immunology*. 40:47-60.
- Fleischer, B., A. Necker, C. Leget, B. Malissen, and F. Romagne. 1996. Reactivity of mouse T-cell hybridomas expressing human Vbeta gene segments with staphylococcal and streptococcal superantigens. *Infection and immunity*. 64:987-994.
- Francisco, L.M., P.T. Sage, and A.H. Sharpe. 2010. The PD-1 pathway in tolerance and autoimmunity. *Immunological reviews*. 236:219-242.
- Fraser, J.D. 2011. Clarifying the mechanism of superantigen toxicity. *PLoS Biol*. 9:e1001145.
- Frujtier-Pöllth, C. 2012. The toxicological mode of action and the safety of synthetic amorphous silica—A nanostructured material. *Toxicology*. 294:61-79.
- Fu, G., L. Nazar, and A. Bain. 1991. Aging processes of alumina sol-gels: characterization of new aluminum polyoxycations by aluminum-27 NMR spectroscopy. *Chemistry of Materials*. 3:602-610.
- Garneau, A.P., G.A. Carpentier, A.-A. Marcoux, R. Frenette-Cotton, C.F. Simard, W. Rémus-Borel, L. Caron, M. Jacob-Wagner, M. Noël, J.J. Powell, R. Bélanger, F. Côté, and P. Isenring. 2015. Aquaporins Mediate Silicon Transport in Humans. *PLoS ONE*. 10:e0136149.
- Gauthy, E., J. Cuende, J. Stockis, C. Huygens, B. Lethé, J.-F. Collet, G. Bommer, P.G. Coulie, and S. Lucas. 2013. GARP is regulated by miRNAs and controls latent TGF- β 1 production by human regulatory T cells. *PloS one*. 8:e76186.
- Gazdar, A.F., B. Gao, and J.D. Minna. 2010. Lung cancer cell lines: Useless artifacts or invaluable tools for medical science? *Lung cancer*. 68:309-318.
- Geginat, J., M. Paroni, S. Maglie, J.S. Alfen, I. Kastirr, P. Gruarin, M. De Simone, M. Pagani, and S. Abrignani. 2015. Plasticity of human CD4 T cell subsets. *CD4⁺ T cell differentiation in infection: amendments to the Th1/Th2 axiom*:67.

- Gibbings, D.J., M. Marcet-Palacios, Y. Sekar, M.C. Ng, and A.D. Befus. 2007. CD8 α is expressed by human monocytes and enhances Fc γ R-dependent responses. *BMC immunology*. 8:12.
- Girardi, M. 2006. Immunosurveillance and immunoregulation by $\gamma\delta$ T cells. *Journal of Investigative Dermatology*. 126:25-31.
- Glinnemann, J. 1992. Erratum: Crystal structures of the low-temperature quartz-type phases of SiO₂ and GeO₂ at elevated pressure. *Zeitschrift für Kristallographie-Crystalline Materials*. 202:269-270.
- González-Muñoz, M.J., A. Peña, and I. Meseguer. 2008. Role of beer as a possible protective factor in preventing Alzheimer's disease. *Food and Chemical Toxicology*. 46:49-56.
- Goodfellow, H.S., M.P. Frushicheva, Q. Ji, D.A. Cheng, T.A. Kadlecck, A.J. Cantor, J. Kuriyan, A.K. Chakraborty, A. Salomon, and A. Weiss. 2015. The catalytic activity of the kinase ZAP-70 mediates basal signaling and negative feedback of the T cell receptor pathway. *Science signaling*. 8:ra49-ra49.
- Gören, R., B. Ersoy, C. Özgür, and T. Alp. 2012. Colloidal stability–slip casting behavior relationship in slurry of mullite synthesized by the USP method. *Ceramics International*. 38:679-685.
- Gorrepati, E.A., P. Wongthahan, S. Raha, and H.S. Fogler. 2010. Silica precipitation in acidic solutions: mechanism, pH effect, and salt effect. *Langmuir*. 26:10467-10474.
- Grant, B.D., and J.G. Donaldson. 2009. Pathways and mechanisms of endocytic recycling. *Nature reviews Molecular cell biology*. 10:597-608.
- Greenberg, M.I., J. Waksman, and J. Curtis. 2007. Silicosis: a review. *Disease-a-Month*. 53:394-416.
- Gryshchuk, V., and N. Galagan. 2016. Silica Nanoparticles Effects on Blood Coagulation Proteins and Platelets. *Biochemistry research international*. 2016.
- Guo, L., and P.H. Santschi. 2007. Ultrafiltration and its applications to sampling and characterisation of aquatic colloids. *IUPAC Series on Analytical and Physical Chemistry of Environmental Systems*. 10:159.
- Hair, M.L., and W. Hertl. 1970. Acidity of surface hydroxyl groups. *The Journal of Physical Chemistry*. 74:91-94.
- Hamilton, R.F., S.A. Thakur, J.K. Mayfair, and A. Holian. 2006. MARCO mediates silica uptake and toxicity in alveolar macrophages from C57BL/6 mice. *Journal of Biological Chemistry*. 281:34218-34226.
- Hanley, C., A. Thurber, C. Hanna, A. Punnoose, J. Zhang, and D.G. Wingett. 2009. The Influences of Cell Type and ZnO Nanoparticle Size on Immune Cell Cytotoxicity and Cytokine Induction. *Nanoscale Research Letters*. 4:1409-1420.
- Hassin, D., O.G. Garber, A. Meiraz, Y.S. Schiffenbauer, and G. Berke. 2011. Cytotoxic T lymphocyte perforin and Fas ligand working in concert even when Fas ligand lytic action is still not detectable. *Immunology*. 133:190-196.
- Hayashi, H. 2010. Peripheral regulatory T cells from silicosis patients are susceptible to CD95-mediated apoptosis. *Kawasaki Medical Journal*. 36:13-21.

- Hayashi, H., Y. Miura, M. Maeda, S. Murakami, N. Kumagai, Y. Nishimura, M. Kusaka, K. Urakami, W. Fujimoto, and T. Otsuki. 2009. Reductive alteration of the regulatory function of the CD4 (+) CD25 (+) T cell fraction in silicosis patients. *International journal of immunopathology and pharmacology*. 23:1099-1109.
- Hayworth, J., K. Kasper, M. Leon-Ponte, C. Herfst, D. Yue, W. Brintnell, D. Mazzuca, D. Heinrichs, E. Cairns, and J. Madrenas. 2009. Attenuation of massive cytokine response to the staphylococcal enterotoxin B superantigen by the innate immunomodulatory protein lactoferrin. *Clinical & Experimental Immunology*. 157:60-70.
- Hench, L.L., I.D. Xynos, and J.M. Polak. 2004. Bioactive glasses for in situ tissue regeneration. *Journal of Biomaterials Science, Polymer Edition*. 15:543-562.
- Hewitt, R.E., L.C. Pele, M. Tremelling, A. Metz, M. Parkes, and J.J. Powell. 2012. Immuno-inhibitory PD-L1 can be induced by a Peptidoglycan/NOD2 mediated pathway in primary monocytic cells and is deficient in Crohn's patients with homozygous NOD2 mutations. *Clinical immunology*. 143:162-169.
- Hirai, T., Y. Yoshioka, H. Takahashi, K.-i. Ichihashi, T. Yoshida, S. Tochigi, K. Nagano, Y. Abe, H. Kamada, and S.-i. Tsunoda. 2012. Amorphous silica nanoparticles enhance cross-presentation in murine dendritic cells. *Biochemical and biophysical research communications*. 427:553-556.
- Hoesel, B., and J.A. Schmid. 2013. The complexity of NF- κ B signaling in inflammation and cancer. *Molecular cancer*. 12:1.
- Hogquist, K.A., and S.C. Jameson. 2014. The self-obsession of T cells: how TCR signaling thresholds affect fate 'decisions' and effector function. *Nature immunology*. 15:815-823.
- Holling, T.M., E. Schooten, A.W. Langerak, and P.J. van den Elsen. 2004. Regulation of MHC class II expression in human T-cell malignancies. *Blood*. 103:1438-1444.
- Huehn, J., J.K. Polansky, and A. Hamann. 2009. Epigenetic control of FOXP3 expression: the key to a stable regulatory T-cell lineage? *Nat Rev Immunol*. 9:83-89.
- Hunter, C.A., and S.A. Jones. 2015. IL-6 as a keystone cytokine in health and disease. *Nature immunology*. 16:448-457.
- Huotari, J., and A. Helenius. 2011. Endosome maturation. *The EMBO journal*. 30:3481-3500.
- Iler, R.K. 1979. *The Chemistry of Silica*. John Wiley & Sons.
- Ivanov, S., S. Zhuravsky, G. Yukina, V. Tomson, D. Korolev, and M. Galagudza. 2012. In vivo toxicity of intravenously administered silica and silicon nanoparticles. *Materials*. 5:1873-1889.
- Iwasaki, A., and R. Medzhitov. 2015. Control of adaptive immunity by the innate immune system. *Nature immunology*. 16:343-353.
- Jacqmin-Gadda, H., D. Commenges, L. Letenneur, and J.-F. Dartigues. 1996. Silica and aluminum in drinking water and cognitive impairment in the elderly. *Epidemiology*. 7:281-285.
- Janeway, C.A., P. Travers, M. Walport, and M.J. Shlomchik. 1997. *Immunobiology: the immune system in health and disease*. Current Biology Singapore.
- Janeway Jr, C.A., P. Travers, M. Walport, and M.J. Shlomchik. 2001. *The complement system and innate immunity*.

- Jantschke, A., K. Spinde, and E. Brunner. 2014. Electrostatic interplay: The interaction triangle of polyamines, silicic acid, and phosphate studied through turbidity measurements, silicomolybdic acid test, and ²⁹Si NMR spectroscopy. *Beilstein journal of nanotechnology*. 5:2026-2035.
- Jenkins, S.J., G. Perona-Wright, and A.S. MacDonald. 2008. Full development of Th2 immunity requires both innate and adaptive sources of CD154. *The Journal of Immunology*. 180:8083-8092.
- Jiang, S., and C. Dong. 2013. A complex issue on CD4+ T-cell subsets. *Immunological reviews*. 252:5-11.
- Jorgensen, I., and E.A. Miao. 2015. Pyroptotic cell death defends against intracellular pathogens. *Immunological reviews*. 265:130-142.
- Joshi, G.N., and D.A. Knecht. 2013. Silica phagocytosis causes apoptosis and necrosis by different temporal and molecular pathways in alveolar macrophages. *Apoptosis*. 18:271-285.
- Jugdaohsingh, R. 2007. Silicon and bone health. *Journal of Nutrition Health & Aging*. 11:99-110.
- Jugdaohsingh, R., S.H. Anderson, K.L. Tucker, H. Elliott, D.P. Kiel, R.P. Thompson, and J.J. Powell. 2002. Dietary silicon intake and absorption. *The American journal of clinical nutrition*. 75:887-893.
- Jugdaohsingh, R., A. Brown, M. Dietzel, and J.J. Powell. 2013. High-Aluminum-Affinity Silica Is a Nanoparticle That Seeds Secondary Aluminosilicate Formation. *PLOS ONE*. 8:e84397.
- Jugdaohsingh, R., S.D. Kinrade, and J.J. Powell. 2008. Is there a biochemical role for silicon? *Metal Ions in Biology and Medicine*. 10:45-55.
- Jugdaohsingh, R., D.M. Reffitt, C. Oldham, J.P. Day, L.K. Fifield, R.P. Thompson, and J.J. Powell. 2000. Oligomeric but not monomeric silica prevents aluminum absorption in humans. *The American journal of clinical nutrition*. 71:944-949.
- Jugdaohsingh, R., K.L. Tucker, N. Qiao, L.A. Cupples, D.P. Kiel, and J.J. Powell. 2004. Dietary silicon intake is positively associated with bone mineral density in men and premenopausal women of the Framingham Offspring cohort. *Journal of Bone and Mineral Research*. 19:297-307.
- Kalia, P., R.A. Brooks, S.D. Kinrade, D.J. Morgan, A.P. Brown, N. Rushton, and R. Jugdaohsingh. 2016. Adsorption of amorphous silica nanoparticles onto hydroxyapatite surfaces differentially alters surface properties and adhesion of human osteoblast cells. *PloS one*. 11:e0144780.
- Kalliny, M.S., and M.I. Bassyouni. 2011. Immune response due to silica exposure in Egyptian phosphate mines. *Journal of health care for the poor and underserved*. 22:91-109.
- Kambayashi, T., and T.M. Laufer. 2014. Atypical MHC class II-expressing antigen-presenting cells: can anything replace a dendritic cell? *Nature Reviews Immunology*. 14:719-730.
- Kaur, G., and J.M. Dufour. 2012. Cell lines: Valuable tools or useless artifacts. *Spermatogenesis*. 2:1-5.
- Kazazi, F., J.-M. Mathijs, P. Foley, and A.L. Cunningham. 1989. Variations in CD4 expression by human monocytes and macrophages and their relationship to infection with the human immunodeficiency virus. *Journal of general virology*. 70:2661-2672.

- Keir, M.E., M.J. Butte, G.J. Freeman, and A.H. Sharpe. 2008. PD-1 and its ligands in tolerance and immunity. *Annu. Rev. Immunol.* 26:677-704.
- Kerek, F. 2010. Biologically active silicic acid. Patent application.
- Kihara, K., T. Matsumoto, and M. Imamura. 1986. Structural change of orthorhombic-I tridymite with temperature: A study based on second-order thermal-vibrational parameters. *Zeitschrift für Kristallographie.* 177:27-38.
- Kinrade, S.D., and T.W. Swaddle. 1988. Silicon-29 NMR studies of aqueous silicate solutions. 1. Chemical shifts and equilibria. *Inorganic Chemistry.* 27:4253-4259.
- Kitamura, T., B.-Z. Qian, and J.W. Pollard. 2015. Immune cell promotion of metastasis. *Nature reviews. Immunology.* 15:73-86.
- Klein, S., M.L. Dell'Arciprete, M. Wegmann, L.V. Distel, W. Neuhuber, M.C. Gonzalez, and C. Kryschi. 2013. Oxidized silicon nanoparticles for radiosensitization of cancer and tissue cells. *Biochemical and biophysical research communications.* 434:217-222.
- Kley, M., A. Kempter, V. Boyko, and K. Huber. 2014. Mechanistic Studies of Silica Polymerization from Supersaturated Aqueous Solutions by Means of Time-Resolved Light Scattering. *Langmuir.* 30:12664-12674.
- Knowles, T.P., M. Vendruscolo, and C.M. Dobson. 2014. The amyloid state and its association with protein misfolding diseases. *Nature reviews Molecular cell biology.* 15:384-396.
- Kobayashi, M., F. Juillerat, P. Galletto, P. Bowen, and M. Borkovec. 2005. Aggregation and charging of colloidal silica particles: effect of particle size. *Langmuir.* 21:5761-5769.
- Koo, H., S.-H. Ryu, H.J. Ahn, W.K. Jung, Y.K. Park, N.H. Kwon, S.H. Kim, J.M. Kim, B.W. Yoo, and S.I. Choi. 2006. Immunostimulatory effects of the anionic alkali mineral complex BARODON on equine lymphocytes. *Clinical and vaccine immunology.* 13:1255-1266.
- Kracker, S., and A. Radbruch. 2004. Immunoglobulin Class Switching. *In B Cell Protocols.* H. Gu and K. Rajewsky, editors. Humana Press, Totowa, NJ. 149-159.
- Krammer, P.H., R. Arnold, and I.N. Lavrik. 2007. Life and death in peripheral T cells. *Nature Reviews Immunology.* 7:532-542.
- Krebs, F.C., S.R. Miller, B.J. Catalone, R. Fichorova, D. Anderson, D. Malamud, M.K. Howett, and B. Wigdahl. 2002. Comparative in vitro sensitivities of human immune cell lines, vaginal and cervical epithelial cell lines, and primary cells to candidate microbicides nonoxynol 9, C31G, and sodium dodecyl sulfate. *Antimicrobial agents and chemotherapy.* 46:2292-2298.
- Kruger, P., M. Saffarzadeh, A.N. Weber, N. Rieber, M. Radsak, H. von Bernuth, C. Benarafa, D. Roos, J. Skokowa, and D. Hartl. 2015. Neutrophils: between host defence, immune modulation, and tissue injury. *PLoS Pathog.* 11:e1004651.
- Kumar, R., I. Roy, T.Y. Ohulchanskyy, L.A. Vathy, E.J. Bergey, M. Sajjad, and P.N. Prasad. 2010. In vivo biodistribution and clearance studies using multimodal organically modified silica nanoparticles. *ACS nano.* 4:699-708.
- Kunzmann, V., E. Bauer, J. Feurle, F. Weißinger, H.-P. Tony, and M. Wilhelm. 2000. Stimulation of $\gamma\delta$ T cells by aminobisphosphonates and induction of antiplasma cell activity in multiple myeloma. *Blood.* 96:384-392.

- Laydon, D.J., C.R. Bangham, and B. Asquith. 2015. Estimating T-cell repertoire diversity: limitations of classical estimators and a new approach. *Phil. Trans. R. Soc. B.* 370:20140291.
- Lazarevic, V., L.H. Glimcher, and G.M. Lord. 2013. T-bet: a bridge between innate and adaptive immunity. *Nat Rev Immunol.* 13:777-789.
- Lehman, S.E., I.A. Mudunkotuwa, V.H. Grassian, and S.C. Larsen. 2016. Nano–Bio Interactions of Porous and Nonporous Silica Nanoparticles of Varied Surface Chemistry: A Structural, Kinetic, and Thermodynamic Study of Protein Adsorption from RPMI Culture Medium. *Langmuir.* 32:731-742.
- Lei, Y., and Y. Takahama. 2012. XCL1 and XCR1 in the immune system. *Microbes and infection.* 14:262-267.
- Leong, A.S., K. Cooper, and F.J.W. Leong. 2003. Manual of diagnostic antibodies for immunohistology. Cambridge University Press.
- Létourneau, S., C. Krieg, G. Pantaleo, and O. Boyman. 2009. IL-2–and CD25-dependent immunoregulatory mechanisms in the homeostasis of T-cell subsets. *Journal of Allergy and Clinical Immunology.* 123:758-762.
- Leung, C.C., I.T.S. Yu, and W. Chen. 2012. Silicosis. *The Lancet.* 379:2008-2018.
- Li, H., A. Llera, D. Tsuchiya, L. Leder, X. Ysern, P.M. Schlievert, K. Karjalainen, and R.A. Mariuzza. 1998. Three-dimensional structure of the complex between a T cell receptor β chain and the superantigen staphylococcal enterotoxin B. *Immunity.* 9:807-816.
- Li, Y., L. Sun, M. Jin, Z. Du, X. Liu, C. Guo, Y. Li, P. Huang, and Z. Sun. 2011. Size-dependent cytotoxicity of amorphous silica nanoparticles in human hepatoma HepG2 cells. *Toxicology in Vitro.* 25:1343-1352.
- Lifshitz, I.M., and V.V. Slyozov. 1961. The kinetics of precipitation from supersaturated solid solutions. *Journal of physics and chemistry of solids.* 19:35-50.
- Lin, W.S., Y.W. Huang, X.D. Zhou, and Y.F. Ma. 2006. In vitro toxicity of silica nanoparticles in human lung cancer cells. *Toxicology and Applied Pharmacology.* 217:252-259.
- Linge, H.M., M. Collin, P. Nordenfelt, M. Mörgelin, M. Malmsten, and A. Egesten. 2008. The human CXC chemokine granulocyte chemotactic protein 2 (GCP-2)/CXCL6 possesses membrane-disrupting properties and is antibacterial. *Antimicrobial agents and chemotherapy.* 52:2599-2607.
- Lison, D., L.C.J. Thomassen, V. Rabolli, L. Gonzalez, D. Napierska, J.W. Seo, M. Kirsch-Volders, P. Hoet, C.E.A. Kirschhock, and J.A. Martens. 2008. Nominal and effective dosimetry of silica nanoparticles in cytotoxicity assays. *Toxicological Sciences.* 104:155-162.
- Liu, X., and J. Sun. 2010. Endothelial cells dysfunction induced by silica nanoparticles through oxidative stress via JNK/P53 and NF- κ B pathways. *Biomaterials.* 31:8198-8209.
- Liu, Y., F. Jiao, Y. Qiu, W. Li, Y. Qu, C. Tian, Y. Li, R. Bai, F. Lao, and Y. Zhao. 2009. Immunostimulatory properties and enhanced TNF- α mediated cellular immunity for tumor therapy by C60 (OH) 20 nanoparticles. *Nanotechnology.* 20:415102.
- Lohmann, C., A. Muschaweckh, S. Kirschnek, L. Jennen, H. Wagner, and G. Häcker. 2009. Induction of tumor cell apoptosis or necrosis by conditional expression of cell death proteins: analysis of cell death pathways and in vitro immune stimulatory potential. *The Journal of Immunology.* 182:4538-4546.

- Lomer, M.C., R.P. Thompson, and J.J. Powell. 2002. Fine and ultrafine particles of the diet: influence on the mucosal immune response and association with Crohn's disease. *Proceedings of the Nutrition Society*. 61:123-130.
- Long, E.O., H.S. Kim, D. Liu, M.E. Peterson, and S. Rajagopalan. 2013. Controlling NK cell responses: integration of signals for activation and inhibition. *Annual review of immunology*. 31.
- Lopez-Castejon, G., and D. Brough. 2011. Understanding the mechanism of IL-1 β secretion. *Cytokine & growth factor reviews*. 22:189-195.
- Love, P.E., and S.M. Hayes. 2010. ITAM-mediated signaling by the T-cell antigen receptor. *Cold Spring Harbor perspectives in biology*. 2:a002485.
- Lu, X., J.C. Qian, H.J. Zhou, Q. Gan, W. Tang, J.X. Lu, Y. Yuan, and C.S. Liu. 2011. In vitro cytotoxicity and induction of apoptosis by silica nanoparticles in human HepG2 hepatoma cells. *International Journal of Nanomedicine*. 6:1889-1901.
- Macdonald, H., A. Hardcastle, R. Jugdaohsingh, D. Reid, and J. Powell. 2005. Dietary silicon intake is associated with bone mineral density in premenopausal women and postmenopausal women taking HRT. *In Journal of Bone and Mineral Research*. Vol. 20. AMER SOC BONE & MINERAL RES 2025 M ST, NW, STE 800, WASHINGTON, DC 20036-3309 USA. S393-S393.
- Macian, F. 2005. NFAT proteins: key regulators of T-cell development and function. *Nature Reviews Immunology*. 5:472-484.
- Macián, F., F. García-Cózar, S.-H. Im, H.F. Horton, M.C. Byrne, and A. Rao. 2002. Transcriptional mechanisms underlying lymphocyte tolerance. *Cell*. 109:719-731.
- Mackay, L.K., A. Braun, B.L. Macleod, N. Collins, C. Tebartz, S. Bedoui, F.R. Carbone, and T. Gebhardt. 2015. Cutting edge: CD69 interference with sphingosine-1-phosphate receptor function regulates peripheral T cell retention. *The Journal of Immunology*. 194:2059-2063.
- Malek, T.R., and I. Castro. 2010. Interleukin-2 receptor signaling: at the interface between tolerance and immunity. *Immunity*. 33:153-165.
- Malissen, B., C. Gregoire, M. Malissen, and R. Roncagalli. 2014. Integrative biology of T cell activation. *Nat Immunol*. 15:790-797.
- Malugin, A., H. Herd, and H. Ghandehari. 2011. Differential toxicity of amorphous silica nanoparticles toward phagocytic and epithelial cells. *Journal of Nanoparticle Research*. 13:5381-5396.
- Marzaioli, V., J.A. Aguilar-Pimentel, I. Weichenmeier, G. Luxenhofer, M. Wiemann, R. Landsiedel, W. Wohlleben, S. Eiden, M. Mempel, and H. Behrendt. 2014. Surface modifications of silica nanoparticles are crucial for their inert versus proinflammatory and immunomodulatory properties. *Int J Nanomed*. 9:2815-2832.
- Matsuzaki, H., S. Lee, N. Kumagai-Takei, S. Yamamoto, T. Hatayama, K. Yoshitome, H. Hayashi, M. Maeda, and T. Otsuki. 2016. Immunological Risks Caused by Fibrous and Particulate Substances. *ENVIRONMENTAL HEALTH*:211.
- Maurer, M., and E. Von Stebut. 2004. Macrophage inflammatory protein-1. *The international journal of biochemistry & cell biology*. 36:1882-1886.
- Mazurek, J.M., and M.D. Attfield. 2008. Silicosis mortality among young adults in the United States, 1968–2004. *American journal of industrial medicine*. 51:568-578.

- McCarthy, J., I. Inkielewicz-Stępniaak, J.J. Corbalan, and M.W. Radomski. 2012. Mechanisms of toxicity of amorphous silica nanoparticles on human lung submucosal cells in vitro: protective effects of Fisetin. *Chemical research in toxicology*. 25:2227-2235.
- McLeod, J.D., L.S. Walker, Y.I. Patel, G. Boulougouris, and D.M. Sansom. 1998. Activation of human T cells with superantigen (staphylococcal enterotoxin B) and CD28 confers resistance to apoptosis via CD95. *The Journal of Immunology*. 160:2072-2079.
- Meddahi-Pellé, A., A. Legrand, A. Marcellan, L. Louedec, D. Letourneur, and L. Leibler. 2014. Organ repair, hemostasis, and in vivo bonding of medical devices by aqueous solutions of nanoparticles. *Angewandte Chemie International Edition*. 53:6369-6373.
- Mellanby, R.J., D.C. Thomas, and J. Lamb. 2009. Role of regulatory T-cells in autoimmunity. *Clinical Science*. 116:639-649.
- Mendoza, A., J.A. Torres-Hernandez, J.G. Ault, J.H. Pedersen-Lane, D. Gao, and D.A. Lawrence. 2014. Silica nanoparticles induce oxidative stress and inflammation of human peripheral blood mononuclear cells. *Cell Stress and Chaperones*. 19:777-790.
- Menten, P., A. Wuyts, and J. Van Damme. 2002. Macrophage inflammatory protein-1. *Cytokine & growth factor reviews*. 13:455-481.
- Merget, R., T. Bauer, H. Küpper, S. Philippou, H. Bauer, R. Breitstadt, and T. Bruening. 2002. Health hazards due to the inhalation of amorphous silica. *Archives of Toxicology*. 75:625-634.
- Miao, E.A., J.V. Rajan, and A. Aderem. 2011. Caspase-1-induced pyroptotic cell death. *Immunological reviews*. 243:206-214.
- Miller, J.F. 2011. The golden anniversary of the thymus. *Nature Reviews Immunology*. 11:489-495.
- Mohamed, B.M., N.K. Verma, A. Prina-Mello, Y. Williams, A.M. Davies, G. Bakos, L. Tormey, C. Edwards, J. Hanrahan, and A. Salvati. 2011. Activation of stress-related signalling pathway in human cells upon SiO₂ nanoparticles exposure as an early indicator of cytotoxicity. *Journal of nanobiotechnology*. 9:1.
- Mosby. 2016. Mosby's Medical Dictionary. Elsevier Health Sciences.
- Mu, Q.S., N.S. Hondow, L. Krzeminski, A.P. Brown, L.J.C. Jeuken, and M.N. Routledge. 2012. Mechanism of cellular uptake of genotoxic silica nanoparticles. *Particle and Fibre Toxicology*. 9.
- Murray, P.J., and T.A. Wynn. 2011. Protective and pathogenic functions of macrophage subsets. *Nat Rev Immunol*. 11:723-737.
- Musić, S., N. Filipović-Vinceković, and L. Sekovanić. 2011. Precipitation of amorphous SiO₂ particles and their properties. *Brazilian Journal of Chemical Engineering*. 28:89-94.
- Nabeshi, H., T. Yoshikawa, K. Matsuyama, Y. Nakazato, S. Tochigi, S. Kondoh, T. Hirai, T. Akase, K. Nagano, and Y. Abe. 2011. Amorphous nanosilica induce endocytosis-dependent ROS generation and DNA damage in human keratinocytes. *Particle and Fibre Toxicology*. 8:1.
- Nancollas, G.H. 1979. The growth of crystals in solution. *Advances in Colloid and Interface Science*. 10:215-252.

- Napetschnig, J., and H. Wu. 2013. Molecular basis of NF- κ B signaling. *Annual review of biophysics*. 42:443.
- Napierska, D., L.C. Thomassen, V. Rabolli, D. Lison, L. Gonzalez, M. Kirsch-Volders, J.A. Martens, and P.H. Hoet. 2009. Size-Dependent Cytotoxicity of Monodisperse Silica Nanoparticles in Human Endothelial Cells. *Small*. 5:846-853.
- Nauseef, W.M. 2014. Myeloperoxidase in human neutrophil host defence. *Cellular microbiology*. 16:1146-1155.
- Neefjes, J., M.L. Jongsma, P. Paul, and O. Bakke. 2011. Towards a systems understanding of MHC class I and MHC class II antigen presentation. *Nature Reviews Immunology*. 11:823-836.
- Netea, M.G., A. Simon, F. van de Veerdonk, B.-J. Kullberg, J.W. Van der Meer, and L.A. Joosten. 2010. IL-1 β processing in host defense: beyond the inflammasomes. *PLoS Pathog*. 6:e1000661.
- Nichols, G., S. Byard, M.J. Bloxham, J. Botterill, N.J. Dawson, A. Dennis, V. Diart, N.C. North, and J.D. Sherwood. 2002. A review of the terms agglomerate and aggregate with a recommendation for nomenclature used in powder and particle characterization. *Journal of pharmaceutical sciences*. 91:2103-2109.
- Nielsen, F.H. 1998. Ultratrace elements in nutrition: Current knowledge and speculation. *Journal of Trace Elements in Experimental Medicine*. 11:251-274.
- Norian, L.A., K.M. Latinis, S.L. Eliason, K. Lyson, C. Yang, T. Ratliff, and G.A. Koretzky. 2000. The Regulation of CD95 (Fas) Ligand Expression in Primary T Cells: Induction of Promoter Activation in CD95LP-Luc Transgenic Mice. *The Journal of Immunology*. 164:4471-4480.
- Nutt, S.L., P.D. Hodgkin, D.M. Tarlinton, and L.M. Corcoran. 2015. The generation of antibody-secreting plasma cells. *Nature Reviews Immunology*. 15:160-171.
- Oeckinghaus, A., M.S. Hayden, and S. Ghosh. 2011. Crosstalk in NF- κ B signaling pathways. *Nat Immunol*. 12:695-708.
- Ohashi, P.S. 2002. T-cell signalling and autoimmunity: molecular mechanisms of disease. *Nature Reviews Immunology*. 2:427-438.
- Olkowska-Truchanowicz, J., K. Bocian, R.B. Maksym, A. Białoszewska, D. Włodarczyk, W. Baranowski, J. Ząbek, G. Korczak-Kowalska, and J. Malejczyk. 2013. CD4+ CD25+ FOXP3+ regulatory T cells in peripheral blood and peritoneal fluid of patients with endometriosis. *Human Reproduction*. 28:119-124.
- Otsuki, T., Y. Miura, Y. Nishimura, F. Hyodoh, A. Takata, M. Kusaka, H. Katsuyama, M. Tomita, A. Ueki, and T. Kishimoto. 2006. Alterations of Fas and Fas-related molecules in patients with silicosis. *Experimental Biology and Medicine*. 231:522-533.
- Palmer, E. 2003. Negative selection—clearing out the bad apples from the T-cell repertoire. *Nature Reviews Immunology*. 3:383-391.
- Park, B.-k., Y.H. Park, and K.-s. Seo. 2000. Relation between lymphocyte subpopulations of peripheral blood and immune responses of modified live hog cholera virus vaccine in pigs treated with an ionized alkali mineral complex. *Journal of veterinary science*. 1:49-52.
- Park, E.-J., and K. Park. 2009. Oxidative stress and pro-inflammatory responses induced by silica nanoparticles in vivo and in vitro. *Toxicology letters*. 184:18-25.

- Park, M.V., I. Lynch, S. Ramírez-García, K.A. Dawson, L. de la Fonteyne, E. Gremmer, W. Slob, J.J. Briedé, A. Elsaesser, and C.V. Howard. 2011. In vitro evaluation of cytotoxic and inflammatory properties of silica nanoparticles of different sizes in murine RAW 264.7 macrophages. *Journal of Nanoparticle Research*. 13:6775-6787.
- Park, Y.-H., H.C. Bae, Y. Jang, S.H. Jeong, H.N. Lee, W.-I. Ryu, M.G. Yoo, Y.-R. Kim, M.-K. Kim, and J.K. Lee. 2013. Effect of the size and surface charge of silica nanoparticles on cutaneous toxicity. *Molecular & Cellular Toxicology*. 9:67-74.
- Parks, W.C., C.L. Wilson, and Y.S. López-Boado. 2004. Matrix metalloproteinases as modulators of inflammation and innate immunity. *Nature Reviews Immunology*. 4:617-629.
- Patiño-Lopez, G., P. Hevezi, J. Lee, D. Willhite, G.M. Verge, S.M. Lechner, V. Ortiz-Navarrete, and A. Zlotnik. 2006. Human class-I restricted T cell associated molecule is highly expressed in the cerebellum and is a marker for activated NKT and CD8+ T lymphocytes. *Journal of neuroimmunology*. 171:145-155.
- Paulsen, M., and O. Janssen. 2011. Pro- and anti-apoptotic CD95 signaling in T cells. *Cell Communication and Signaling*. 9:7.
- Pennock, N.D., J.T. White, E.W. Cross, E.E. Cheney, B.A. Tamburini, and R.M. Kedl. 2013. T cell responses: naïve to memory and everything in between. *Advances in Physiology Education*. 37:273-283.
- Pereira, D.I., B. Lederer, and J.J. Powell. 2015. A balanced salt solution that prevents agglomeration of nano iron oxo-hydroxides in serum-free cellular assays. *Materials Research Express*. 2:015403.
- Pernis, B. 2004. Silica and the immune system. *Acta Bio-Medica: Atenei Parmensis*. 76:38-44.
- Pernis, B., and E.C. Vigliani. 1960. Recenti acquisizioni sulla patogenesi della silicosi. Università di Milano.
- Petrarca, C., A. Perrone, N. Verna, F. Verginelli, J. Ponti, E. Sabbioni, L. Di Giampaolo, V. Dadorante, C. Schiavone, and P. Boscolo. 2005. Cobalt nano-particles modulate cytokine in vitro release by human mononuclear cells mimicking autoimmune disease. *International journal of immunopathology and pharmacology*. 19:11-14.
- Pfau, J.C., J.M. Brown, and A. Holian. 2004. Silica-exposed mice generate autoantibodies to apoptotic cells. *Toxicology*. 195:167-176.
- Poon, I.K.H., M.D. Hulett, and C.R. Parish. 2010. Molecular mechanisms of late apoptotic/necrotic cell clearance. *Cell Death & Differentiation*. 17:381-397.
- Porter, A.E., N. Patel, J.N. Skepper, S.M. Best, and W. Bonfield. 2004. Effect of sintered silicate-substituted hydroxyapatite on remodelling processes at the bone-implant interface. *Biomaterials*. 25:3303-3314.
- Powell, J.J., S.F.A. Bruggraber, N.J.R. Faria, and D.I.A. Pereira. 2008. Ligand modified poly oxo-hydroxy metal ion materials, their uses and processes for their preparation. Google Patents.
- Powell, J.J., N. Faria, E. Thomas-McKay, and L.C. Pele. 2010. Origin and fate of dietary nanoparticles and microparticles in the gastrointestinal tract. *Journal of autoimmunity*. 34:J226-J233.

- Radonski, M., and C. Medina-Martin. 2011. Amorphous silica nanoparticles trigger nitric oxide/peroxynitrite imbalance in human endothelial cells inflammatory and cytotoxicity effects.
- Radulovic, K., V. Rossini, C. Manta, K. Holzmann, H.A. Kestler, and J.H. Niess. 2013. The early activation marker CD69 regulates the expression of chemokines and CD4 T cell accumulation in intestine. *PLoS one*. 8:e65413.
- Ramesh, N., A. Horner, D. Ahern, and R.S. Geha. 1995. Bacterial superantigens induce the proliferation of resting γ/δ receptor bearing T cells. *Immunological investigations*. 24:713-724.
- Ratcliffe, S., R. Jugdaohsingh, J. Vivancos, A. Marron, R. Deshmukh, J.F. Ma, N. Mitani-Ueno, J. Robertson, J. Wills, M.V. Boekschoten, M. Müller, R.C. Mawhinney, S.D. Kinrade, P. Isenring, R.R. Bélanger, and J.J. Powell. 2017. Identification of a Mammalian Silicon Transporter. *American Journal of Physiology - Cell Physiology*.
- Reddy, M., E. Eirikis, C. Davis, H.M. Davis, and U. Prabhakar. 2004. Comparative analysis of lymphocyte activation marker expression and cytokine secretion profile in stimulated human peripheral blood mononuclear cell cultures: an in vitro model to monitor cellular immune function. *Journal of immunological methods*. 293:127-142.
- Reffitt, D.M., N. Ogston, R. Jugdaohsingh, H.F.J. Cheung, B.A.J. Evans, R.P.H. Thompson, J.J. Powell, and G.N. Hampson. 2003. Orthosilicic acid stimulates collagen type 1 synthesis and osteoblastic differentiation in human osteoblast-like cells in vitro. *Bone*. 32:127-135.
- Rieger, H., and M. Welter. 2015. Integrative models of vascular remodeling during tumor growth. *Wiley Interdisciplinary Reviews. Systems Biology and Medicine*. 7:113-129.
- Rimstidt, J.D. 1997. Quartz solubility at low temperatures. *Geochimica et Cosmochimica Acta*. 61:2553-2558.
- Roche, P.A., and K. Furuta. 2015. The ins and outs of MHC class II-mediated antigen processing and presentation. *Nature Reviews Immunology*. 15:203-216.
- Rock, K.L., J.J. Lai, and H. Kono. 2011. Innate and adaptive immune responses to cell death. *Immunological reviews*. 243:191-205.
- Rondeau, V., D. Commenges, H. Jacqmin-Gadda, and J.-F. Dartigues. 2000. Relation between aluminum concentrations in drinking water and Alzheimer's disease: an 8-year follow-up study. *American journal of epidemiology*. 152:59-66.
- Rondeau, V., H. Jacqmin-Gadda, D. Commenges, and J.-F. Dartigues. 2001. Re: aluminum in drinking water and cognitive decline in elderly subjects: the Paquid cohort. *American journal of epidemiology*. 154:288-290.
- Rust, C., and F. Koning. 1993. γ/δ T cell reactivity towards bacterial superantigens. *In Seminars in immunology*. Vol. 5. Elsevier. 41-46.
- Safi, M., J. Courtois, M. Seigneuret, H. Conjeaud, and J.-F. Berret. 2011. The effects of aggregation and protein corona on the cellular internalization of iron oxide nanoparticles. *Biomaterials*. 32:9353-9363.
- Saha, A., and E.S. Robertson. 2011. Epstein-Barr Virus–Associated B-cell Lymphomas: Pathogenesis and Clinical Outcomes. *Clinical Cancer Research*. 17:3056-3063.
- Sahoo, A., S. Wali, and R. Nurieva. 2016. T helper 2 and T follicular helper cells: Regulation and function of interleukin-4. *Cytokine & growth factor reviews*. 30:29-37.

- Sakaguchi, S., M. Miyara, C.M. Costantino, and D.A. Hafler. 2010. FOXP3+ regulatory T cells in the human immune system. *Nature Reviews Immunology*. 10:490-500.
- Sancho, D., M.a. Yáñez-Mó, R. Tejedor, and F. Sánchez-Madrid. 1999. Activation of peripheral blood T cells by interaction and migration through endothelium: role of lymphocyte function antigen-1/intercellular adhesion molecule-1 and interleukin-15. *Blood*. 93:886-896.
- Sandberg, W.J., M. Låg, J.A. Holme, B. Friede, M. Gualtieri, M. Kruszewski, P.E. Schwarze, T. Skuland, and M. Refsnes. 2012. Comparison of non-crystalline silica nanoparticles in IL-1 β release from macrophages. *Particle and fibre toxicology*. 9:1.
- Sandberg, Y., B. Verhaaf, E. van Gastel-Mol, I. Wolvers-Tettero, J. de Vos, R. MacLeod, J. Noordzij, W. Dik, J. van Dongen, and A. Langerak. 2007. Human T-cell lines with well-defined T-cell receptor gene rearrangements as controls for the BIOMED-2 multiplex polymerase chain reaction tubes. *Leukemia*. 21:230-237.
- Sapir, T., and Y. Shoenfeld. 2005. Uncovering the hidden potential of intravenous immunoglobulin as an anticancer therapy. *Clinical reviews in allergy & immunology*. 29:307-310.
- Satpathy, S.R., V.R. Jala, S.R. Bodduluri, E. Krishnan, B. Hegde, G.W. Hoyle, M. Fraig, A.D. Luster, and B. Haribabu. 2015. Crystalline silica-induced leukotriene B4-dependent inflammation promotes lung tumour growth. *Nature communications*. 6.
- Scaramuzzi, K., G.D. Tanaka, F.M. Neto, P.R.A.F. Garcia, J.J.M. Gabrili, D.C.A. Oliveira, D.V. Tambourgi, J.S. Mussalem, D. Paixão-Cavalcante, M.T. D'Azeredo Orlando, V.F. Botosso, C.L.P. Oliveira, M.C.A. Fantini, and O.A. Sant'Anna. 2016. Nanostructured SBA-15 silica: An effective protective vehicle to oral hepatitis B vaccine immunization. *Nanomedicine: Nanotechnology, Biology and Medicine*. 12:2241-2250.
- Schroder, K., P.J. Hertzog, T. Ravasi, and D.A. Hume. 2004. Interferon- γ : an overview of signals, mechanisms and functions. *Journal of leukocyte biology*. 75:163-189.
- Schwartz, R.H. 2003. T cell anergy*. *Annual review of immunology*. 21:305-334.
- Schwartzberg, P.L., K.L. Mueller, H. Qi, and J.L. Cannons. 2009. SLAM receptors and SAP influence lymphocyte interactions, development and function. *Nature Reviews Immunology*. 9:39-46.
- Sckisel, G.D., M.N. Bouchlaka, A.M. Monjazeb, M. Crittenden, B.D. Curti, D.E. Wilkins, K.A. Alderson, C.M. Sungur, E. Ames, and A. Mirsoian. 2015. Out-of-Sequence Signal 3 Paralyzes Primary CD4+ T-Cell-Dependent Immunity. *Immunity*. 43:240-250.
- Serra, P., and P. Santamaria. 2015. Nanoparticle-based autoimmune disease therapy. *Clinical Immunology*. 160:3-13.
- Shatrova, A., E. Mityushova, N. Aksenov, and I. Marakhova. 2015. CD25 expression on the surface of Jurkat cells. *Cell and Tissue Biology*. 9:364-370.
- Silva-Filho, J., C. Caruso-Neves, and A. Pinheiro. 2014. IL-4: an important cytokine in determining the fate of T cells. *Biophysical Reviews*. 6:111-118.
- Silva-Santos, B., K. Serre, and H. Norell. 2015. [gamma][delta] T cells in cancer. *Nature Reviews Immunology*.
- Skrastina, D., I. Petrovskis, I. Lieknina, J. Bogans, R. Renhofa, V. Ose, A. Dishlers, Y. Dekhtyar, and P. Pumpens. 2014. Silica nanoparticles as the adjuvant for the immunisation of mice using hepatitis B core virus-like particles. *PLoS one*. 9:e114006.

- Smith-Garvin, J.E., G.A. Koretzky, and M.S. Jordan. 2009. T cell activation. *Annual review of immunology*. 27:591.
- Solan, J.L., M.D. Fry, E.M. TenBroek, and P.D. Lampe. 2003. Connexin43 phosphorylation at S368 is acute during S and G2/M and in response to protein kinase C activation. *Journal of cell science*. 116:2203-2211.
- Sommer, M., D. Kaczorek, Y. Kuzyakov, and J. Breuer. 2006. Silicon pools and fluxes in soils and landscapes - a review. *Journal of Plant Nutrition and Soil Science-Zeitschrift Fur Pflanzenernahrung Und Bodenkunde*. 169:310-329.
- Spector, T.D., M.R. Calomme, S.H. Anderson, G. Clement, L. Bevan, N. Demeester, R. Swaminathan, R. Jugdaohsingh, D.A. Berghe, and J.J. Powell. 2008. Choline-stabilized orthosilicic acid supplementation as an adjunct to calcium/vitamin D3 stimulates markers of bone formation in osteopenic females: a randomized, placebo-controlled trial. *BMC Musculoskeletal Disorders*. 9:85.
- Sprangers, S., T.J.d. Vries, and V. Everts. 2016. Monocyte Heterogeneity: Consequences for Monocyte-Derived Immune Cells. *Journal of Immunology Research*. 2016.
- Sprent, J., Z. Cai, A. Brunmark, M.R. Jackson, and P.A. Peterson. 1997. Constructing Artificial Antigen-Presenting Cells from Drosophila Cells. *In Dendritic Cells in Fundamental and Clinical Immunology: Volume 3*. P. Ricciardi-Castagnoli, editor. Springer US, Boston, MA. 249-254.
- Sripanyakorn, S., R. Jugdaohsingh, W. Dissayabutr, S.H. Anderson, R.P. Thompson, and J.J. Powell. 2009. The comparative absorption of silicon from different foods and food supplements. *British journal of nutrition*. 102:825-834.
- Stavnezer, J. 1996. Antibody class switching. *Advances in immunology*. 61:79-146.
- Steeg, P.S. 2016. Targeting metastasis. *Nat Rev Cancer*. 16:201-218.
- Stinchcombe, J.C., and G.M. Griffiths. 2007. Secretory mechanisms in cell-mediated cytotoxicity. *Annu. Rev. Cell Dev. Biol*. 23:495-517.
- Stöber, W., A. Fink, and E. Bohn. 1968. Controlled growth of monodisperse silica spheres in the micron size range. *Journal of colloid and interface science*. 26:62-69.
- Stockis, J., D. Colau, P.G. Coulie, and S. Lucas. 2009. Membrane protein GARP is a receptor for latent TGF- β on the surface of activated human Treg. *European journal of immunology*. 39:3315-3322.
- Stumm, W., and J.J. Morgan. 1981. Aquatic chemistry. An introduction emphasizing chemical equilibria in natural waters. John Wiley & Sons, New York.
- Sun, Z.-Y.J., S.T. Kim, I.C. Kim, A. Fahmy, E.L. Reinherz, and G. Wagner. 2004. Solution structure of the CD3 $\epsilon\delta$ ectodomain and comparison with CD3 $\epsilon\gamma$ as a basis for modeling T cell receptor topology and signaling. *Proceedings of the National Academy of Sciences of the United States of America*. 101:16867-16872.
- Suntharalingam, G., M.R. Perry, S. Ward, S.J. Brett, A. Castello-Cortes, M.D. Brunner, and N. Panoskaltsis. 2006. Cytokine storm in a phase 1 trial of the anti-CD28 monoclonal antibody TGN1412. *New England Journal of Medicine*. 355:1018-1028.
- Tavare, A.N., N.J.S. Perry, L.L. Benzonana, M. Takata, and D. Ma. 2012. Cancer recurrence after surgery: Direct and indirect effects of anesthetic agents*. *International Journal of Cancer*. 130:1237-1250.

- Taylor, P.D., R. Jugdaohsingh, and J.J. Powell. 1997. Soluble silica with high affinity for aluminum under physiological and natural conditions. *Journal of the American Chemical Society*. 119:8852-8856.
- Terman, D.S., A. Serier, O. Dauwalder, C. Badiou, A. Dutour, D. Thomas, V. Brun, J. Biennu, J. Etienne, and F. Vandenesch. 2013. Staphylococcal enterotoxins of the enterotoxin gene cluster (egcSEs) induce nitric oxide- and cytokine dependent tumor cell apoptosis in a broad panel of human tumor cells. *Frontiers in cellular and infection microbiology*. 3.
- Thäle, C., and A.F. Kiderlen. 2005. Sources of interferon-gamma (IFN- γ) in early immune response to *Listeria monocytogenes*. *Immunobiology*. 210:673-683.
- Tourdot, S., and K.G. Gould. 2002. Competition between MHC class I alleles for cell surface expression alters CTL responses to influenza A virus. *The Journal of Immunology*. 169:5615-5621.
- Trickett, A., and Y.L. Kwan. 2003. T cell stimulation and expansion using anti-CD3/CD28 beads. *Journal of Immunological Methods*. 275:251-255.
- Tscharke, D.C., N.P. Croft, P.C. Doherty, and N.L. La Gruta. 2015. Sizing up the key determinants of the CD8+ T cell response. *Nat Rev Immunol*. 15:705-716.
- Tummers, B., and D.R. Green. 2017. Caspase-8: regulating life and death. *Immunological Reviews*. 277:76-89.
- Turvey, S.E., and D.H. Broide. 2010. Innate immunity. *Journal of Allergy and Clinical Immunology*. 125:S24-S32.
- Ueki, A., M. Yamaguchi, H. Ueki, Y. Watanabe, G. Ohsawa, K. Kinugawa, Y. Kawakami, and F. Hyodoh. 1994. Polyclonal human T-cell activation by silicate in vitro. *Immunology*. 82:332.
- Valmori, D., A. Merlo, N.E. Souleimanian, C.S. Hesdorffer, and M. Ayyoub. 2005. A peripheral circulating compartment of natural naive CD4(+) Tregs. *Journal of Clinical Investigation*. 115:1953-1962.
- Van Belle, K., J. Herman, L. Boon, M. Waer, B. Sprangers, and T. Louat. 2016. Comparative In Vitro Immune Stimulation Analysis of Primary Human B Cells and B Cell Lines. *Journal of immunology research*. 2016.
- Vantourout, P., and A. Hayday. 2013. Six-of-the-best: unique contributions of $\gamma\delta$ T cells to immunology. *Nature Reviews Immunology*. 13:88-100.
- Vivier, E., E. Tomasello, M. Baratin, T. Walzer, and S. Ugolini. 2008. Functions of natural killer cells. *Nature immunology*. 9:503-510.
- Vivier, E., S. Ugolini, D. Blaise, C. Chabannon, and L. Brossay. 2012. Targeting natural killer cells and natural killer T cells in cancer. *Nature Reviews Immunology*. 12:239-252.
- Voskoboinik, I., J.C. Whisstock, and J.A. Trapani. 2015. Perforin and granzymes: function, dysfunction and human pathology. *Nat Rev Immunol*. 15:388-400.
- Walker, L.S.K., and D.M. Sansom. 2015. Confusing signals: Recent progress in CTLA-4 biology. *Trends in Immunology*. 36:63-70.
- Wang, B., R. Maile, R. Greenwood, E.J. Collins, and J.A. Frelinger. 2000. Naive CD8+ T cells do not require costimulation for proliferation and differentiation into cytotoxic effector cells. *The Journal of Immunology*. 164:1216-1222.

- Wang, F., F. Gao, M. Lan, H. Yuan, Y. Huang, and J. Liu. 2009a. Oxidative stress contributes to silica nanoparticle-induced cytotoxicity in human embryonic kidney cells. *Toxicology in Vitro*. 23:808-815.
- Wang, X., X. Li, K. Yoshiyuki, Y. Watanabe, Y. Sogo, T. Ohno, N.M. Tsuji, and A. Ito. 2016. Comprehensive Mechanism Analysis of Mesoporous-Silica-Nanoparticle-Induced Cancer Immunotherapy. *Advanced healthcare materials*. 5:1169-1176.
- Wang, Y., D. Becker, T. Vass, J. White, P. Marrack, and J.W. Kappler. 2009b. A conserved CXXC motif in CD3 ϵ is critical for T cell development and TCR signaling. *PLoS Biol*. 7:e1000253.
- Warren, R.L., J.D. Freeman, T. Zeng, G. Choe, S. Munro, R. Moore, J.R. Webb, and R.A. Holt. 2011. Exhaustive T-cell repertoire sequencing of human peripheral blood samples reveals signatures of antigen selection and a directly measured repertoire size of at least 1 million clonotypes. *Genome research*. 21:790-797.
- Waters, K.M., L.M. Masiello, R.C. Zangar, B.J. Tarasevich, N.J. Karin, R.D. Quesenberry, S. Bandyopadhyay, J.G. Teeguarden, J.G. Pounds, and B.D. Thrall. 2009. Macrophage responses to silica nanoparticles are highly conserved across particle sizes. *Toxicological Sciences*. 107:553-569.
- Watson, A.R., and W.T. Lee. 2006. Defective T cell receptor-mediated signal transduction in memory CD4 T lymphocytes exposed to superantigen or anti-T cell receptor antibodies. *Cellular immunology*. 242:80-90.
- Wells, A.D. 2009. New insights into the molecular basis of T cell anergy: anergy factors, avoidance sensors, and epigenetic imprinting. *The Journal of Immunology*. 182:7331-7341.
- Wesley, J.D., M.S. Tessmer, D. Chaukos, and L. Brossay. 2008. NK cell-like behavior of V α 14i NK T cells during MCMV infection. *PLoS Pathog*. 4:e1000106.
- White, K.N., A.I. Ejim, R.C. Walton, A.P. Brown, R. Jugdaohsingh, J.J. Powell, and C.R. McCrohan. 2008. Avoidance of aluminum toxicity in freshwater snails involves intracellular silicon–aluminum biointeraction. *Environmental science & technology*. 42:2189-2194.
- Wiest, D.L. 2016. Development of $\gamma\delta$ T Cells, the Special-Force Soldiers of the Immune System. In *T-Cell Development: Methods and Protocols*. R. Bosselut and M. S. Vacchio, editors. Springer New York, New York, NY. 23-32.
- Wikenheiser, D.J., and J.S. Stumhofer. 2016. ICOS Co-Stimulation: Friend or Foe? *Frontiers in Immunology*. 7.
- Winkles, J.A. 2008. The TWEAK–Fn14 cytokine–receptor axis: discovery, biology and therapeutic targeting. *Nature reviews Drug discovery*. 7:411-425.
- Winter, M. 2012. WebElements. Vol. 2012. WebElement Ltd. UK.
- Wooldridge, L., M. Clement, A. Lissina, E.S.J. Edwards, K. Ladell, J. Ekeruche, R.E. Hewitt, B. Laugel, E. Gostick, D.K. Cole, R. Debets, C. Berrevoets, J.J. Miles, S.R. Burrows, D.A. Price, and A.K. Sewell. 2010. Major histocompatibility complex class I molecules with super-enhanced CD8 binding properties bypass the requirement for cognate TCR recognition and non-specifically activate cytotoxic T lymphocytes. *Journal of immunology (Baltimore, Md. : 1950)*. 184:3357-3366.
- Wottrich, R., S. Diabate, and H.F. Krug. 2004. Biological effects of ultrafine model particles in human macrophages and epithelial cells in mono- and co-culture. *International Journal of Hygiene and Environmental Health*. 207:353-361.

- Wright, A., and M. Lehmann. 1981. The structure of quartz at 25 and 590 C determined by neutron diffraction. *Journal of solid state chemistry*. 36:371-380.
- Wu, H., R.M. Gower, H. Wang, X.-Y. Dai Perrard, R. Ma, D.C. Bullard, A.R. Burns, A. Paul, C.W. Smith, and S.I. Simon. 2009. Functional role of CD11c+ monocytes in atherogenesis associated with hypercholesterolemia. *Circulation*. 119:2708-2717.
- Wu, P., F. Hyodoh, T. Hatayama, H. Sakaguchi, S. Hatada, Y. Miura, A. Takata-Tomokuni, H. Katsuyama, and T. Otsuki. 2005a. Induction of CD69 antigen expression in peripheral blood mononuclear cells on exposure to silica, but not by asbestos/chrysotile-A. *Immunology letters*. 98:145-152.
- Wu, P., Y. Miura, F. Hyodoh, Y. Nishimura, T. Hatayama, S. Hatada, H. Sakaguchi, M. Kusaka, H. Katsuyama, and M. Tomita. 2005b. Reduced function of CD4+ 25+ regulatory T cell fraction in silicosis patients. *International journal of immunopathology and pharmacology*. 19:357-368.
- Wu, Y.-L., Y.-P. Ding, Y. Tanaka, L.-W. Shen, C.-H. Wei, N. Minato, and W. Zhang. 2014. $\gamma\delta$ T cells and their potential for immunotherapy. *Int J Biol Sci*. 10:119-135.
- Xie, G., J. Sun, G. Zhong, L. Shi, and D. Zhang. 2010. Biodistribution and toxicity of intravenously administered silica nanoparticles in mice. *Archives of toxicology*. 84:183-190.
- Ye, Y., J. Liu, J. Xu, L. Sun, M. Chen, and M. Lan. 2010. Nano-SiO₂ induces apoptosis via activation of p53 and Bax mediated by oxidative stress in human hepatic cell line. *Toxicology in Vitro*. 24:751-758.
- Yong, P.F., U. Salzer, and B. Grimbacher. 2009. The role of costimulation in antibody deficiencies: ICOS and common variable immunodeficiency. *Immunological reviews*. 229:101-113.
- Yoo, B.W., S.I. Choi, S.H. Kim, S.J. Yang, H.C. Koo, S.H. Seo, B.K. Park, H.S. Yoo, and Y.H. Park. 2001. Immunostimulatory effects of anionic alkali mineral complex solution Barodon in porcine lymphocytes. *Journal of veterinary science*. 2:15-24.
- Young, I.T. 1972. The classification of white blood cells. *IEEE Transactions on Biomedical Engineering*:291-298.
- Yu, Y., Y. Li, W. Wang, M. Jin, Z. Du, Y. Li, J. Duan, Y. Yu, and Z. Sun. 2013. Acute toxicity of amorphous silica nanoparticles in intravenously exposed ICR mice. *PloS one*. 8:e61346.
- Yuseff, M.-I., P. Pierobon, A. Reversat, and A.-M. Lennon-Duménil. 2013. How B cells capture, process and present antigens: a crucial role for cell polarity. *Nature Reviews Immunology*. 13:475-486.
- Zhang, H., D.R. Dunphy, X. Jiang, H. Meng, B. Sun, D. Tarn, M. Xue, X. Wang, S. Lin, and Z. Ji. 2012. Processing pathway dependence of amorphous silica nanoparticle toxicity: colloidal vs pyrolytic. *Journal of the American Chemical Society*. 134:15790-15804.
- Zhang, M., X.-X. Fang, M.-E. Li, C.-H. Zheng, X.-H. Zhou, and X.-Q. Lyu. 2014. Handgrip exercise elevates basilic venous hemodynamic parameters in healthy subjects. *International Journal of Nursing Sciences*. 1:389-393.
- Zhen, A., S.R. Krutzik, B.R. Levin, S. Kasparian, J.A. Zack, and S.G. Kitchen. 2014. CD4 ligation on human blood monocytes triggers macrophage differentiation and enhances HIV infection. *Journal of virology*. 88:9934-9946.

Zheng, Y., Y. Zha, and T.F. Gajewski. 2008. Molecular regulation of T-cell anergy. *EMBO reports*. 9:50-55.

Zhu, J., and W.E. Paul. 2008. CD4 T cells: fates, functions, and faults. *Blood*. 112:1557-1569.

Zimmerman, B., B. Canono, and P. Campbell. 1986. Silica decreases phagocytosis and bactericidal activity of both macrophages and neutrophils in vitro. *Immunology*. 59:521.

Zou, W. 2005. Immunosuppressive networks in the tumour environment and their therapeutic relevance. *Nature Reviews Cancer*. 5:263-274.

Zwirner, N.W., and C.I. Domaica. 2010. Cytokine regulation of natural killer cell effector functions. *Biofactors*. 36:274-288.

Appendix 1 – Examples of gating strategies used in flow cytometry studies and integrations used in western blot studies

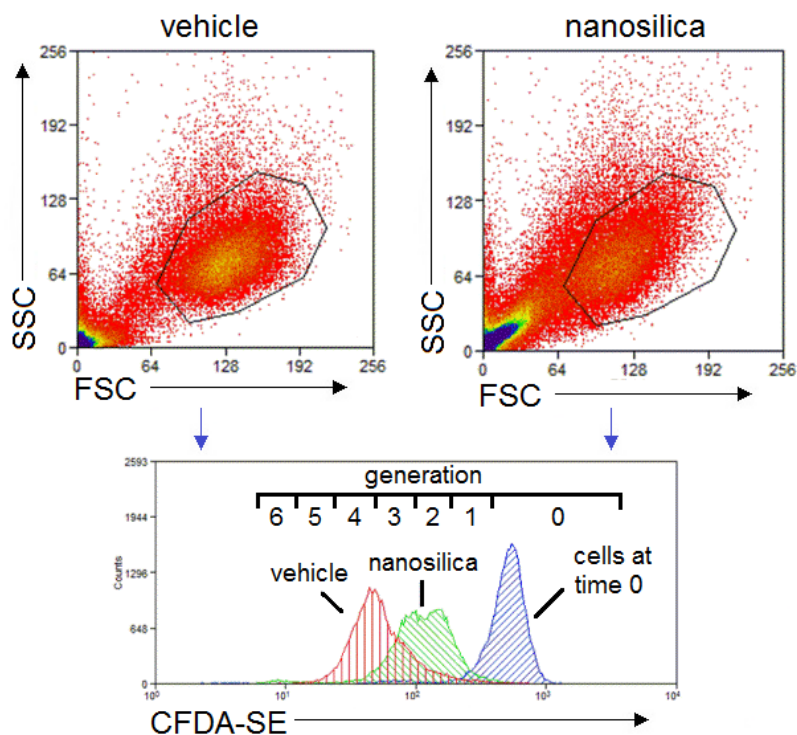


Figure 9.01. Gating strategy for the assessing transformed EBV B cell proliferation without a viability stain. EBV B cells were selected based on FSC versus SSC profiles which also excluded debris. Examples of cells at time 0 (blue) and those treated with vehicle (red) or nanosilica (green) and incubated for 48 h are shown. The generational gates were set according to the intensity mean of the CFSE stained cells fixed at experimental time 0 (generation 0) and gating in between the calculated mean intensities of each generation (the daughter generation has half the intensity of the parent generation)

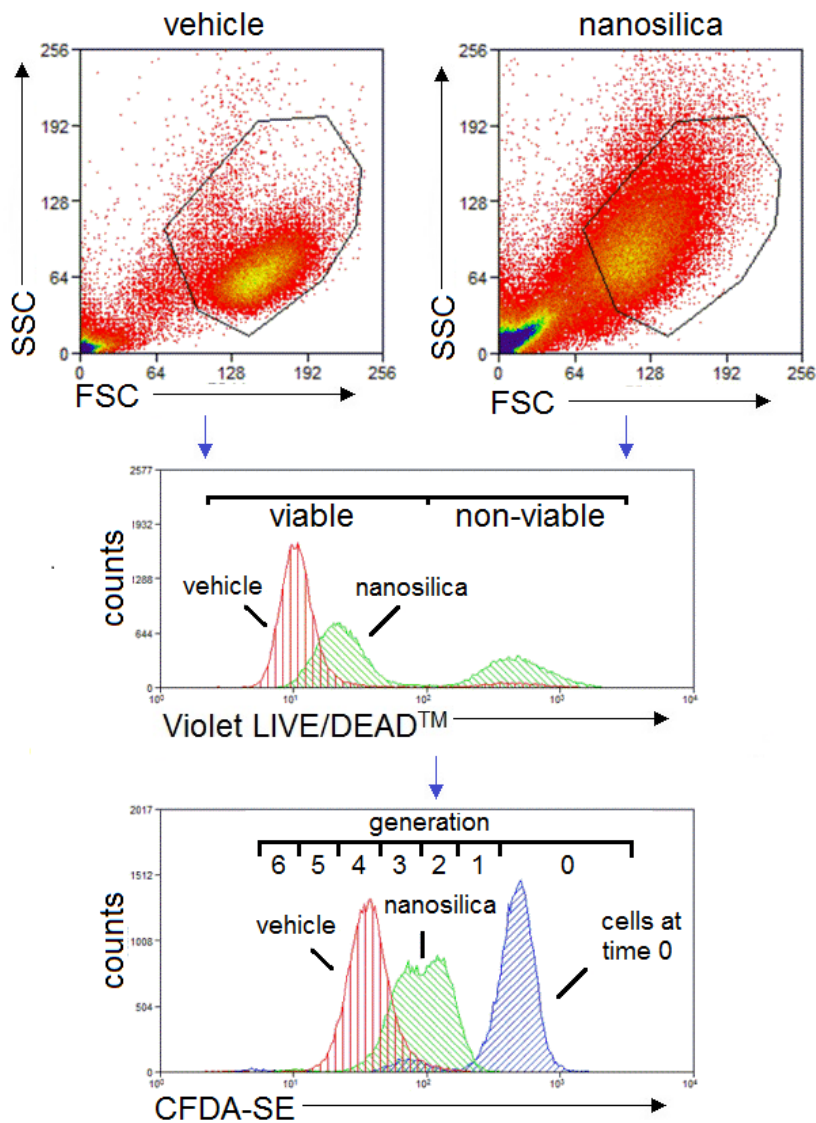


Figure 9.02. Gating strategy for the assessing transformed EBV B cell proliferation with a viability stain. EBV B cells were selected based on FSC versus SSC profiles which also excluded debris followed by a viability gate (Violet LIVE/DEAD^{low}). Examples of cells at time 0 (blue) and those treated with vehicle (red) or nanosilica (green) and incubated for 48 h are shown. The generational gates were set according to the intensity mean of the CFSE stained cells fixed at experimental time 0 (generation 0) and gating in between the calculated mean intensities of each generation (the daughter generation has half the intensity of the parent generation)

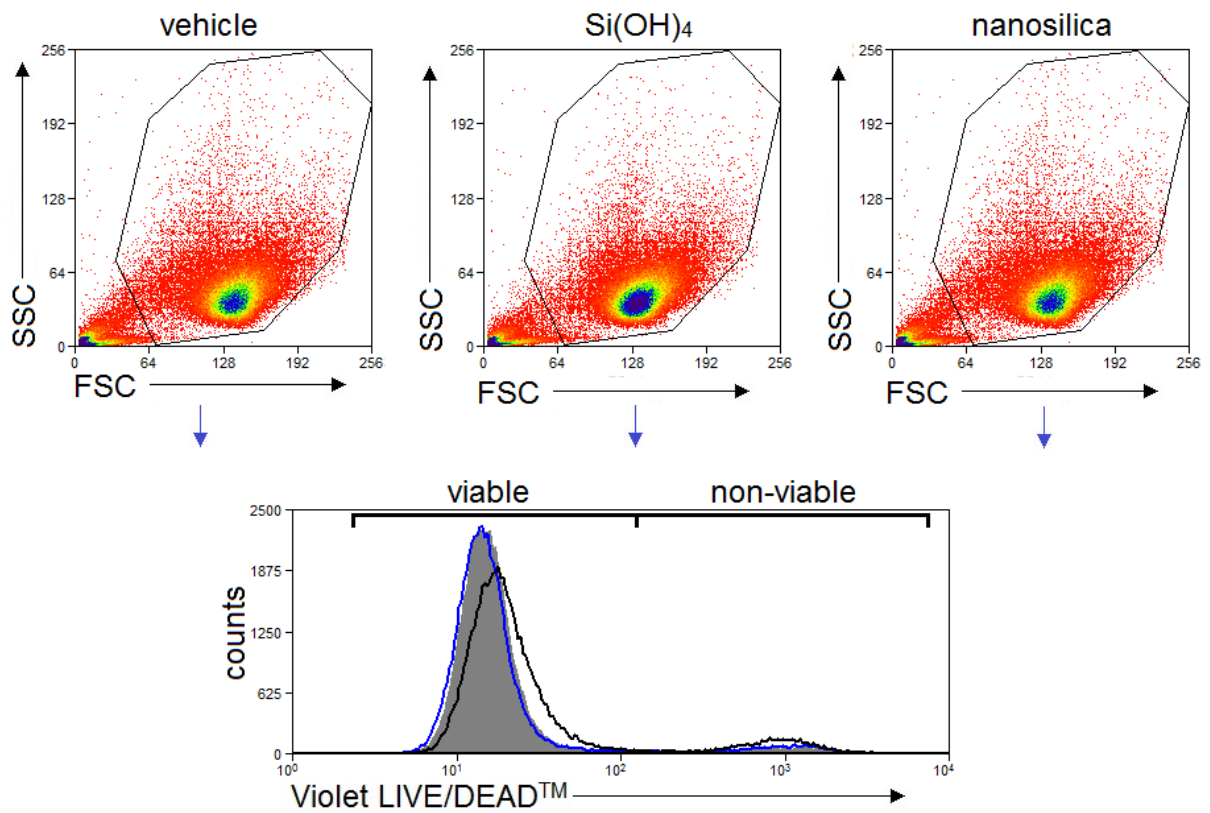


Figure 9.03. Gating strategy for assessing THP-1 viability. THP-1 cells were selected based on FSC versus SSC profiles which also excluded debris, and viability was assessed with a Violet LIVE/DEAD stain, where Violet LIVE/DEAD^{low} cells were considered viable. Examples of untreated (grey filled), Si(OH)₄ treated (blue) and nanosilica treated (black) cells are shown.

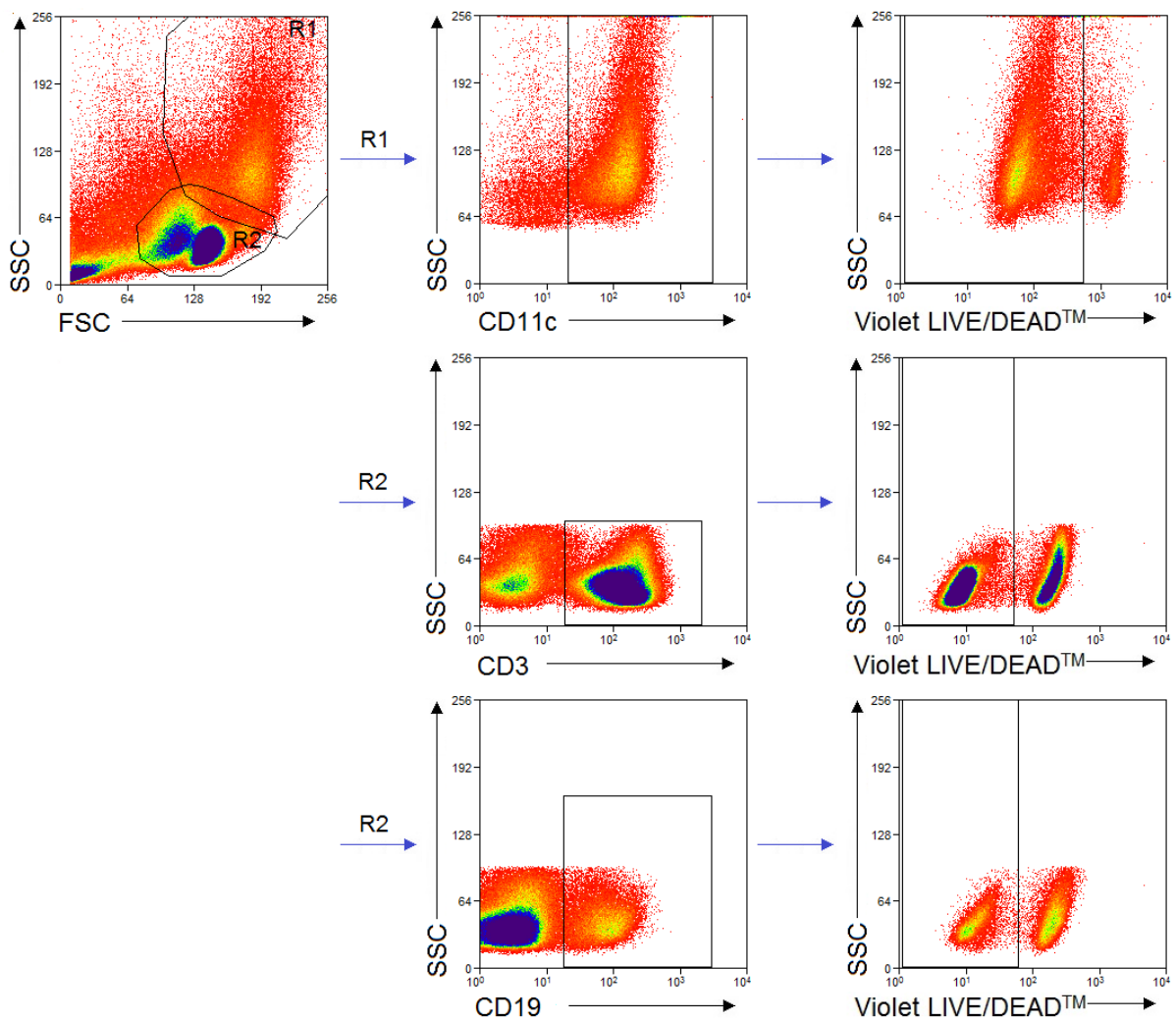


Figure 9.04. Gating strategy for assessing viability of monocytes (CD11c(+)), T cells (CD3(+)) and B cells (CD19(+)) in PBMC cultures. Monocytes were first selected based on FSC versus SSC profiles through a monocyte gate (R1) which also excluded debris, followed by a CD11c(+) gate. T cells and B cells were first selected based on FSC versus SSC profiles through a lymphocyte gate (R2) which also excluded debris, followed by CD3(+) and CD19(+) gate, respectively. Viability was assessed with a Violet LIVE/DEAD stain, where Violet LIVE/DEAD^{low} cells were considered viable.

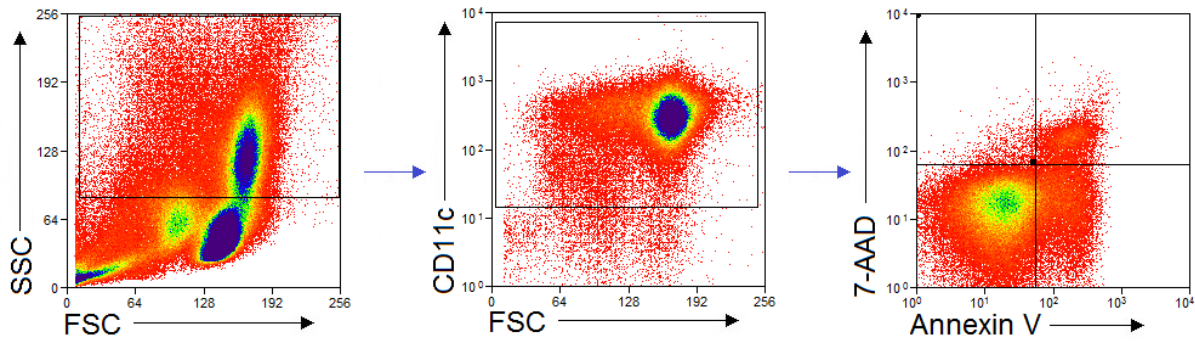


Figure 9.05. Gating strategy for assessing apoptosis and necrosis of monocytes (CD11c+) in PBMC cultures. Monocytes were first selected based on FSC versus SSC profiles through a monocyte gate which also excluded debris, followed by a CD11c(+) gate. Apoptosis and necrosis was assessed using a intracellular DNA stain (7-AAD) and a phosphatidylserine stain (Annexin V), where Annexin V(+)7-AAD(-) cells were considered apoptotic and Annexin V(+) 7-AAD(+) cells were considered necrotic.

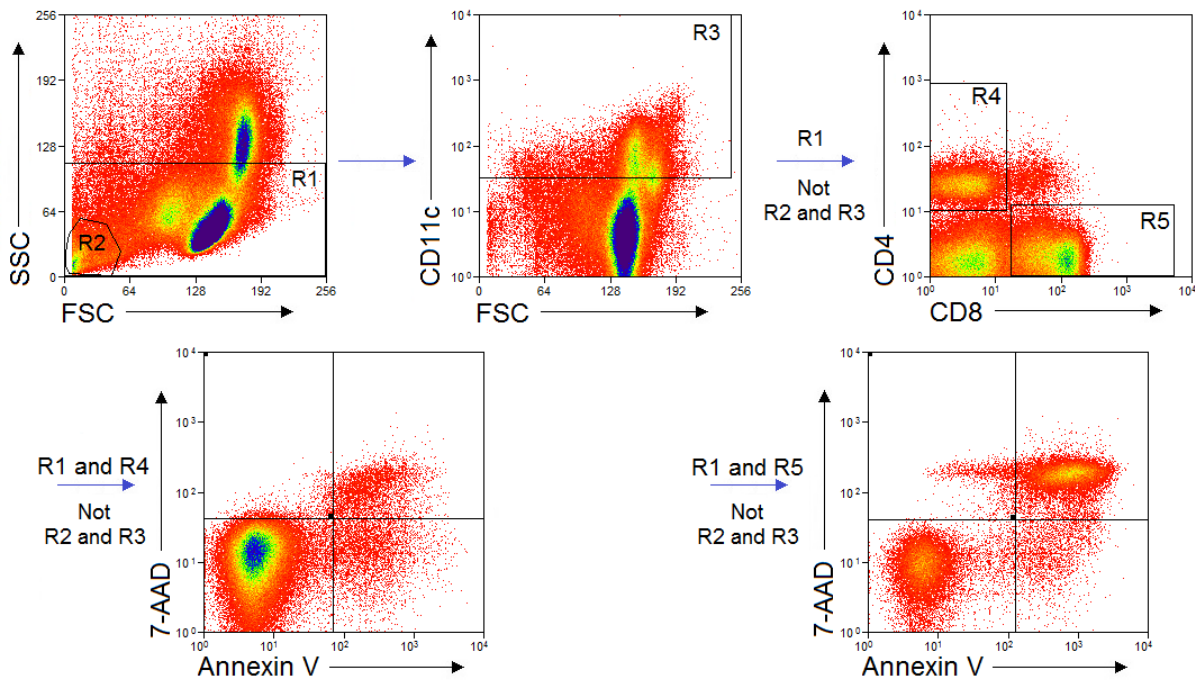


Figure 9.06. Gating strategy for assessing apoptosis and necrosis of CD4(+) and CD8(+) cells in PBMC cultures. T cells were first selected based on FSC versus SSC profiles through a lymphocyte gate (R1), followed by negatively gating out debris (R2) and monocytes (CD11c(+), R3). Helper and cytotoxic T cells were then selected with respective CD4(+) and CD8(+) gates. Apoptosis and necrosis was assessed using a intracellular DNA stain (7-AAD) and a phosphatidylserine stain (Annexin V), where Annexin V(+)7-AAD(-) were considered apoptotic and Annexin V(+)7-AAD(+) were considered necrotic. A TCR/CD3 stain was not included due to the inhibition of its staining by nanosilica from 0-2 h (Figure 4.10 and in Chapter 6).

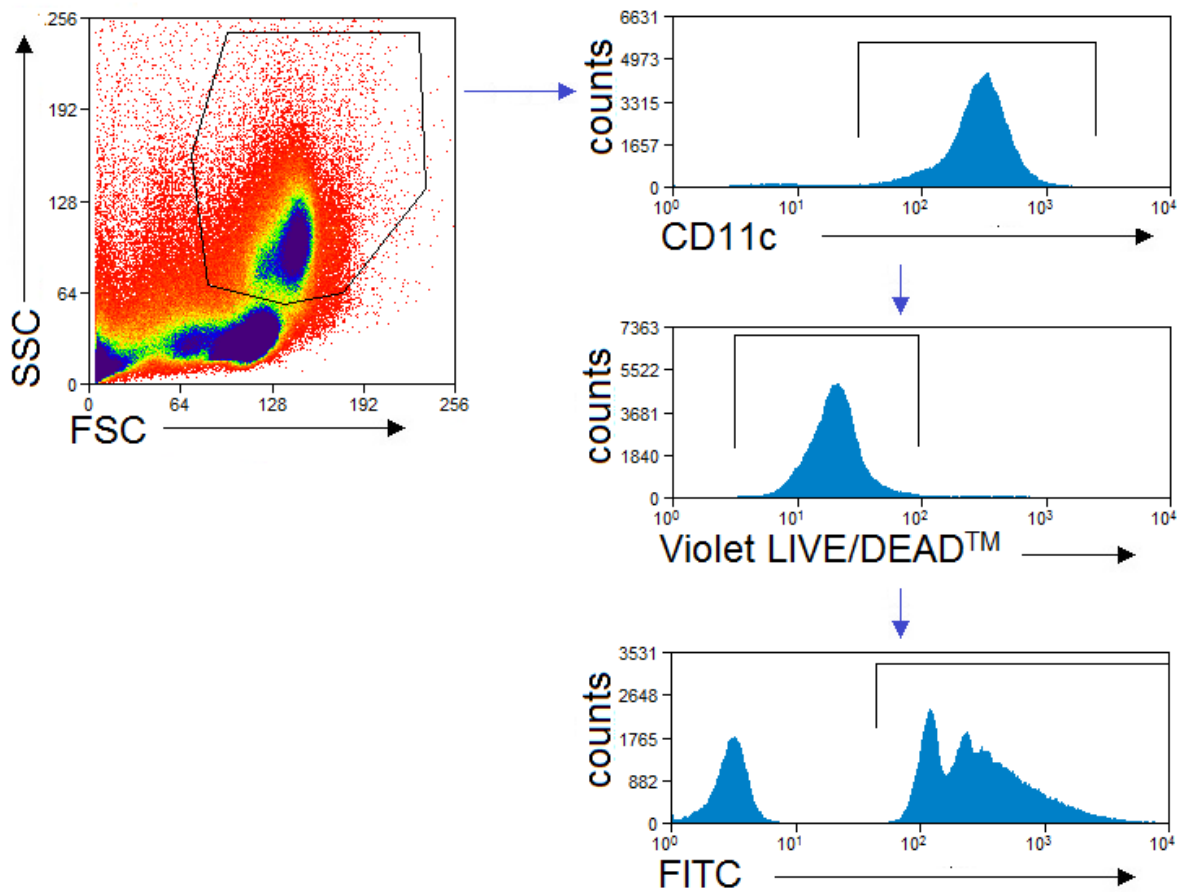


Figure 9.07. Gating strategy for assessing fluorescent bead and bacteria by monocytes in enriched monocyte cultures. Monocytes were first selected based on FSC versus SSC profiles through a monocyte gate, followed by a monocyte gate (CD11c(+)) and a viability gate (Violet LIVE/DEAD^{LOW}). Uptake was assessed with a FITC(+) gate.

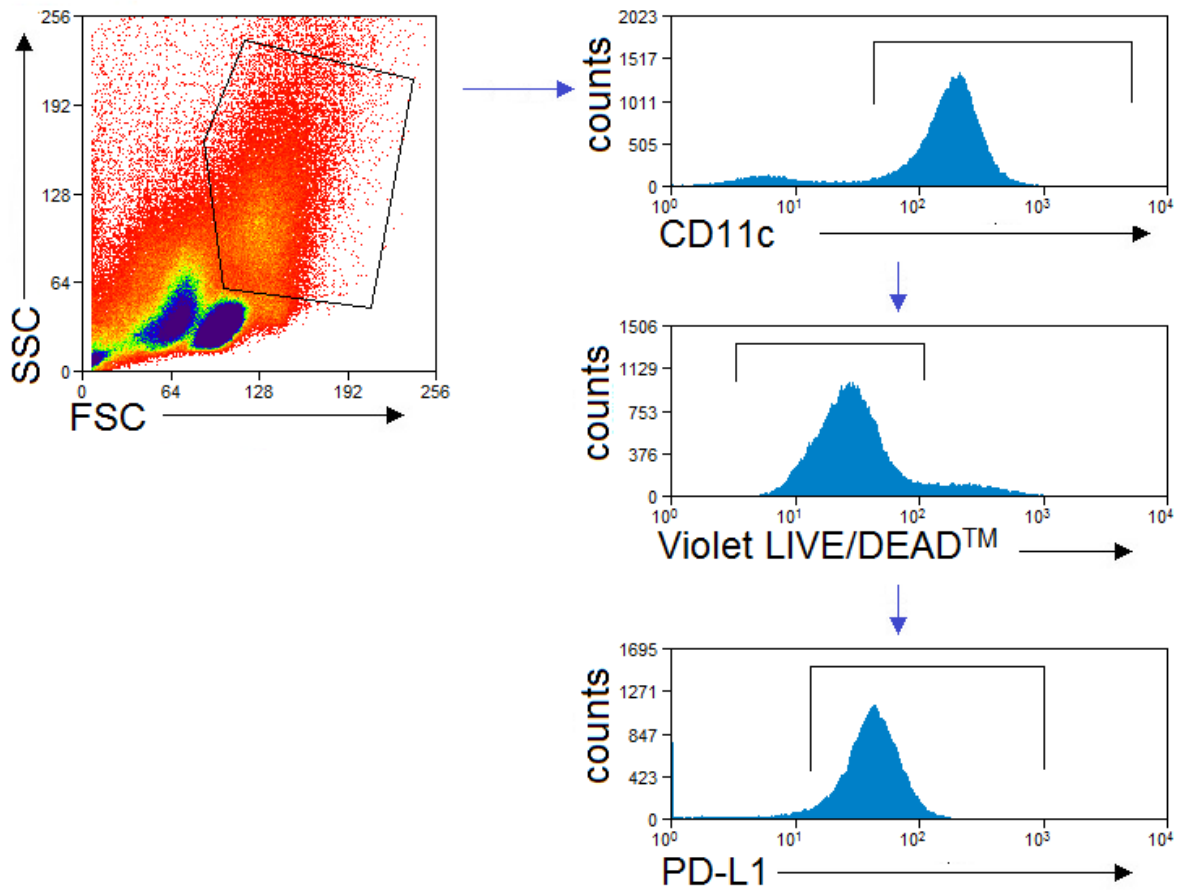


Figure 9.08. Gating strategy for assessing PD-L1 expression by monocytes in PBMC cultures. Monocytes were first selected based on FSC versus SSC profiles through a monocyte gate, followed by a monocyte gate (CD11c(+)) and a viability gate (Violet LIVE/DEAD^{LOW}). PD-L1 expression was assessed with a PD-L1(+) gate.

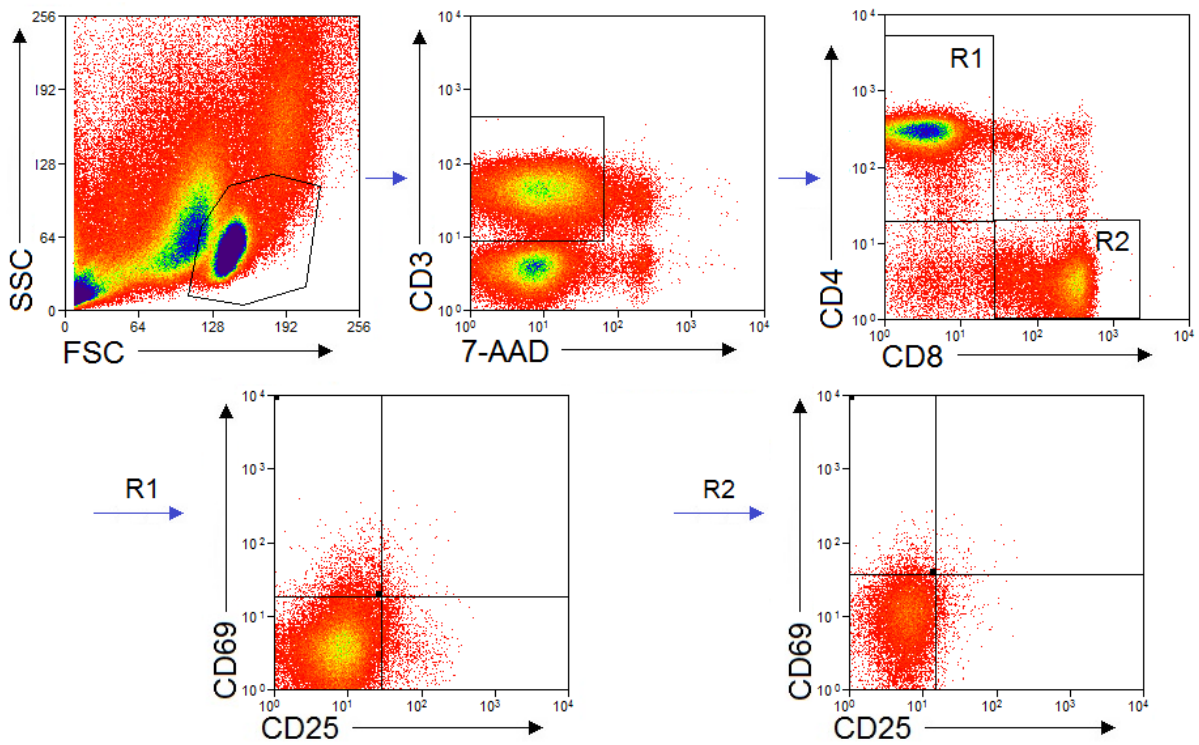


Figure 9.09. Gating strategy for assessing CD25 and CD69 expression on CD4(+) and CD8(+) T cells in PBMC cultures. T cells were first selected based on FSC versus SSC profiles through a T cell gate also which excluded debris, followed by a viable T cell gate (7-AAD(-)CD3(+)) and a CD4(+) (R1) or a CD8(+) (R2) gate for helper and cytotoxic T cells, respectively. Expression of activation markers were assessed through CD25 vs CD69 dot plots and quadrant gating.

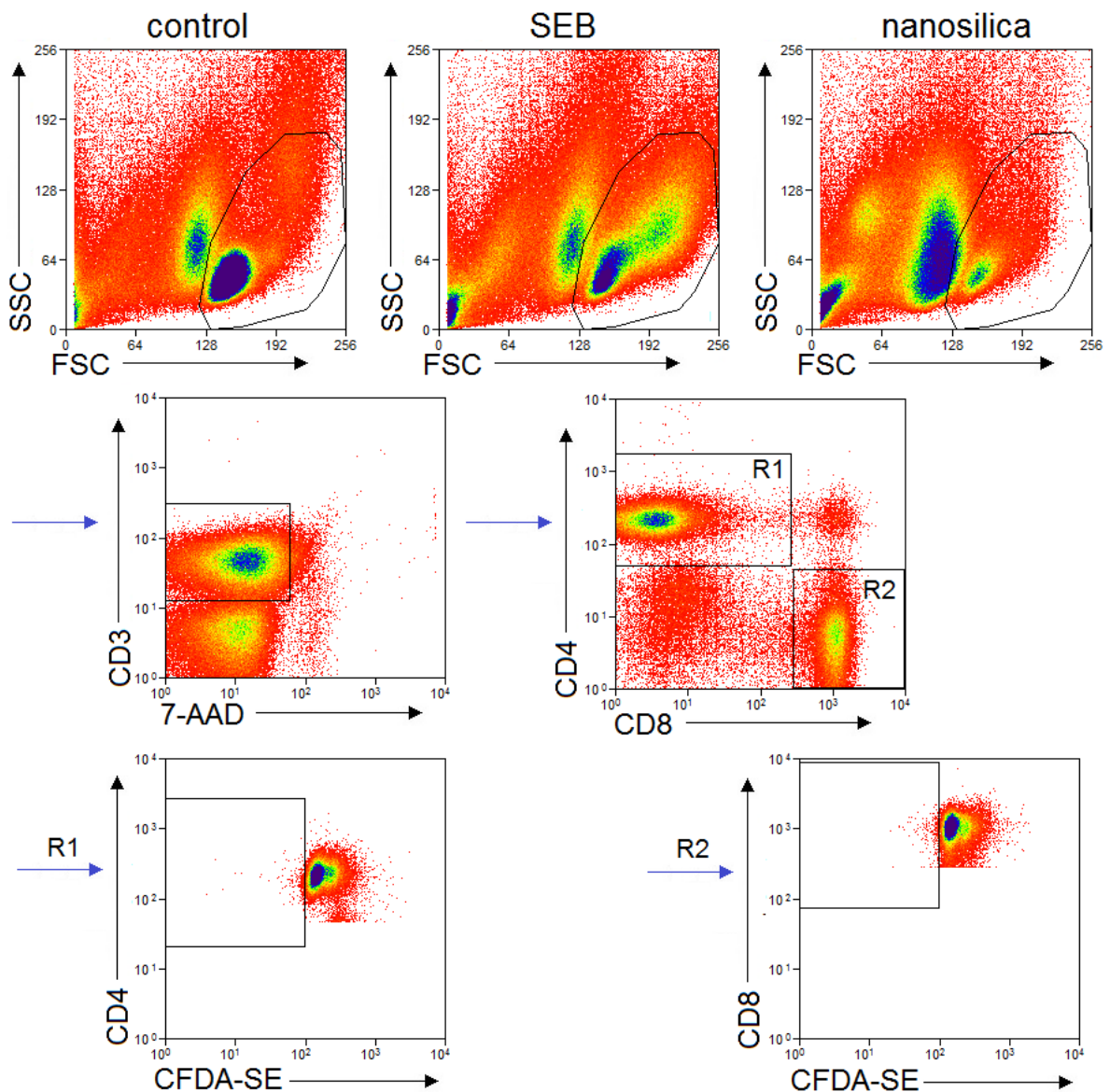


Figure 9.10. Gating strategy for assessing proliferation of CD4(+) and CD8(+) T cells in PBMC cultures. T cells were first selected based on FSC versus SSC profiles through a T cell gate also which excluded debris, followed by a viable T cell gate (7-AAD(-)CD3(+)) and a CD4(+) (R1) or a CD8(+) (R2) gate for helper and cytotoxic T cells, respectively. Proliferation was assessed through CD4/CD8 vs CFDA-SE dot plots, where divided cells were selected with a CFDA-SE^{low} gate. The linear forward scatter (FSC)-side scatter gate used was generous to accommodate the cell size increase prior to division (as evident in the example SEB histogram plot)

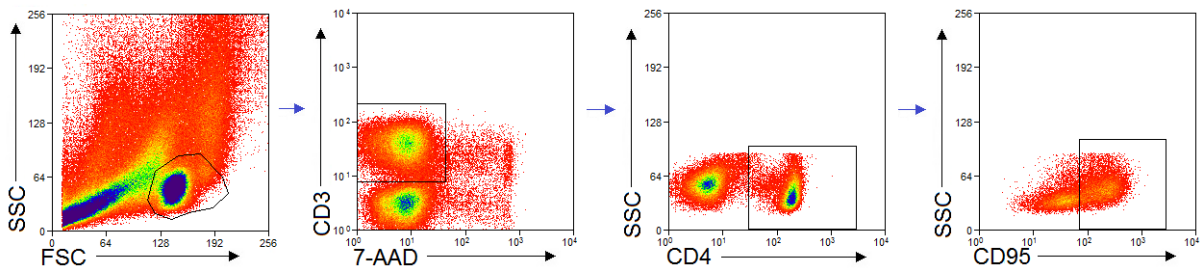


Figure 9.11. Gating strategy for assessing CD95 (Fas) expression on CD4(+) T cells in PBMC cultures. T cells were first selected based on FSC versus SSC profiles through a T cell gate also which excluded debris, followed by a viable T cell gate (7-AAD(-)CD3(+)) and a CD4(+) gate. CD95 expression was assessed through SSC vs CD95 dot plots, where CD95(+) cells were selected

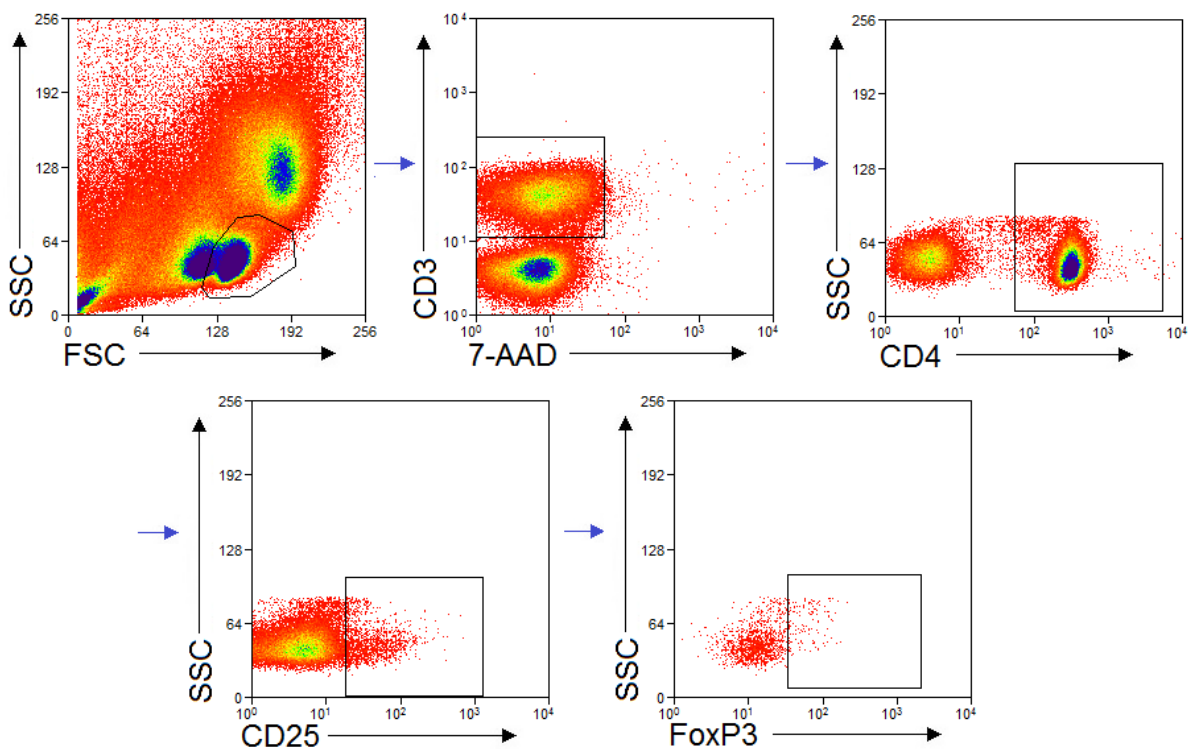


Figure 9.12. Gating strategy for assessing FoxP3 levels in activated CD4(+) T cells in PBMC cultures. T cells were first selected based on FSC versus SSC profiles through a T cell gate also which excluded debris, followed by a viable T cell gate (7-AAD(-)CD3(+)), a CD4(+) gate and a CD25(+) gate. FoxP3 expression was assessed through SSC vs FoxP3 dot plots, where FoxP3(+) cells were selected

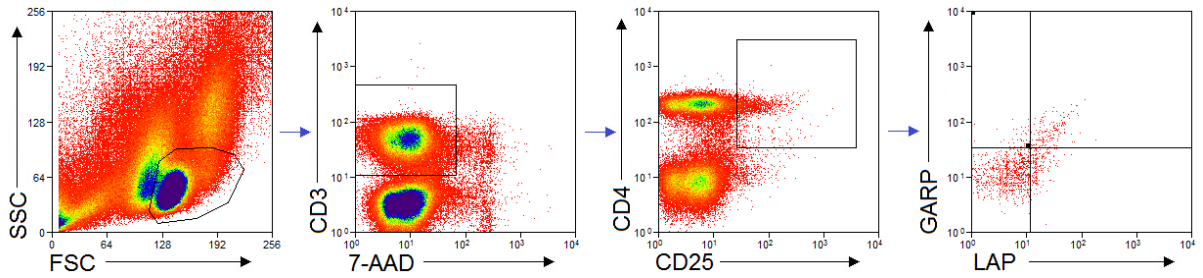


Figure 9.13. Gating strategy for assessing LAP/GARP expression on activated CD4(+) T cells in PBMC cultures. T cells were first selected based on FSC versus SSC profiles through a T cell gate also which excluded debris, followed by a viable T cell gate (7-AAD(-)CD3(+)) and a CD4(+)CD25(+) gate. LAP/GARP double positive cells were assessed with LAP vs GARP dot plots and quadrant gating.

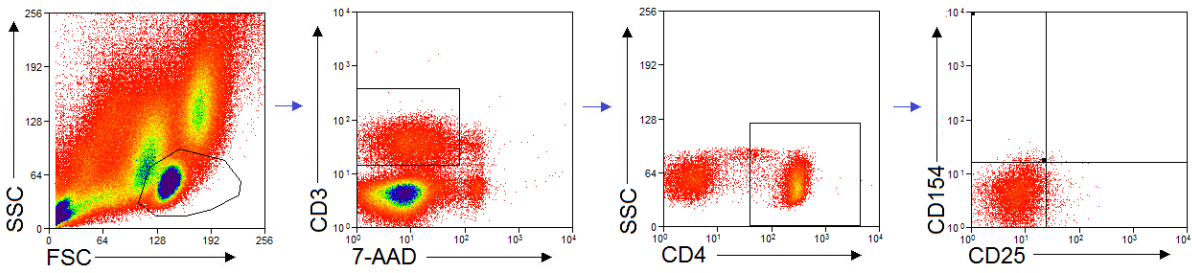


Figure 9.14. Gating strategy for assessing CD40L (CD154) expression on CD4(+) T cells in PBMC cultures. T cells were first selected based on FSC versus SSC profiles through a T cell gate also which excluded debris, followed by a viable T cell gate (7-AAD(-)CD3(+)) and a CD4(+) gate. CD154 positivity was assessed with CD154 vs CD25 dot plots and quadrant gating.

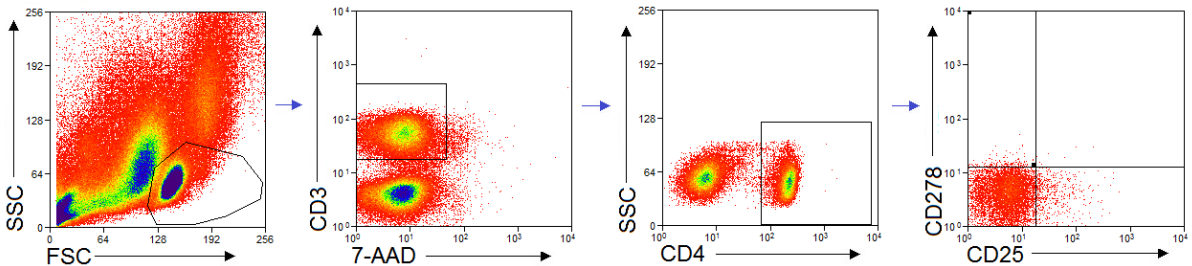


Figure 9.15. Gating strategy for assessing iCOS (CD278) expression on CD4(+) T cells in PBMC cultures. T cells were first selected based on FSC versus SSC profiles through a T cell gate also which excluded debris, followed by a viable T cell gate (7-AAD(-)CD3(+)) and a CD4(+) gate. CD278 positivity was assessed with CD278 vs CD25 dot plots and quadrant gating.

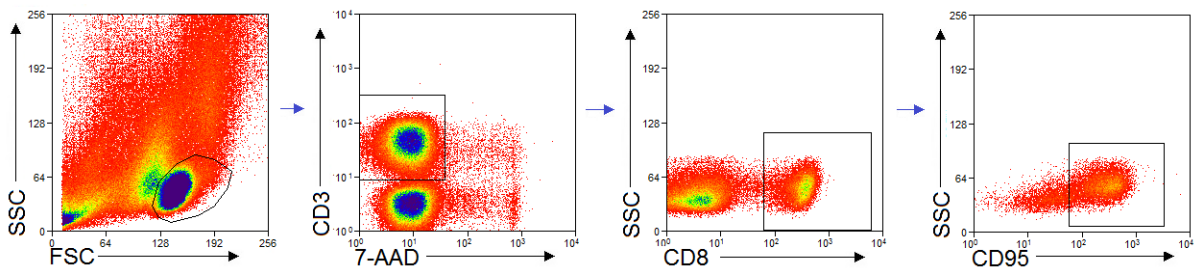


Figure 9.16. Gating strategy for assessing CD95 (Fas) expression on CD8(+) T cells in PBMC cultures. T cells were first selected based on FSC versus SSC profiles through a T cell gate also which excluded debris, followed by a viable T cell gate (7-AAD(-)CD3(+)) and a CD8(+)gate. CD95 expression was assessed through SSC vs CD95 dot plots, where CD95(+) cells were selected

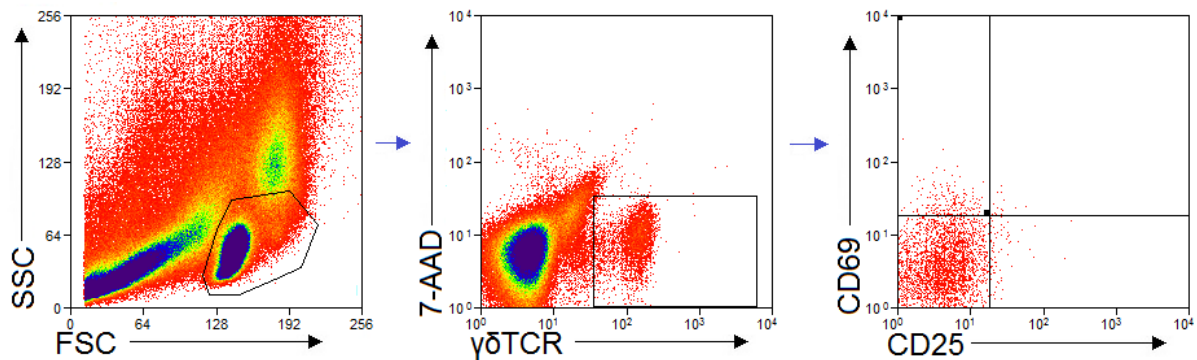


Figure 9.17. Gating strategy for assessing CD25 and CD69 expression on $\gamma\delta$ T cells in PBMC cultures. T cells were first selected based on FSC versus SSC profiles through a T cell gate also which excluded debris, followed by a viable $\gamma\delta$ T cell gate (7-AAD(-) $\gamma\delta$ TCR(+)). Expression of activation markers were assessed through CD25 vs CD69 dot plots and quadrant gating.

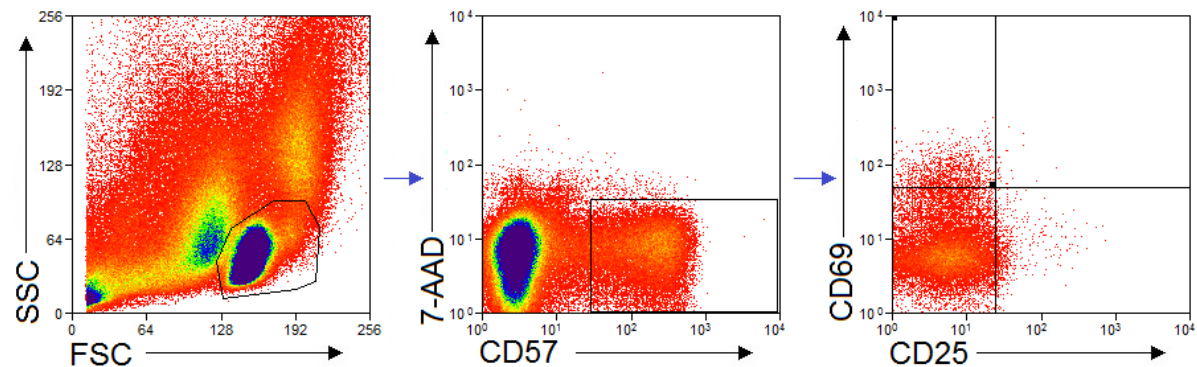
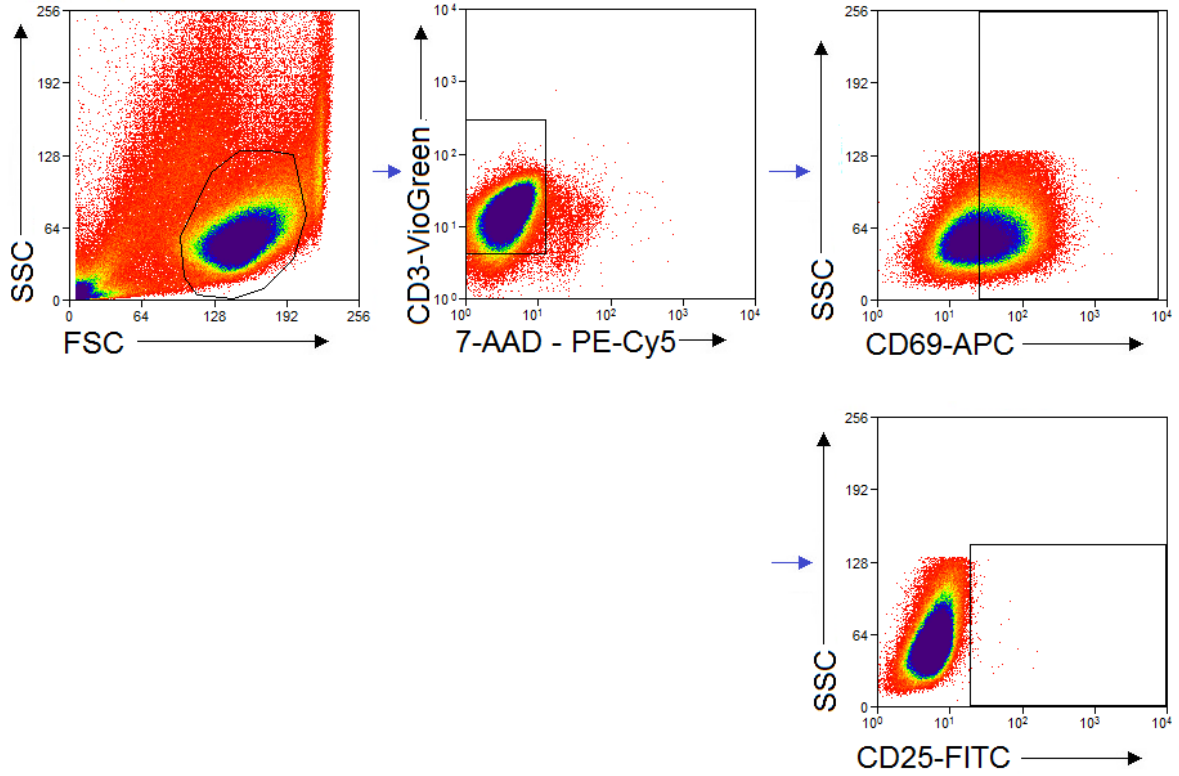


Figure 9.18. Gating strategy for assessing CD25 and CD69 expression on NK/NKT (CD57(+)) cells in PBMC cultures. NK/NKT cells were first selected based on FSC versus SSC profiles through a lymphocyte gate also which excluded debris, followed by a viable NK/NKT cell gate (7-AAD(-)CD57(+)). Expression of activation markers were assessed through CD25 vs CD69 dot plots and quadrant gating.

Jurkat



Karpas299

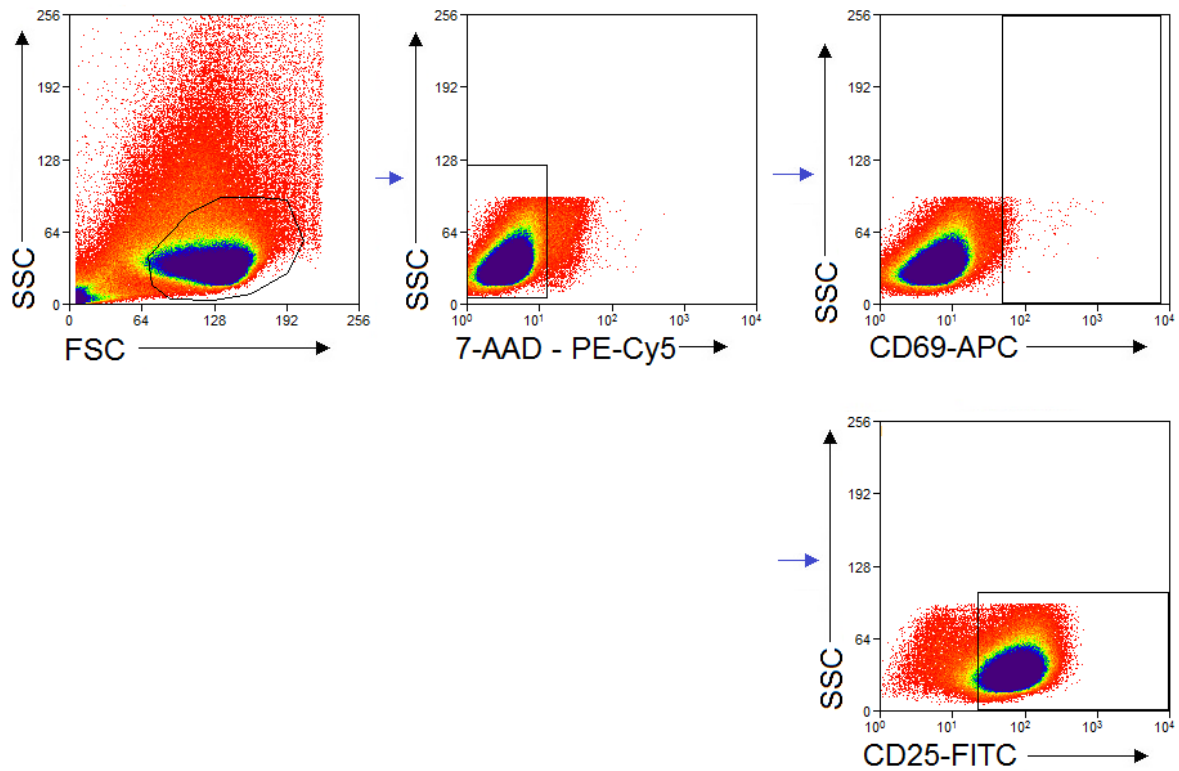


Figure 9.19. Gating strategy for assessing CD25 and CD69 expression on Jurkat and Karpas 299 cells. Cells were gated through a FS-SS gate to exclude debris followed by either a viable T cell gate (7-AAD(-)CD3(+), Jurkat) or a viable cell gate (7-AAD(-), Karpas 299).

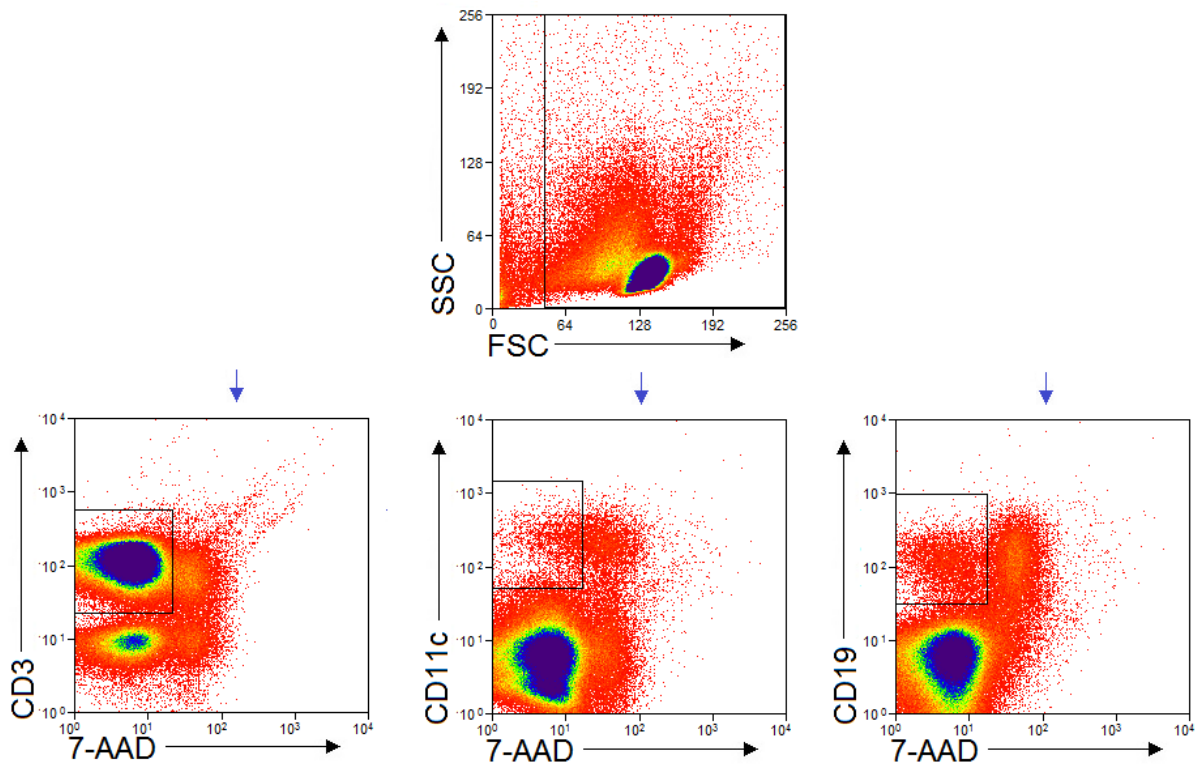


Figure 9.20. Gating strategy for assessing cell distribution in enriched T cell cultures. Cells were first selected based on a generous FSC versus SSC profiles which also excluded debris first, followed by viable T cell, monocyte and B cell gates ((7-AAD(-)CD3/11c/19(+))

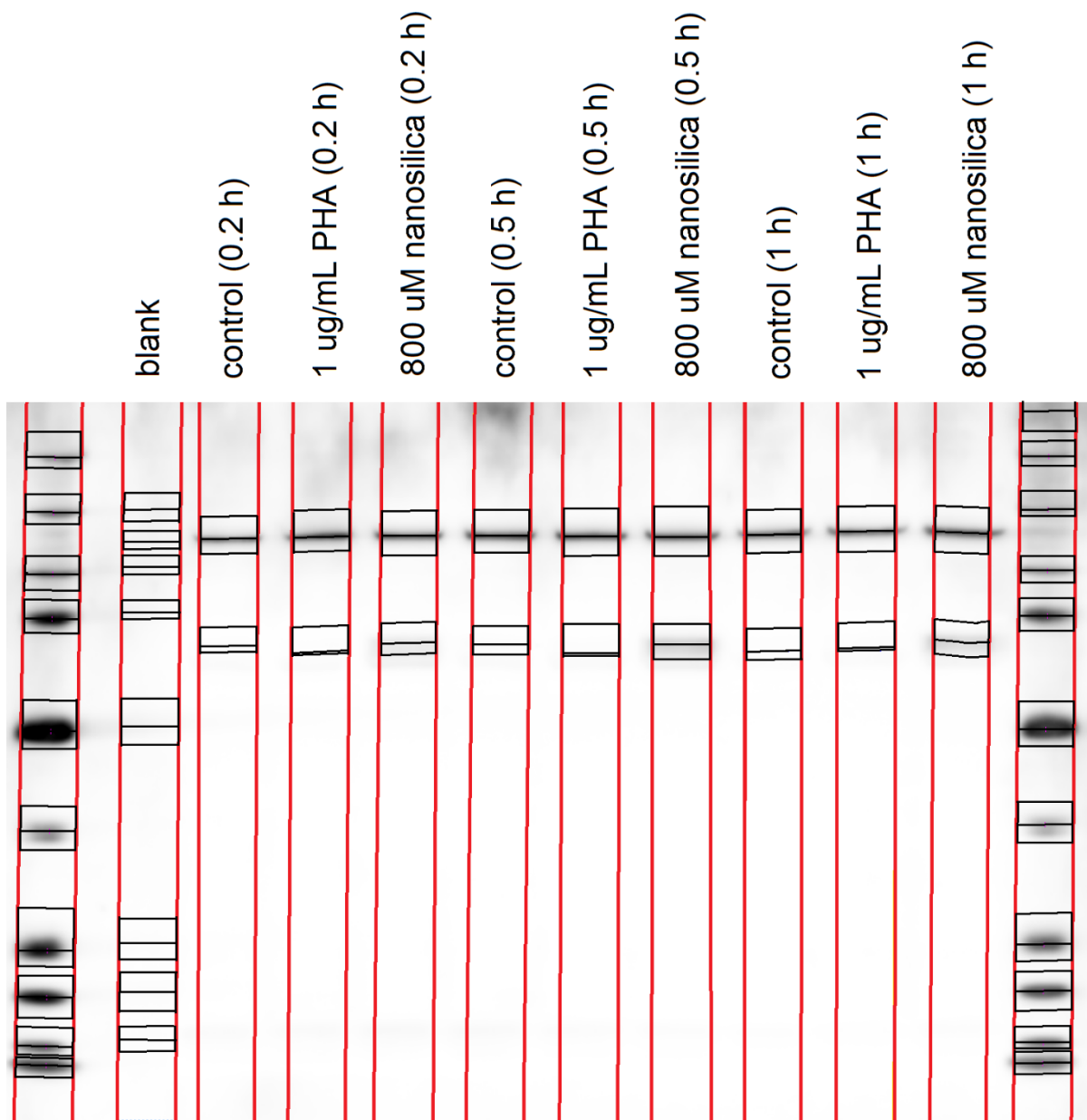


Figure 9.21. Integration strategy for the determination of pZap70 and vinculin levels in cell lysates. The volume (intensity of chemiluminescence) was determined between top and bottom lines, and the middle line denotes the maximum peak height. Similar integration strategy was used for pLAT.

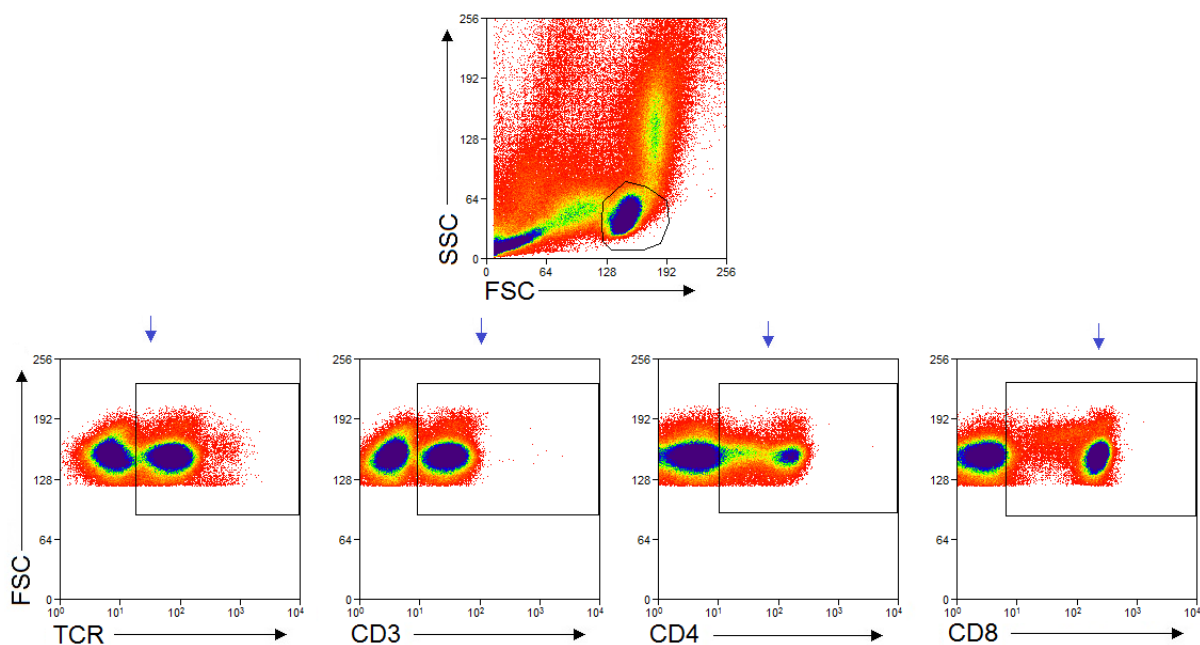


Figure 9.22. Gating strategy for assessing $\alpha\beta$ TCR, CD3, CD4 and CD8 antibody binding inhibition in PBMC cultures. T cells were selected based on FSC versus SSC profiles through a T cell gate also which excluded debris. $\alpha\beta$ TCR, CD3, CD4 and CD8 expression was plotted against FCS and positive cells were selected.

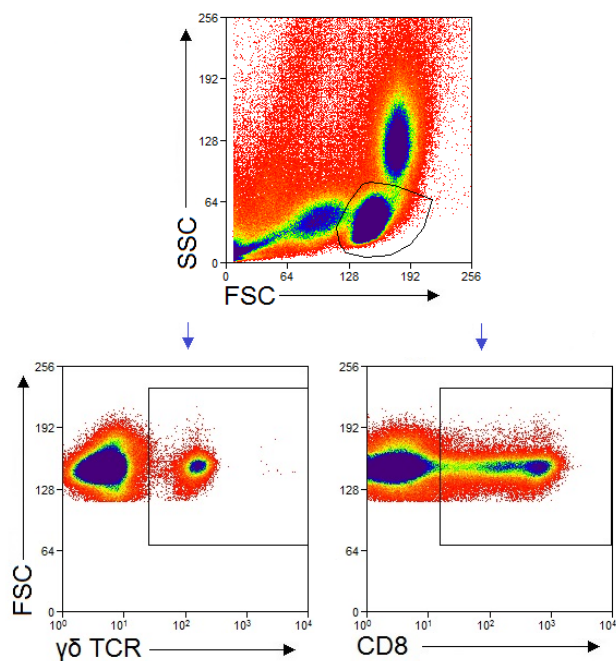


Figure 9.23. Gating strategy for assessing $\gamma\delta$ TCR and CD8 antibody binding inhibition in PBMC cultures. T cells were selected based on FSC versus SSC profiles through a T cell gate also which excluded debris. $\gamma\delta$ TCR expression was plotted against FCS and positive cells were selected.

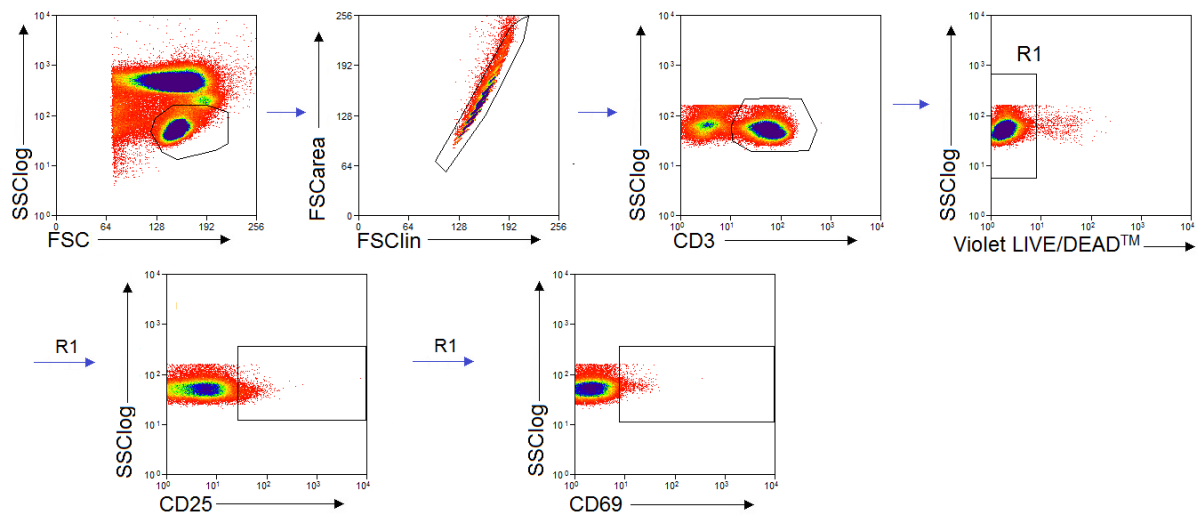


Figure 9.24. Gating strategy for assessing CD25 and CD69 expression on CD3(+) T cells in whole blood cultures. T cells were first selected based on FSC versus SSClog profiles through a T cell gate which also excluded debris, followed by a singlets gate (FSClin vs FSCarea), a T cell gate (CD3(+)) and a viability gate (Invitrogen LIVE/DEAD, Violet^{LOW}, R1). The expression of the activation markers were assessed with CD25 vs SSClog and CD69 vs SSClog dot plots, where positive cells were identified.

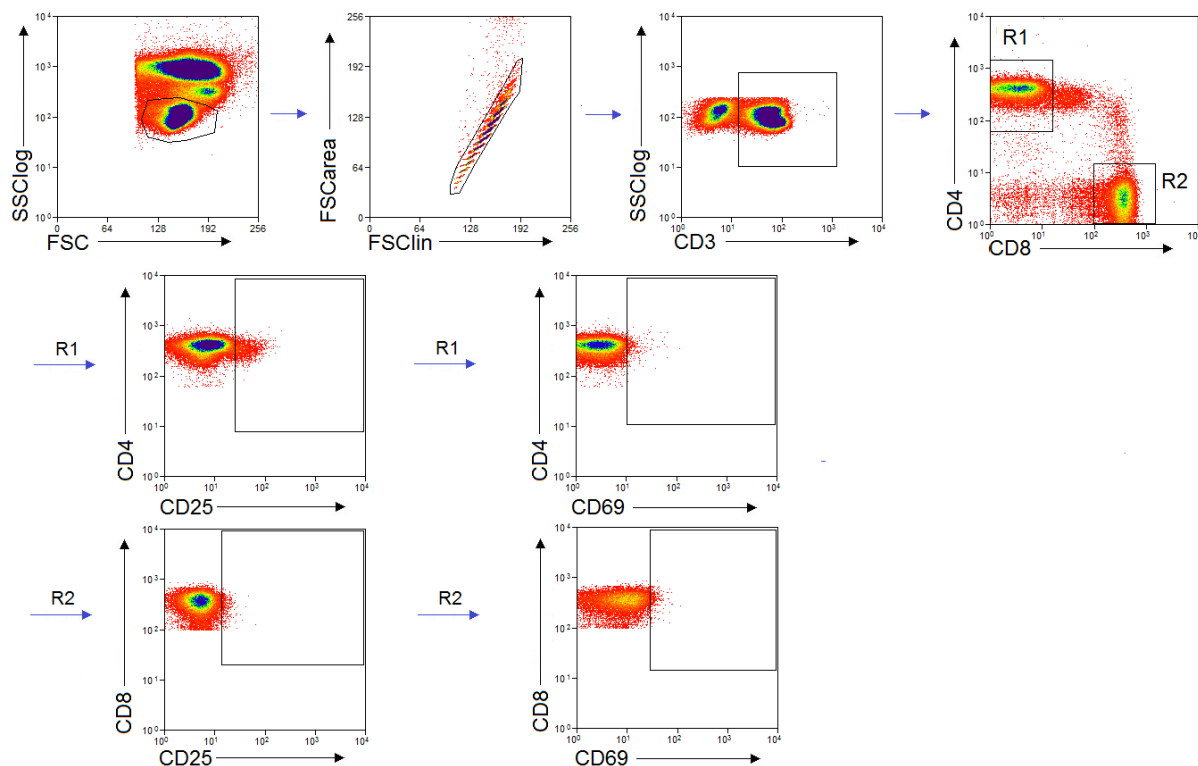


Figure 9.25. Gating strategy for assessing CD25 and CD69 expression on CD4(+) and CD8(+) T cells in whole blood cultures. T cells were first selected based on FSC versus SSClog profiles through a T cell gate which also excluded debris, followed by a singlets gate (FSClin vs FSCarea), a T cell gate (CD3(+)), and a CD4(+) (R1) or a CD8(+) (R2) gate for helper and cytotoxic T cells, respectively. The expression of the activation markers were assessed with CD25 vs SSClog and CD69 vs SSClog dot plots, where positive cells were identified.

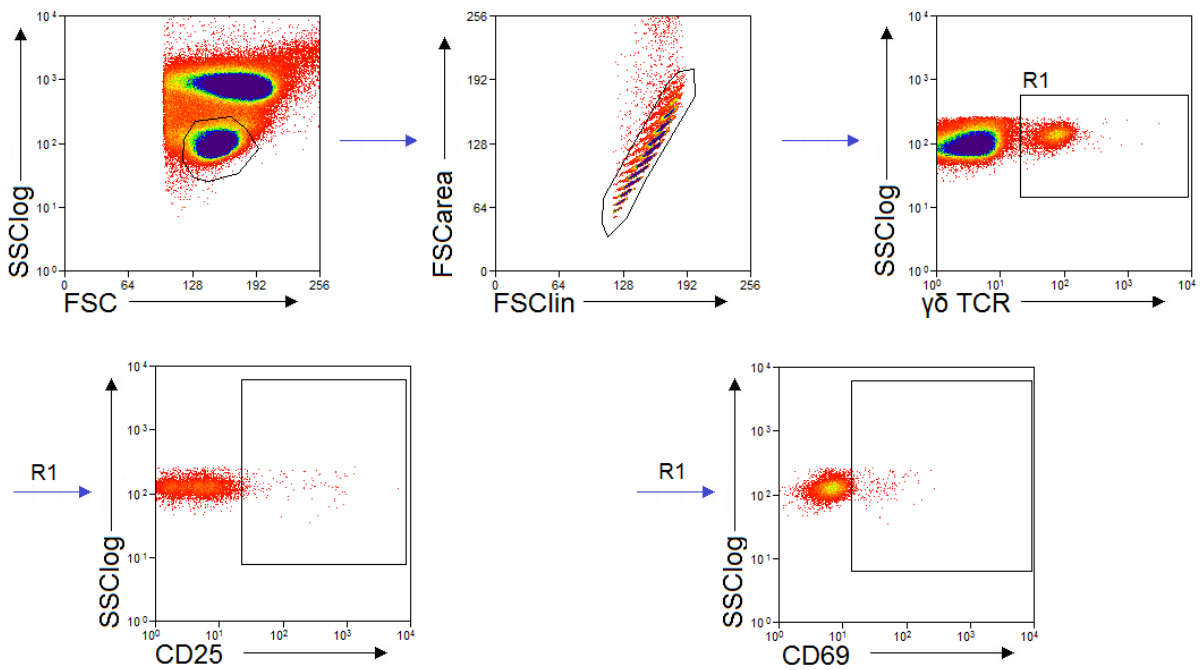


Figure 9.26. Gating strategy for assessing CD25 and CD69 expression on $\gamma\delta$ T cells in whole blood cultures. T cells were first selected based on FSC versus SSClog profiles through a T cell gate which also excluded debris, followed by a singlets gate (FSClin vs FSCarea), and a $\gamma\delta$ T cell gate ($\gamma\delta$ TCR(+)). The expression of the activation markers were assessed with CD25 vs SSClog and CD69 vs SSClog dot plots, where positive cells were identified.

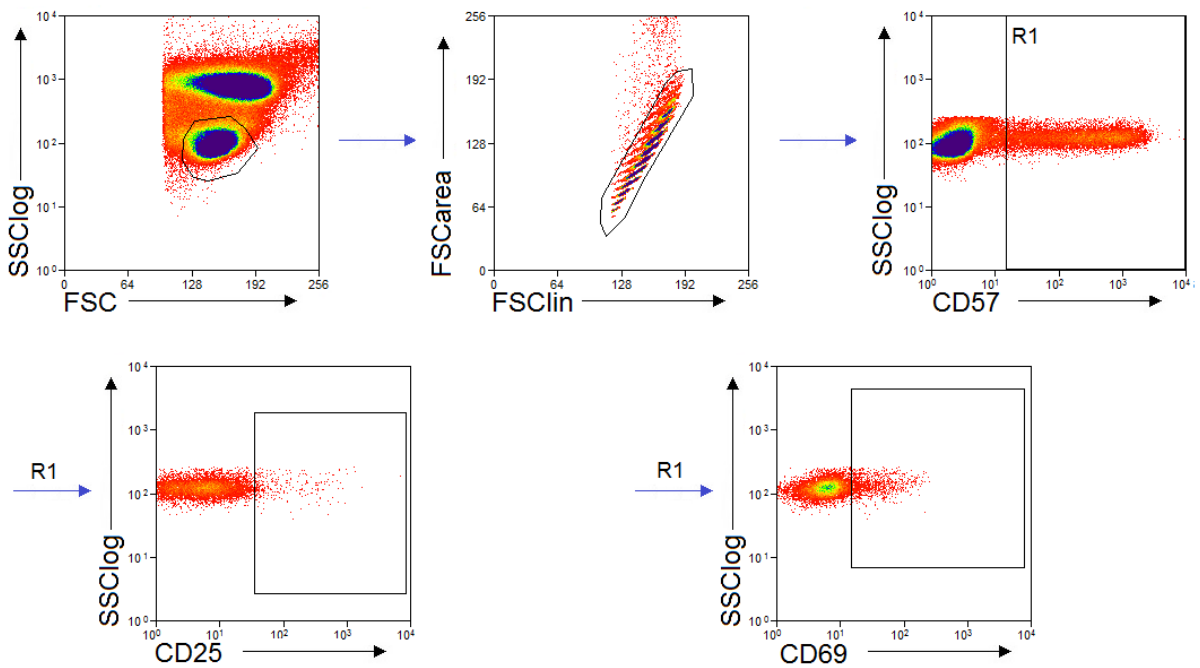


Figure 9.27. Gating strategy for assessing CD25 and CD69 expression on NK/NKT cells in whole blood cultures. NK/NKT cells were first selected based on FSC versus SSClog profiles through a NK/NKT cell gate which also excluded debris, followed by a singlets gate (FSClin vs FSCarea), and a NK/NKT cell gate (CD57(+)). The expression of the activation markers were assessed with CD25 vs SSClog and CD69 vs SSClog dot plots, where positive cells were identified.

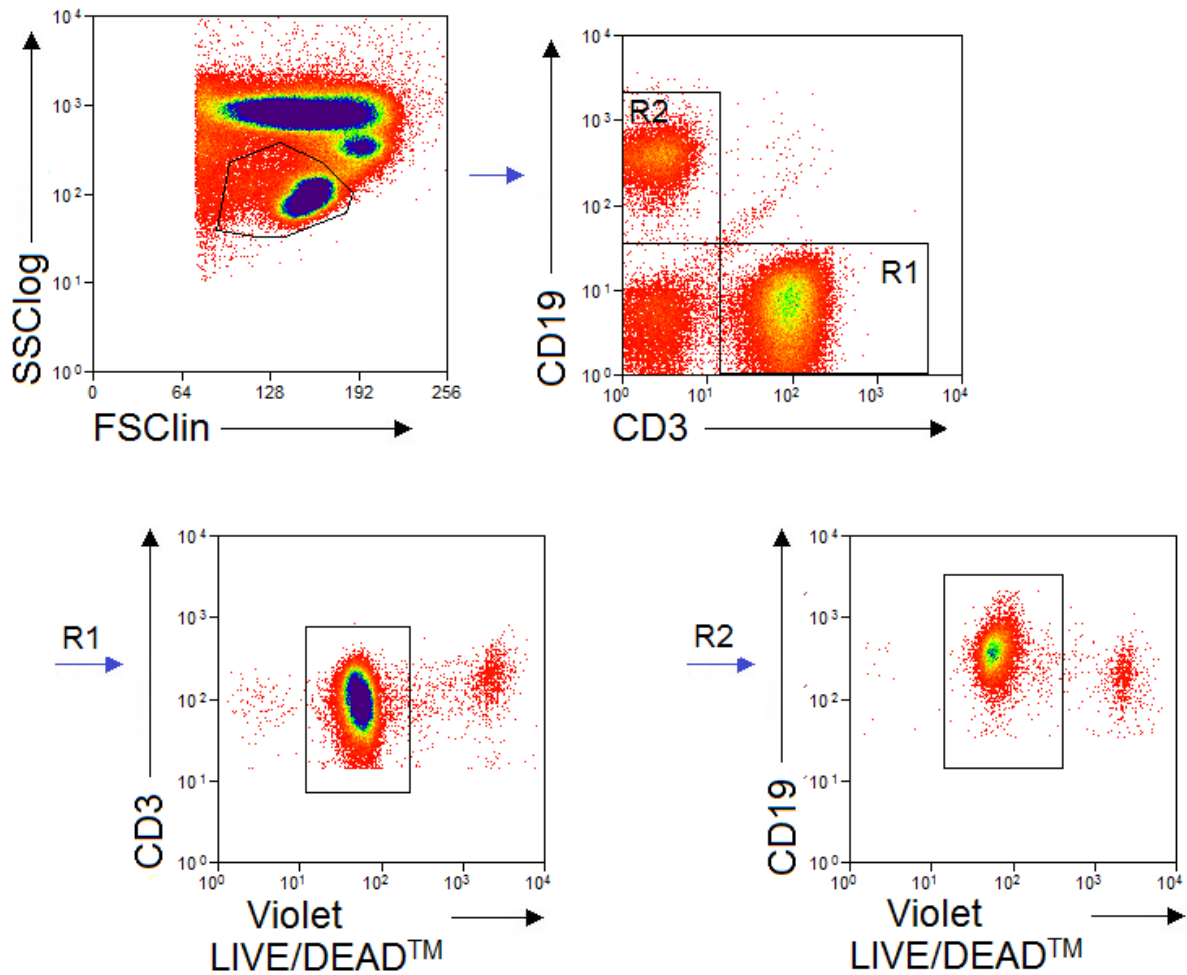


Figure 9.28. Gating strategy for assessing viability of T cells and B cells in whole blood cultures. T cells and B cells were first selected based on FSC versus SSClog profiles through a lymphocyte cell gate which also excluded debris, followed by respective T cell (CD3(+), R1) and B cell (CD19(+), R2) gates. Viability was assessed with a Violet LIVE/DEAD stain, where Violet LIVE/DEAD^{low} cells were considered viable.

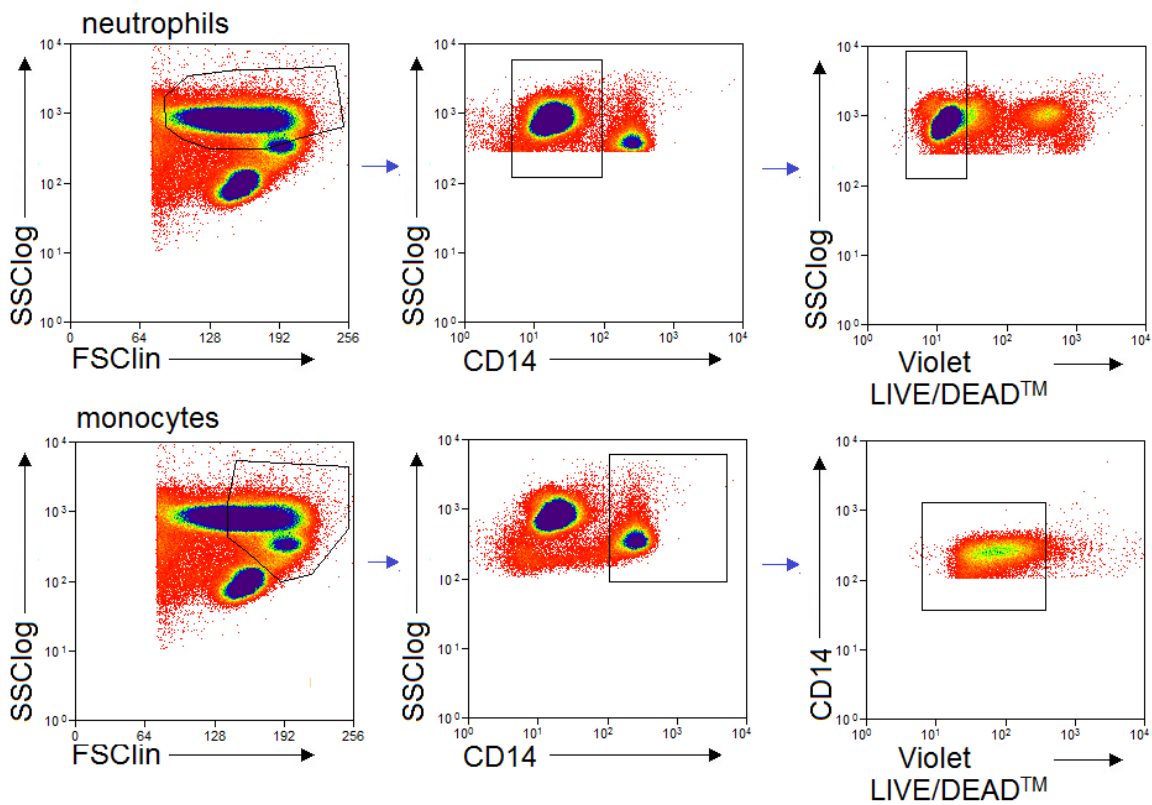


Figure 9.29. Gating strategy for assessing viability of neutrophils and monocytes in whole blood cultures. Monocytes were first selected based on FSC versus SSClog profiles through a monocyte cell gate which also excluded debris, followed by a monocyte gate (CD14^{high}). Neutrophils were first selected based on FSC versus SSClog profiles through a neutrophil cell gate which also excluded debris, followed by a negative monocyte gate (CD14^{low}). Viability was assessed with a Violet LIVE/DEAD stain, where Violet LIVE/DEAD^{low} cells were considered viable.

Appendix 2 – Clearance of amorphous nanosilica from the periphery after intravenous injection

10.1. Introduction

Silicon absorbed from diet is rapidly cleared in urine, peripheral levels return to baseline within ca. 6 h after consumption of a silicate containing material (Jugdaohsingh et al., 2002; Sripanyakorn et al., 2009). The clearance of intravenous administered nanosilica particles is less well understood. The excretion and retention of intravenously administered silica nanoparticles (of varying sizes and functionalities) has been investigated (Cho et al., 2009; Ivanov et al., 2012; Kumar et al., 2010; Xie et al., 2010; Yu et al., 2013), but the short term clearance of these particles from the periphery has not. Here, the clearance of a nanosilica dispersion (3-5 nm) from the periphery after intravenous administration was assessed.

10.2 Methods

Nanosilica dispersions (40 mM, 3-5 nm in diameter) were prepared by Mr C. Bastos. *In vivo* studies were conducted under project licence 80/2574 by Drs J. Shields and L. Pedro. Briefly, C57BL6 mice were injected with a subcutaneous tumour on day 0 and left untreated for 6 days. Mice were then injected with 200 μ L nanosilica or saline and were sacrificed at 4 or 24 h for collection of blood. At each timepoint, 3 mice (1 saline, 2 nanosilica treated) were sacrificed. An identical protocol was used with healthy mice without the subcutaneous injection of tumour cells and only 2 mice were sacrificed at each timepoint (1 saline, 1 nanosilica treated). ICP-OES on the blood was conducted by Dr R. Jugdaohsingh.

10.3 Results and discussion

Figure 10.01 shows the blood silicon levels after intravenous injection of a 40 mM Si nanosilica dispersion. The concentration at the time of injection was estimated using the approximate blood volume (C57BL6 mice contain approximately 2 mL). More than 75% of the silicon injected was cleared from circulation within 4 h, were the tumour bearing animals had lower levels than healthy animals. Whether these differences are real or just an artefact from the low numbers ($n=2$ for tumour-bearing animals, $n=1$ for healthy animals) is unknown. At 24 h, blood silicon levels were below 5 μ g/mL. These results would suggest that nanosilica particles (3-5 nm) are rapidly cleared from the periphery after intravenous injection. A curve of best fit (one phase decay) would suggest that the concentration of nanosilica would decrease below Si solubility (ca. 1.7 mM Si (48 μ g/mL) at pH 7.4 (Jugdaohsingh et al., 2008; Mosby, 2016)) within 2 h. The nanosilica particles would likely dissolve relatively quickly in these conditions. It is important to note that the levels of Si injected into the mice are 100-1000 times higher than peripheral levels after ingestion of a highly bioavailable silicate containing material (Sripanyakorn et al., 2009).

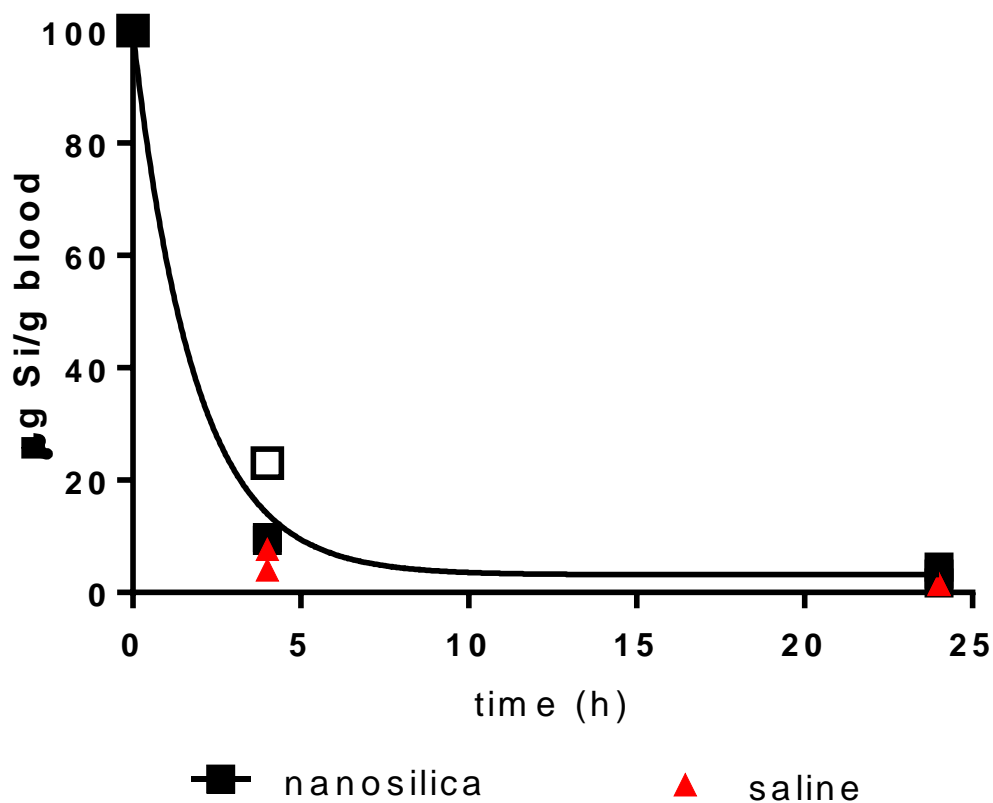


Figure 10.01. Concentration of silicon in blood after mice were intravenously injected with 200 µL nanosilica (40 mM Si). The concentration at time of injection was estimated using the approximate blood volume. Open squares correspond to clearance in healthy mice and closed squares correspond to tumour bearing mice. A curve of best fit (one phase decay) was used to estimate rate of nanosilica dilution.

10.4 Conclusions

It was shown here that intravenous administered nanosilica particles are rapidly cleared from the periphery. It is likely that the concentration of Si drops below Si solubility within hours after injection, which would promote the dissolution of the particles.

Appendix 3 – The effect of nanosilica on bead and bacterial uptake by monocytes in enriched cultures from PBMC – flow imaging analysis.

11.1. Introduction

The effects of amorphous nanosilica particles on phagocyte function have been extensively studied. There have been studies showing both positive and negative effects on monocyte function (Brandenberger et al., 2013; Chen et al., 2014; Fedeli et al., 2014; Fedeli et al., 2013; Hirai et al., 2012; Marzaioli et al., 2014; Mendoza et al., 2014). The effect of 3-5 nm nanosilica particles on uptake of bacteria and beads by monocytes was investigated in Chapter 4. Nanosilica was found to decrease the percentage of monocytes positive for the fluorescent beads/bacteria. Whether the decrease in fluorescence is due to degradation of the foreign material in the endosome/lysosome or a decrease in monocyte phagocytosis was investigated here using imaging flow cytometry.

11.2 Methods

Nanoparticle dispersions (3-5 nm) were prepared by diluting sodium silicate (cat. # 338443) in distilled deionized water to 23 mM Si and adjusting to pH 6.7 (pH strips) with hydrochloric acid. The dispersions were left to equilibrate for 12-24 h at room temperature. Low doses were used to avoid significant cell death.

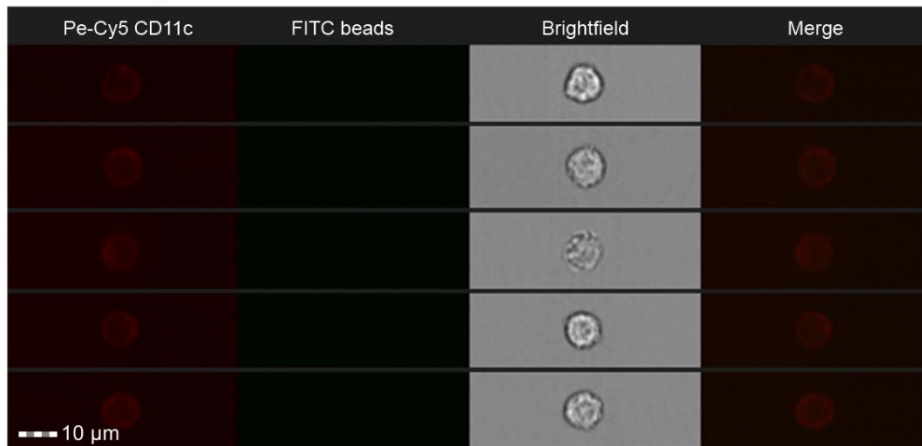
Peripheral blood mononuclear cells (PBMC) were isolated from single leukocyte cones purchased from the National Blood Service (Cambridge, UK) using density gradient centrifugation. Cells were frozen down in freezing media (10% DMSO, 50% FBS, 40% RPMI 1640). Frozen cells were thawed, washed in RPMI, and rested 2 h in RPMI containing 10% FBS, 0.3 g/L L-glutamine, 1% penicillin-streptomycin and 0.01 µg/mL DNase. Enrichment of monocytes was conducted through monocyte adherence. Briefly, PBMC cultures were added to a 6 well plate and incubated for >1 h. Non-adherent cells were then discarded and adherent cells were scraped and transferred to a fresh 6 well plate. After repeating 3 times, cells were counted and rested for a minimum of 2 h prior to use.

Enriched monocytes cultures were treated with nanosilica followed immediately by addition of fluorescent beads (final concentration 25 µg/mL) or bacteria (final concentration 3 µg/mL) (details of beads and bacterial can be found in Table 2.01). Cultures were incubated for 1 h, stained (using the Invitrogen live-dead stain) and flow imaging was conducted immediately by Dr. R. Hewitt. The same samples that were used in flow cytometry analyses were split for Image Stream IsX analysis. Antibody, bead and bacteria details can be found in Table 2.01 (Chapter 2).

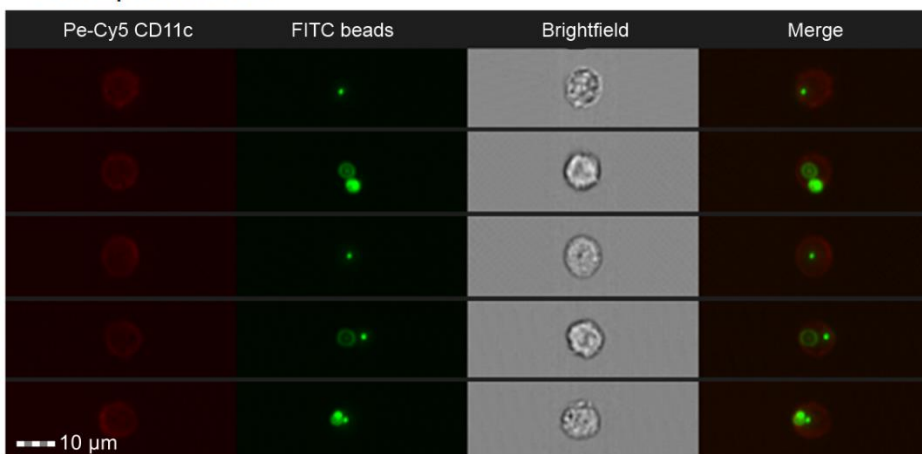
11.3 Results and discussion

Figure 11.01 shows the effect of nanosilica on bead uptake by monocytes. The representative images show monocytes (CD11c(+)) negative and positive for the beads. As with the flow cytometry analyses, the percentage of cells positive for beads decreased when co-incubated with nanosilica. There was no indication of a decrease in fluorescence intensity of the beads after treatment with nanosilica. The decrease in bacterial phagocytosis after nanosilica treatment as determined by flow cytometry was also confirmed with imaging flow analyses, where there was no decrease in bacterial fluorescent intensity (Figure 11.02). These results would indicate that nanosilica negatively effects monocyte phagocytosis.

A. Bead negative cells



Bead positive cells



B.

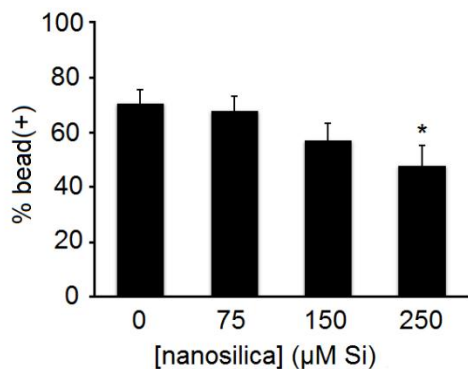
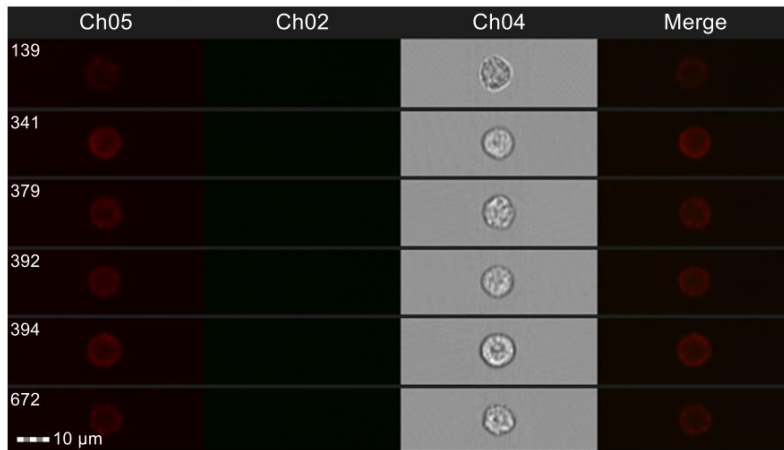
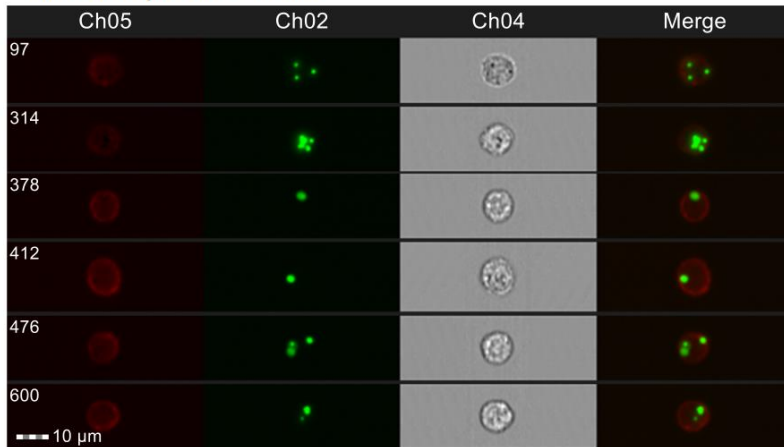


Figure 11.01. The effect of nanosilica on the phagocytosis of polystyrene fluorescent beads by monocytes. **A.** Representative flow images showing the CD11c cells negative and positive for fluorescent beads after 1 h incubation. **B.** The percentage of CD11c cells positive for fluorescent beads after nanosilica treatment for 1 h. Tabulated data represents the means \pm standard deviation for 3 donors (* denotes a significance compared to the control, two-tailed paired T test, $p < 0.05$). Monocytes were first selected through area (defined as the size of the masked cells in square microns) versus aspect ratio (the ratio of the minor axis divided the major axis) of the brightfield cell images to identify cell populations of interest as well as doublet and debris exclusion. The cells were then gated through a CD11c(+) gate. Uptake was assessed with a bead(+) gate.

A. Bacteria negative cells



Bacteria positive cells



B.

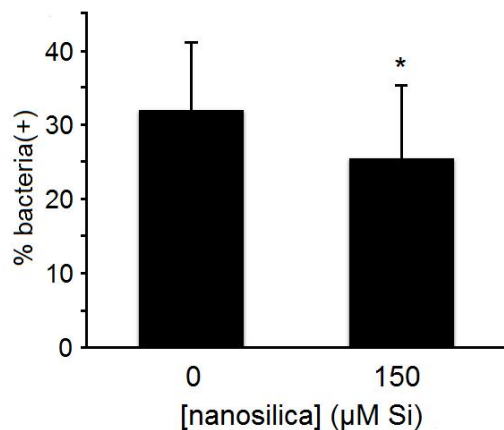


Figure 11.02. The effect of nanosilica on the phagocytosis of fluorescent *S. aureus* by monocytes. **A.** Representative flow images showing the CD11c cells negative and positive for fluorescent bacteria after 1 h incubation. **B.** The percentage of CD11c cells positive for fluorescent bacteria after nanosilica treatment for 1 h. Tabulated data represents the means \pm standard deviation for 3 donors (* denotes a significance compared to the control, two-tailed paired T test, $p < 0.05$). Monocytes were first selected through area (defined as the size of the masked cells in square microns) versus aspect ratio (the ratio of the minor axis divided the major axis) of the brightfield cell images to identify cell populations of interest as well as doublet and debris exclusion. The cells were then gated through a CD11c(+) gate. Uptake was assessed with a bacteria(+) gate.

11.4 Conclusions

Nanosilica decreased bead and bacteria phagocytosis by monocytes as determined by imaging flow cytometry. These results would suggest that the decrease in phagocytosis as determined by flow cytometry is not due to degradation of the fluorescent foreign material (beads/bacteria) but a decrease in phagocytosis.